

Summary of the
Bulletin of the
International Seismological Centre

2013

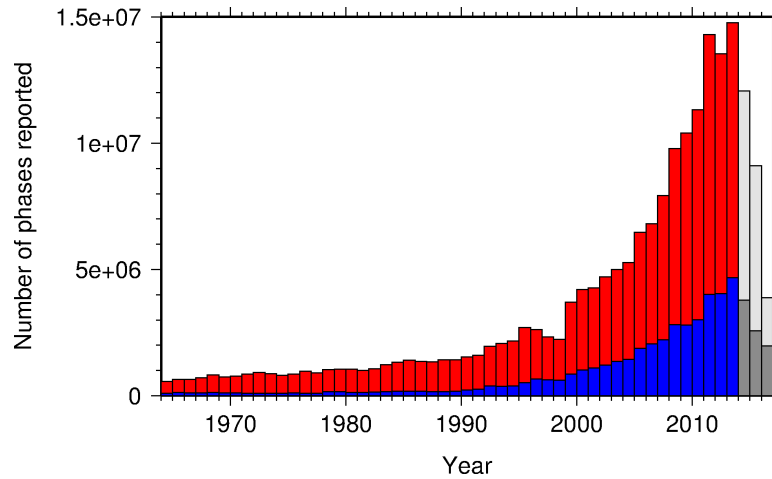
July – December

Volume 50 Issue 7-12

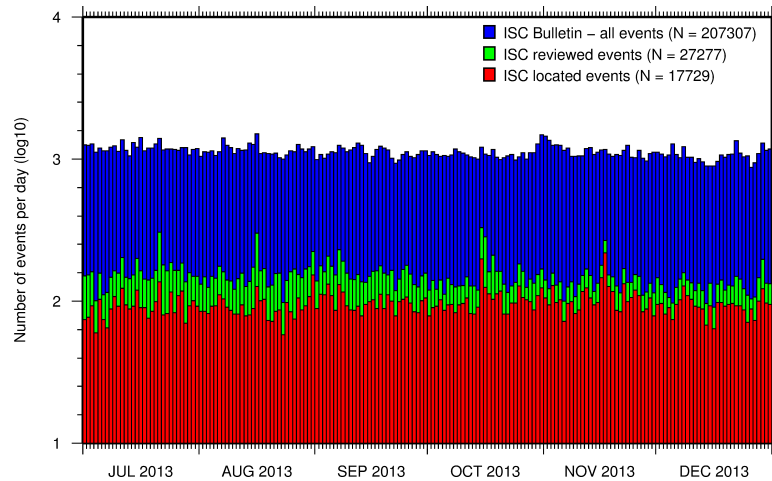
www.isc.ac.uk

isc-mirror.iris.washington.edu

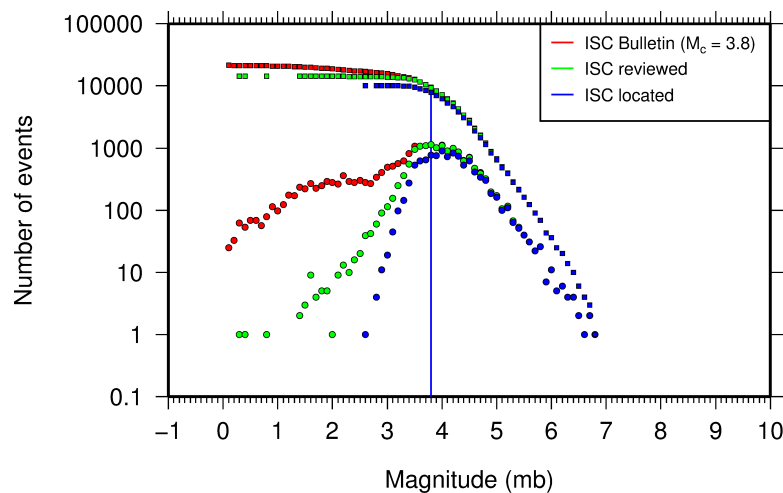
ISSN 2309-236X



The number of phases (red) and number of amplitudes (blue) collected by the ISC for events each year since 1964. The data in grey covers the current period where data are still being collected before the ISC review takes place and are accurate at the time of publication. See Section 7.3.



The number of events within the Bulletin for the current summary period. The vertical scale is logarithmic. See Section 8.1.



Frequency and cumulative frequency magnitude distribution for all events in the ISC Bulletin, ISC reviewed events and events located by the ISC. The magnitude of completeness (M_C) is shown for the ISC Bulletin. Note: only events with values of m_b are represented in the figure. See Section 8.4.

Contents

1	Preface	1
2	The International Seismological Centre	2
2.1	The ISC Mandate	2
2.2	Brief History of the ISC	3
2.3	Former Directors of the ISC and its U.K. Predecessors	4
2.4	Member Institutions of the ISC	5
2.5	Sponsoring Organisations	11
2.6	Data Contributing Agencies	12
2.7	ISC Staff	21
3	Availability of the ISC Bulletin	26
4	Citing the International Seismological Centre	27
5	Summary of Seismicity, July - December 2013	29
6	Notable Events	34
6.1	Notable events of Kamchatka in 2013	34
6.2	The February 28, 2013, M_W 6.8 South Kamchatka Earthquake	34
6.2.1	Introduction	34
6.2.2	Focal mechanism of the earthquake	36
6.2.3	Main features of the aftershocks process	36
6.2.4	Macroseismic data	38
6.2.5	Ground motion	41
6.2.6	Conclusion	45
6.3	The largest deep-focus Sea of Okhotsk earthquake May 24, 2013, $M_W = 8.3$	47
6.3.1	Introduction	47
6.3.2	Tectonic setting and the focal mechanism of the earthquake	50
6.3.3	Main features of the aftershock sequence	58
6.3.4	Macroseismic data	59
6.3.5	Conclusion	63
6.4	References	63
7	Statistics of Collected Data	66

7.1	Introduction	66
7.2	Summary of Agency Reports to the ISC	66
7.3	Arrival Observations	71
7.4	Hypocentres Collected	78
7.5	Collection of Network Magnitude Data	80
7.6	Moment Tensor Solutions	86
7.7	Timing of Data Collection	89
8	Overview of the ISC Bulletin	91
8.1	Events	91
8.2	Seismic Phases and Travel-Time Residuals	100
8.3	Seismic Wave Amplitudes and Periods	106
8.4	Completeness of the ISC Bulletin	108
8.5	Magnitude Comparisons	109
9	The Leading Data Contributors	114
9.1	The Largest Data Contributors	114
9.2	Contributors Reporting the Most Valuable Parameters	116
9.3	The Most Consistent and Punctual Contributors	120
10	Appendix	122
11	Glossary of ISC Terminology	141
12	Acknowledgements	145
	References	146

1

Preface

Dear Colleague,

This is the second and concluding 2013 issue of the Summary of the ISC Bulletin that remains the most fundamental reason for continued operations at the ISC. This issue covers seismic events that occurred during the period from July to December 2013.

This publication contains a description of the ISC data available on the attached DVD-ROM and from the ISC website. It contains information on the ISC, its Members, Sponsors and Data Providers. It offers analysis of the data contributed to the ISC by many seismological agencies worldwide as well as analysis of the data in the ISC Bulletin itself. This somewhat smaller issue misses some of the standard information on routine procedures usually published in the first issue of each year.

We continue publishing invited articles describing notable seismic events during the year - the M_W 6.8 earthquake in Kamchatka and the largest deep focus M_W 8.3 earthquake in the Sea of Okhotsk.

We hope that you find this relatively new publication useful in your work. If your home-institution or company is unable, for one reason or another, to support the long-term international operations of the ISC in full by becoming a Member, then, please, consider subscribing to this publication by contacting us at admin@isc.ac.uk.

With kind regards to our Data Contributors, Members, Sponsors and users,

Dr Dmitry A. Storchak

Director

International Seismological Centre (ISC)

2

The International Seismological Centre

2.1 The ISC Mandate

The International Seismological Centre (ISC) was set up in 1964 with the assistance of UNESCO as a successor to the International Seismological Summary (ISS) to carry forward the pioneering work of Prof. John Milne, Sir Harold Jeffreys and other British scientists in collecting, archiving and processing seismic station and network bulletins and preparing and distributing the definitive summary of world seismicity.

Under the umbrella of the International Association of Seismology and Physics of the Earth Interior (IASPEI/IUGG), the ISC has played an important role in setting international standards such as the International Seismic Bulletin Format (ISF), the IASPEI Standard Seismic Phase List (SSPL) and both the old and New IASPEI Manual of the Seismological Observatory Practice (NMSOP-2) (www.iaspei.org/projects/NMSOP.html).

The ISC has contributed to scientific research and prominent scientists such as John Hodgson, Eugene Herrin, Hal Thirlaway, Jack Oliver, Anton Hales, Ola Dahlman, Shigeji Suehiro, Nadia Kondorskaya, Vit Karnik, Stephan Müller, David Denham, Bob Engdahl, Adam Dziewonski, John Woodhouse and Guy Masters all considered it an important duty to serve on the ISC Executive Committee and the Governing Council.

The current mission of the ISC is to maintain:

- the ISC **Bulletin** – the longest continuous definitive summary of World seismicity (collaborating with 130 seismic networks and data centres around the world). (www.isc.ac.uk/iscbulletin/)
- the International Seismographic Station Registry (**IR**, jointly with the World Data Center for Seismology, Denver). (www.isc.ac.uk/registries/)
- the IASPEI Reference Event List (Ground Truth, **GT**, jointly with IASPEI). (www.isc.ac.uk/gtevents/)

These are fundamentally important tasks. Bulletin data produced, archived and distributed by the ISC for almost 50 years are the definitive source of such information and are used by thousands of seismologists worldwide for seismic hazard estimation, for tectonic studies and for regional and global imaging of the Earth's structure. Key information in global tomographic imaging is derived from the analysis of ISC data. The ISC Bulletin served as a major source of data for such well known products as the ak135 global 1-D velocity model and the EHB (*Engdahl et al.*, 1998) and Centennial (*Engdahl and Villaseñor*, 2002) catalogues. It presents an important quality-control benchmark for the Comprehensive Nuclear-Test-Ban Treaty Organization (CTBTO). Hypocentre parameters from the ISC Bulletin are used

by the Data Management Center of the Incorporated Research Institutions for Seismology (IRIS DMC) to serve event-oriented user-requests for waveform data. The ISC-GEM Bulletin is a cornerstone of the ISC-GEM Global Instrumental Reference Earthquake Catalogue for Global Earthquake risk Model (GEM).

The ISC Bulletin contains over 6 million seismic events: earthquakes, chemical and nuclear explosions, mine blasts and mining induced events. At least 1.7 million of them are regional and teleseismically recorded events that have been reviewed by the ISC analysts. The ISC Bulletin contains approximately 200 million individual seismic station readings of arrival times, amplitudes, periods, SNR, slowness and azimuth, reported by approximately 17,000 seismic stations currently registered in the IR. Over 6,000 stations have contributed to the ISC Bulletin in recent years. This number includes the numerous sites of the USArray. The IASPEI GT List currently contains 8969 events for which latitude, longitude and depth of origin are known with high confidence (to 5 km or better) and seismic signals were recorded at regional and/or teleseismic distances.

2.2 Brief History of the ISC



Figure 2.1: *The steel globe bearing positions of early seismic stations was used for locating positions of earthquakes for the International Seismological Summaries.*

(BCIS).

Following Milne's death in 1913, Seismological Bulletins of the BAAS were continued under Prof. H.H. Turner, later based at Oxford University. Upon formal post-war dissolution of the International Association of Seismology in 1922 the newly founded Seismological Section of the International Union of Geodesy and Geophysics (IUGG) set up the International Seismological Summary (ISS) to continue at Oxford under Turner, to produce the definitive global catalogues from the 1918 data-year onwards, under the auspices of IUGG and with the support of the BAAS.

ISS production, led by several professors at Oxford University, and Sir Harold Jeffreys at Cambridge

University, continued until it was superseded by the ISC Bulletin, after the ISC was formed in Edinburgh in 1964 with Dr P.L. Willmore as its first director.

During the period 1964 to 1970, with the help of UNESCO and other international scientific bodies, the ISC was reconstituted as an international non-governmental body, funded by interested institutions from various countries. Initially there were supporting members from seven countries, now there are almost 60, and member institutions include national academies, research foundations, government departments and research institutes, national observatories and universities. Each member, contributing a minimum unit of subscription or more, appoints a representative to the ISC's Governing Council, which meets every two years to decide the ISC's policy and operational programme. Representatives from the International Association of Seismology and Physics of the Earth's Interior also attend these meetings. The Governing Council appoints the Director and a small Executive Committee to oversee the ISC's operations.



Figure 2.2: ISC building in Thatcham, Berkshire, UK.

In 1975, the ISC moved to Newbury in southern England to make use of better computing facilities there. The ISC subsequently acquired its own computer and in 1986 moved to its own building at Pipers Lane, Thatcham, near Newbury. The internal layout of the new premises was designed for the ISC and includes not only office space but provision for the storage of extensive stocks of ISS and ISC publications and a library of seismological observatory bulletins, journals and books collected over many tens of years.

In 1997 the first set of the ISC Bulletin CD-ROMs was produced (not counting an earlier effort at USGS). The first ISC website appeared in 1998 and the first ISC database was put in day-to-day operations from 2001.

Throughout 2009-2011 a major internal reconstruction of the ISC building was undertaken to allow for more members of staff working in mainstream ISC operations as well as major development projects such as the CTBTO Link, ISC-GEM Catalogue and the ISC Bulletin Rebuild.

2.3 Former Directors of the ISC and its U.K. Predecessors



John Milne
Publisher of the *Slide Circular Reports on Earthquakes*
1899-1913



Herbert Hall Turner
Seismological Bulletins of the BAAS
1913-1922
Director of the ISS
1922-1930



Harry Hemley Plaskett
Director of the ISS
1931-1946



Harold Jeffreys
Director of the ISS
1946-1957



Robert Stoneley
Director of the ISS
1957-1963



P.L. (Pat) Willmore
Director of the ISS
1963-1970
Director of the ISC
1964-1970



Edouard P. Arnold
Director of the ISC
1970-1977



Anthony A. Hughes
Director of the ISC
1977-1997



Raymond J. Willemann
Director of the ISC
1998-2003



Avi Shapira
Director of the ISC
2004-2007

2.4 Member Institutions of the ISC

Article IV(a-b) of the ISC Working Statutes stipulates that any national academy, agency, scientific institution or other non-profit organisation may become a Member of the ISC on payment to the ISC of a sum equal to at least one unit of subscription and the nomination of a voting representative to serve on the ISC's governing body. Membership shall be effective for one year from the date of receipt at the ISC of the annual contribution of the Member and is thereafter renewable for periods of one year.

The ISC is currently supported with funding from its 62 Member Institutions and a four-year Grant Award EAR-1417970 from the US National Science Foundation.

Figures 2.3 and 2.4 show major sectors to which the ISC Member Institutions belong and proportional

financial contributions that each of these sectors make towards the ISC’s annual budget.

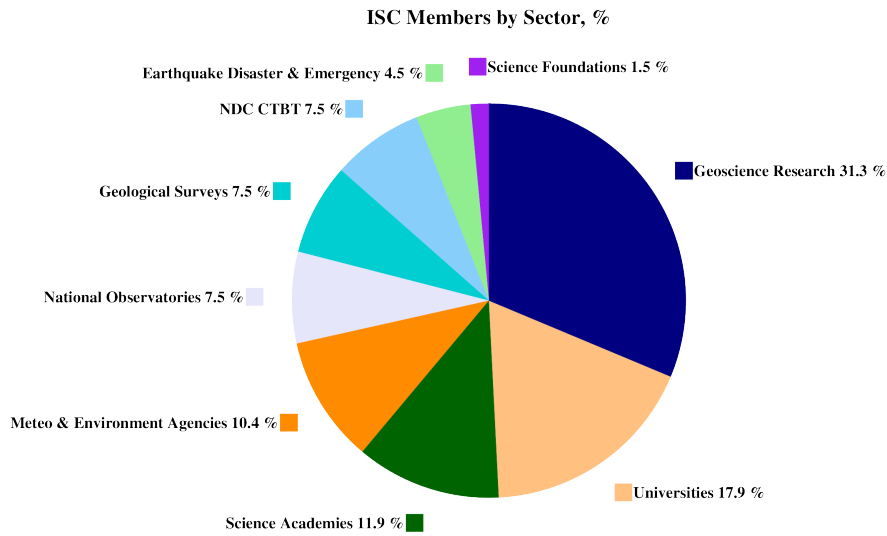


Figure 2.3: Distribution of the ISC Member Institutions by sector in year 2013 as a percentage of total number of Members.

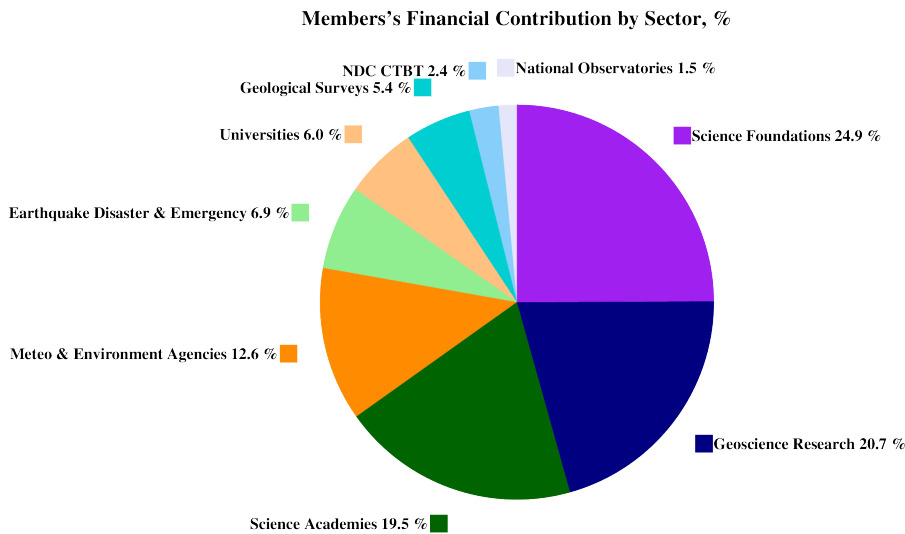


Figure 2.4: Distribution of Member’s financial contributions to the ISC by sector in year 2013 as a percentage of total annual Member contributions.

There follows a list of all current Member Institutions with a category (1 through 9) assigned according to the ISC Working Statutes. Each category relates to the number of membership units contributed.



Centre de Recherche en Astronomie, Astrophysique et Géophysique (CRAAG)
 Algeria
www.craag.dz
 Category: 1



Instituto Nacional de Prevención Sísmica (INPRES)
 Argentina
www.inpres.gov.ar
 Category: 1



Seismology Research Centre
Australia
www.seis.com.au
Category: 1



The University of Melbourne
Australia
www.unimelb.edu.au
Category: 1



Geoscience Australia
Australia
www.ga.gov.au
Category: 3



Bundesministerium für Wis-
senschaft, Forschung und
Wirtschaft (BMWFW)
Austria
www.bmbwk.gv.at
Category: 2



Centre of Geophysical Moni-
toring (CGM) of the National
Academy of Sciences of Belarus
Belarus
www.cgm.org.by
Category: 1



Belgian Science Policy Office
(BELSPO)
Belgium

Category: 1



Seismological Observatory, Insti-
tute of Geosciences, University of
Brasilia
Brazil
www.obsis.unb.br
Category: 1



Universidade de São Paulo, Cen-
tro de Sismologia
Brazil
www.sismo.iag.usp.br
Category: 1



The Geological Survey of Canada
Canada
gsc.nrcan.gc.ca
Category: 4



Department of Geophysics, Uni-
versity of Chile
Chile
ingenieria.uchile.cl
Category: 1



China Earthquake Administra-
tion
China
www.gov.cn
Category: 5



Institute of Earth Sciences,
Academia Sinica
Chinese Taipei
www.earth.sinica.edu.tw
Category: 1



Geological Survey Department
Cyprus
www.moa.gov.cy
Category: 1



Academy of Sciences of the Czech
Republic
Czech Republic
www.cas.cz
Category: 2



Geological Survey of Denmark
and Greenland - GEUS
Denmark
www.geus.dk
Category: 2

Korea Earthquake Administra-
tion
DPR Korea

Category: 1



National Research Institute
for Astronomy and Geophysics
(NRIAG), Cairo
Egypt
www.nriag.sci.eg
Category: 1



The University of Helsinki
Finland
www.helsinki.fi
Category: 2



Institute National des Sciences de
l'Univers
France
www.insu.cnrs.fr
Category: 4



Laboratoire de Détection et de
Géophysique/CEA
France
www-dase.cea.fr
Category: 2



GeoForschungsZentrum Potsdam
Germany
www.gfz-potsdam.de
Category: 2



Bundesanstalt für Geowis-
senschaften und Rohstoffe
Germany
www.bgr.bund.de
Category: 4



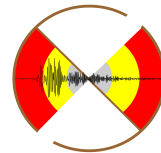
The Seismological Institute, Na-
tional Observatory of Athens
Greece
www.noa.gr
Category: 1



The Hungarian Academy of Sci-
ences
Hungary
www.mta.hu
Category: 1



The Icelandic Meteorological Of-
fice
Iceland
www.vedur.is
Category: 1



National Centre for Seismology of
the Ministry of Earth Sciences of
India
India
www.moes.gov.in
Category: 4



Iraqi Seismic Network
Iraq
www.imos-tm.com
Category: 1



Soreq Nuclear Research Centre
(SNRC)
Israel
www.soreq.gov.il
Category: 1



The Geophysical Institute of Is-
rael
Israel
www.gii.co.il
Category: 1



Istituto Nazionale di Geofisica e
Vulcanologia
Italy
www.ingv.it
Category: 3



Istituto Nazionale di
Oceanografia e di Geofisica
Sperimentale
Italy
www.ogs.trieste.it
Category: 1



University of the West Indies
Jamaica
www.mona.uwi.edu
Category: 1



Japan Agency for Marine-Earth
Science and Technology (JAM-
STEC)
Japan
www.jamstec.go.jp
Category: 3



National Institute of Polar Re-
search (NIPR)
Japan
www.nipr.ac.jp
Category: 1



The Japan Meteorological
Agency (JMA)
Japan
www.jma.go.jp
Category: 5



Earthquake Research Institute,
University of Tokyo
Japan
www.eri.u-tokyo.ac.jp
Category: 3



Natural Resources Authority,
Amman
Jordan
www.nra.gov.jo
Category: 1



Institute of Geophysics, National
University of Mexico
Mexico
www.igeofcu.unam.mx
Category: 1



The Royal Netherlands Meteoro-
logical Institute
Netherlands
www.knmi.nl
Category: 2



Institute of Geological and Nu-
clear Sciences
New Zealand
www.gns.cri.nz
Category: 3



The University of Bergen
Norway
www.uib.no
Category: 2



Stiftelsen NOR SAR
Norway
www.norsar.no
Category: 2



Institute of Geophysics, Polish
Academy of Sciences
Poland
www.igf.edu.pl
Category: 1



Instituto Português do Mar e da
Atmosfera
Portugal
www.ipma.pt
Category: 2



Red Sísmica de Puerto Rico
Puerto Rico
redsismica.uprm.edu
Category: 1



Korean Meteorological Adminis-
tration
Republic of Korea
www.kma.go.kr
Category: 1



National Institute for Earth
Physics
Romania
www.infp.ro
Category: 1



Russian Academy of Sciences
Russia
www.ras.ru
Category: 5



Earth Observatory of Singapore
(EOS), an autonomous Institute
of Nanyang Technological Uni-
versity
Singapore
www.earthobservatory.sg
Category: 1



Environmental Agency of Slove-
nia
Slovenia
www.arso.gov.si
Category: 1



Council for Geoscience
South Africa
www.geoscience.org.za
Category: 1



Institut Cartogràfic i Geològic de
Catalunya (ICGC)
Spain
www.igc.cat
Category: 1



Uppsala Universitet
Sweden
www.uu.se
Category: 2



National Defence Research Es-
tablishment
Sweden
www.foi.se
Category: 1



The Swiss Academy of Sciences
Switzerland
www.scnat.ch
Category: 2



University of the West Indies
Trinidad and Tobago
sta.uwi.edu
Category: 1



AFAD Disaster and Emergency
Management Authority
Turkey
www.deprem.gov.tr
Category: 2



Kandilli Observatory and Earth-
quake Research Institute
Turkey
www.koeri.boun.edu.tr
Category: 1



AWE Blacknest
United Kingdom
www.blacknest.gov.uk
Category: 1



British Geological Survey
United Kingdom
www.bgs.ac.uk
Category: 2



The Royal Society of London
United Kingdom
www.royalsociety.org
Category: 6



Incorporated Research Institu-
tions for Seismology
U.S.A.
www.iris.edu
Category: 1



University of Texas at Austin
U.S.A.
www.utexas.edu
Category: 1



National Earthquake Informa-
tion Center, U.S. Geological Sur-
vey
U.S.A.
www.neic.usgs.gov
Category: 2



The National Science Foundation
of the United States. (Grant No.
EAR-1417970)
U.S.A.
www.nsf.gov
Category: 9

In addition the ISC is currently in receipt of grants from the International Data Centre (IDC) of the Preparatory Commission of the Comprehensive Nuclear-Test-Ban Treaty Organization (CTBTO), FM Global, Lighthill risk Network, OYO, USGS (Award G15AC00202), Innovate UK (Grant KTP009092) and Aspen Re.



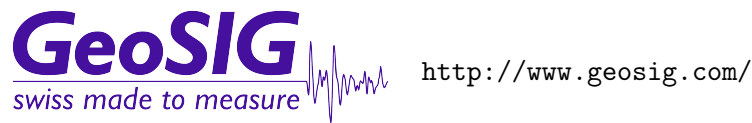
2.5 Sponsoring Organisations

Article IV(c) of the ISC Working Statutes stipulates any commercial organisation with an interest in the objectives and/or output of the ISC may become an Associate Member of the ISC on payment of an Associate membership fee, but without entitlement to representation with a vote on the ISC's governing body.



REF TEK designs and manufactures application specific, high-performance, battery-operated, field-portable geophysical data acquisition devices for the global market. With over 35 years of experience, REF TEK provides customers with complete turnkey solutions that include high resolution recorders, broadband sensors, state-of-the-art communications (V-SAT, GPRS, etc), installation, training, and continued customer support. Over 7,000 REF TEK instruments are currently being used globally for multiple applications. From portable earthquake monitoring to telemetry earthquake monitoring, earth-

quake aftershock recording to structural monitoring and more, REF TEK equipment is suitable for a wide variety of application needs.



GeoSIG provides earthquake, seismic, structural, dynamic and static monitoring and measuring solutions. As an ISO Certified company, GeoSIG is a world leader in design and manufacture of a diverse range of high quality, precision instruments for vibration and earthquake monitoring. GeoSIG instruments are at work today in more than 100 countries around the world with well-known projects such as the NetQuakes installation with USGS and Oresund Bridge in Denmark. GeoSIG offers off-the-shelf solutions as well as highly customised solutions to fulfil the challenging requirements in many vertical markets including the following:

- Earthquake Early Warning and Rapid Response (EEWRR)
- Seismic and Earthquake Monitoring and Measuring
- Industrial Facility Seismic Monitoring and Shutdown
- Structural Analysis and Ambient Vibration Testing
- Induced Vibration Monitoring
- Research and Scientific Applications

2.6 Data Contributing Agencies

In addition to its Members and Sponsors, the ISC owes its existence and successful long-term operations to its 145 seismic bulletin data contributors. These include government agencies responsible for national seismic networks, geoscience research institutions, geological surveys, meteorological agencies, universities, national data centres for monitoring the CTBT and individual observatories. There would be no ISC Bulletin available without the regular stream of data that are unselfishly and generously contributed to the ISC on a free basis.



The Institute of Seismology,
Academy of Sciences of Albania
Albania
TIR



Centre de Recherche en As-
tronomie, Astrophysique et Géo-
physique
Algeria
CRAAG



Universidad Nacional de La Plata
Argentina
LPA



Instituto Nacional de Prevención
Sísmica
Argentina
SJA



National Survey of Seismic Protection
Armenia
NSSP



Geoscience Australia
Australia
AUST



International Data Centre,
CTBTO
Austria
IDC



Zentralanstalt für Meteorologie
und Geodynamik (ZAMG)
Austria
VIE



Republic Center of Seismic Survey
Azerbaijan
AZER



Centre of Geophysical Monitoring
Belarus
BELR



Royal Observatory of Belgium
Belgium
UCC



Observatorio San Calixto
Bolivia
SCB



Republic Hydrometeorological
Service, Seismological Observa-
tory, Banja Luka
Bosnia-Herzegovina
RHSSO



Instituto Astronomico e Ge-
ofisico
Brazil
VAO



Geophysical Institute, Bulgarian
Academy of Sciences
Bulgaria
SOF



Canadian Hazards Information
Service, Natural Resources
Canada
Canada
OTT



Centro Sismológico Nacional,
Universidad de Chile
Chile
GUC



China Earthquake Networks
Center
China
BJI



Institute of Earth Sciences,
Academia Sinica
Chinese Taipei
ASIES



Red Sismológica Nacional de
Colombia
Colombia
RSNC



Sección de Sismología, Vul-
canología y Exploración Ge-
ofisica
Costa Rica
UCR



Seismological Survey of the Re-
public of Croatia
Croatia
ZAG



Servicio Sismológico Nacional
Cubano
Cuba
SSNC



Cyprus Geological Survey De-
partment
Cyprus
NIC



West Bohemia Seismic Network
Czech Republic
WBNET



The Institute of Physics of the
Earth (IPEC)
Czech Republic
IPEC



Geophysical Institute, Academy
of Sciences of the Czech Republic
Czech Republic
PRU



Geological Survey of Denmark
and Greenland
Denmark
DNK



Observatoire Géophysique
d'Arta
Djibouti
ARO

Observatorio Sismologico Po-
litecnico Loyola
Dominican Republic
OSPL



Servicio Nacional de Sismología y
Vulcanología
Ecuador
IGQ



National Research Institute of
Astronomy and Geophysics
Egypt
HLW



Servicio Nacional de Estudios
Territoriales
El Salvador
SNET



University of Addis Ababa
Ethiopia
AAE



Institute of Seismology, Univer-
sity of Helsinki
Finland
HEL



Institut de Physique du Globe
France
STR



Laboratoire de Détection et de
Géophysique/CEA
France
LDG

Laboratoire de Géo-
physique/CEA
French Polynesia
PPT



Seismological Observatory
Skopje
FYR Macedonia
SKO



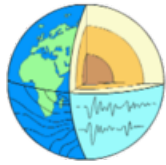
Seismic Monitoring Centre of
Georgia
Georgia
TIF



Alfred Wegener Institute for Po-
lar and Marine Research
Germany
AWI



Seismological Observa-
tory Berggießhübel, TU
Bergakademie Freiberg
Germany
BRG



Geophysikalisches Observatorium Collm
Germany
CLL



Bundesanstalt für Geowissenschaften und Rohstoffe
Germany
BGR



Department of Geophysics, Aristotle University of Thessaloniki
Greece
THE



National Observatory of Athens
Greece
ATH



INSIVUMEH
Guatemala
GCG



Hong Kong Observatory
Hong Kong
HKC



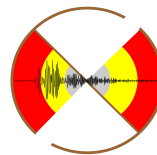
Geodetic and Geophysical Research Institute
Hungary
BUD



Icelandic Meteorological Office
Iceland
REY



National Geophysical Research Institute
India
HYB



National Centre for Seismology of the Ministry of Earth Sciences of India
India
NDI



Badan Meteorologi, Klimatologi dan Geofisika
Indonesia
DJA



Tehran University
Iran
TEH



International Institute of Earthquake Engineering and Seismology (IIEES)
Iran
THR



Iraqi Meteorological and Seismology Organisation
Iraq
ISN



The Geophysical Institute of Israel
Israel
GII



Dipartimento per lo Studio del Territorio e delle sue Risorse (RSNI)
Italy
GEN



Laboratory of Research on Experimental and Computational Seimology
Italy
RISSC



MedNet Regional Centroid - Moment Tensors
Italy
MED_RCMT



Istituto Nazionale di
Oceanografia e di Geofisica
Sperimentale (OGS)
Italy
TRI



Istituto Nazionale di Geofisica e
Vulcanologia
Italy
ROM

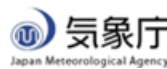


Osservatorio Sismologico Univer-
sità di Bari
Italy
OSUB

Station Géophysique de Lamto
Ivory Coast
LIC



Jamaica Seismic Network
Jamaica
JSN



Japan Meteorological Agency
Japan
JMA



The Matsushiro Seismological
Observatory
Japan
MAT



National Institute of Polar Re-
search
Japan
SYO



National Research Institute for
Earth Science and Disaster Pre-
vention
Japan
NIED



Jordan Seismological Observa-
tory
Jordan
JSO



Seismological Experimental
Methodological Expedition
Kazakhstan
SOME



National Nuclear Center
Kazakhstan
NNC



Institute of Seismology, Academy
of Sciences of Kyrgyz Republic
Kyrgyzstan
KRNET

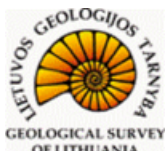
Kyrgyz Seismic Network
Kyrgyzstan
KNET



Latvian Seismic Network
Latvia
LVSN



National Council for Scientific
Research
Lebanon
GRAL



Geological Survey of Lithuania
Lithuania
LIT



Macao Meteorological and Geo-
physical Bureau
Macao, China
MCO



Geological Survey Department
Malawi
Malawi
GSDM

Malaysian Meteorological Service
Malaysia
KLM



Instituto de Geofísica de la
UNAM
Mexico
MEX



Red Sismica del Noroeste de
Mexico (RESOM)
Mexico
ECX



Institute of Geophysics and Ge-
ology
Moldova
MOLD



Seismological Institute of Mon-
tenegro
Montenegro
PDG



Centre National de Recherche
Morocco
CNRM



The Geological Survey of
Namibia
Namibia
NAM



National Seismological Centre,
Nepal
Nepal
DMN



Koninklijk Nederlands Meteorol-
ogisch Instituut
Netherlands
DBN



Institute of Geological and Nu-
clear Sciences
New Zealand
WEL



University of Bergen
Norway
BER



Stiftelsen NOR SAR
Norway
NAO



Sultan Qaboos University
Oman
OMAN



Micro Seismic Studies Pro-
gramme, PNSTECH
Pakistan
MSSP



Universidad de Panama
Panama
UPA



Manila Observatory
Philippines
QCP



Philippine Institute of Volcanology and Seismology
Philippines
MAN



Institute of Geophysics, Polish
Academy of Sciences
Poland
WAR



Instituto Geofísico do Infante
Dom Luiz
Portugal
IGIL



Instituto Português do Mar e da
Atmosfera, I.P.
Portugal
INMG

Sistema de Vigilância Sismológica dos Açores
Portugal
SVSA



Korea Meteorological Administration
Republic of Korea
KMA



National Institute for Earth
Physics
Romania
BUC



Institute of Environmental Problems of the North,
Russian Academy of Sciences
Russia
IEPN

Sakhalin Experimental and
Methodological Seismological
Expedition, GS RAS
Russia
SKHL



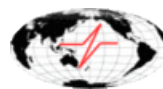
Altai-Sayan Seismological Centre, GS SB RAS
Russia
ASRS



Yakutiya Regional Seismological
Center, GS SB RAS
Russia
YARS



Kamchatkan Experimental and
Methodical Seismological Department, GS RAS
Russia
KRSC



Geophysical Survey of Russian
Academy of Sciences
Russia
MOS



Baykal Regional Seismological
Centre, GS SB RAS
Russia
BYKL



North Eastern Regional Seismological
Centre, GS RAS
Russia
NERS



Kola Regional Seismic Centre,
GS RAS
Russia
KOLA



Mining Institute of the Ural
Branch of the Russian Academy
of Sciences
Russia
MIRAS



Saudi Geological Survey
Saudi Arabia
SGS



Seismological Survey of Serbia
Serbia
BEO



Geophysical Institute, Slovak
Academy of Sciences
Slovakia
BRA



Environmental Agency of the Re-
public of Slovenia
Slovenia
LJU



Ministry of Mines, Energy and
Rural Electrification
Solomon Islands
HNR



Council for Geoscience
South Africa
PRE



Instituto Andaluz de Geofísica
Spain
IAG

Real Instituto y Observatorio de
la Armada
Spain
SFS



Institut Cartogràfic i Geològic de
Catalunya
Spain
MRB



Instituto Geográfico Nacional
Spain
MDD



University of Uppsala
Sweden
UPP



Swiss Seismological Service
(SED)
Switzerland
ZUR



National Syrian Seismological
Center
Syria
NSSC



Thai Meteorological Department
Thailand
BKK



The University of the West Indies
Trinidad and Tobago
TRN



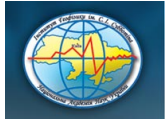
Institut National de la
Météorologie
Tunisia
TUN



Kandilli Observatory and Re-
search Institute
Turkey
ISK



Disaster and Emergency Man-
agement Presidency
Turkey
DDA



Subbotin Institute of Geophysics,
National Academy of Sciences
Ukraine
SIGU



Dubai Seismic Network
United Arab Emirates
DSN



British Geological Survey
United Kingdom
BGS

Department of Geosciences
U.S.A.
UAF



The Global CMT Project
U.S.A.
GCMT



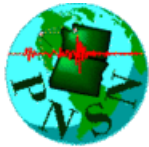
National Earthquake Informa-
tion Center
U.S.A.
NEIC



IRIS Data Management Center
U.S.A.
IRIS



Red Sísmica de Puerto Rico
U.S.A.
RSPR



Pacific Northwest Seismic Net-
work
U.S.A.
PNSN



National Center for Scientific Re-
search
Vietnam
PLV

Geological Survey Department of
Zambia
Zambia
LSZ



Goetz Observatory
Zimbabwe
BUL

Seismic Institute of Kosovo
SIK

East African Network
EAF



CWB
Chinese Taipei
TAP

2.7 ISC Staff

Listed below are the staff (and their country of origin) who were employed at the ISC at the time of this ISC Bulletin Summary.

- Dmitry Storckh
- Director
- Russia/United Kingdom



- Maureen Aspinwall
- Administration Officer
- United Kingdom



- Lynn Elms
- Administration Officer
- United Kingdom



- James Harris
- Senior System and Database Administrator
- United Kingdom



- Przemek Ozgo
- System Administrator
- Poland



- John Eve
- Data Collection Officer
- United Kingdom



- Edith Korger
- Data Collection Seismologist
- Austria



- Domenico Di Giacomo
- Seismologist
- Italy



- Konstantinos Lentas
- Seismologist/Developer
- Greece



- Rosemary Hulin (née Wylie)
- Analyst/Administrator
- United Kingdom



- Blessing Shumba
- Seismologist/Analyst
- Zimbabwe



- Rebecca Verney
- Analyst
- United Kingdom



- Jennifer Weston
- Seismologist/Analyst
- United Kingdom



- Elizabeth Entwistle
- Seismologist/Analyst
- United Kingdom



- Elizabeth Ayres (née Ball)
- Analyst/Historical Data Entry Officer
- United Kingdom



- Kathrin Lieser
- Seismologist/Analyst
- Germany



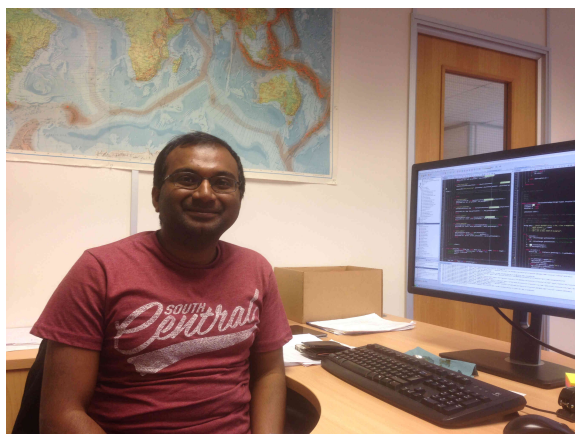
- Lonn Brown
- Seismologist/Analyst
- Canada



- Daniela Olaru
- Historical Data Entry Officer
- Romania



- Saiful Khan
- VBAS Developer
- India



3

Availability of the ISC Bulletin

The ISC Bulletin is available from the following sources:

- Web searches

The entire ISC Bulletin is available directly from the ISC website via tailored searches.

(www.isc.ac.uk/iscbulletin/search)

(isc-mirror.iris.washington.edu/iscbulletin/search)

- Bulletin search - provides the most verbose output of the ISC Bulletin in ISF or QuakeML.
- Event catalogue - only outputs the prime hypocentre for each event, producing a simple list of events, locations and magnitudes.
- Arrivals - search for arrivals in the ISC Bulletin. Users can search for specific phases for selected stations and events.

- CD-ROMs/DVD-ROMs

CDs/DVDs can be ordered from the ISC for any published volume (one per year), or for all back issues of the Bulletin (not including the latest volume). The data discs contain the Bulletin as a PDF, in IASPEI Seismic Format (ISF), and in Fixed Format Bulletin (FFB) format. An event catalogue is also included, together with the International Registry of seismic station codes.

- FTP site

The ISC Bulletin is also available to download from the ISC ftp site, which contains the Bulletin in PDF, ISF and FFB formats. (<ftp://www.isc.ac.uk>)

(<ftp://isc-mirror.iris.washington.edu>)

Mirror service

A mirror of the ISC database, website and ftp site is available at IRIS DMC (isc-mirror.iris.washington.edu), which benefits from their high-speed internet connection, providing an alternative method of accessing the ISC Bulletin.

4

Citing the International Seismological Centre

Data from the ISC should always be cited. This includes use by academic or commercial organisations, as well as individuals. A citation should show how the data were retrieved and may be in one of these suggested forms:

Data retrieved from the ISC web site:

- International Seismological Centre, On-line Bulletin, <http://www.isc.ac.uk>, Internatl. Seismol. Cent., Thatcham, United Kingdom, 2016.

Data transcribed from the IASPEI reference event bulletin:

- International Seismological Centre, Reference Event Bulletin, <http://www.isc.ac.uk>, Internatl. Seismol. Cent., Thatcham, United Kingdom, 2016.

Data transcribed from the EHB bulletin:

- International Seismological Centre, EHB Bulletin, <http://www.isc.ac.uk>, Internatl. Seismol. Cent., Thatcham, United Kingdom, 2016.

Data copied from ISC CD-ROMs/DVD-ROMs:

- International Seismological Centre, Bulletin Disks 1-24 [CD-ROM], Internatl. Seismol. Cent., Thatcham, United Kingdom, 2016.

Data transcribed from the printed Bulletin:

- International Seismological Centre, Bull. Internatl. Seismol. Cent., 46(1), Thatcham, United Kingdom, 2016.

Data transcribed from the printed Summary of the Bulletin:

- International Seismological Centre, Summ. Bull. Internatl. Seismol. Cent., 48(7-12), Thatcham, United Kingdom, 2016.

The ISC is named as a valid data centre for citations within American Geophysical Union (AGU) publications. As such, please follow the AGU guidelines when referencing ISC data in one of their journals. The ISC may be cited as both the institutional author of the Bulletin and the source from which the data were retrieved.

BibTex entry example:

```
@manual{ISCcitation2016,  
author = "International Seismological Centre",  
title = "On-line Bulletin",  
organization = "Internatl. Seismol. Cent.",  
note = "http://www.isc.ac.uk",  
address = "Thattham, United Kingdom",  
year = "2016"  
}
```

5

Summary of Seismicity, July - December 2013

In the second half of 2013 no events larger than magnitude 8 were reported. The two largest events with a magnitude of M_W 7.8 occurred at shallow depths in the Scotia Sea and Pakistan.

The largest earthquake yet along the South Scotia ridge transform occurred on 17 November 2013 (09:04:56 UTC, 60.3783°S, 46.5876°W, 7.9 km, 2216 stations (ISC)). The M_W 7.8 event is the largest of a series of earthquakes along the South Scotia ridge transform in 2013 (*USGS(a); Ye et al., 2014*) and re-ruptured a fault segment that was affected by a M_W 7.5 earthquake only ten years before on 4 August 2003 (60.5323S, 43.4511W, 7.3 km, 865 stations (ISC)). The short time between two major events affecting the same fault segment is very unusual. Usually, the rupture of the 2013 earthquake would be expected to stop at the limit of the 2003 earthquake rupture area because of a strong lowering of tectonic stresses in that area. *Vallée and Satriano (2014)* suggest that the 2013 earthquakes ruptured large zones that have been unloaded by the 2003 earthquake. *Ye et al. (2014)* believe that while the aftershock zones of the 2003 and 2013 events overlap, the peak slip patterns are largely complementary and the 2013 event did not re-rupture a previously slipped region. They infer that the fault planes are inherited underthrusting fault geometries from past convergence.

With 17 linked articles in the ISC Event Bibliography (*Di Giacomo et al., 2014; International Seismological Centre, 2016*), the M_W 7.8 Balochistan event in Pakistan is the one that raised most interest in the scientific community in this Summary time period, mainly because of its complex faulting behaviour in a tectonic setting where three tectonic plates collide (e.g. *Avouac et al. 2014; Jolivet et al., 2014; Zhou et al., 2015*). The event occurred on 24 September 2013 (11:29:48 UTC, 26.91°N, 65.53°E, 15.5 km, 2881 stations (ISC)) and ruptured about 200 km of the Hoshab fault. The Provincial Disaster Management Authority of Balochistan reported 399 people killed and 599 people injured (*PDMA Balochistan*). Although the epicentre is located about 200 km inland, the Balochistan event caused a tsunami with about 1 m height by triggering a submarine landslide which in turn triggered the tsunami (*Heidarzadeh and Satake, 2014; Hoffmann et al., 2014*). Shortly after the main shock, a new island most likely a mud volcano that got pushed up, rose from the sea floor in the Arabian Sea (*Heidarzadeh and Satake, 2014; NASA*).

The number of events in this Bulletin Summary categorised by type are given in Table 5.1.

The period between July and December 2013 produced 7 earthquakes with $M_W \geq 7$; these are listed in Table 5.2.

Figure 5.1 shows the number of moderate and large earthquakes in the second half of 2013. The distribution of the number of earthquakes should follow the Gutenberg-Richter law.

Figures 5.2 to 5.5 show the geographical distribution of moderate and large earthquakes in various magnitude ranges.

damaging earthquake	6
felt earthquake	1433
known earthquake	184797
known chemical explosion	5859
known induced event	2049
known mine explosion	886
known rockburst	15
known experimental explosion	38
suspected earthquake	7115
suspected chemical explosion	392
suspected induced event	76
suspected mine explosion	3535
suspected rockburst	893
unknown	245
total	207343

Table 5.1: Summary of events by type between July and December 2013.

Date	lat	lon	depth	M_W	Flinn-Engdahl Region
2013-11-17 09:04:56	-60.38	-46.59	7	7.8	Scotia Sea
2013-09-24 11:29:48	26.91	65.53	15	7.8	Pakistan
2013-07-15 14:03:41	-61.05	-25.23	19	7.3	South Sandwich Islands region
2013-07-07 18:35:31	-4.01	153.93	387	7.3	New Ireland region
2013-10-25 17:10:17	37.15	144.75	14	7.1	Off east coast of Honshu
2013-10-15 00:12:33	9.83	124.12	23	7.1	Mindanao
2013-09-25 16:42:43	-15.90	-74.60	38	7.0	Near coast of Peru

Table 5.2: Summary of the earthquakes of magnitude $M_W \geq 7$ between July and December 2013.

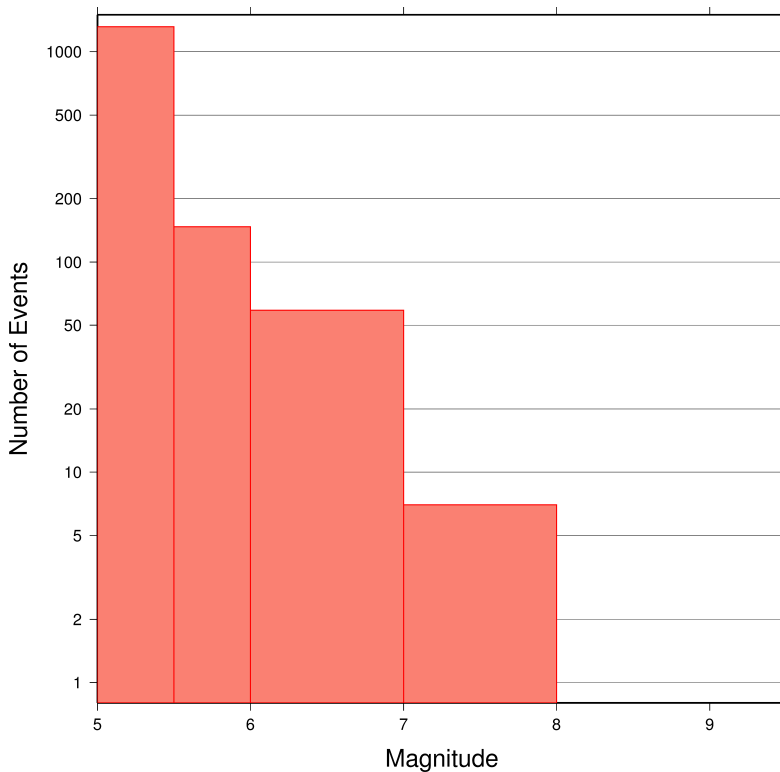


Figure 5.1: Number of moderate and large earthquakes between July and December 2013. The non-uniform magnitude bias here correspond with the magnitude intervals used in Figures 5.2 to 5.5

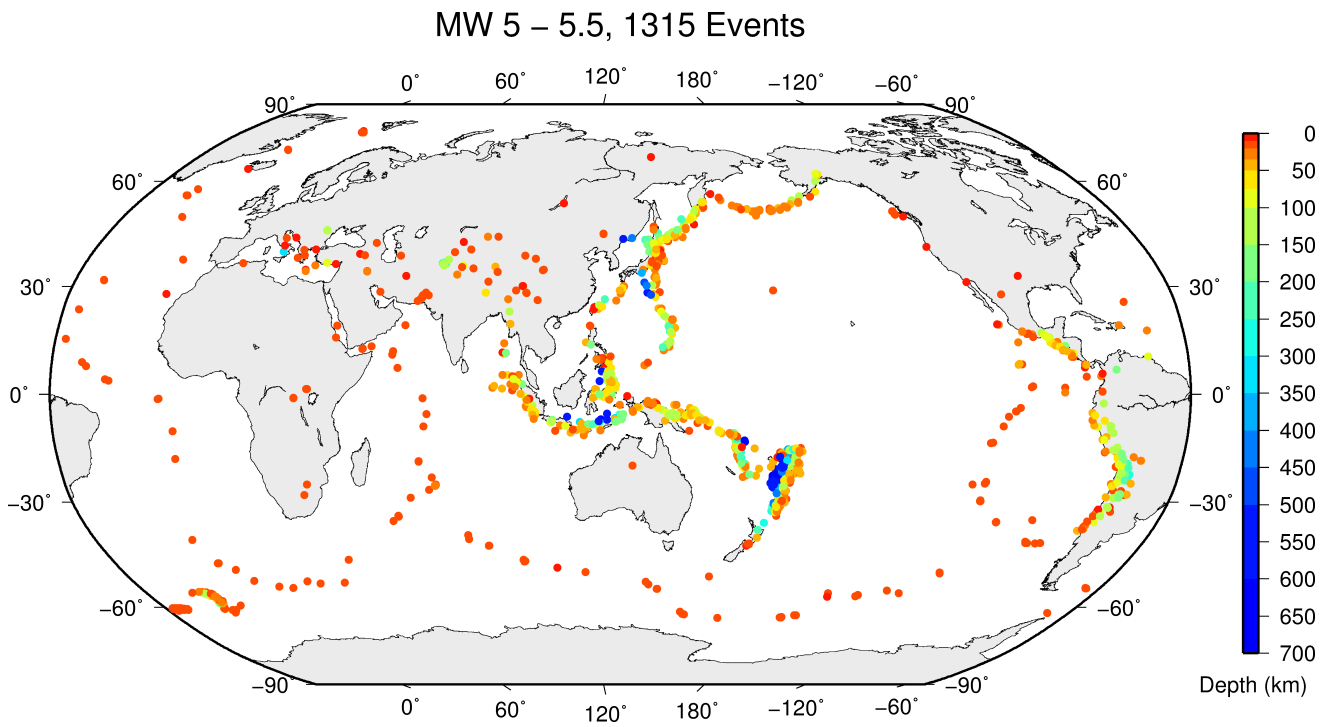


Figure 5.2: Geographic distribution of magnitude 5-5.5 earthquakes between July and December 2013.

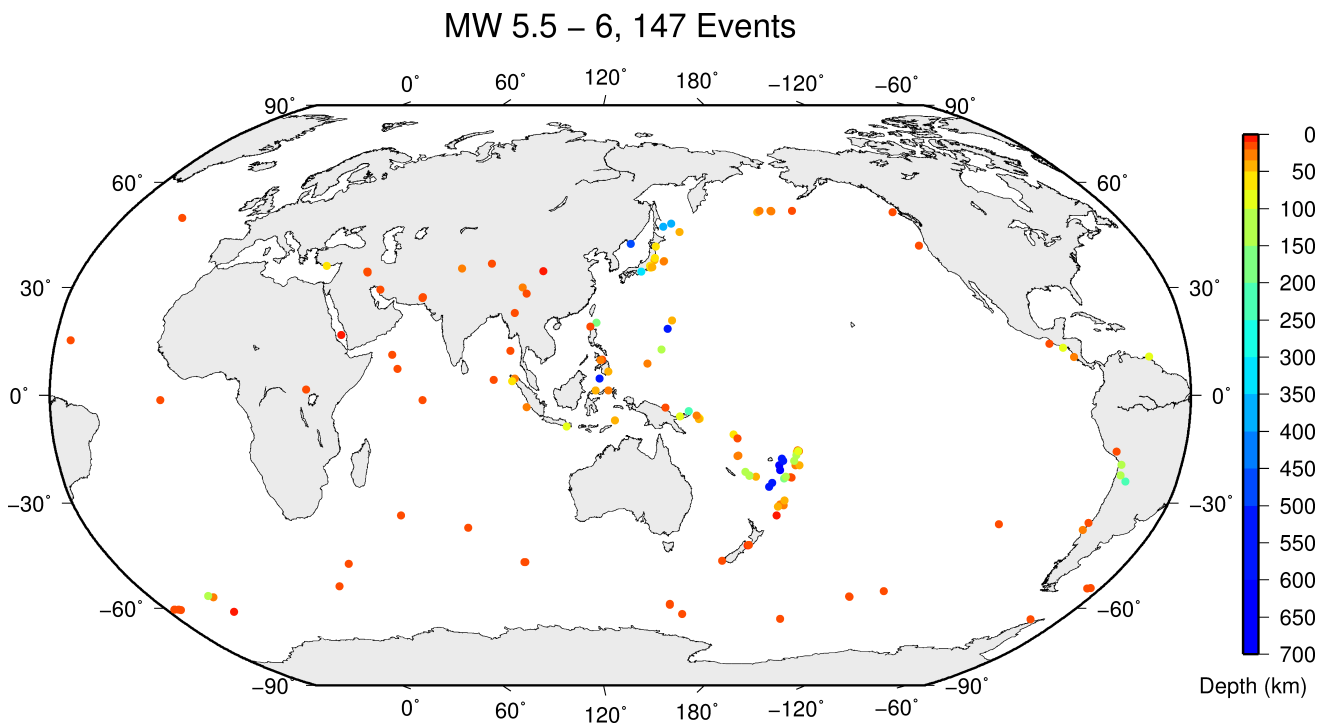


Figure 5.3: Geographic distribution of magnitude 5.5-6 earthquakes between July and December 2013.

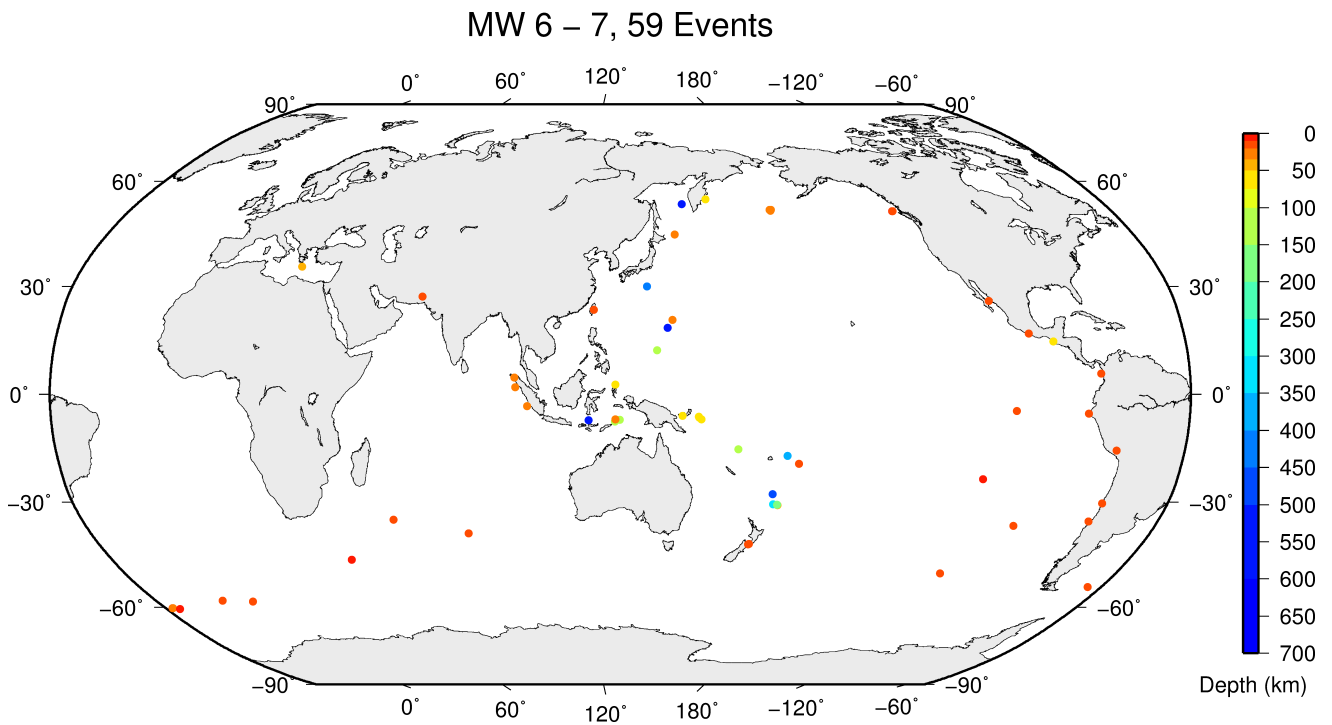


Figure 5.4: Geographic distribution of magnitude 6-7 earthquakes between July and December 2013.

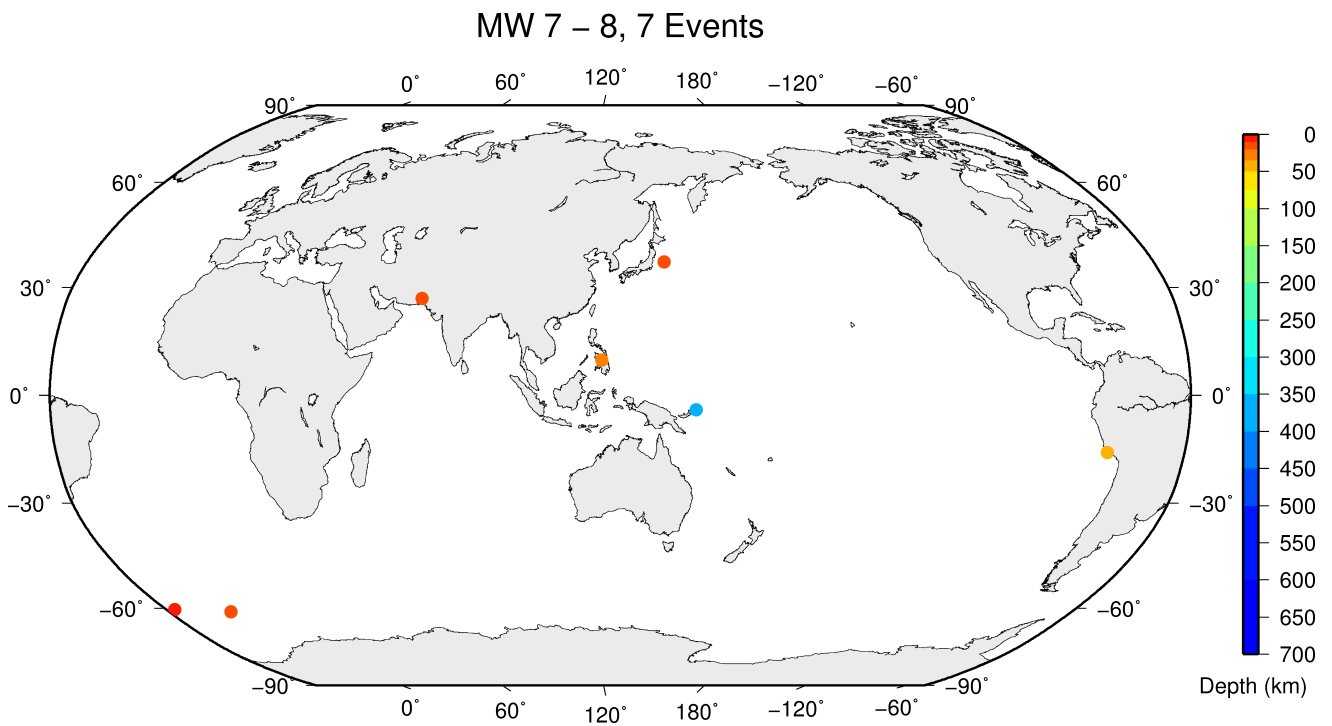


Figure 5.5: Geographic distribution of magnitude 7-8 earthquakes between July and December 2013.

References

- Avouac, J.-P., Ayoub, F., Wei, S., Ampuero, J.-P., Meng, L., et al., 2014, The 2013, M_W 7.7 Balochistan earthquake, energetic strike-slip reactivation of a thrust fault. *Earth Planet Sci. Lett.*, **391**, pp.128-134, doi: 10.1016/j.epsl.2014.01.036, <https://hal.archives-ouvertes.fr/hal-01068760>.
- Di Giacomo, D., Storchak, D.A., Safronova, N., Ozgo, P., Harris, J., Verney, R. and Bondár, I., (2014), A New ISC Service: The Bibliography of Seismic Events, *Seismol. Res. Lett.*, **85**, 2, pp. 354-360, doi: 10.1785/0220130143.
- Heidarzadeh, M. and Satake, K. (2014), Possible sources of the tsunami observed in the northwestern Indian Ocean following the 2013 September 24 M_W 7.7 Pakistan inland earthquake. *Geophysical Journal International*, **199**, 2, pp.752-766, doi: 10.1093/gji/ggu297.
- Hoffmann, G., Al-Yahyai, S., Naeem, G., Kociok, M. and Grützner, C. (2014), An Indian Ocean tsunami triggered remotely by an onshore earthquake in Balochistan, Pakistan. *Geology*, **42**, 10, pp.883-886, doi: 10.1130/G35756.1.
- International Seismological Centre, On-line Event Bibliography, http://www.isc.ac.uk/event_bibliography, Internatl. Seis. Cent., Thatcham, United Kingdom, 2016.
- Jolivet, R., Duputel, Z., Riel, B., Simons, M., Rivera, L., Minson, S.E., Zhang, H., Aivazis, M.A.G., Ayoub, F., Leprince, S. and Samsonov, S. (2014), The 2013 M_W 7.7 Balochistan earthquake: Seismic potential of an accretionary wedge, *Bulletin of the Seismological Society of America*, **104**, 2, pp.1020-1030, doi: 10.1785/0120130313.
- NASA, <http://earthobservatory.nasa.gov/IOTD/view.php?id=82146>, (visited on 7 Dec 2016)
- PDMA Balochistan (Provincial Disaster Management Authority of Balochistan), <http://www.pdma.gob.pk/?cat=42>, (visited on 7 Dec 2016).
- USGS(a), <http://earthquake.usgs.gov/earthquakes/eqarchives/poster/2013/20131117.pdf>, (visited on 7 Dec 2016)
- Vallée, M., and Satriano, C., (2014), Ten year recurrence time between two major earthquakes affecting the same fault segment, *Geophysical Research Letters* **41**, 7, pp. 2312-2318, doi: 10.1002/2014GL059465.
- Ye, L., Lay, T., Koper, K.D., Smalley, R., Rivera, L., Bevis, M.G., Zakrajsek, A.F. and Teferle, F.N., (2014), Complementary slip distributions of the August 4, 2003 M_W 7.6 and November 17, 2013 M_W 7.8 South Scotia Ridge earthquakes, *Earth and Planetary Science Letters*, **401**, pp. 215-226, doi: 10.1016/j.epsl.2014.06.007.
- Zhou, Y., Elliott, J.R., Parsons, B. and Walker, R.T. (2015), The 2013 Balochistan earthquake: An extraordinary or completely ordinary event?, *Geophysical Research Letters*, **42**, 15, pp.6236-6243, doi: 10.1002/2015GL065096.

6

Notable Events

6.1 Notable events of Kamchatka in 2013

V. N. Chebrov¹ (1949-2016), D. V. Chebrov¹, I. R. Abubakirov¹, A. Yu. Chebrova¹, A. A. Gusev^{1&2}, E. M. Guseva¹, D. V. Droznin¹, S. Ya. Droznina¹, E. M. Ivanova¹, N. M. Kravchenko¹, Yu. A. Kugaenko¹, A. V. Lander³, E. A. Matveenko¹, S. V. Mitushkina¹, D. A. Ototiuk¹, V. M. Pavlov¹, A. A. Raevskaya¹, V. A. Saltykov¹, A. A. Skorkina¹, N. N. Titkov¹



Viktor N. Chebrov (1949-2016)



Danila V. Chebrov

1. Kamchatka Branch of Geophysical Survey of Russian Academy of Sciences (RAS), Petropavlovsk-Kamchatsky
2. Institute of Volcanology and Seismology, RAS, Petropavlovsk-Kamchatsky
3. Institute of Earthquake Prediction Theory and Mathematical Geophysics of RAS, Moscow

6.2 The February 28, 2013, M_W 6.8 South Kamchatka Earthquake

6.2.1 Introduction

On February 28, 2013, at 14:05 (UTC) a magnitude M_W 6.8 earthquake occurred near the South-East Coast of Kamchatka (Figure 6.1). The source is located in the Pacific Ocean, 120 km east of Severo-Kurilsk, and 270 km south of Petropavlovsk-Kamchatsky. Hypocenter parameters of the earthquake, its

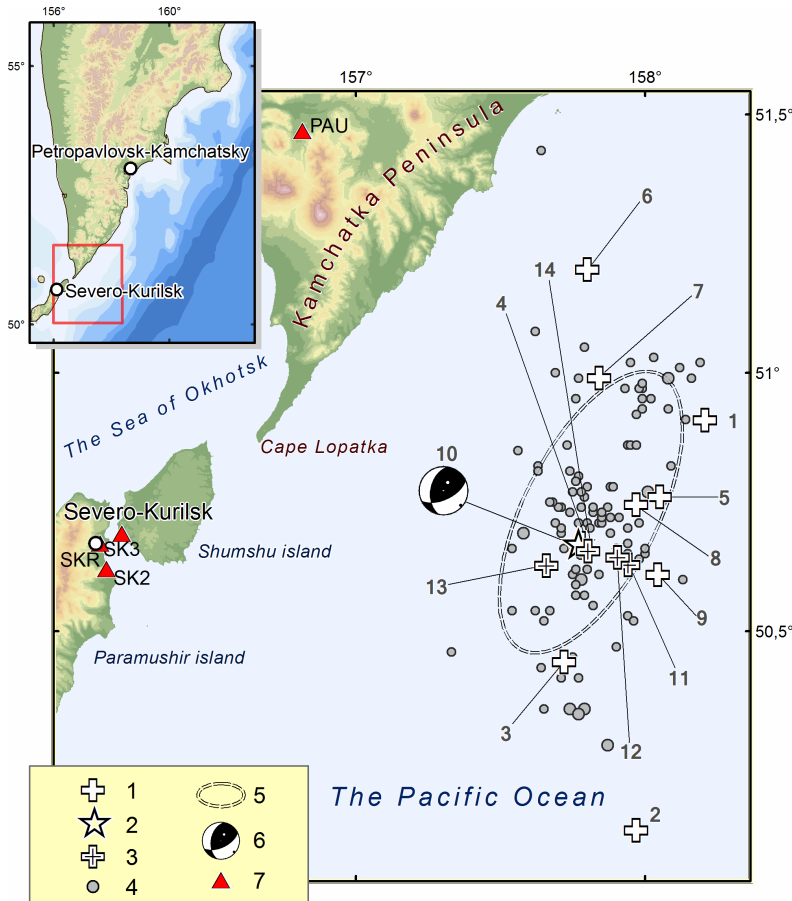


Figure 6.1: Location scheme for epicenters of the February 28, 2013 earthquake, its aftershocks with $ML > 3.5$, and strong earthquakes ($ML > 6.0$) of this region for the period from 1962 to February 28, 2013, according to the catalogue of Kamchatka and the Commander Islands earthquakes ($ML > 3.5$ corresponds to the catalogue completeness threshold for the Kamchatka regional network within area of responsibility). 1 - epicenters of strong earthquakes of this region for the period from 1962 to February 28, 2013; 2 - the epicenter of the February 28, 2013 earthquake; 3 - epicenters of strong aftershocks ($ML > 6.0$); 4 - epicenters of aftershocks with $3.5 \leq ML \leq 6.0$; 5 - 2σ -ellipse approximation of the aftershock zone; 6 - stereogram of the focal mechanism by Global CMT for the main earthquake; 7 - seismic stations. Numeration of earthquakes corresponds to Table 6.1.

strong aftershocks with $ML > 6.0$ and strong earthquakes ($ML > 6.0$) of this area from 1962 to the main event of February 28, 2013 and their magnitude estimations according to several seismological agencies of Russia and the world are given in Table 6.1. According to the Kamchatka Branch of the Geophysical Survey of Russian Academy of Sciences (GS RAS) the earthquake intensities were reported to be up to V-VI on the Medvedev-Sponheuer-Karnik scale (MSK-64) (Medvedev *et al.*, 1965) in settlements on Kamchatka peninsula.

Real-time earthquake processing by Seismological Subsystem of Tsunami Warning System (SS TWS by KB GS RAS) was performed in accordance with accepted time limits. Earthquake alerts and hypocenter parameters were released three times, in 1, 4 and 6 minutes from the first arrival at the closest seismic station. The final SS TWS solution was: 14:05:50 (UTC); 50.89°N , 157.55°E , depth $h = 61$ km, $M_S = 6.4$, $M_S(20R) = 6.6$, $ML = 6.9$. Tsunami alert was not issued. There were no tsunami waves registered by mareographs of Kamchatka Tsunami Warning Center of Roshydromet (Petropavlovsk-Kamchatsky).

The 65 strongest earthquakes final solutions have been published with a delay of no more than a day. In total, during the first 10 days there were 102 aftershocks registered with a magnitude of $ML = 2.6-6.8$. Final processing of the event sequence for the first 10 days was completed by March 10. Further events were processed in the normal mode with a delay of no more than a day.

№	Hypocenter					Energy class / Magnitudes								
	Date YYYY.MM DD.	Time hh:mm:ss	ϕ°, N	λ°, E	h, km	KB GS RAS			Global CMT	NEIC(USGS)			Obninsk	
						K^{F68}	ML	M_c	M_W	m_b	M_S	M_W	m_b	M_S
Strong earthquakes of this area for the period from 1962 to February 28, 2013														
1	1966.04.08	01:46:43.4	50.91	158.21	18	13.9	6.2	-	-	6.0	-	-	-	-
2	1966.06.21	23:06:29.2	50.12	157.97	25	13.5	6.0	-	-	5.5	-	-	$M = 5$	
3	1973.03.12	19:39:19.6	50.44	157.72	39	14.3	6.4	-	-	6.1	-	-	6.0	6.2
4	1973.04.12	13:49:14.2	50.67	157.78	20	14.2	6.4	-	-	6.1	-	-	6.1	6.4
5	1992.07.13	15:34:03.3	50.76	158.05	39	13.7	6.1	-	6.1	5.7	5.8	6.2	5.8	5.9
6	1993.06.08	13:03:37.0	51.20	157.80	40	15.0	6.8	7.3	7.5	6.4	7.3	7.1	6.5	7.4
7	1999.09.18	21:28:34.2	50.99	157.84	40	13.8	6.2	6.0	6.0	5.9	5.6	6.0	6.2	5.6
8	2006.08.24	21:50:34.1	50.75	157.97	38	14.3	6.4	6.4	6.5	5.9	6.2	6.5	6.0	6.3
9	2008.07.24	01:43:15.8	50.61	158.04	40	13.8	6.2	6.1	6.2	6.0	6.0	6.2	6.1	6.1
The February 28, 2013 earthquake and its strong aftershocks														
10	2013.02.28	14:05:48	50.672	157.773	61	15.2	6.9	6.6	6.8	6.4	6.7	6.9	6.3	6.8
11	2013.03.01	12:53:49	50.628	157.941	52	14.2	6.4	5.9	6.4	5.7	5.8	6.4	5.8	6.4
12	2013.03.01	13:20:48	50.643	157.904	62	15.1	6.8	6.5	6.5	6.3	6.3	6.5	6.2	6.6
13	2013.03.04	20:56:33	50.627	157.658	51	13.6	6.1	5.1	5.3	5.3	4.8	0	5.4	4.7
14	2013.03.09	14:56:27	50.655	157.803	49	13.7	6.1	5.6	5.8	5.7	5.3	5.8	5.7	5.5

Note: K^{F68} - K-class magnitude of S-wave; ML - local magnitude; M_c - coda magnitude; M_W - moment magnitude; m_b - short-period body-wave magnitude; M_S - surface-wave magnitude.

Table 6.1: Parameters of strong earthquakes in the South Kamchatka region from 1962 to March 2013, including February 28, 2013 earthquake and its strongest aftershocks

6.2.2 Focal mechanism of the earthquake

Table 6.2 shows parameters and stereograms of focal mechanisms for the February 28, 2013 earthquake and its strongest aftershocks mentioned in Table 6.1 according to catalogues of Global CMT and KB GS RAS. (Estimates from KB GS RUS are determined by using the polarity of P wave onsets at regional stations). All the mechanisms are consistent with the tectonic condition of sub-horizontal compression in the NW-SE direction. For most mechanisms the flat plane dips under the Kamchatka peninsula, which corresponds to the geometry of the subduction zone.

6.2.3 Main features of the aftershocks process

The aftershock sequence of the February 28, 2013 earthquake ($M_W = 6.8$) was selected from the preliminary catalogue using a method after Molchan and Dmitrieva (1991); the software was developed by V. B. Smirnov (Lomonosov Moscow State University). This data collection includes 254 earthquakes with magnitudes in the range of $ML = 2.2-6.8$ where ML is calculated from K^{F68} as $ML = K^{F68}/2 - 0.75$, where K^{F68} is the K-class magnitude (Fedotov, 1972; Bormann, 2002). The cumulative frequency-magnitude plot (Figure 6.2) indicates a catalogue completeness threshold of $ML_{min} = 3.3$ which corresponds to the left edge of the linear part of the plot. Based on this threshold 121 out of 254 earthquakes were obtained from the preliminary catalogue until the end of 2013 for further analysis.

In Figure 6.1 aftershocks are contoured by the dispersion ellipse containing 90% of the aftershocks for the first month after the main earthquake, allowing to estimate the size of the rupture area of the February 28, 2013 earthquake ($M_W = 6.8$) as 90 km (length) \times 40 km (width).

The frequency-magnitude plot shows a gap of $\Delta M = 1.3$ between the largest aftershocks and the rest of the sequence (Figure 6.2). Such gaps can be observed between a main shock and the aftershocks.

№	Date YYYY.MM .DD	Time hh:mm:ss	h, km	The axes of the principal stresses						Nodal planes						Agency	
				T		N		P		NP1			NP2				
				pl	azm	pl	azm	pl	azm	stk	dip	slip	stk	dip	slip		
10	2013.02.28	14:05:59	45	77	313	2	215	13	124	36	58	92	212	32	86	Global CMT	
		14:05:48	61	59	27	30	225	8	131	65	59	126	191	46	46	KB GS RAS	
11	2013.03.01	12:53:58	44	78	300	0	30	12	120	30	57	90	210	33	90	Global CMT	
		12:53:49	52	62	327	9	221	27	126	43	72	99	196	20	64	KB GS RAS	
12	2013.03.01	13:20:55	41	77	313	2	216	13	126	214	32	87	37	58	92	Global CMT	
		13:20:48	62	66	71	16	201	17	296	193	64	73	49	31	122	KB GS RAS	
13	2013.03.04	20:56:36	44	78	297	1	33	12	124	32	57	88	216	33	93	Global CMT	
		20:56:33	51	79	267	6	32	9	123	27	54	82	221	37	101	KB GS RAS	
14	2013.03.09	14:56:32	47	79	330	3	323	11	132	45	56	94	218	34	84	Global CMT	
		14:56:27	49	81	229	9	49	0	139	41	46	78	238	46	102	KB GS RAS	

Table 6.2: Parameters of focal mechanisms of the main earthquake and its aftershocks with $ML \geq 6.0$ from Table 6.1 according to the Global CMT and KB GS RAS data

However, in this study the gap is observed between the group of the five strongest events (earthquakes with magnitudes $ML \geq 6.1$, including the main event and 4 strongest aftershocks) and the remaining aftershocks sequence with magnitudes $ML \leq 4.8$. The only earthquake in the magnitude range of $ML = 4.8-6.0$ occurred a month after the main event when the seismic process probably came out of the active phase. Thus, the observed sequence of earthquakes has features of both a swarm and an aftershock sequence with $ML \leq 4.8$.

Figure 6.3 shows the cumulative number of aftershocks over time in log-log scale.

Until the end of day 1 the trend is linear thus following Omori's Law with a decay exponent $p=1$. However, after two earthquakes on March 01, 2013 with $M_W = 6.4$ and $M_W = 6.5$, the behaviour of the sequence changes dramatically, indicating new aftershock process initiated by these two earthquakes. In more detail, the following characteristic stages (Figure 6.3) can be distinguished:

1. Hyperbolic (standard Omori) stage with

$$\frac{dN}{dt} \sim \frac{1}{t} \tag{6.1}$$

, where N is the cumulative number of aftershocks and t is time, until the strongest aftershocks

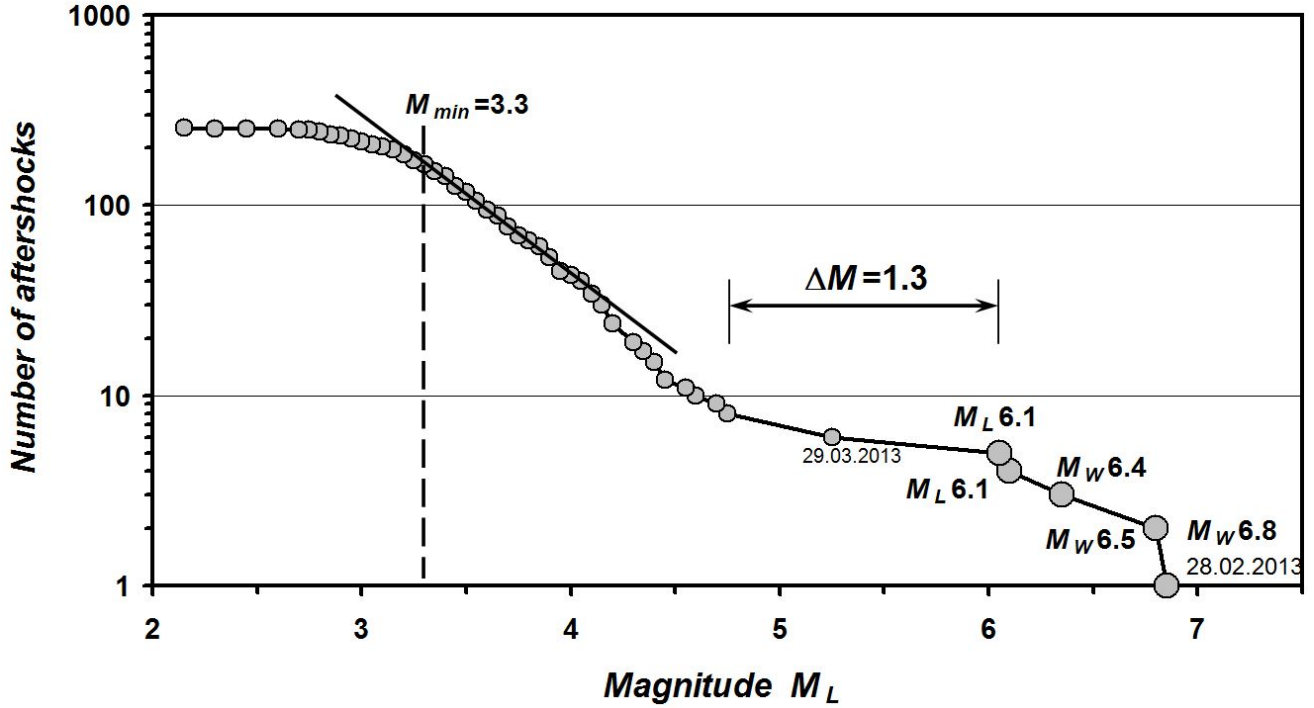


Figure 6.2: Cumulative frequency-magnitude plot for the aftershocks sequence of the February 28, 2013 earthquake ($M_W = 6.8$)

occur on March 01, 2013. The duration of this stage is ~ 23 hours. In this stage, the catalogue completeness threshold is equal to $M_L = 3.3$;

2. Strongest aftershocks occur on March 01, 2013 with $M_W = 6.4$ and $M_W = 6.5$; these are accompanied by decaying aftershocks following Omori's law

$$\frac{dN}{dt} \sim \frac{1}{t^p} \quad (6.2)$$

with $p = 0.7$. The duration of this stage is ~ 33 hours. The catalogue completeness of the mode is equal $M_L = 3.3$, except for the first 40 minutes;

3. The next stage showing a regular hyperbolic-law aftershock decay is the longest one, and lasts until June 2013. This date can be regarded as the end of the aftershock process that began with the earthquake on February 28, 2013, $M_W = 6.8$; therefore total duration of the aftershock sequence can be estimated as ~ 100 days. After this date, events in the area in question occur with intervals longer than one month.

6.2.4 Macroseismic data

Macroseismic information is collected for the 46 settlements of the Kamchatka region and the Northern Kuriles based on 109 reports of various sources. For the first time residents of the Kamchatka peninsula actively used an online questionnaire, which can be found on the official website of KB GS RAS (<http://www.emsd.ru/lspool/poll.php>). 59 respondents shared their experience from 9 locations. Although the earthquake occurred late at night on March 01, 2013 at 02:05 local time the online questionnaire system immediately began to receive reports from the respondents. By the beginning of the

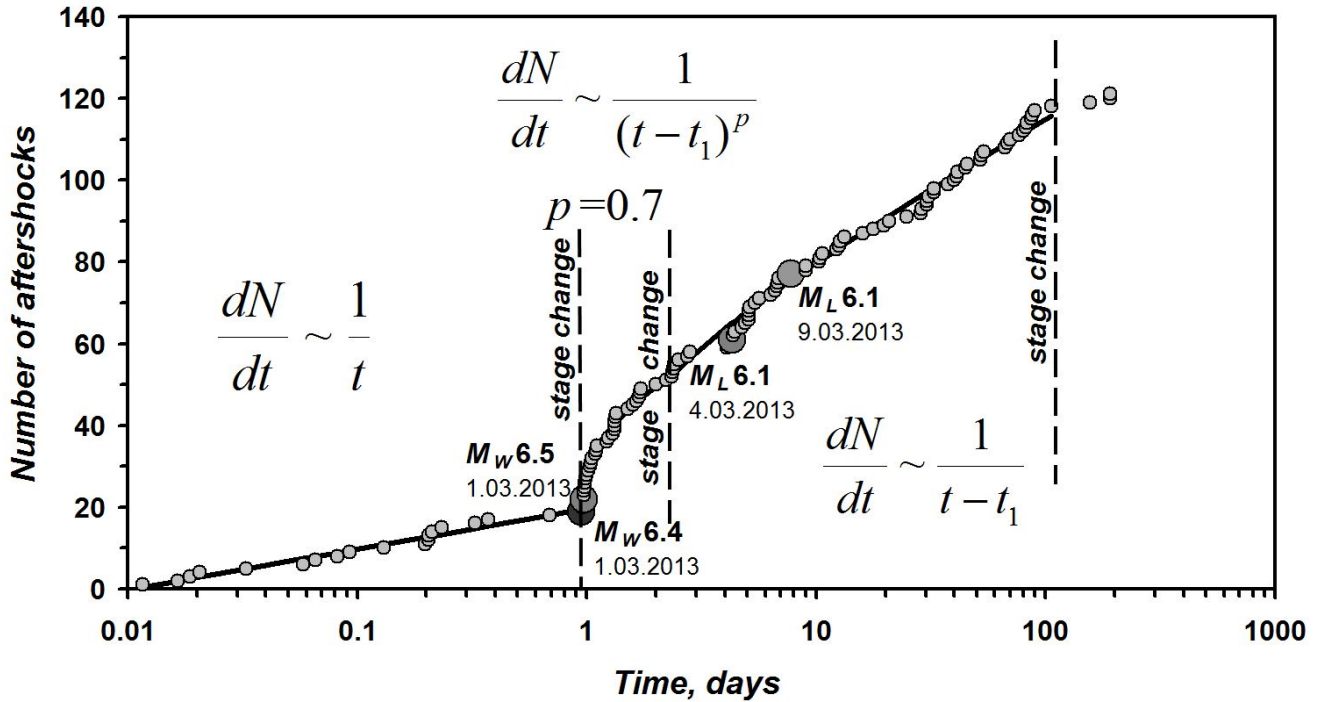


Figure 6.3: Development of the aftershock sequence with time. Origin time of the plot is set at the moment of the main shock on February 28, 2013 with $M_W = 6.8$, plus 0.01 day. The cumulative number of aftershocks is shown. The strongest earthquakes of the series are indicated.

next working day the database of KB GS RAS already collected preliminary information about the intensity of ground shaking in 4 places: Petropavlovsk-Kamchatsky, Viluchinsk, Elizovo and Paratunka.

The earthquake was felt with intensities up to V-VI on the MSK-64 scale in 34 settlements located at epicentral distances from 82 to 492 km. The area of macroseismic effects is about 56 000 km². A list of locations with epicentral distance, macroseismic intensity and effects description is given in Chebrov (2014).

Figure 6.4 shows a map of isoseismals and reported intensities for the earthquake. Isoseismals are drawn schematically because of the small amount of data due to the lack of settlements in the study area. Isoseismals are elongated along the east coast of Kamchatka; this pattern is typical for Kamchatka earthquakes.

Figure 6.5 shows the reported intensities over hypocentral distance, $I(r)$, and theoretical decay curves of macroseismic intensity, calculated using the equation after Fedotov and Shumilina (1971):

$$I = 1.5 \cdot M - 2.63 \cdot \lg(r) - 0.0087 \cdot r + 2.5 \tag{6.3}$$

where I - macroseismic intensity; r - hypocentral distance; M - magnitude (In our calculations we used M_W).

The macroseismic magnitude was estimated as $M = 6.6$; this value was chosen as providing the best fit between intensity decay and observed data. In this fitting, the macroseismic earthquake hypocenter was assumed to coincide with the instrumental one. The graph shows that at equal distances from the hypocenter seismic intensity values in the settlements of the east coast are higher than values in central

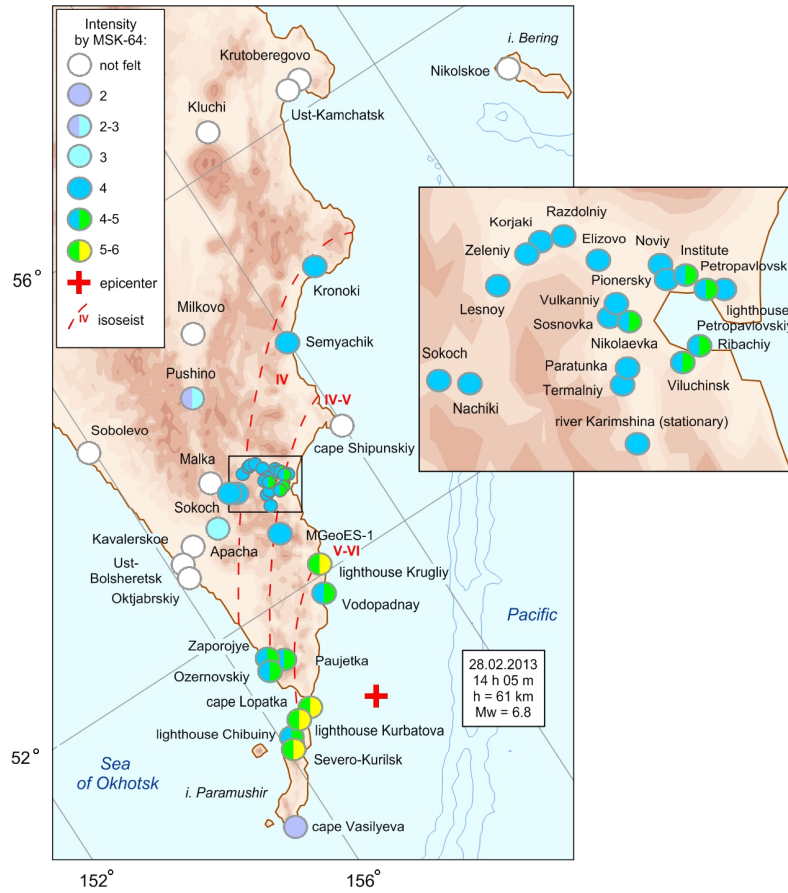


Figure 6.4: Macroseismic intensity distribution of the February 28, 2013 earthquake

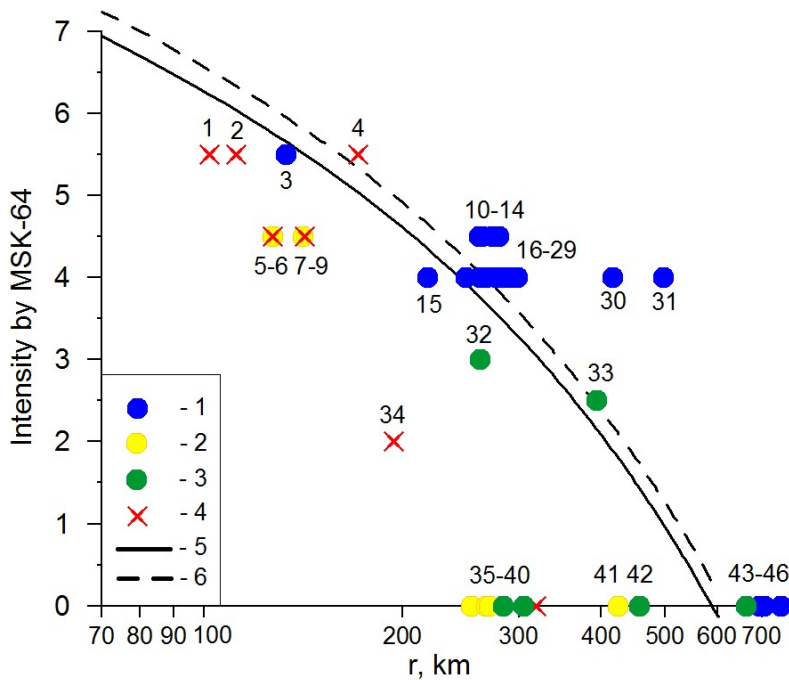


Figure 6.5: Intensity (I) decay with hypocentral distance (r). 1 - observation sites located at the east coast of the Kamchatka Peninsula and Paramushir island; 2 - sites at the west coast; 3 - sites in central Kamchatka; 4 - sites with seismic intensity estimation from transmitted radiogram without text description (lighthouses and the Vodopadnaya meteorological station); 5, 6 - intensity decay curves calculated for $M_W = 6.6$ and 6.8 , respectively, with Equation (6.3).

Kamchatka and the western coast where the earthquake was not felt at distances over 260 km. It should be noted that there is a lack of reported effects at Cape Shipunskiy (Figure 6.4), located on the east coast. Strong winds and storms often mask macroseismic effects at this site. Seismic intensities at the Vodopadnay meteorological station, Chibuiny lighthouses, and Cape Vasilyeva are significantly lower than expected. This may be related to local site conditions, or due to a human bias of intensity values based on the reports of very small staff at the lighthouse.

After the February 28, 2013 earthquake four aftershocks with $ML > 6.0$ (Table 6.1) occurred during the first 9 days and could be felt in Kamchatka (Figure 6.6). All events, including the main one, have a similar pattern in isoseismal maps: the macroseismic effect is higher on the eastern coast of Kamchatka with the strongest shaking recorded at Severo-Kurilsk on the Paramushir island (Figure 6.6).

6.2.5 Ground motion

Figure 6.7 illustrates the records of ground motion at the Severo-Kurilsk seismic station. Peak amplitudes for 29 stations are presented on Figure 6.8 (accelerations) and Figure 6.9 (velocities). When both accelerometer and velocimeter are present at a station, results recovered from records of both instruments are plotted.

There are sometimes significant discrepancies between the estimates of the amplitudes from an accelerometer and a velocimeter. This fact can result from various factors. At some stations the accelerometer is installed on a pedestal, usually in a building (single-storey), while the velocimeter is installed outside the building, at distances of ≈ 40 m, in a borehole at depths of 5-30 m. Additionally, instrument orientation azimuths for borehole instruments could bear large errors.

The decay of amplitudes with hypocentral distance r is analysed in the next paragraphs. Figure 6.8 shows the peak acceleration of the vertical and horizontal components with hypocentral distance. For comparison, two peak acceleration decay curves from other sources are plotted. Of the two parallel solid gray lines, the lower one is after Fukushima and Tanaka (1990) (with their epicentral distances converted to hypocentral ones). It follows the trend

$$A \sim r^{-1.218} \quad (6.4)$$

Its intersection with the y-axis corresponds to $M_W = 7.0$. The upper line is plotted through an anchor point at $r = 200$ km using a point estimate derived from empirical scaling after Gusev *et al.* (1997). In that paper, only epicentral distances between 50-200 km were considered. Therefore, the line was plotted through the anchor point with the slope identical to that of Fukushima and Tanaka (1990). None of these approximations is acceptable. At distances above 300 km data points are below both straight lines. An alternative linear approximation of the data was found, based on the least squares method (dot-dashed line), with a slope of -2.55. Despite some improvement of the fit, the general agreement was still poor. As a final approximation we prefer three-segment broken line (dashes), with corner points at $r = 300$ and 600 km, and slopes that vary, from left to right, from -1.37 to -2.42 and to -5.8.

In Figure 6.9, peak velocities are depicted. The reference straight line represents the calibration curve of the local K-class magnitude scale K^{F68} (Fedotov, 1972) with the standard slope of -1.75, and with its

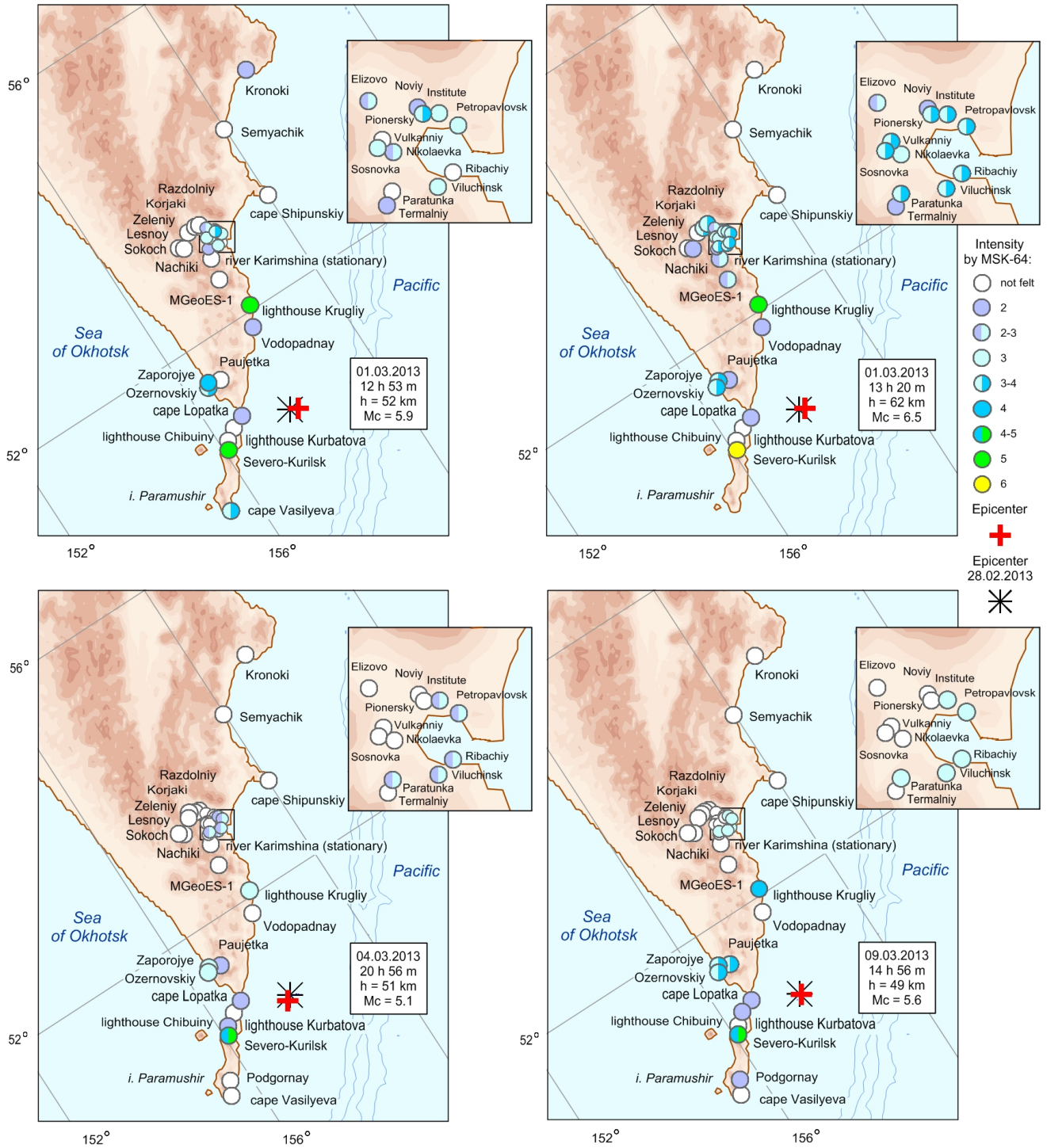


Figure 6.6: Macroseismic effects of aftershocks of the February 28, 2013 earthquake, see also Table 6.1

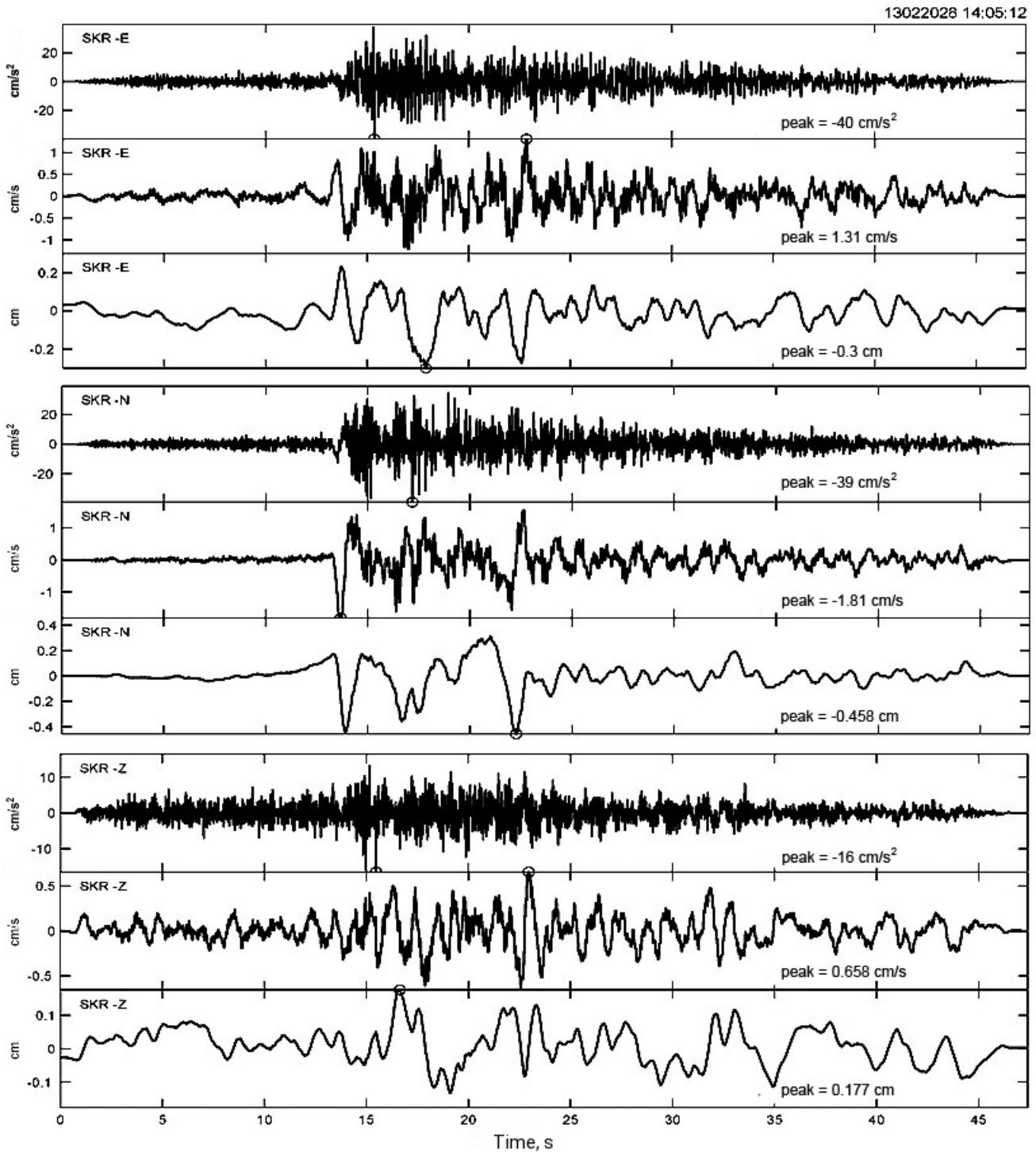


Figure 6.7: Example of acceleration records at channels of digital Guralp CMG-5 accelerograph with the GEOSIG recorder at Severo-Kurilsk station (SKR), one of the closest to the epicenter, and recovered signals of velocity and displacement from these records in the frequency range from 0.1 to 40 Hz.

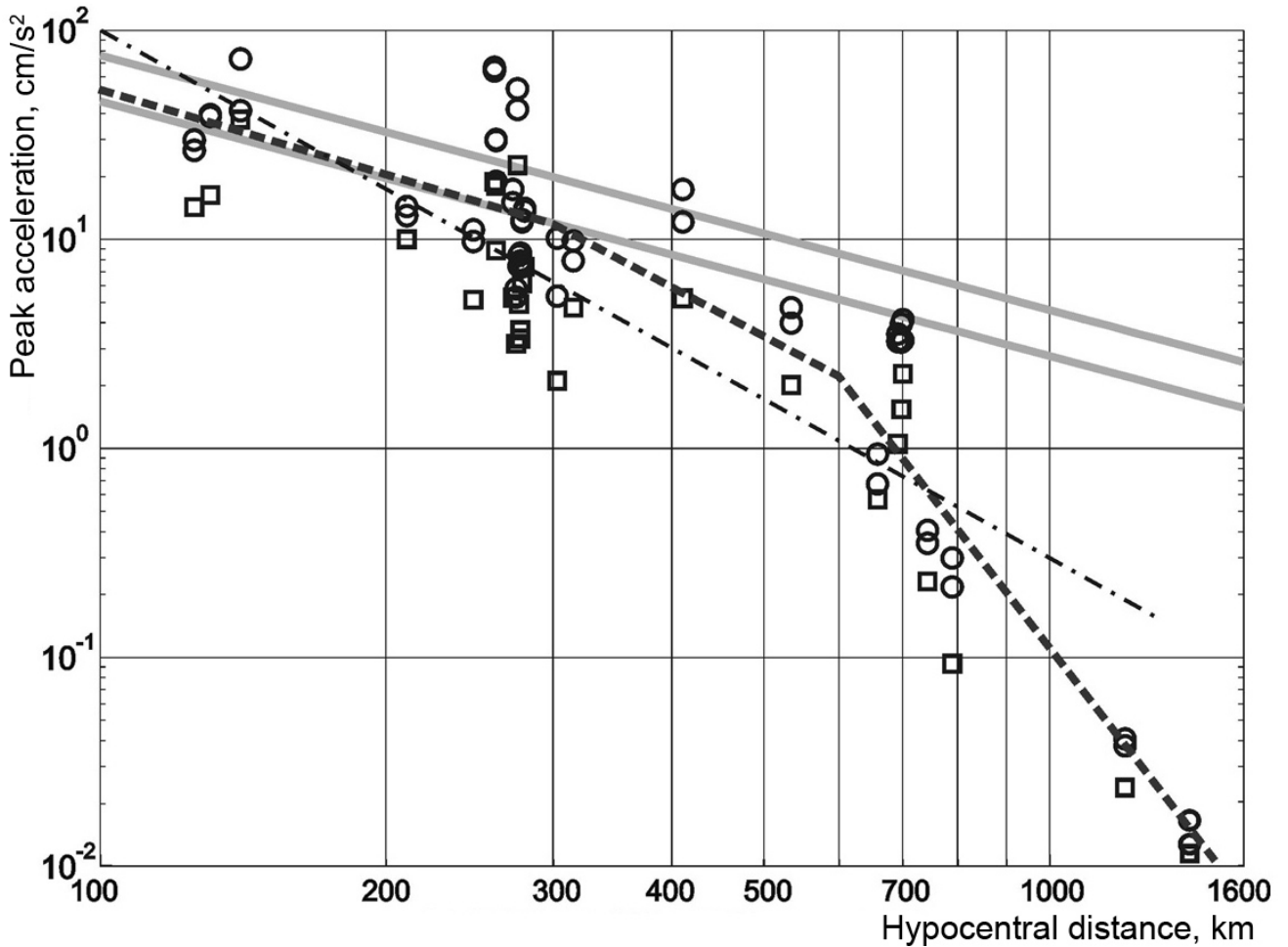


Figure 6.8: Peak acceleration with hypocentral distance. Circles and squares correspond to acceleration values on the horizontal and vertical components, respectively. Gray lines follow decay approximations based on Fukushima and Tanaka (1990) (lower) and Gusev et al. (1997) (top), for details see the text. Dot-dashed line shows a linear approximation of the data, which is not acceptable. The dashed line is the accepted 3-segment approximation.

position along the y-axis selected for the best fit. This selection gives the corresponding magnitude value $K^{F68} = 16.3$. The peak velocity was estimated as $2\pi (A/T)$ where A/T is the standard input of K^{F68} magnitude calculation. The actual value of K^{F68} for the main shock is 15.3, indicating amplitudes about 3.2 times lower than expected from the above estimate of $K^{F68}=16.3$. The discrepancy appears to be associated with significantly broader bandwidth of the digital velocimeter as compared to the emulated band-limited signal of 1.2s VEGIK seismograph channel used for the K^{F68} calculation. The qualitative agreement of the trend for observed data with the trend of the calibration curve is quite acceptable. It should be noted that the original calibration curve was constructed up to the 600 km distance; the success of its extrapolation up to 1600 km was unexpected.

A more detailed analysis of amplitudes can be carried out after careful classification of stations by their soil types. According to the analysis of limited data for amplitudes of the February 28, 2013 earthquake, preliminary conclusions can be made:

- (1) the level of acceleration and velocity amplitudes for the earthquake is approximately consistent with average tendencies for Kamchatka;

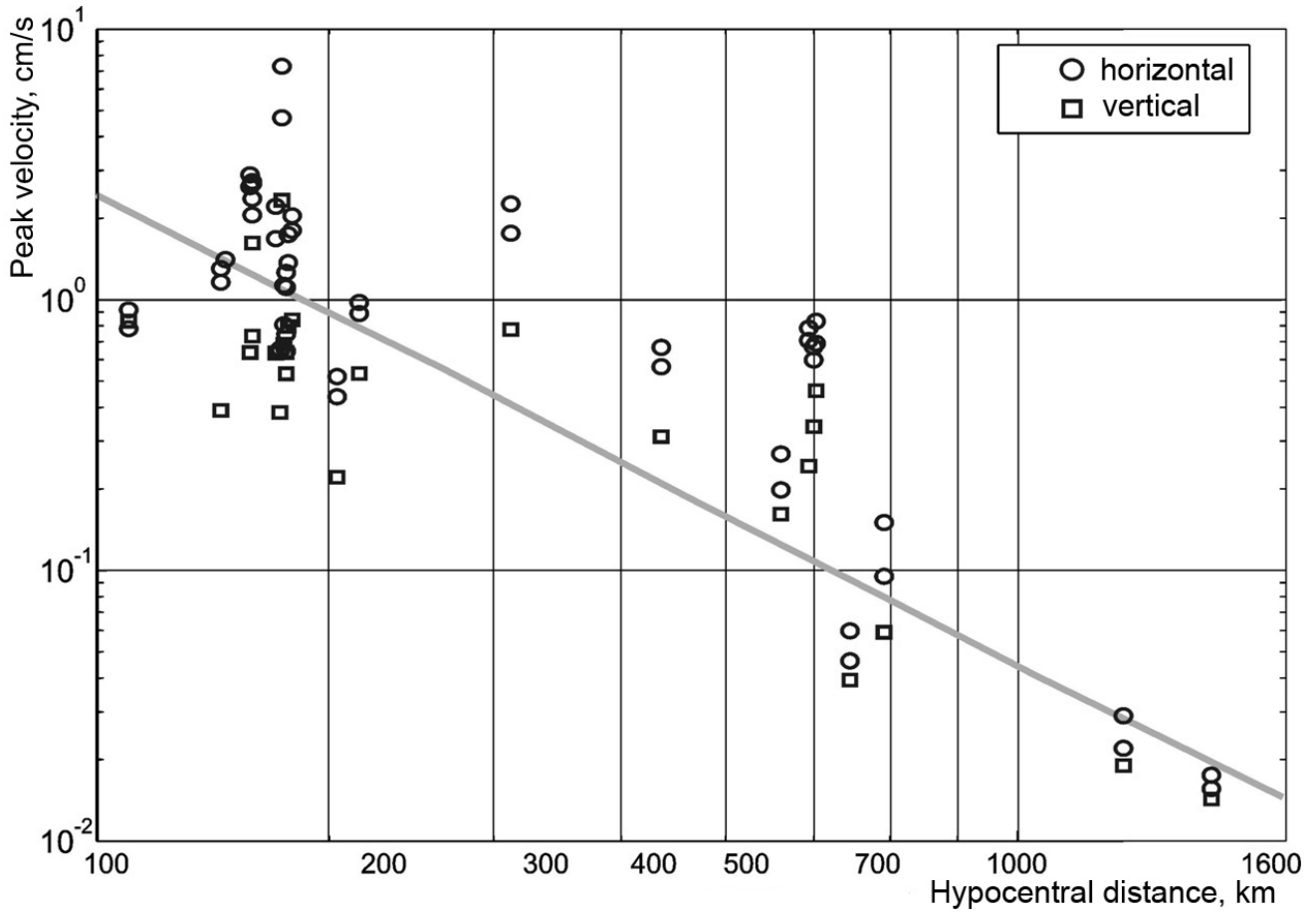


Figure 6.9: Peak velocities with hypocentral distance. The line shows the calibration curve of the Kamchatka K-class magnitude scale K^{F68} (Fedotov, 1972), with a value of $K^{F68} = 16.3$.

(2) the distance decay for peak accelerations over the 100-300 km range is comparable to that for earthquakes of Kamchatka and Japan. The trend of $A \sim r^{-1.218}$ is consistent with the data. At larger distances, the decay becomes much steeper.

(3) the distance decay for peak velocities in the entire investigated distance range of 100-1600 km matches the calibration curve for regional K-class magnitude, K^{F68} , with its trend $V \sim r^{-1.75}$.

6.2.6 Conclusion

The February 28, 2013 earthquake of $M_W = 6.8$ is a regular event in the seismic process of the Kuril-Kamchatka subduction zone. The earthquake occurred at the latitude of the Cape Lopatka. This segment of the Kuril-Kamchatka arc is one of the most seismically active areas in the North-West Pacific. There have been repeatedly earthquakes with $M > 8$ that caused tsunamis and intensities of ground shaking up to IX on the MSK-64 scale in the south of Kamchatka (Godzikovskaya 2010; Kondorskaya and Shebalin, 1977).

The last earthquakes with magnitudes of $M \geq 7.0$ were recorded in the area of the North Kuriles in 1955 (on November 23, 1955, $M = 7.3$ (Kondorskaya and Shebalin, 1977) and in 1973 (on February 28, 1973, $M_W = 7.4$ (Gusev and Shumilina, 2004), and off the coast of south Kamchatka - in 1993 (on June 08, 1993, $M_W = 7.5$ (Gusev and Shumilina, 2004) and in 1999 (on March 08, 1999, $M_W = 6.9$).

This area is located in an extensive fault zone that was ruptured by the strong catastrophic Kamchatka earthquake on April 11, 1952 with $M_W = 9.0$ (Gusev and Shumilina, 2004), and probably lies in the fault zone of the first historical earthquake in Kamchatka on October 17, 1737 with $M_W = 9.2$ (Gusev and Shumilina, 2004) described by S. P. Krasheninnikov (1949) and Godzikovskaya (2010) as well.

Parameters of the February 28, 2013 earthquake have been evaluated by SS TWS within 6 minutes, what is in accordance with accepted time limits. In urgent mode aftershocks have been processed. Macro seismic data have been collected for the region of Kamchatka and Northern Kuriles.

The actual time-magnitude pattern of the observed earthquake sequence is specific, with its properties between a standard aftershock sequence with a single mainshock, and a typical swarm with no main event. The aftershock cloud approximately covers an area of 90 km (length) \times 40 km (width); these figures provide a maximum estimate for the main shock fault size.

The analysis of peak accelerations shows typical amplitudes and decay within 250 km epicentral distance. At larger distances, a much stronger decay was revealed. The decay of peak amplitudes with epicentral distance matches the average trend for the Kamchatka region well. The February 28, 2013 earthquake of $M_W = 6.8$ is the first earthquake of such magnitude in the Kamchatka region, that is recorded by the digital new system of seismic observations set by KB GS RAS between 2005 and 2010 (Chebrov *et al.*, 2013).

6.3 The largest deep-focus Sea of Okhotsk earthquake May 24, 2013, $M_W = 8.3$

6.3.1 Introduction

On May 24, 2013, at 05:44 (UTC) a magnitude M_W 8.3 earthquake occurred in the Sea of Okhotsk, to the west of the Kamchatka Peninsula (Figure 6.10). The scalar seismic moment of the event is $M_0 = 3.95 \cdot 10^{21} N \cdot m$ (Ekström *et al.*, 2012). This is the strongest earthquake recorded in the Kamchatka region during the years of instrumental seismological observations (from 1962 to present) and the most powerful earthquake in the world among events of comparable depths. A similar strong deep-focus event (647 km depth, $M_0 = 2.63 \cdot 10^{21} Nm$) occurred in Bolivia, on June 9, 1994, but this event turned out to be weaker than the Sea of Okhotsk one.

Co-seismic displacement signals of the Sea of Okhotsk earthquake were recorded by many Far Eastern stations of the Global Navigation Satellite System (GNSS) (Chebrov *et al.*, 2013) and the macroseismic effect could be felt globally.

According to KB GS RAS, the epicenter of the May 24, 2013 earthquake is about 360 km north-west of Petropavlovsk-Kamchatsky, the hypocenter is located in the Kamchatka Benioff zone at a depth of 630 km, which corresponds to the lower depth limit for seismic events. The earthquake was followed by an aftershock sequence. Parameters of hypocenters for the earthquake and its strongest aftershocks with $ML \geq 6.0$, energy characteristics according to several seismological agencies of Russia and the world are given in Table 6.3.

Previous strong deep-focus earthquakes in the Sea of Okhotsk area occurred on July 05, 2008 at a depth of 665 km with $M_W = 7.7$ and on November 24, 2008 at a depth of 564 km with $M_W = 7.3$.

The 2013 Sea of Okhotsk earthquake was felt in the Kamchatka region with intensities up to V-VI, and in the rest of Russia - up to IV-V degrees, as well as in several countries of Europe, Asia and North America. Macroseismic manifestations of the May 24, 2013 earthquake have been reported at epicentral distances up to 9500 km.

According to the SS TWS regulations real-time data processing started when an alarm signal was released (i.e. when the amplitude on a station exceeds the predetermined threshold value) after registering the P-wave onset at the "Karymshina" station (KRM). Processing was carried out within accepted time limits despite the strong ground shaking with intensities up to IV-V at the office's location. A preliminary assessment of source parameters was obtained within 4 minutes since the alarm, and a final one was released within 8 minutes since the alarm. All the relevant messages were sent according to the circulation list. The on-duty staff decided not to issue a tsunami alarm because the earthquake hypocenter was located at a depth greater than 600 km.

The reference magnitude to assess the tsunamigenic potential of an earthquake in the SS TWS is the surface-wave magnitude M_S . It should be noted that this magnitude has been underestimated in the preliminary solution ($M_S = 6.7$). It is well known that deep earthquakes produce significantly reduced surface waves what leads to magnitude underestimation. Earthquake records are shown in Figure 6.11.

Thus, the earthquake processing time of SS TWS is about 8 minutes, which is within the approved

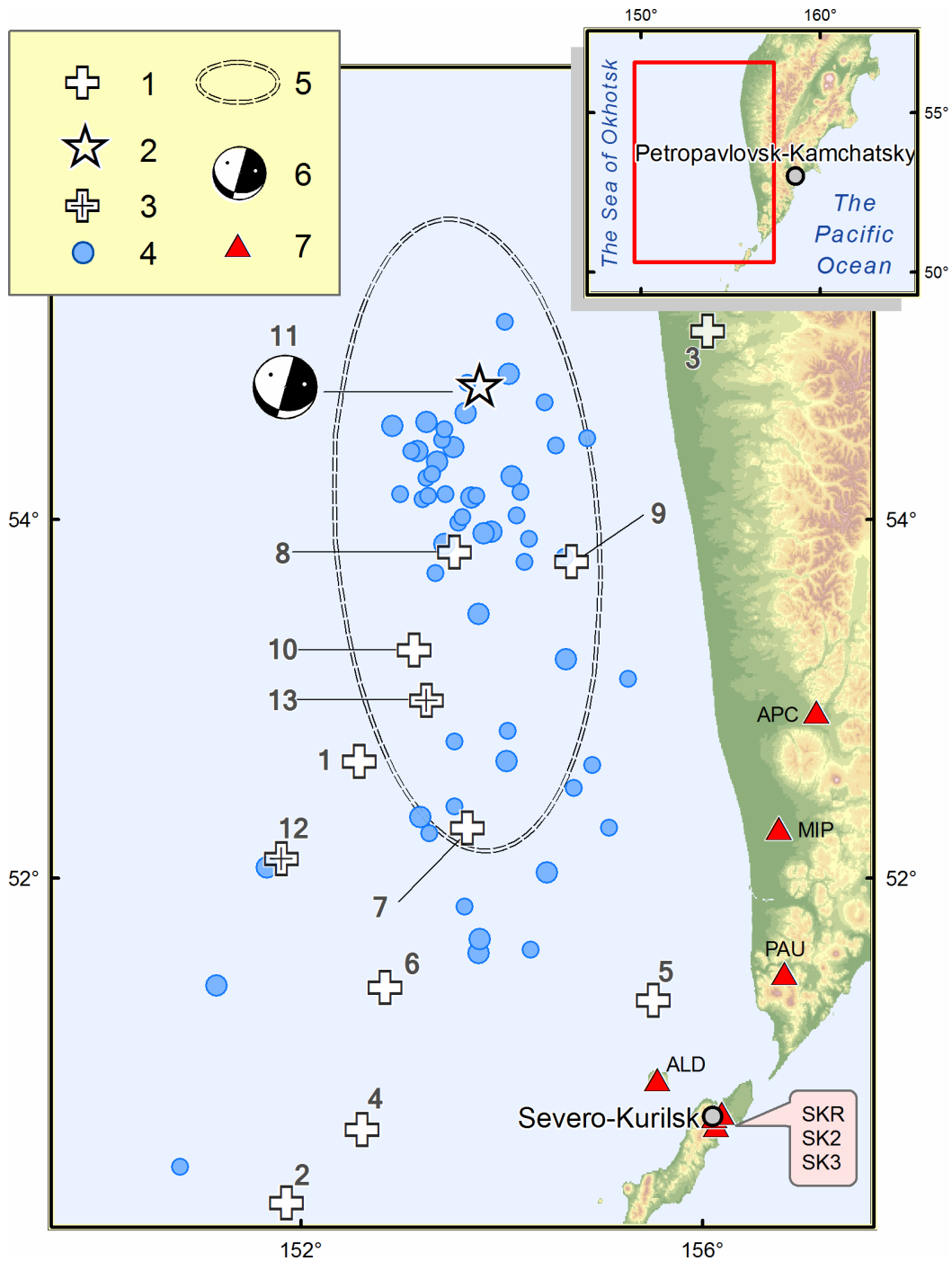


Figure 6.10: Location scheme for epicenters of the May 24, 2013 earthquake, its aftershocks with magnitudes of $ML \geq 4.2$ and strong earthquakes ($ML > 6.0$) of this region for the period from 1962 to May 24, 2013 according to the catalogue of Kamchatka and the Commander Islands earthquakes ($ML \geq 4.2$ corresponds to the catalogue completeness threshold for the Kamchatka regional network in the Sea of Okhotsk region): 1 - epicenters of strong earthquakes ($ML > 6.0$) of this region for the period from 1962 to May 24, 2013, 2 - the epicenter of the May 24, 2013 earthquake; 3 - epicenters of strong aftershocks ($ML > 6.0$); 4 - epicenters of aftershocks with $4.2 \leq ML \leq 6.0$; 5 - 2σ -ellipse approximation of the aftershock zone; 6 - stereogram of the focal mechanism by Global CMT for the main shock; 7 - seismic stations. Numeration of earthquakes corresponds to Table 6.3.

№	Hypocenter					Energy class / Magnitudes							
	Date YYYY.MM DD.	Time hh:mm:ss	ϕ°, N	λ°, E	h, km	KB GS RAS			Global CMT	NEIC(USGS)		Obninsk	
						K^{F68}	ML	M_c	M_W	m_b	M_W	m_b	M_S
Strong earthquakes of this area for the period from 1962 to May 24, 2013													
1	1965.08.01	16:41:07	52.65	152.58	460	14.1	6.3	—	—	5.1	—	—	—
2	1971.01.29	21:57:51	50.19	151.86	710	15.2	7.3	—	—	6.1	—	6.8	—
3	1972.05.27	04:06:45	55.05	156.05	467	14.0	6.2	—	—	5.7	—	6.2	—
4	1975.12.21	10:54:06	50.60	152.61	701	15.2	6.8	—	—	6.0	—	6.4	—
5	1977.09.21	21:01:42	51.32	155.51	247	13.7	6.1	—	—	5.6	—	6.1	—
6	1979.12.30	04:18:21	51.39	152.84	682	13.6	6.0	—	—	5.4	—	5.8	5.0
7	2001.02.07	15:16:10	52.28	153.66	476	14.2	6.4	5.0	5.7	5.6	5.7	5.9	—
8	2008.07.05	02:12:06	53.82	153.53	610	15.7	7.1	6.9	7.7	6.8	7.7	6.9	6.5
9	2008.11.24	09:02:52	53.76	154.69	564	15.2	6.8	6.7	7.3	6.5	7.3	6.5	6.2
10	2009.12.10	02:30:51	53.40	152.61	621	14.8	6.6	5.4	6.3	6.1	6.3	6.2	—
The May 24, 2013 earthquake and its strongest aftershocks													
11	2013.05.24	05:44:47	54.76	153.79	630	17.0	7.8	7.4	8.3	7.5	8.3	7.7	—
12	2013.05.24	14:56:29	52.11	151.81	642	15.0	6.8	5.8	6.7	6.7	6.7	7.0	—
13	2013.10.01	03:38:19	52.99	153.25	605	15.2	6.9	6.1	6.7	—	—	6.7	—

Note: K^{F68} - K-class magnitude of S-wave; ML - local magnitude; M_c - coda magnitude; M_W - moment magnitude; m_b - short-period body-wave magnitude; M_S - surface-wave magnitude.

Table 6.3: Parameters of strong earthquakes ($ML \geq 6.0$) in the Sea of Okhotsk region from 1962 to May 2013, including the May 24, 2013 earthquake and its strongest aftershocks

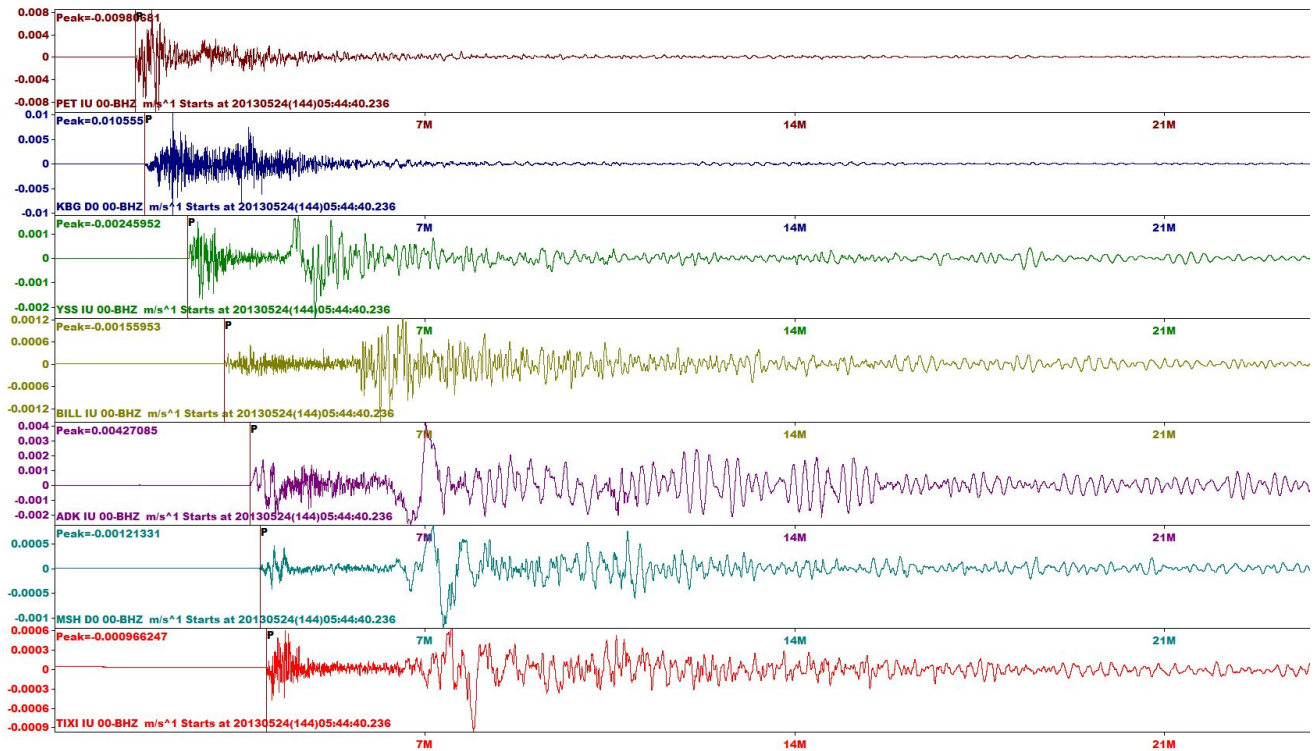


Figure 6.11: Examples of earthquake records of the May 24, 2013 earthquake at broadband seismic stations (vertical channels): PET - “Petropavlovsk”; KBG - “Krutoberegovo”; YSS - “Yuzhno-Sahalinsk”; BILL - “Bilibino”; ADK - “Adyak”; MSH - “Schultz Cape”; TIXI - “Tiksi”

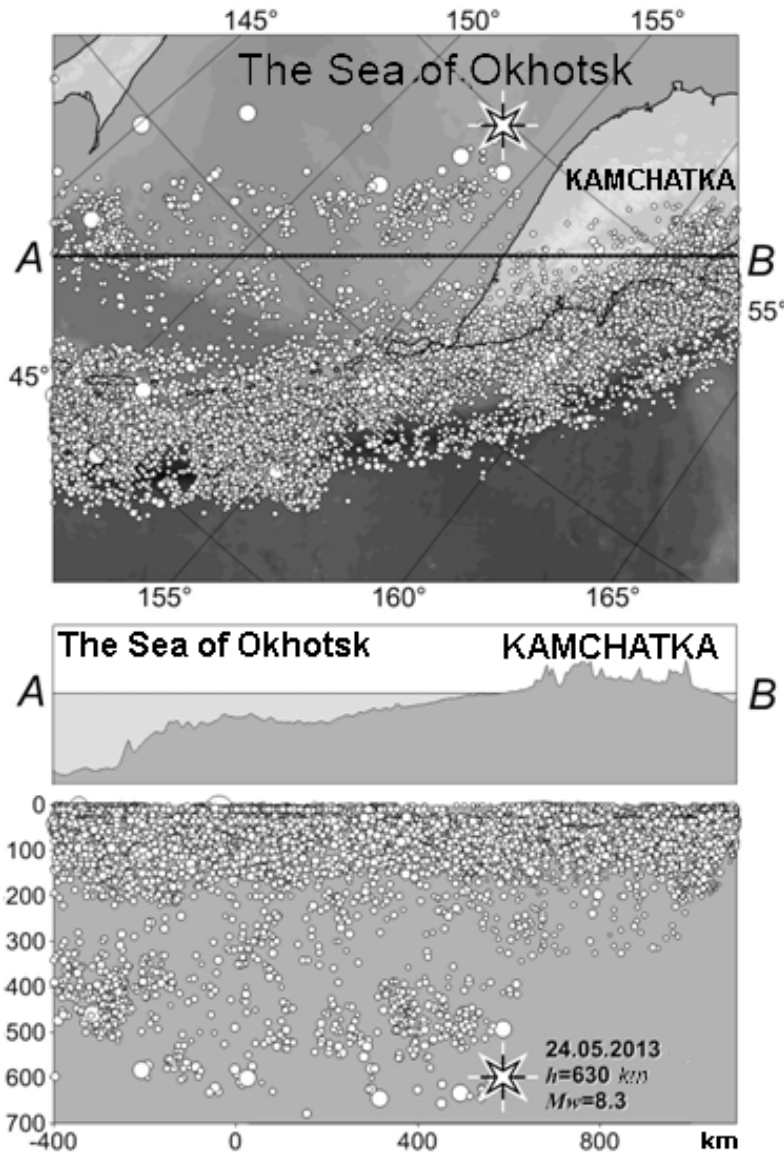


Figure 6.12: Locations for the epicenters of the May 24, 2013 earthquake and other events of the focal zone from 1962 to August 2013 according to USGS NEIC PDE catalogue and the projection of its hypocenters on the vertical plane along a profile (AB)

time limit (according to current regulations it should take not more than 10 minutes for processing earthquakes at epicentral distances of up to 1000 km). The processing centre "Petropavlovsk" in a challenging situation demonstrated sufficient accuracy in determination of earthquake parameters within their mission as an urgent service of tsunami warning system.

6.3.2 Tectonic setting and the focal mechanism of the earthquake

The Kuril-Kamchatka subduction zone can be divided along strike into two segments: the Kurile-South-Kamchatsky and the North-Kamchatsky segment (Levina *et al.*, 2013). The boundary between them is located in the Avacha Gulf area. Numerous geological and seismological data confirm the difference in ages of subduction on these two segments. The observed seismic focal zones are characterized in the southern and northern segments by fundamentally different depths, 650-700 km to the south and only 350-400 km to the north, respectively (Figure 6.12).

The deep-focus May 24, 2013 earthquake occurred almost at this boundary, or to be more specific at the north-eastern end of the Kuril-South-Kamchatka segment of the subducting Pacific plate. NE of the

epicenter, the depth position of the lower boundary of the Benioff zone moves up, from about 400 km at latitude 53.5N to about 120 km at 56N.

Focal mechanisms were determined using three types of data: (1) polarities of P waves; (2) co-seismic offsets at the GNSS stations (static case); and (3) waveforms registered at regional broadband seismic stations (dynamic case).

Parameters and stereograms of focal mechanisms for the May 24, 2013 earthquake and its strongest aftershocks with $ML \geq 6.0$ according to catalogues of Global CMT and KB GS RAS (the latter estimates are determined using P wave polarities at regional and global stations) are given in Table 6.4. The most interesting fact is that all the solutions indicate compression down dip of the subducting Pacific plate.

№	Date YYYY.MM .DD	Time hh:mm:ss	h, km	The axes of the principal stresses						Nodal planes						Agency	
				T		N		P		NP1			NP2				
				pl	azm	pl	azm	pl	azm	stk	dip	slip	stk	dip	slip		
11	2013.05.24	05:45:08	611	34	102	1	192	56	283	12	79	-89	189	11	-93	Global CMT	
		05:44:47	630	39	81	28	196	39	311	196	90	62	106	28	180	KB GS RAS1)	
12	2013.05.24	14:56:34	642	19	124	11	30	68	272	25	64	-102	231	28	-67	Global CMT	
		14:56:29	642	9	138	9	229	78	3	56	55	-79	218	37	-105	KB GS RAS1)	
13	2013.10.01	03:38:24	585	13	171	28	74	59	284	59	64	-121	293	40	-44	Global CMT	
		03:38:19	605	25	190	21	90	56	325	83	73	-112	318	28	-39	KB GS RAS1)	

Note. 1) Input data are polarities of P-waves.

Table 6.4: Parameters of focal mechanisms of the May 24, 2013 earthquake and its strongest aftershocks with $ML \geq 6.0$ from Table 6.3 according to the Global CMT and KB GS RAS data

The determination of focal mechanism in a general approach as a full seismic moment tensor (SMT) is described in Abubakirov *et al.* (2015), where six SMT components are calculated. The seismic moment tensor was determined using either co-seismic static offsets or waveforms (displacements) by a least-square linear inversion providing error estimations for each of the SMT components as standard deviations. Then the SMT eigenvalues and corresponding principal axes were estimated which allowed to determine (1) the best double couple (DC), (2) scalar seismic moment, $M_0 = (E_3 - E_1)/2$, and (3) Lode-Nadai coefficient, $\eta = (2E_2 - E_1 - E_3)/(E_3 - E_1)$, where $E_1 \leq E_2 \leq E_3$ are SMT eigenvalues. The η value varies from -1 to 1 ($\eta = 0$ corresponds to the pure double-couple source) and characterizes a discrepancy between a SMT solution and a DC.

In addition to the SMT, in the dynamic case the source is characterized by its source time function (STF), which describes the slip rate. In this study we assume the STF to be an isosceles triangle of unit area and the source epicenter is known from USGS PDE catalogue. The duration of the STF and the source depth are found by best fit during the inversion process.

All calculated variables are accompanied by error estimates. For variables that are functions of SMT

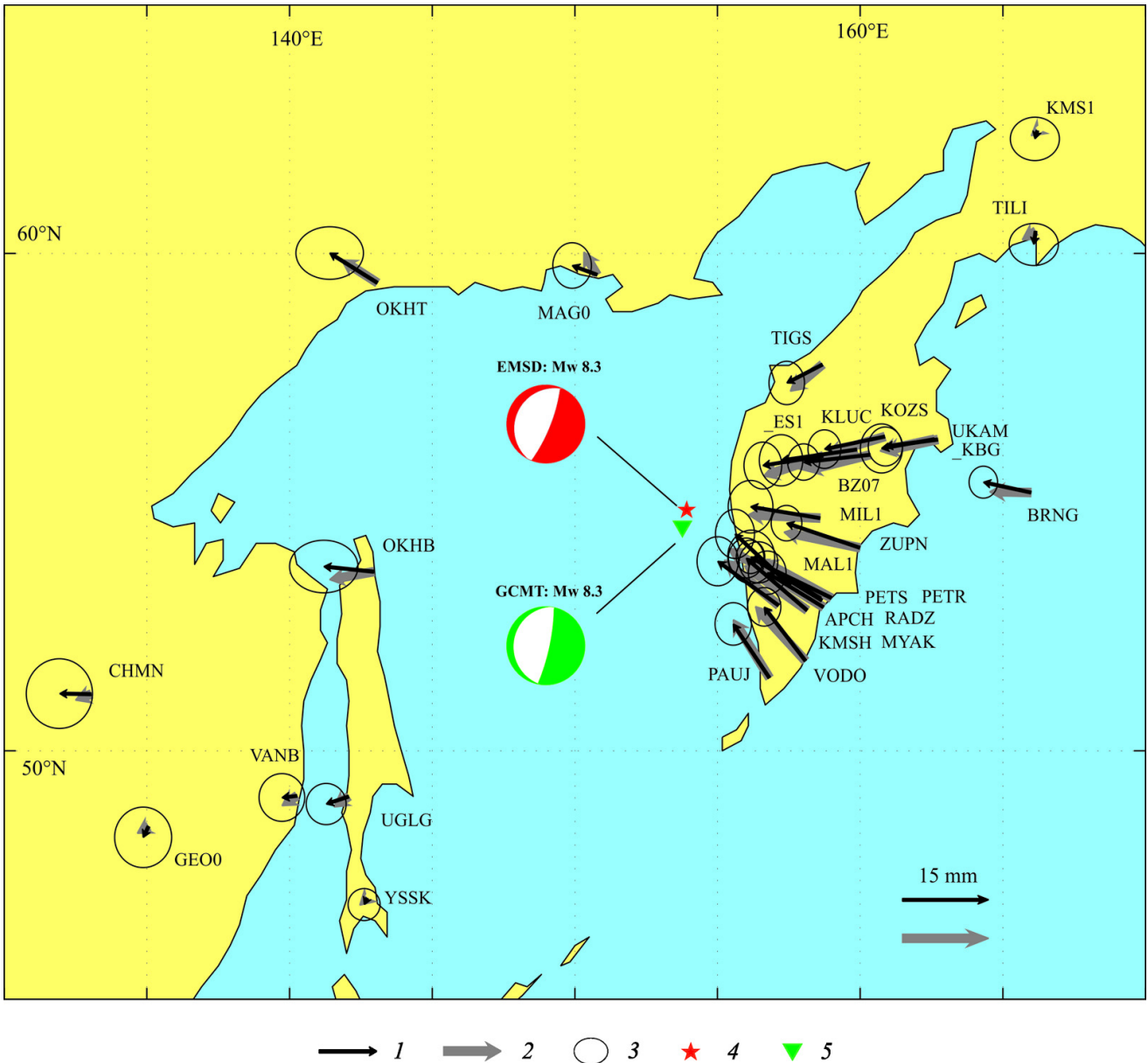


Figure 6.13: Horizontal components of observed offsets and simulated static displacements for the *ES_1* option (parameters used for calculation are given in Table 6.5). 1 - observed horizontal offsets; 2 - simulated static offsets; 3 - error ellipses; 4 - epicenter as located by the KB GS (EMSD); 5 - epicenter according to the GCMT

components error estimates are obtained by the Monte-Carlo method. Namely, each optimal SMT component is disturbed by random normally distributed quantities with zero mean and standard deviation obtained by the LS inversion. For N realizations ($N = 1000$) of the SMT, the set of values of a dependent scalar quality, say the largest eigenvalue, is generated. The estimate for such scalar quantity is the half-width of the interval (centered at the undisturbed value) that contains 68% of the points. Note that if a data distribution is normal then 68% of the data values are within one standard deviation of the mean. When we deal with a vector, we find half the angle at the vertex of a circular cone that contains 68% of the vectors based on the disturbed tensors. The axis of the cone is determined by the undisturbed vector.

For the static case we used three-component data from GNSS observations carried out by KB GS

RAS and networks of other institutions of the Far Eastern Branch of the Russian Academy of Sciences (Figure 6.13 shows horizontal offsets vectors). We assume that the source is a point source and located at the GCMT centroid. For SMT inversion we used the functions of influence of the SMT components or partial derivatives of Green’s functions with respect of source spatial coordinates. The influence functions - synthetic static displacements from unit couple corresponding to each of SMT component - were calculated for a layered sphere using an original algorithm (Abubakirov *et al.*, 2015).

For the dynamic case we used seismic broadband seismograms (Figure 6.14). Four seismic networks were used for processing: GSN (global seismic network), Japanese F-net network, Alaska Regional Network and China National Seismic Network. Additionally, we used reference stations of SS TWS by KB GS RAS and Tsunami Warning Center of USA West Coast and Alaska (West Coast & Alaska Tsunami Warning Center). For the SMT inversion we used records of stations with a low-frequency corner in the velocity transfer function at frequencies less than 8.33 mHz (period of at least 120 s). This condition allows us to reconstruct long-period ground motion with a sufficient enough signal-noise ratio.

The algorithm of dynamic inversion is presented in Pavlov and Abubakirov (2012). The functions of influence for the dynamic case were calculated for a layered half-space using the algorithm described in Pavlov (2013).

Seismic stations were selected in the epicentral distances of 8-25°. The upper limit of this range is set to ensure the applicability of the flat layered model of media used for the inversion, and the lower one is to ensure far-field conditions as calculations are based on a point-source model.

Calculation cases are described in Table 6.5. Besides the input data type (static or dynamic), they vary by number of components used and/or the number of unknown SMT components.

Used paramters	ES_1	ES14	ES35	ES25	ES35	ES36
Input data	Co-seismic offsets	Co-seismic offsets	Co-seismic offsets	Co-seismic offsets	Wave forms ¹⁾	Wave forms ²⁾
Method of static offsets evaluation	1-1 ³⁾	14-14 ⁴⁾	14-14 ⁴⁾	14-14 ⁴⁾	-	-
Number of SMT components	3	3	3	2 ⁵⁾	3	3
Number of unknowns	6	6	5 ⁶⁾	5	5	6

Note.

- 1) In the interval $[t_P, t_P + 900]$ s;
- 2) in the interval $[t_P, t_S]$ s;
- 3) difference of observations after and before the earthquake;
- 4) difference of observations based on linear interpolations of data for 2 weeks after and 2 weeks before the earthquake;
- 5) horizontal components only;
- 6) SMT is assumed to have zero trace ($M_{11} + M_{22} + M_{33} = 0$).

Table 6.5: Codes of calculation cases

The inversion results (Table 6.6, Table 6.7 and Figure 6.15) are compared to three SMT solutions available on the website of the USGS. All of these cases use the same condition (SMT is assumed to

Code	M_{11}	M_{12}	M_{13}	M_{22}	M_{23}	M_{33}	ξ	$\varepsilon, \%$
	$10^{21} N \cdot m$							
GCMT ¹⁾	1.28 ± 0.01	-0.16 ± 0.01	-3.57 ± 0.01	0.38 ± 0.01	0.78 ± 0.01	-1.67 ± 0.01	-	-
ES_1	1.11 ± 0.91	-0.52 ± 0.36	-3.37 ± 0.24	0.27 ± 1.19	1.29 ± 0.19	-2.48 ± 0.46	-0.37 ± 0.52	2.6
ES14	1.41 ± 0.96	-0.66 ± 0.39	-3.71 ± 0.24	1.86 ± 1.34	1.46 ± 0.21	-0.85 ± 0.51	0.81 ± 0.57	3.7
ES35	0.57 ± 0.42	-0.51 ± 0.36	-3.74 ± 0.24	0.62 ± 0.44	1.47 ± 0.21	-1.19 -	-	3.8
ES25	0.58 ± 0.42	-0.59 ± 0.35	-3.84 ± 0.24	0.57 ± 0.44	1.60 ± 0.22	-1.15 -	-	2.6
ED35	0.87 ± 0.07	-0.06 ± 0.07	-3.77 ± 0.09	0.41 ± 0.07	1.13 ± 0.07	-1.29 -	-	20.8
ED36	0.62 ± 0.20	-0.22 ± 0.22	-5.06 ± 0.37	0.46 ± 0.28	1.52 ± 0.33	-1.24 ± 0.60	-0.06 ± 0.23	20.8

Note. 1) It is given in full format (rounded) from GCMT catalogue (rounded).

Table 6.6: CMT-components M_{ij} , values of isotropic part ξ and residuals ε

have zero trace). In the tables SMT solutions are coded as follows:

USGSW - The W-phase is used as raw data (seismogram segments from direct P wave to surface wave onsets) at regional and teleseismic distances, with filtering in a period range of 100-1000 s;

GCMT - the global catalogue of centroids and moment tensors. For calculations broadband seismograms are used at epicentral distances of $\sim 30^\circ$ to $\sim 90^\circ$. In this case, the body waves are used (with periods of > 50 s) and the mantle waves (with periods of > 200 s);

USGSC - a version of CMT by National Information Center (NEIC) of US Geological Survey. Medium- and long-period body and surface waves were used for the calculations.

Table 6.6 shows the SMT components obtained by inversions and error estimates by the least-squares method. For cases of USGSW and USGSC error estimates are not provided. Also this table shows the values of the isotropic part of the SMT, if it is not assumed to be equal to zero. Table 6.7 shows such calculated variables as: SMT eigenvalues, strike, dip, slip, scalar seismic moment M_0 for the best double couple (DC), discrepancy between SMT solution from DC - η , and also the value of moment magnitude M_W . All these values are given with error estimates. For cases of USGSW and USGSC error estimates are not available.

The duration of rupture process was estimated as 32 seconds. The calculation also gives an independent estimate of the depth, $h = 640$ km, which allowed to estimate the error of about ± 50 km. This estimate is consistent with other definitions given in Table 6.4. The duration value is consistent with the independent evaluation of ~ 30 s from the work of Ye *et al.* (2013). The value of the duration in the GCMT catalogue is $\tau = 71.4$ s, which is more than double our estimate. However, the GCMT estimate is not a result of direct fitting, but assigned by the magnitude using a correlation equation (Ekström *et al.*, 2012).

Code	Eigenvalues, $10^{21} N \cdot m$			Focal mechanism			η , %	M_0 10^{21} $N \cdot m$	M_W
				Planes ¹⁾		Rake ²⁾			
	E_1	E_2	E_3	φ (°)	δ (°)	λ_s (°)			
USGSW ³⁾	-4.00	0.31	3.67	12/184	81/10	-89/-98	12	3.84	8.3
GCMT	-4.13 ± 0.01	0.36 ± 0.01	3.76 ± 0.01	12/189 $\pm 0.1/1$	79/11 ± 0.1	-89/-93 $\pm 0.2/1$	14 \pm 0.3	3.96 ± 0.01	8.331 ± 0.001
USGSC ⁴⁾	-4.58	0.40	4.18	15/177	81/10	-87/-107	14	4.40	8.4
ES_1	-4.65 ± 0.45	0.02 ± 1.0	3.52 ± 0.66	22/207 $\pm 4/33$	76/14 $\pm 3/4$	-91/-84 $\pm 8/29$	14 \pm 24	4.09 ± 0.31	8.34 ± 0.02
ES14	-3.71 ± 0.51	1.30 ± 1.07	4.84 ± 0.67	25/246 $\pm 5/33$	80/13 $\pm 4/5$	-98/-50 $\pm 9/27$	17 \pm 22	4.27 ± 0.31	8.35 ± 0.02
ES35	-4.30 ± 0.37	0.25 ± 0.44	4.05 ± 0.31	23/238 $\pm 3/26$	83/9 $\pm 3/4$	-95/-55 $\pm 5/26$	9 \pm 16	4.17 ± 0.26	8.35 ± 0.02
ES25	-4.39 ± 0.36	0.14 ± 0.44	4.25 ± 0.32	24/240 $\pm 3/25$	83/9 $\pm 3/4$	-95/-53 $\pm 4/25$	5 \pm 15	4.32 ± 0.26	8.36 ± 0.02
ED35	-4.29 ± 0.09	0.42 ± 0.07	3.87 ± 0.09	16/188 $\pm 1/7$	82/8 $\pm 1/1$	-89/-98 $\pm 1/7$	15 \pm 3	4.08 ± 0.08	8.34 ± 0.01
ED36	-5.64 ± 0.51	0.35 ± 0.29	5.12 ± 0.45	17/213 $\pm 4/22$	85/5 $\pm 2/2$	-91/-74 $\pm 2/22$	11 \pm 8	5.38 ± 0.37	8.42 ± 0.02

Note.

1) The plane orientation is defined by two angles - the strike φ and dip δ (angle for the second plane is given after the slash);

2) rake λ_s - the angle in the focal plane between the strike direction and the slip vector (measured anti clockwise from the strike direction);

3) obtained by W-phase

(http://earthquake.usgs.gov/earthquakes/eventpage/usb000h4jh#moment-tensor?source=us&code=usb000h4jh_Mww);

4) CMT obtained by USGS NEIC

(http://earthquake.usgs.gov/earthquakes/eventpage/usb000h4jh#moment-tensor?source=us&code=pde20130524054448980_598_C_UCMT)

Table 6.7: Parameters of the Sea of Okhotsk earthquake: eigenvalues, mechanism, discrepancy between SMT solution and double couple η , scalar seismic moment M_0 , and moment magnitude M_W

For the ES_1 case (using co-seismic offsets, details are in Table 6.5) Figure 6.15 shows the focal mechanism, cones, characterizing error estimates, eigenvectors positions and the neutral axis and quantities for other cases of this study and those obtained by other agencies. All cases show similar solutions.

The M_0 values for all the cases are consistent. The only exception is the ED36 dynamic case. Input data used for ED36 (excluding S waves) are not sufficient enough.

Using seismological data parameters of the finite source, such as rupture velocity (V_r), duration time, rupture area were estimated by Ye *et al.* (2013). They found that the radiated seismic energy E_R is $E_R = 1.5 \times 10^{17}$ J, rupture velocity is $V_r = 4$ km/s, and average stress drop is $\Delta\sigma = 15$ MPa. The estimated slip distribution along the fault plane is heterogeneous, with an average slip of 1.9-2.3 m, and a maximum slip of 9.9 m. The rupture area is 180×60 km.

Another interpretation of GNSS data for the Sea of Okhotsk earthquake in terms of a dislocation model are described in Steblov *et al.* (2014) and Shestakov *et al.* (2014), using the shallow dipping plane of the GCMT focal mechanism. Shestakov's input data set is similar to ours; Steblov's data set is not as

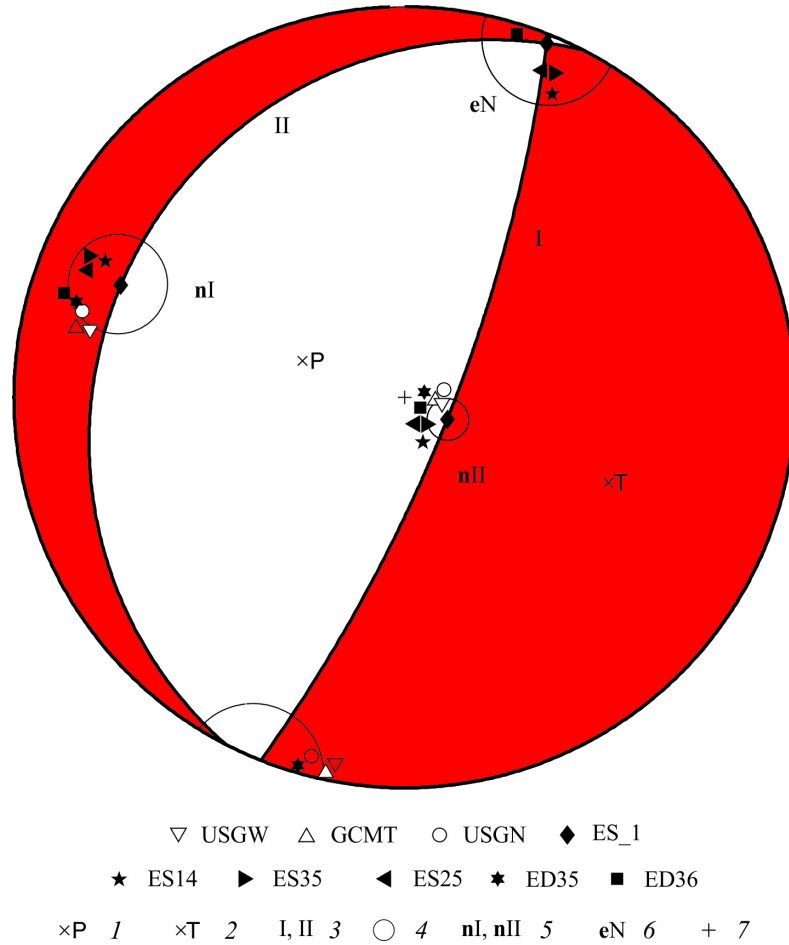


Figure 6.15: The mechanism for *ES_1* case on a stereogram of the lower hemisphere. 1, 2 - axis of stress and strain; 3 - nodal planes; 4 - projection of the part of focal sphere that belongs to a cone reflecting error estimates; eigenvectors position (5) and the neutral axis (6) for all the cases from Table 6.7; 7 - the center of projection. The value of the half-angle of the axial section of the cone equals to 6° for the cone at *nI*, 9° - at *nII* and 10° - at *eN*

dense for the Kamchatka part as the other two sets, but includes additional GNSS stations in the Kuril Islands. All three working groups use different methods to determine static offsets from raw data.

The individual determination of such values as fault area (A) and slip (D), instead of $A \cdot D$, is a challenging task as mentioned in Steblov *et al.* (2014). When the second plane, instead of the preferred one, of the GCMT focal mechanism is used for inversion, a similar misfit is found (Shestakov *et al.*, 2014). In general, observed data are not sufficient to distinguish the true plane orientation; with available GNSS data for this deep-focus earthquake, the only values confidently determined are parameters characterizing an equivalent point source. In other words, due to the focal depth and station network configuration, all the GNSS stations are in the far-field.

The fault center or the source point is (1) assumed as GCMT centroid (Shestakov *et al.*, 2014), (2) found for the best solution as about 60 km southeast from the GCMT centroid (Steblov *et al.*, 2014), or (3) assumed as NEIC PDE coordinates of the epicenter for the dynamic case and GCMT centroid for the static case (Abubakirov *et al.*, 2015); while the M_0 values are consistent: (1) $M_0 = 4.69 \cdot 10^{21} N \cdot m$, (2) $M_0 = 4.25 \cdot 10^{21} N \cdot m$, and (3) $M_0 = (4.08 - 4.32 \pm 0.31) \cdot 10^{21} N \cdot m$, respectively.

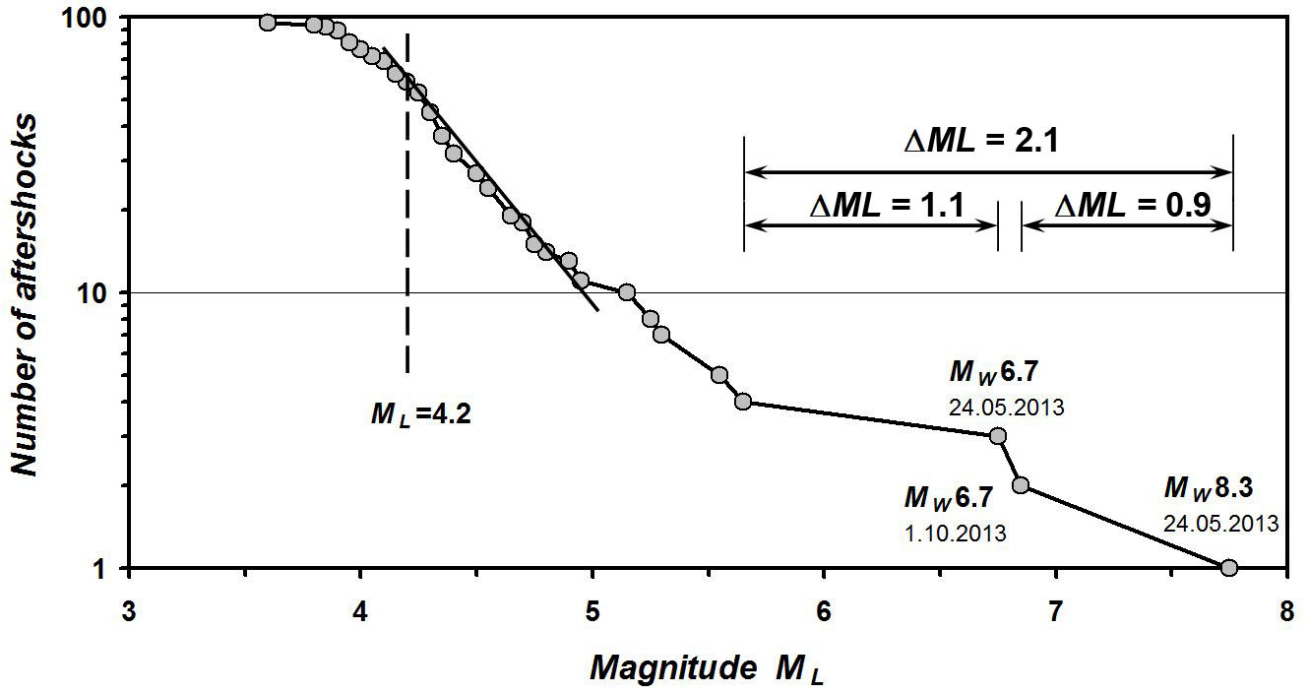


Figure 6.16: Cumulative frequency-magnitude plot for the aftershocks sequence of the May 24, 2013 earthquake with $M_W = 8.3$

6.3.3 Main features of the aftershock sequence

The aftershock sequence of the May 24, 2013 earthquake, $M_W = 8.3$, consists of 94 earthquakes with magnitudes in the range of $M_L = 3.8-6.9$. By its cumulative frequency-magnitude plot (Figure 6.16) the catalogue completeness threshold can be determined as $M_L = 4.2$, which corresponds to the left edge of the linear part of the curve. For further analysis 62 earthquakes that occurred prior to April 2014 were selected from the preliminary catalogue based on this threshold.

Figure 6.10 shows an ellipse containing 90% of the aftershocks for the first 14 hours after the major earthquake, allowing to estimate the rupture area of the May 24, 2013 earthquake, $M_W = 8.3$ as 400 km (length) \times 180 km (width).

According to the frequency-magnitude plot (Figure 6.16) the energy interval between the main event and the strongest aftershock $\Delta M_L = 0.9$ is comparable to the interval between the two strongest aftershocks and a relatively numerous group of aftershocks with a continuous energy distribution ($\Delta M_L = 1.1$).

Figure 6.17 shows the cumulative number of aftershocks over time in logarithmic time scale. The aftershock sequence can be divided into several stages based on the change of the slope of the plot.

First of all, it is necessary to exclude the initial stage with a duration of an hour and consisting of 6 aftershocks with magnitudes between $M_L = 4.4-5.3$ from consideration because we believe that powerful coda-waves of the main shock could have masked several events.

The remaining sequence of earthquakes can be divided into three stages, each of which is approximated by a straight line on the plot of Figure 6.17 that has a semi-log scale. This approximation corresponds to a hyperbolic decay of dN/dt where the slope of the line is represented by a proportionality coefficient A . Note that the last segment of the hyperbolic-law approximation is less reliable because of the small

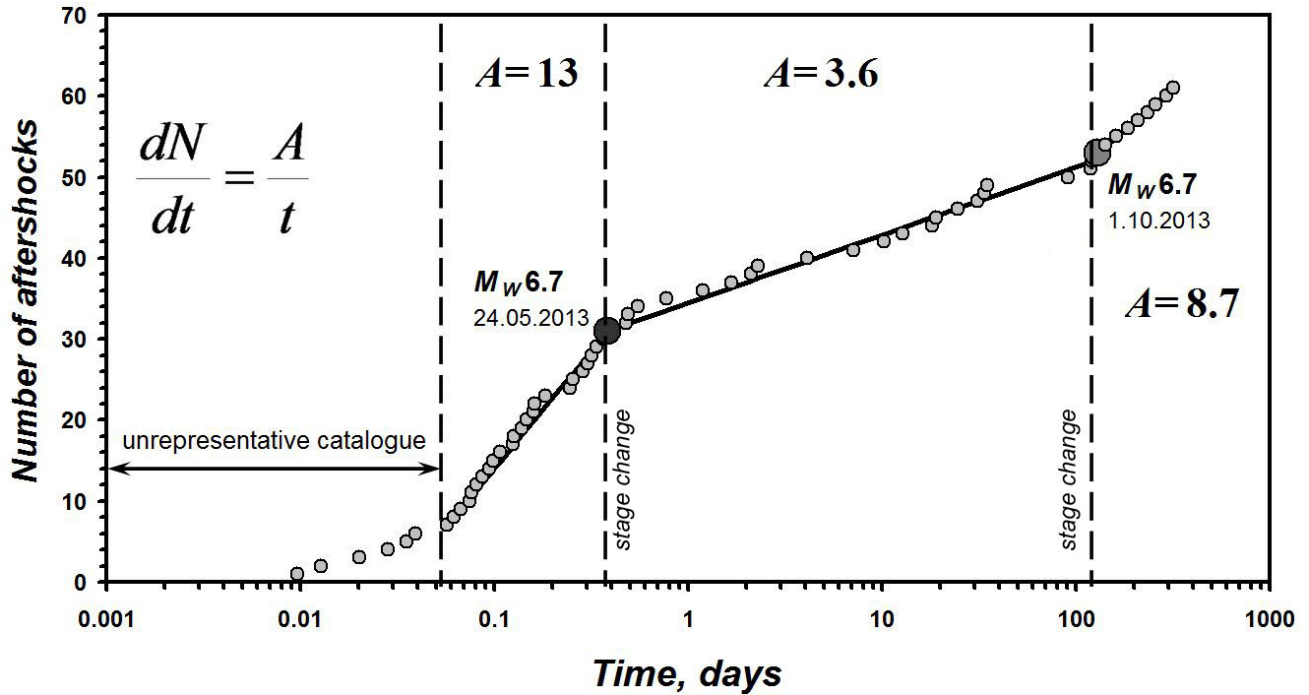


Figure 6.17: The typical stages of the aftershock process of the May 24, 2013 earthquake, $M_W = 8.3$. The starting point corresponds to the main event origin. Time bounds of the stages with linear trends are indicated.

amount of data.

A peculiar feature is the coincidence of the two stage changes and the two most powerful aftershocks with magnitude $M_W = 6.7$ each: on May 24, 2013 (9 hours after the main shock) and on October 01, 2013 (after >4 months). None of these earthquakes triggered its own aftershock sequence.

It should also be noted that the May 24, 2013 earthquake with $M_W = 6.7$ at the end of the most intense part of the aftershock sequence occurred outside the ellipse containing 90% of aftershocks of the $M_W = 8.3$ earthquake, and it can be alternatively qualified as a separate event, not as an aftershock in a narrow sense (№12 in Figure 6.10).

6.3.4 Macroseismic data

Macroseismic information was collected for 190 settlements. From various sources, 546 responses were processed, of which 90 messages of 29 sites were received through the Internet-based questionnaire (<http://www.emsd.ru/lisopol/poll.php>).

The Sea of Okhotsk earthquake on May 24, 2013 had a great area of macroseismic impact, while it nowhere had any catastrophic manifestations. This event was felt with intensities up to VI degrees on the MSK-64 scale in the settlements located from the epicenter at distances from 139 to 9470 km. In the northern hemisphere of the Earth on a significant part of Eurasia and North America its effect was reported in Russia, Kazakhstan, Japan, China, India, the United Arab Emirates, Poland, Canada, the USA, Mexico, Italy, Estonia and Kyrgyzstan; in the southern hemisphere - in Indonesia on the Java island.

In the Kamchatka area macroseismic data from 64 settlements, were collected. In 50 of them the earthquake was reported to be felt with intensities of II to VI degrees (Figure 6.18). The nearest site to the epicenter, Krutogorovo village, and other towns of the western coast of the Kamchatka Peninsula reported intensities of no more than IV degrees, with the exception of the Oktiabrsky village (I = V degrees). The strongest ground shaking was reported in areas of the eastern coast: I = VI degrees on the Semyachik meteorological station and in the Valley of Geysers, I = V-VI degrees at the Krugly lighthouse. Thus, the highest intensities were reported close to the deep sea trench. This feature is typical for deep island arcs earthquakes, and was first seen in the early 20th century for events in the Benioff zone in Japan (Utsu, 1966). It was concluded that this phenomenon was caused by large inhomogeneities within island arcs.

To collect macroseismic information for the Sea of Okhotsk earthquake outside of Kamchatka official requests were sent to the Russian Ministry of Emergency Situations, all the Branches of the Geophysical Service RAS and Siberian Branch of the Geophysical Survey RAS, The Schmidt Institute of Physics of the Earth RAS, Mining Institute of the Ural Branch of RAS and other scientific institutions in different regions of Russia. Letters were sent to fellow seismologists from Azerbaijan, Kyrgyzstan, Uzbekistan, Belarus, Moldova, as well as in Kazakhstan National Data Center with a kind request to provide all the available information about the manifestations of this earthquake. There were 17 responses received out of 29 requests sent. The most detailed information was sent by A. D. Zavyalov (IPE RAS), E. P. Semenova (Sakhalin Branch of GS RAS), N. A. Gileva (Baikal Branch of GS RAS), L.I. Karpenko (Magadan Branch of GS RAS), and R.A. Diagilev (Mining Institute of the Ural Branch of RAS, Perm). In addition, information was collected from a variety of news and other Internet resources. We express our sincere gratitude to all those who assisted in the collection of macroseismic data.

As a result, in addition to the Kamchatka region, macroseismic information was obtained from 82 settlements in the territory of Russia, of which 75 reported intensities from II to IV-V degrees. The earthquake was felt by the residents of the Far East (except Primorsky region, Figure 6.19), Siberian, Volga, Central, Southern, North Caucasus and the North-West Federal District (FD) of the Russian Federation.

In Russia, outside Kamchatka, the strongest ground shaking with I = IV-V degrees were reported at two sites: Severo-Kurilsk and Gornoe in the Sakhalin region. Shaking of the intensity of IV was felt in the city of Magadan and Klepka in the Magadan region, Ulegorsk, Aniva, Tymovskoe and Troitskoye in the Sakhalin region. In Moscow and Khabarovsk the earthquake intensity manifestations varied from II to IV, obviously, depending on the soil type and construction quality. In other Russian towns the earthquake was felt with almost equal intensity of about II to III. From Kazakhstan National Data Center macroseismic information was obtained for 7 settlements located on the territory of Kazakhstan, which allowed to specify the data featured at the US Geological Survey (USGS) (<http://earthquake.usgs.gov/earthquakes/dyfi/>).

According to information received from the Seismological Service of Moldova, Belarus and Azerbaijan, the earthquake in these countries was not felt. On the website of the European Mediterranean Seismological Centre (EMSC) (<http://www.emsc-csem.org/Earthquake/Testimonies/comments.php?id=318696>) testimonies of the Sea of Okhotsk earthquake from Estonia, Italy, Kyrgyzstan are available. However, intensities are not available.

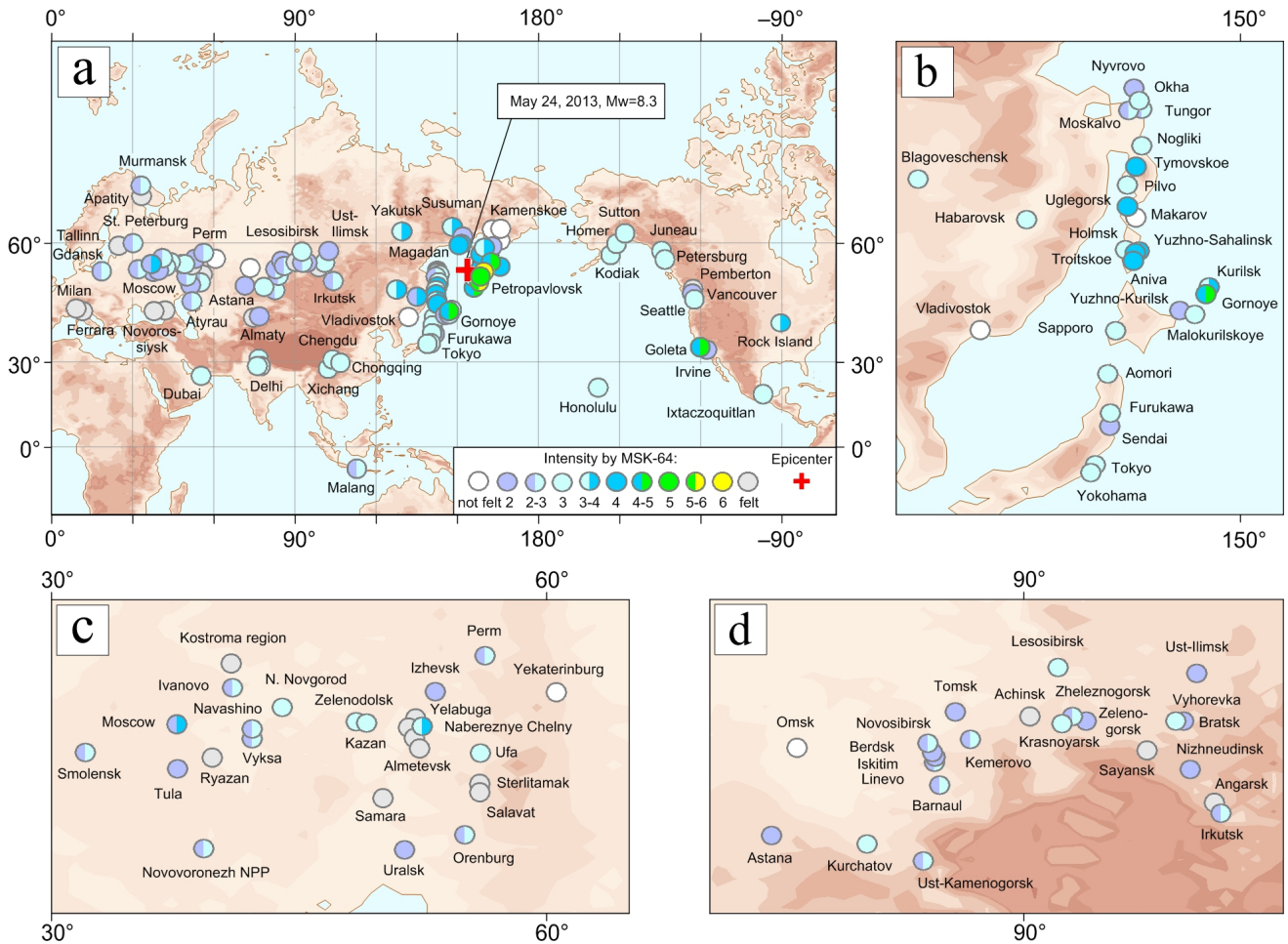


Figure 6.19: a) Macroseismic map of the Sea of Okhotsk earthquake on May 24, 2013 (MSK-64 intensity scale). More details: b) Japan - Sakhalin - Primorye, epicentral distances, $\Delta = 10\text{-}20^\circ$; (C) Central Russia - Ural, $\Delta = 50\text{-}60^\circ$; (G) Siberia - North Kazakhstan, $\Delta = 30\text{-}40^\circ$

Figure 6.19 also provides information about macroseismic manifestations in different areas of the world, compiled by the US Geological Survey (USGS) using their DYFI system (Did You Feel It?) (Wald *et al.*, 2011). Texts of received questionnaires were kindly provided to us by the USGS employee, D.J. Wald. The analysis of the text messages received allowed assessing ground shaking intensities at these sites using the MSK-64 scale (Medvedev *et al.*, 1965). In most reports the intensities do not exceed III. Only in the United States there were 2 sites with more notable shaking: the greatest intensity with I = IV-V degrees in Goleta and with I = III-IV degrees in the city of Rock Island, IL.

Thus, macroseismic effects of the 2013 Sea of Okhotsk earthquake were manifested globally. It was felt in almost all major cities of Russia and caused a considerable interest of seismologists. Macroseismic effects of the Sea of Okhotsk earthquake are studied in a number of papers, for example, Zhigalin *et al.* (2013), Tatevosian *et al.* (2014) and others. The most complete descriptions of the macroseismic impact worldwide are shown in Chebrov (2014) and Chebrova *et al.* (2015).

6.3.5 Conclusion

On May 24, 2013 under the Sea of Okhotsk in the area of responsibility of the Kamchatka regional seismological network, at a depth of 630 km the strongest earthquake recorded in the years of detailed observations (from 1961 to the present time) occurred with a magnitude of $M_W = 8.3$.

The main features of the deep-focus May 24, 2013 earthquake are:

- tectonic setting: the hypocentre is located at the north-eastern end of the Kuril-South-Kamchatka segment of the subducting Pacific plate;
- the main shock as well as the aftershocks are located near the depth limit of earthquake occurrence;
- abnormal range of macroseismic manifestations: the earthquake was felt at teleseismic distances in many settlements of Russia from Kamchatka to the territory of the East European Plain, as well as in countries of Asia (Japan, China, India and others), North America and Pacific;
- co-seismic offsets were observed at the majority of GNSS stations in Far East of Russia.

The parameters of the May 24, 2013 earthquake have been evaluated within 8 minutes from the time of registration of the earthquake within Urgent Message Service and SS TWS, which were sent to the Ministry of Emergency Situations and other relevant agencies.

In the preliminary stage macroseismic information was collected in the Kamchatka area, and the aftershock sequence was processed revealing several stages of the aftershock process.

From the aftershock distribution the rupture area of the May 24, 2013 earthquake is estimated as 400 km (length) \times 180 km (width) with a depth range of 425-720 km.

Estimates of focal mechanisms produced by various methods show similar solutions.

Despite the global macroseismic effect, in nearby settlements (Kamchatka region) the earthquake was felt with intensity of up to V-VI degrees and did not cause any damages.

6.4 References

- Abubakirov, I. R., Pavlov, V. M. and Titkov, N. N. (2015). The mechanism of the deep-focus, Sea of Okhotsk earthquake of May 24, 2013 as inferred from static displacements and broadband seismograms, *Journal of Volcanology and Seismology*, 9(4), 242-257, DOI: 10.1134/S0742046315040028.
- Bormann, P. (Ed.) (2002): *New Manual of Seismological Observatory Practice (NMSOP)*, IASPEI, GFZ GeoForschungsZentrum Potsdam, Potsdam, Vol. 1-2, DOI: 10.2312/GFZ.NMSOP-2.
- Chebrov, V. N., Droznin, D. V., Kugaenko, Yu. A., Levina, V. I., Senyukov, S. L., Sergeev, V. A., Shevchenko, Yu. V. and Yashchuk, V. V. (2013). The system of detailed seismological observations in Kamchatka in 2011, *Journal of Volcanology and Seismology*, 7(1), 16-36, DOI:10.1134/S0742046313010028.

- Chebrov V. N. (Ed.) (2014) *Strong earthquakes of Kamchatka in 2013*. Petropavlovsk-Kamchatsky: New Book Company, 2014. 252 p. ISBN 978-5-87750-298-7. [In Russian]
- Chebrova A. Yu., V. N. Chebrov, A. A. Gusev, A. V. Lander, E. M. Guseva, S. V. Mityushkina, and A. A. Raevskaya (2015) The Impacts of the M_W 8.3 Sea of Okhotsk Earthquake of May 24, 2013 in Kamchatka and Worldwide, *Journal of Volcanology and Seismology*, 9(4), p. 223-241, DOI:10.1134/S074204631504003X.
- Ekström, G., Nettles, M. and Dziewonski, A. M. (2012). The global CMT project 2004-2010: centroid-moment tensors for 13,017 earthquakes, *Phys. Earth Planet. Inter.*, 200, 1-9, DOI:10.1016/j.pepi.2012.04.002.
- Fedotov, S. A. (1972). *Energy classification of the Kuril-Kamchatka earthquakes and problem of magnitude determination*, Nauka. 117 p. [in Russian]
- Fedotov, S. A. and Shumilina, L. S. (1971). Seismic hazard of Kamchatka, *Izv. Akad. Nauk SSSR Fiz. Zemli.*, 9, 3-15.
- Fukushima, Y. and Tanaka, T. (1990) A new attenuation relation for peak horizontal acceleration of strong earthquake ground motion in Japan, *Bull. Seismol. Soc. Am.*, 80(4), 757-783.
- Godzikovskaya, A. A. (2010). Macroseismic descriptions and parameters of Kamchatka earthquakes that occurred during the preinstrumental period of observation, *Journal of Volcanology and Seismology*, 4(5), 354-366, DOI:10.1134/S0742046310050052.
- Gusev, A. A., Gordeev, E. I., Guseva, E. M., Petukhin, A. G. and Chebrov, V. N. (1997). The first version of the Amax (M_w , R) relationship for Kamchatka, *Pure and applied geophysics*, 149(2), 299-312, DOI:doi:10.1007/s000240050027.
- Gusev, A. A. and Shumilina, L. S. (2004). Recurrence of Kamchatka strong earthquakes on a scale of moment magnitudes, *Izvestiya Physics of the Solid Earth*, 40(3), 206-215.
- Kondorskaya, N. V. and Shebalin, N. V. (1977). New catalog of strong earthquakes in the territory of the USSR from ancient times to 1975, Academy of Sciences, Moscow (English translation, updated through 1977, available as Report SE-31, World Data Center A for Solid Earth Geophysics, NOAA, Boulder, CO, 1982, 606 p.)
- Krashennnikov, S. P. (1949). The description of land Kamchatka, reprinted by the USSR Academy of Sciences Press, Moscow. 840 p. [in Russian]
- Levina, V. I., Mityushkina, S. V., Lander, A. V. and Chebrova, A. Yu. (2013). The seismicity of the Kamchatka region: 1962-2011, *Journal of Volcanology and Seismology*, 7(1), 37-57, DOI:10.1134/S0742046313010053.
- Medvedev, S. V., Shponhoyer, V. and Karnik, V. (1965). Scale of seismic intensity MSK-64, *Academy of Science of USSR*, 11.
- Molchan, G. M. and Dmitrieva, O. E. (1991). Identification of aftershocks: review and new approaches, *Computational Seismology*, 24, 19-50.
- Pavlov, V. M. and Abubakirov, I. R. (2012). Algorithm for calculation of seismic moment tensor of

strong earthquakes using regional broadband seismograms of body waves, Bulletin of Kamchatka regional association «Educational-scientific center». *Earth sciences*, 2(20), 149-158 [in Russian].

Pavlov, V. M. (2013). Algorithm for calculating synthetic seismograms in a layered half-space with application of matrix impedance, *Izvestiya Physics of the Solid Earth*, 49(1), 24-33,

DOI:10.1134/S1069351313010102.

Shestakov, N. V., Ohzono, M., Takahashi, H., Gerasimenko, M. D., Bykov, V. G., Gordeev, E. I., Chebrov, V. N., Titkov, N. N., Serovetnikov, S. S., Vasilenko, N. F., Prytkov, A. S., Sorokin, A. A., Serov, M. A., Kondratyev, M. N. and Pupatenko, V. V. (2014). Modeling of coseismic crustal movements initiated by the May 24, 2013, $M_W = 8.3$ Okhotsk deep focus earthquake, *Doklady Earth Sciences*, 457(2), 976-981, DOI:10.1134/S1028334X1408008X.

Steblov, G. M., Ekström, G., Kogan, M. G., Freymueller, J. T., Titkov, N. N., Vasilenko, N. F., Nettles, M., Gabsatarov, Yu. V., Prytkov, A. S., Frolov, D. I. and Kondratyev, M. N. (2014). First geodetic observations of a deep earthquake: The 2013 Sea of Okhotsk M_w 8.3, 611 km-deep, event, *Geophys. Res. Lett.*, 41, 3826-3832, DOI:10.1002/2014GL060003.

Tatevossian, R. E., Kosarev, G. L., Bykov, V. V., Maciejewski, S. A., Ulomov, I. V., Aptekman, Z. Y. and Vakarchuk, R. N. (2014). Deep earthquake with $M_W = 8.3$ was felt at a distance of 6500 km, *Izvestiya Physics of the Solid Earth*, 3, 154-162, DOI:10.1134/S1069351314030124.

Utsu, T. (1966). Regional differences in absorption of seismic waves in the upper mantle as inferred from abnormal distributions of seismic intensities, *Geophysics*, 2(4), 359-374.

Wald, D. J., Quitoriano, V., Dengler, L. A. and Dewey, J. W. (1999). Utilization of the Internet for rapid community intensity maps, *Seismological Research Letters*, 70(6), 680-697, DOI:10.1785/gssrl.70.6.680.

Ye, L., Lay, T., Kanamori, H. and Koper, K. D. (2013). Energy release of the 2013 $M_W = 8.3$ Sea of Okhotsk earthquake and deep slab stress heterogeneity, *Science*, 341(6152), 1380-1384, DOI:10.1126/science.1242032.

Zhigalin, A. D., Zav'yalov, A. D., Mindel', I. G., Nikonov, A. A., Popova, O. G., Rogozhin, E. A., Ruzaiкин, A. I. and Sevost'yanov, V. V. (2014). The phenomenon of the Sea of Okhotsk Earthquake of May 24, 2013, in Moscow, *Herald of the Russian Academy of Sciences*, 84(4), 283-291, DOI:10.1134/S1019331614040

7

Statistics of Collected Data

7.1 Introduction

The ISC Bulletin is based on the parametric data reports received from seismological agencies around the world. With rare exceptions, these reports include the results of waveform review done by analysts at network data centres and observatories. These reports include combinations of various bulletin elements such as event hypocentre estimates, moment tensors, magnitudes, event type and felt and damaging data as well as observations of the various seismic waves recorded at seismic stations.

Data reports are received in different formats that are often agency specific. Once an authorship is recognised, the data are automatically parsed into the ISC database and the original reports filed away to be accessed when necessary. Any reports not recognised or processed automatically are manually checked, corrected and re-processed. This chapter describes the data that are received at the ISC before the production of the reviewed Bulletin.

Notably, the ISC integrates all newly received data reports into the automatic ISC Bulletin (available on-line) soon after these reports are made available to ISC, provided it is done before the submission deadline that currently stands at 12 months following an event occurrence.

With data constantly being reported to the ISC, even after the ISC has published its review, the total data shown as collected, in this chapter, is limited to two years after the time of the associated reading or event, i.e. any hypocentre data collected two years after the event are not reflected in the figures below.

7.2 Summary of Agency Reports to the ISC

A total of 145 agencies have reported data for July 2013 to December 2013. The parsing of these reports into the ISC database is summarised in Table 7.1.

	Number of reports
Total collected	2857
Automatically parsed	2014
Manually parsed	843

Table 7.1: Summary of the parsing of reports received by the ISC from a total of 145 agencies, containing data for this summary period.

Data collected by the ISC consists of multiple data types. These are typically one of:

- Bulletin, hypocentres with associated phase arrival observations.

- Catalogue, hypocentres only.
- Unassociated phase arrival observations.

In Table 7.2, the number of different data types reported to the ISC by each agency is listed. The number of each data type reported by each agency is also listed. Agencies reporting indirectly have their data type additionally listed for the agency that reported it. The agencies reporting indirectly may also have ‘hypocentres with associated phases’ but with no associated phases listed - this is because the association is being made by the agency reporting directly to the ISC. Summary maps of the agencies and the types of data reported are shown in Figure 7.1 and Figure 7.2.

Table 7.2: Agencies reporting to the ISC for this summary period. Entries in bold are for new or renewed reporting by agencies since the previous six-month period.

Agency	Country	Directly or indirectly reporting (D/I)	Hypocentres with associated phases	Hypocentres without associated phases	Associated phases	Unassociated phases	Amplitudes
TIR	Albania	D	320	14	3255	154	0
CRAAG	Algeria	D	393	0	1765	335	0
LPA	Argentina	D	0	0	0	385	0
SJA	Argentina	D	4169	29	78735	0	16371
NSSP	Armenia	D	88	3	785	0	0
AUST	Australia	D	786	12	18131	0	0
IDC	Austria	D	14651	0	379566	0	299782
VIE	Austria	D	4683	67	42498	184	41111
AZER	Azerbaijan	D	179	0	6524	0	0
BELR	Belarus	D	0	0	0	2866	612
UCC	Belgium	D	0	0	0	4736	865
SCB	Bolivia	D	43	0	1005	0	111
RHSSO	Bosnia-Herzegovina	D	732	0	12689	7775	0
VAO	Brazil	D	659	0	16030	0	0
SOF	Bulgaria	D	463	1	2476	2027	0
OTT	Canada	D	1208	66	36156	0	2232
PGC	Canada	I OTT	869	0	26212	0	0
GUC	Chile	D	3086	100	64878	1421	16974
BJI	China	D	2336	19	106671	23935	66199
ASIES	Chinese Taipei	D	0	48	0	0	0
TAP	Chinese Taipei	D	20105	14	669658	0	0
RSNC	Colombia	D	6560	7	151831	22684	48091
ICE	Costa Rica	I UCR	0	1	0	0	0
UCR	Costa Rica	D	1027	6	17192	190	749
ZAG	Croatia	D	0	0	0	38823	0
SSNC	Cuba	D	88	0	1266	0	0
NIC	Cyprus	D	363	0	7769	48	3897
IPEC	Czech Republic	D	441	0	2773	22361	1311
PRU	Czech Republic	D	3839	0	38107	262	10273
WBNET	Czech Republic	D	192	0	3453	0	3448
DNK	Denmark	D	0	76	0	6391	1853
ARO	Djibouti	D	27	0	275	0	0
OSPL	Dominican Republic	D	264	10	3064	3	0
IGQ	Ecuador	D	151	0	4847	0	0
HLW	Egypt	D	203	4	1846	0	0
SNET	El Salvador	D	1273	21	19536	66	3473
SSS	El Salvador	I UCR	0	2	0	0	0
EST	Estonia	I HEL	300	0	0	0	0
AAE	Ethiopia	D	43	1	324	467	0
SKO	FYR Macedonia	D	1431	1	19675	3115	4281
FIA0	Finland	I HEL	117	11	0	0	0
HEL	Finland	D	5564	3011	100369	0	16130

Table 7.2: (continued)

Agency	Country	Directly or indirectly reporting (D/I)	Hypocentres with associated phases	Hypocentres without associated phases	Associated phases	Unassociated phases	Amplitudes
CSEM	France	I BJI	1445	370	0	0	0
LDG	France	D	2355	48	51942	8	20634
STR	France	D	926	0	11965	0	0
PPT	French Polynesia	D	1276	10	10182	607	10757
TIF	Georgia	D	0	384	0	7354	0
AWI	Germany	D	2465	1	9534	91	0
BGR	Germany	D	149	213	6192	0	181
BNS	Germany	I BGR	3	23	0	0	0
BRG	Germany	D	0	0	0	5237	3955
BUG	Germany	I BGR	8	0	0	0	0
CLL	Germany	D	6	0	74	8096	2636
GDNRW	Germany	I BGR	2	15	0	0	0
GFZ	Germany	I NEIC	21	1	0	0	0
LEDBW	Germany	I BGR	16	8	0	0	0
ATH	Greece	D	13286	12	402911	0	134152
THE	Greece	D	5130	39	116291	7144	35202
GCG	Guatemala	D	1032	0	6333	0	0
HKC	Hong Kong	D	0	0	0	22	0
BUD	Hungary	D	0	1	0	6623	0
REY	Iceland	D	24	0	799	0	0
HYB	India	D	605	164	1548	13	258
NDI	India	D	630	451	16186	7818	5659
DJA	Indonesia	D	3003	61	55783	0	38866
TEH	Iran	D	646	54	24092	0	6053
THR	Iran	D	629	30	4791	0	1421
ISN	Iraq	D	427	0	3962	12	873
GII	Israel	D	422	0	7700	0	0
GEN	Italy	D	1904	1	16994	2964	0
MED_RCMT	Italy	D	0	158	0	0	0
OSUB	Italy	D	0	0	0	1591	0
RISSC	Italy	D	16	0	218	0	0
ROM	Italy	D	14082	150	804900	405539	549892
TRI	Italy	D	0	0	0	5511	0
LIC	Ivory Coast	D	866	0	2772	0	1768
JSN	Jamaica	D	95	0	671	0	1
JMA	Japan	D	66247	0	566316	906	0
MAT	Japan	D	0	0	0	8282	0
NIED	Japan	D	0	794	0	0	0
SYO	Japan	D	0	0	0	4616	0
JSO	Jordan	D	930	49	6307	0	7416
NNC	Kazakhstan	D	9076	1	102433	0	96016
SOME	Kazakhstan	D	4848	240	64070	0	61925
KNET	Kyrgyzstan	D	1375	0	11784	0	2393
KRNET	Kyrgyzstan	D	4276	0	70336	0	0
LVSN	Latvia	D	295	0	3408	0	1717
GRAL	Lebanon	D	365	0	2521	418	0
LIT	Lithuania	D	197	197	2506	2750	2026
MCO	Macao, China	D	0	0	0	48	0
GSDM	Malawi	D	0	0	0	234	0
KLM	Malaysia	D	396	0	1814	0	0
ECX	Mexico	D	629	11	8724	0	1424
MEX	Mexico	D	3198	145	24836	0	1
MOLD	Moldova	D	0	0	0	2112	761
PDG	Montenegro	D	345	0	8118	0	4252
CNRM	Morocco	D	1852	15	19758	0	0
NAM	Namibia	D	9	0	41	0	0
DMN	Nepal	D	1888	0	18374	0	13846
DBN	Netherlands	D	0	8	0	1291	283
WEL	New Zealand	D	2019	13	114298	171	74334
INET	Nicaragua	I UCR	0	1	0	0	0
BER	Norway	D	2047	1922	38619	2270	7960
NAO	Norway	D	2512	1166	6976	0	2046

Table 7.2: (continued)

Agency	Country	Directly or indirectly reporting (D/I)	Hypocentres with associated phases	Hypocentres without associated phases	Associated phases	Unassociated phases	Amplitudes
OMAN	Oman	D	697	0	13136	0	0
MSSP	Pakistan	D	0	0	0	1034	0
UPA	Panama	D	338	0	6514	0	61
ARE	Peru	I NEIC	17	32	0	0	0
LIM	Peru	I IRIS	2	2	0	0	0
MAN	Philippines	D	0	2524	0	54920	17902
QCP	Philippines	D	0	0	0	166	0
WAR	Poland	D	0	0	0	23069	700
IGIL	Portugal	D	618	3	2655	7	871
INMG	Portugal	D	1233	0	34557	2194	11555
PDA	Portugal	I NEIC	0	1	13	0	0
SVSA	Portugal	D	528	0	8998	3178	4113
KMA	Republic of Korea	D	40	0	439	0	0
BUC	Romania	D	1353	10	22696	77439	9238
ASRS	Russia	D	150	58	5895	0	1933
BYKL	Russia	D	125	2	11071	0	3532
CMWS	Russia	I MOS	0	5	0	0	0
DRS	Russia	I MOS	72	154	0	0	0
IDG	Russia	I MOS	0	284	0	0	0
IEPN	Russia	D	174	1	1389	1878	884
KOLA	Russia	D	166	228	630	0	0
KRAR	Russia	I MOS	0	268	0	0	0
KRSC	Russia	D	531	0	19018	0	0
MIRAS	Russia	D	67	45	527	0	265
MOS	Russia	D	2276	1558	356496	0	128793
NERS	Russia	D	26	57	779	0	365
NORS	Russia	I MOS	54	207	0	0	0
SKHL	Russia	D	619	624	16319	0	8148
VLA	Russia	I MOS	0	66	0	0	0
YARS	Russia	D	837	837	12519	0	7843
SGS	Saudi Arabia	D	24	24	370	0	0
BEO	Serbia	D	1481	1	28956	0	1
BRA	Slovakia	D	0	0	0	22550	0
LJU	Slovenia	D	1392	731	20062	3725	6362
HNR	Solomon Islands	D	0	0	0	1070	0
PRE	South Africa	D	924	0	13718	0	4574
IAG	Spain	D	0	8	0	0	0
MDD	Spain	D	3194	7	98891	0	66414
MRB	Spain	D	425	0	10936	0	4134
SFS	Spain	D	536	0	3424	484	0
UPP	Sweden	D	1197	1484	13325	0	0
ZUR	Switzerland	D	418	21	6062	0	2427
NSSC	Syria	D	466	0	4665	26	2185
BKK	Thailand	D	1841	320	11415	0	12370
TRN	Trinidad and Tobago	D	13	881	577	28521	0
TUN	Tunisia	D	41	0	205	0	0
DDA	Turkey	D	9601	2	153643	18436	52619
ISK	Turkey	D	7950	16	113897	6577	70061
AEIC	U.S.A.	I NEIC	1420	168	31131	0	0
ANF	U.S.A.	I IRIS	1925	852	0	0	0
BRK	U.S.A.	I NEIC	0	0	0	0	0
BUT	U.S.A.	I NEIC	31	10	0	0	0
CERI	U.S.A.	I NEIC	25	8	0	0	0
GCMT	U.S.A.	D	0	2737	0	0	0
HON	U.S.A.	I NEIC	0	16	0	0	0
HVO	U.S.A.	I NEIC	80	5	0	0	0
IRIS	U.S.A.	D	3730	2737	295644	0	0
LDO	U.S.A.	I NEIC	4	6	0	0	0
NCEDC	U.S.A.	I NEIC	413	71	17069	0	0
NEIC	U.S.A.	D	14305	7401	1034375	0	430051

Table 7.2: (continued)

Agency	Country	Directly or indirectly reporting (D/I)	Hypocentres with associated phases	Hypocentres without associated phases	Associated phases	Unassociated phases	Amplitudes
OGSO	U.S.A.	I NEIC	3	1	0	0	0
PAL	U.S.A.	I IRIS	1	0	0	0	0
PAS	U.S.A.	I NEIC	204	39	2454	0	0
PMR	U.S.A.	I NEIC	0	43	0	0	0
PNNL	U.S.A.	I NEIC	0	1	0	0	0
PNSN	U.S.A.	D	0	153	0	0	0
REN	U.S.A.	I NEIC	55	20	0	0	0
RSPR	U.S.A.	D	1940	16	24351	0	0
SCEDC	U.S.A.	I IRIS	238	114	0	0	0
SEA	U.S.A.	I NEIC	60	2	927	0	0
SLC	U.S.A.	I IRIS	1	0	0	0	0
SLM	U.S.A.	I NEIC	21	1	0	0	0
TUL	U.S.A.	I NEIC	203	2	6	0	0
UAF	U.S.A.	D	0	1	0	0	0
UUSS	U.S.A.	I NEIC	44	1	0	0	0
WES	U.S.A.	I NEIC	8	1	0	0	0
SIGU	Ukraine	D	81	81	1983	0	716
DSN	United Arab Emirates	D	576	0	6762	0	0
BGS	United Kingdom	D	290	22	10131	67	3994
EAF	Unknown	D	753	5	4639	10008	0
SIK	Unknown	D	0	98	0	0	0
UNK	Unknown	I ASRS	432	230	5896	0	0
CAR	Venezuela	I NEIC	1	1	0	0	0
PLV	Vietnam	D	8	0	104	0	47
LSZ	Zambia	D	176	0	593	97	35
BUL	Zimbabwe	D	346	1	2087	1331	0

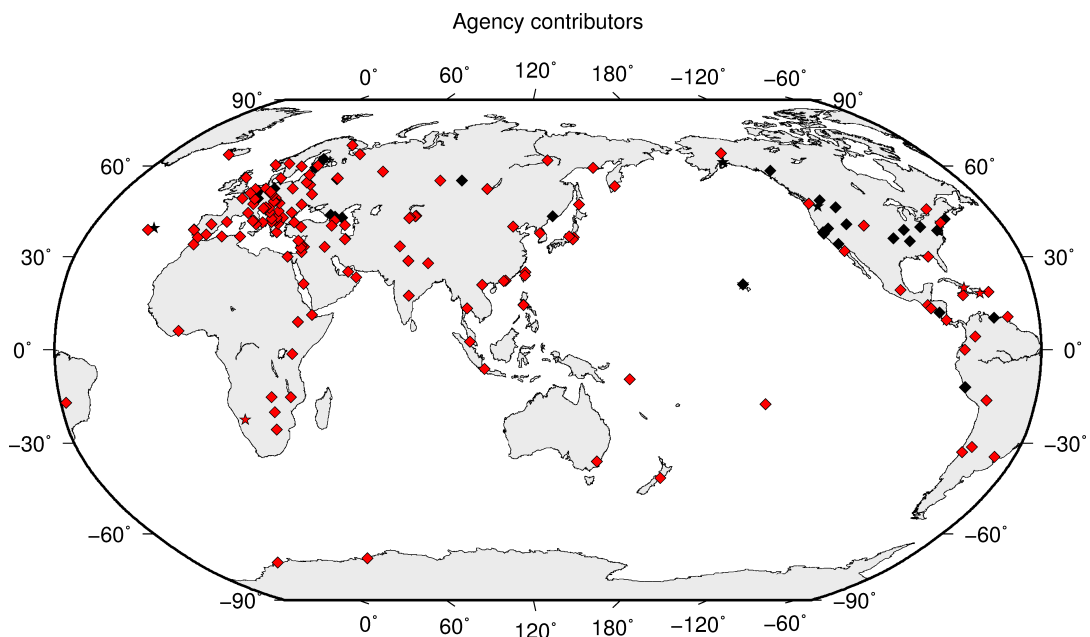


Figure 7.1: Map of agencies that have contributed data to the ISC for this summary period. Agencies that have reported directly to the ISC are shown in red. Those that have reported indirectly (via another agency) are shown in black. Any new or renewed agencies, since the last six-month period, are shown by a star. Each agency is listed in Table 7.2.

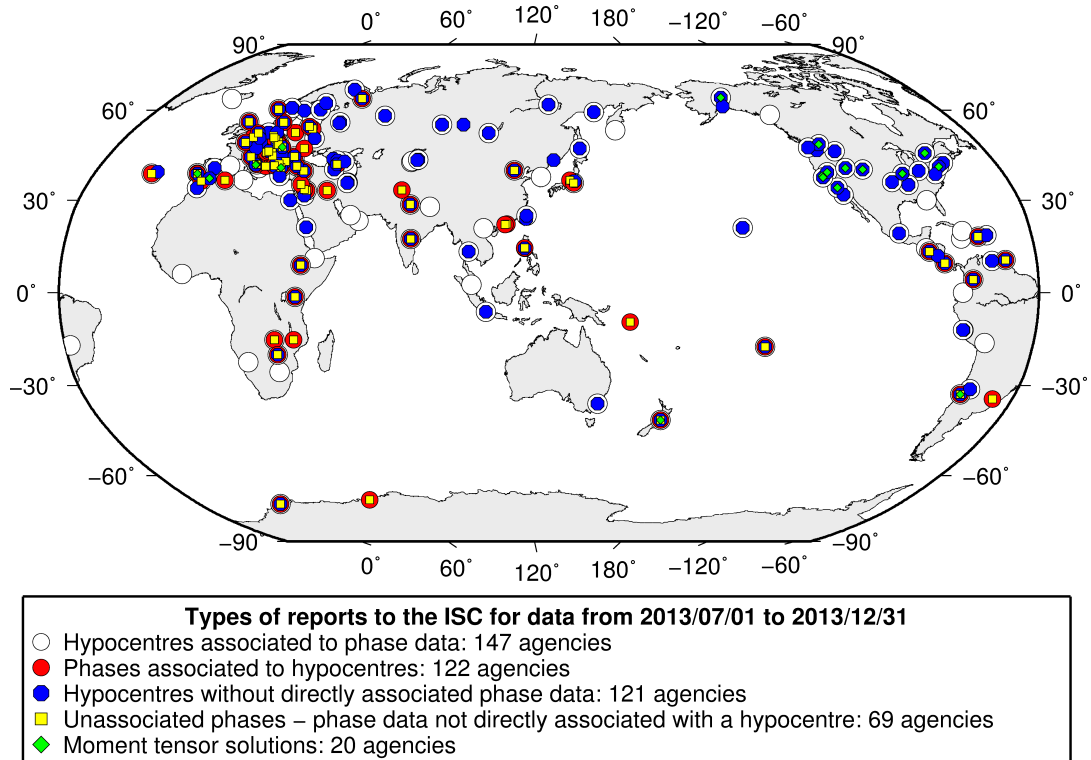


Figure 7.2: Map of the different data types reported by agencies to the ISC. A full list of the data types reported by each agency is shown in Table 7.2.

7.3 Arrival Observations

The collection of phase arrival observations at the ISC has increased dramatically with time. The increase in reported phase arrival observations is shown in Figure 7.3.

The reports with phase data are summarised in Table 7.3. This table is split into three sections, providing information on the reports themselves, the phase data, and the stations reporting the phase data. A map of the stations contributing these phase data is shown in Figure 7.4.

The ISC encourages the reporting of phase arrival times together with amplitude and period measurements whenever feasible. Figure 7.5 shows the percentage of events for which phase arrival times from each station are accompanied with amplitude and period measurements.

Figure 7.6 indicates the number of amplitude and period measurement for each station.

Together with the increase in the number of phases (Figure 7.3), there has been an increase in the number of stations reported to the ISC. The increase in the number of stations is shown in Figure 7.7. This increase can also be seen on the maps for stations reported each decade in Figure 7.8.

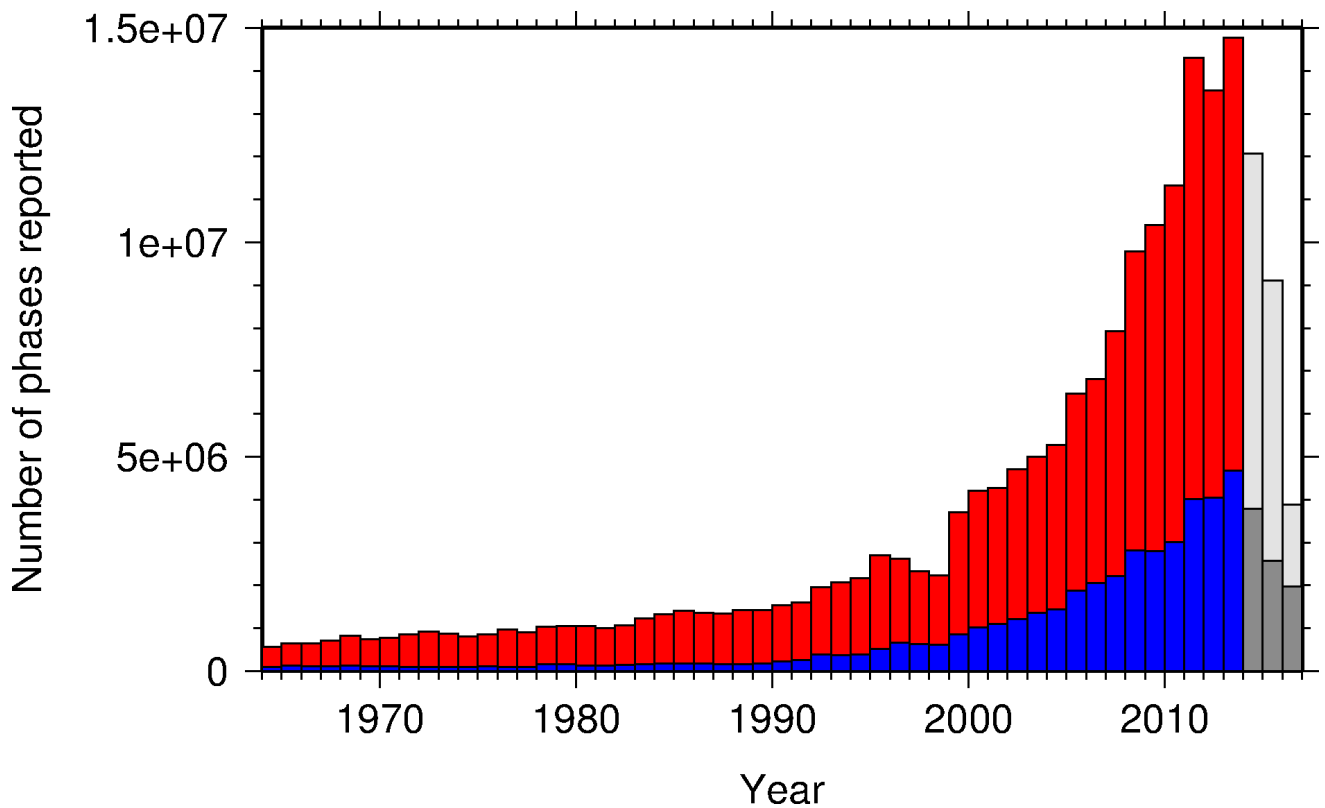
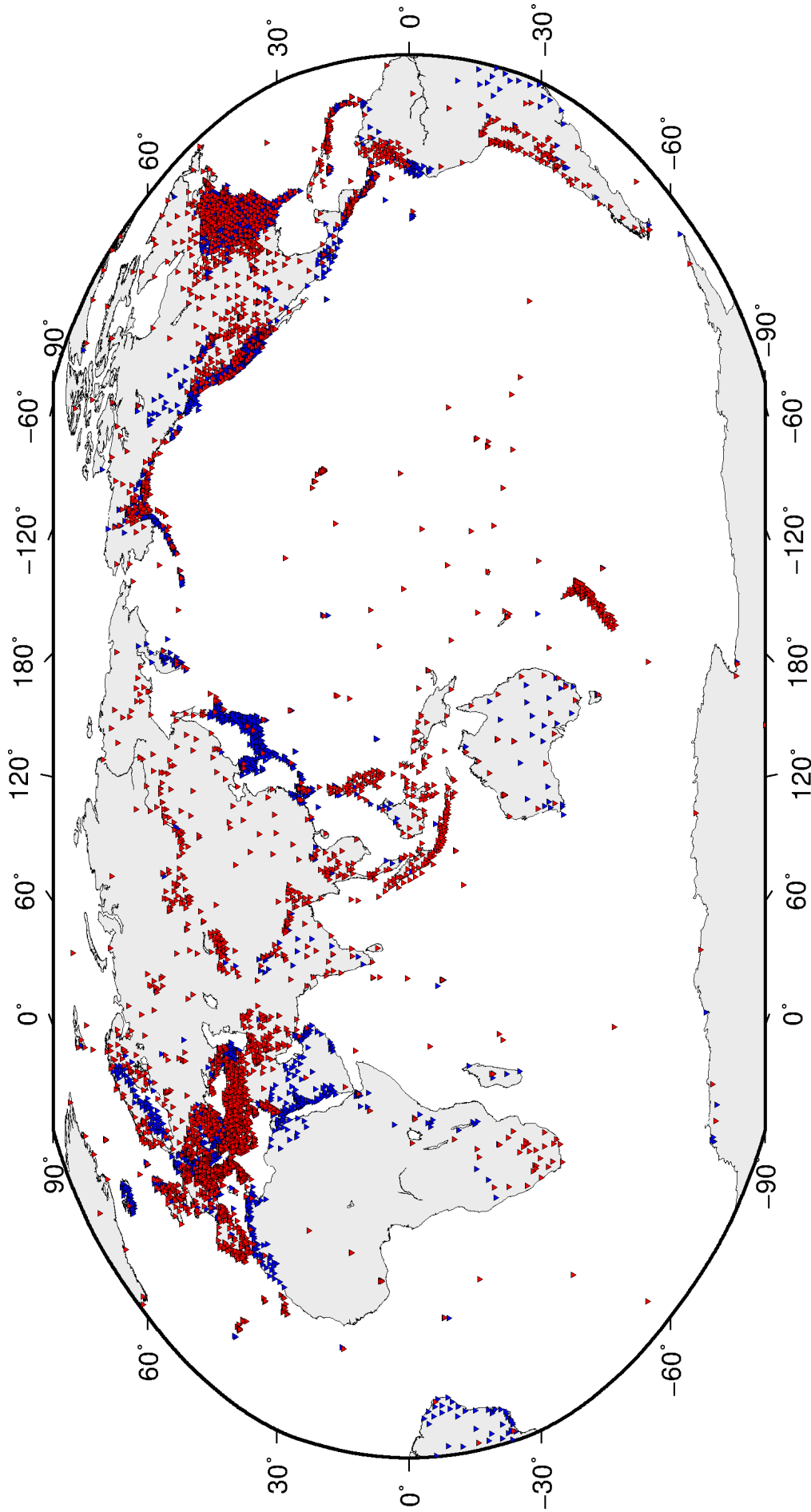


Figure 7.3: Histogram showing the number of phases (red) and number of amplitudes (blue) collected by the ISC for events each year since 1964. The data in grey covers the current period where data are still being collected before the ISC review takes place and is accurate at the time of publication.

Reports with phase arrivals	2533
Reports with phase arrivals including amplitudes	704
Reports with only phase arrivals (no hypocentres reported)	252
Total phase arrivals received	7593109
Total phase arrival-times received	6780895
Number of duplicate phase arrival-times	706569 (10.4%)
Number of amplitudes received	2475061
Stations reporting phase arrivals	7268
Stations reporting phase arrivals with amplitude data	3974
Max number of stations per report	1928

Table 7.3: Summary of reports containing phase arrival observations.



Phase arrival data were collected by the ISC from 7268 stations
for readings from 2013/07/01 to 2013/12/31

Figure 7.4: Stations contributing phase data to the ISC for readings from July 2013 to the end of December 2013. Stations in blue provided phase arrival times only; stations in red provided both phase arrival times and amplitude data.

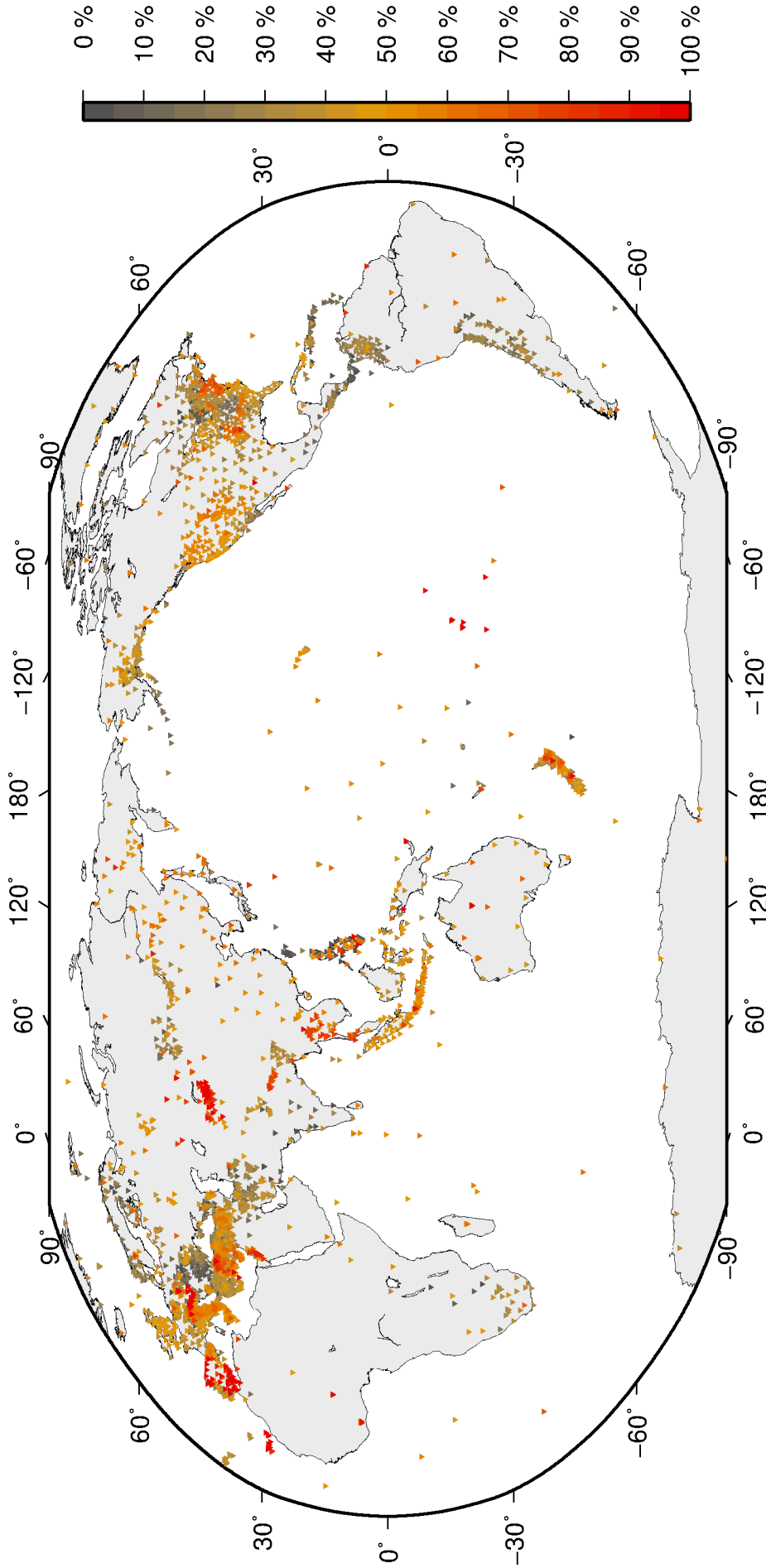
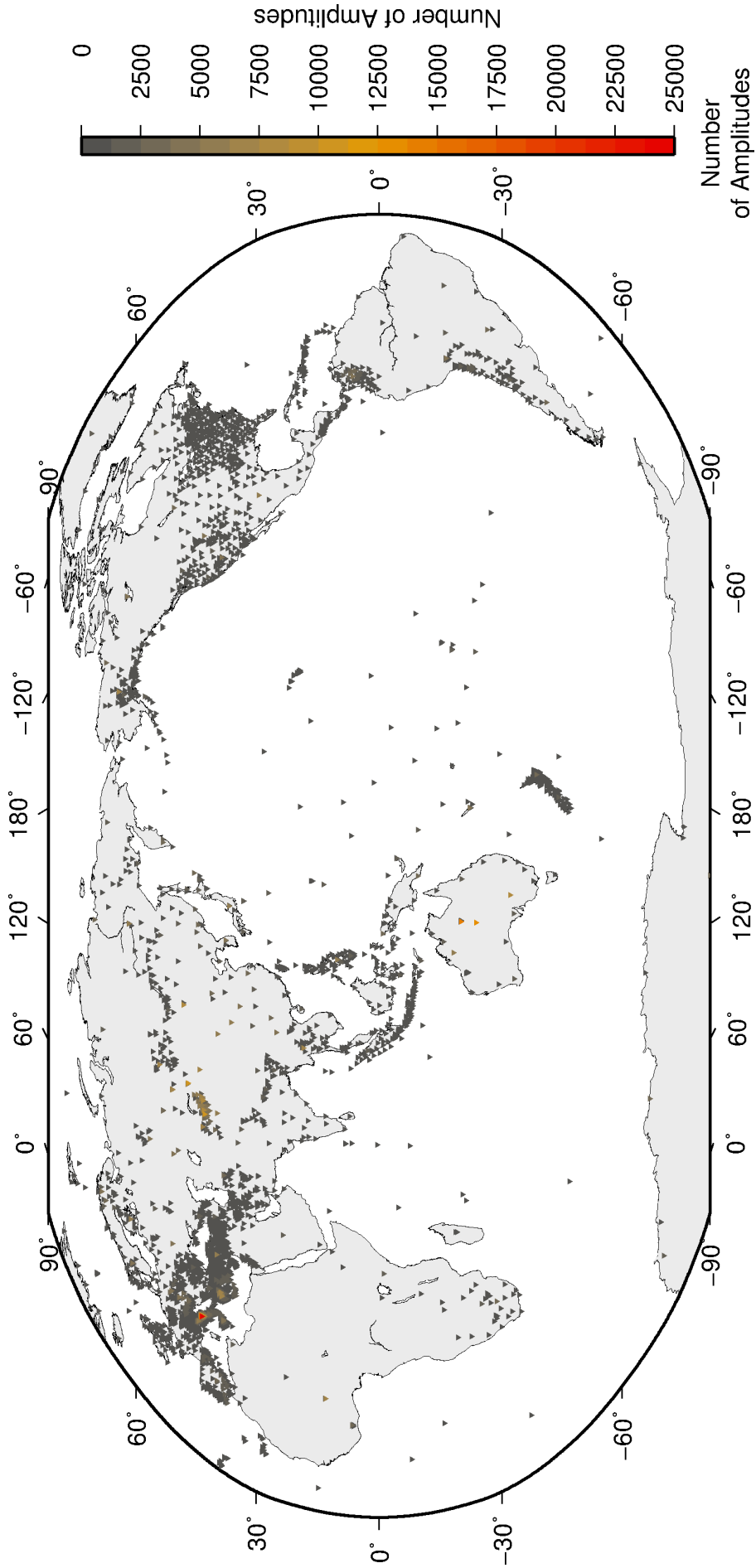


Figure 7.5: Percentage of events for which phase arrival times from each station are accompanied with amplitude and period measurements.



Amplitude data were collected by the ISC from **3932** stations sent by **83** agencies for readings from **2013/07/01** to **2013/12/31**

Figure 7.6: Number of amplitude and period measurements for each station.

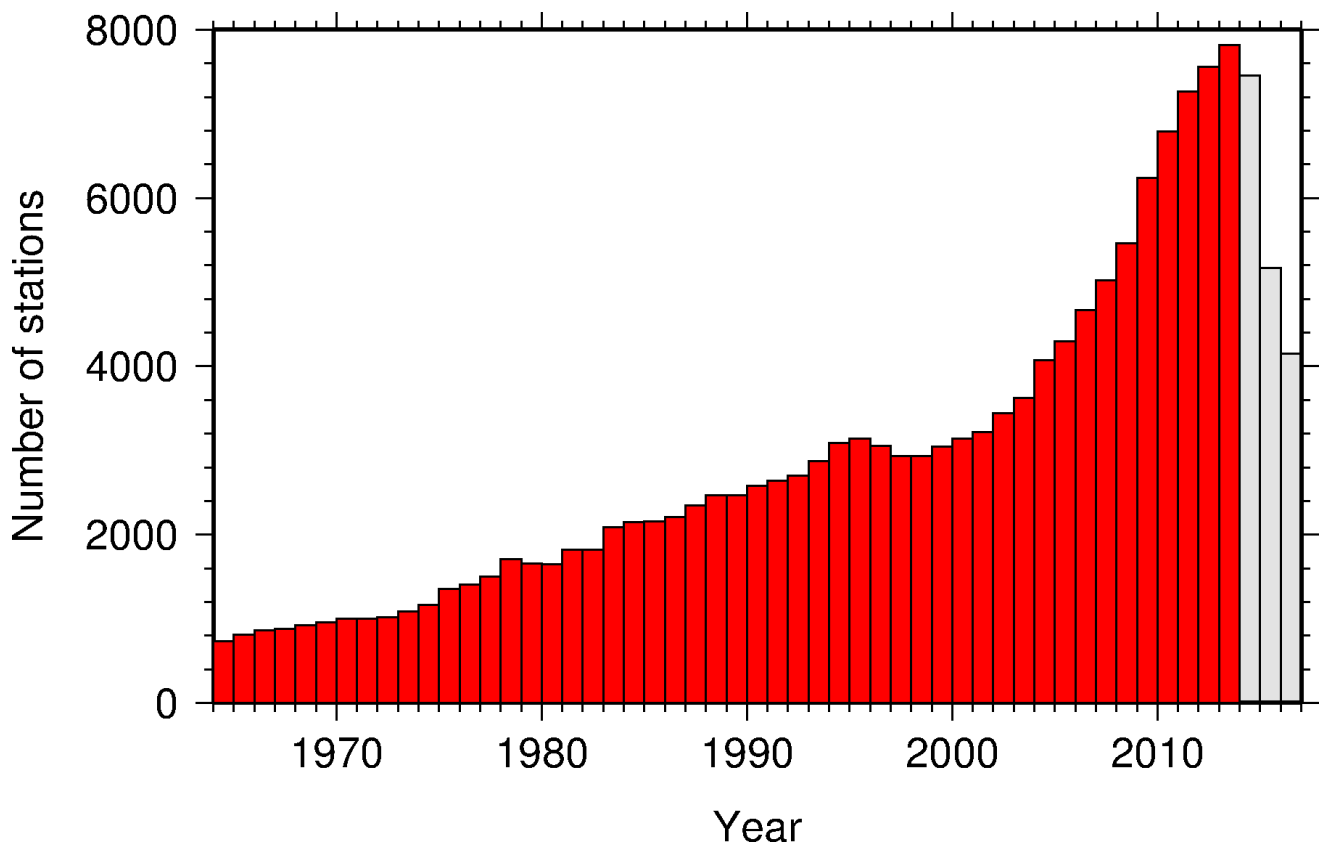


Figure 7.7: Histogram showing the number of stations reporting to the ISC each year since 1964. The data in grey covers the current period where station information is still being collected before the ISC review of events takes place and is accurate at the time of publication.

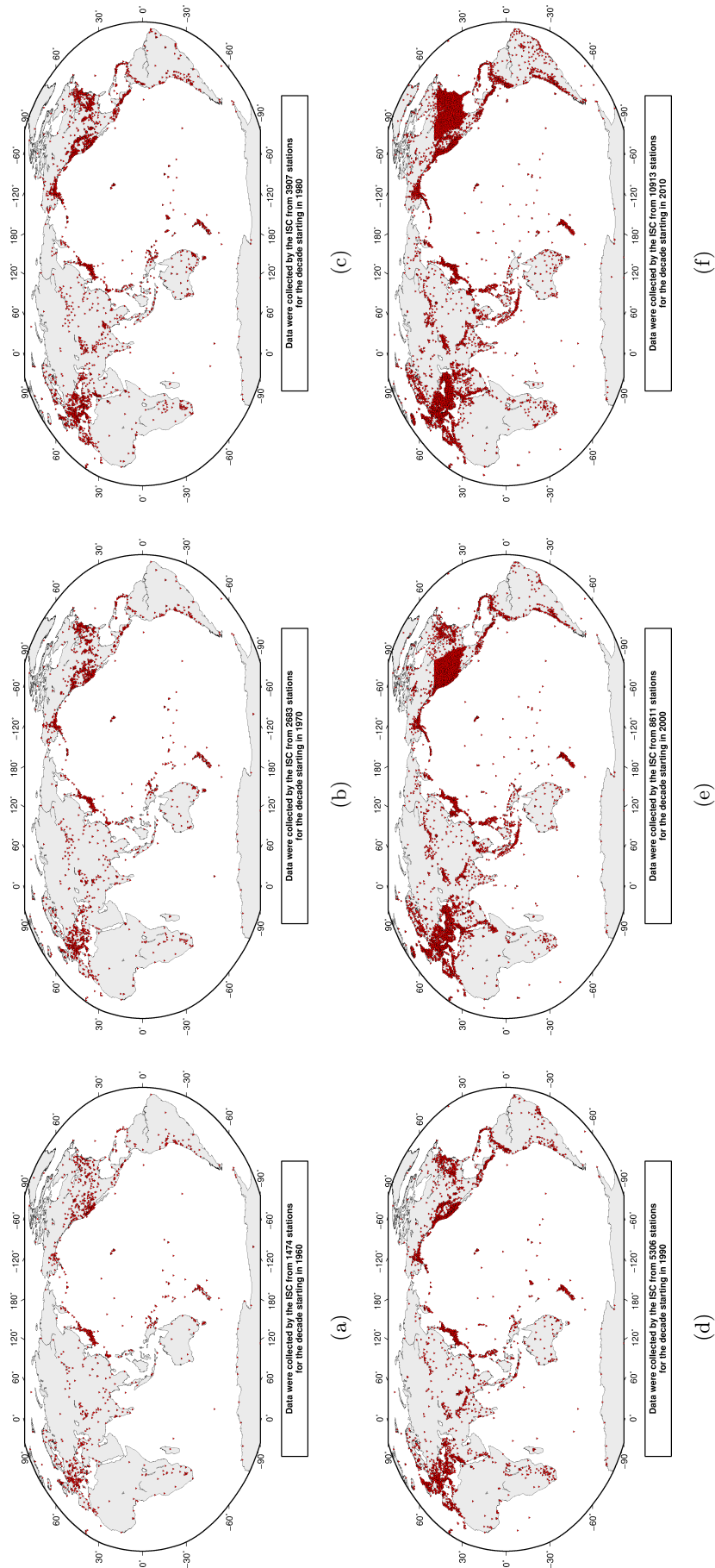


Figure 7.8: Maps showing the stations reported to the ISC for each decade since 1960. Note that the last map covers a shorter time period.

7.4 Hypocentres Collected

The ISC Bulletin groups multiple estimates of hypocentres into individual events, with an appropriate prime hypocentre solution selected. The collection of these hypocentre estimates are described in this section.

The reports containing hypocentres are summarised in Table 7.4. The number of hypocentres collected by the ISC has also increased significantly since 1964, as shown in Figure 7.9. A map of all hypocentres reported to the ISC for this summary period is shown in Figure 7.10. Where a network magnitude was reported with the hypocentre, this is also shown on the map, with preference given to reported values, first of M_W followed by M_S , m_b and M_L respectively (where more than one network magnitude was reported).

Reports with hypocentres	2605
Reports of hypocentres only (no phase readings)	324
Total hypocentres received	308961
Number of duplicate hypocentres	6824 (2.2%)
Agencies determining hypocentres	171

Table 7.4: Summary of the reports containing hypocentres.

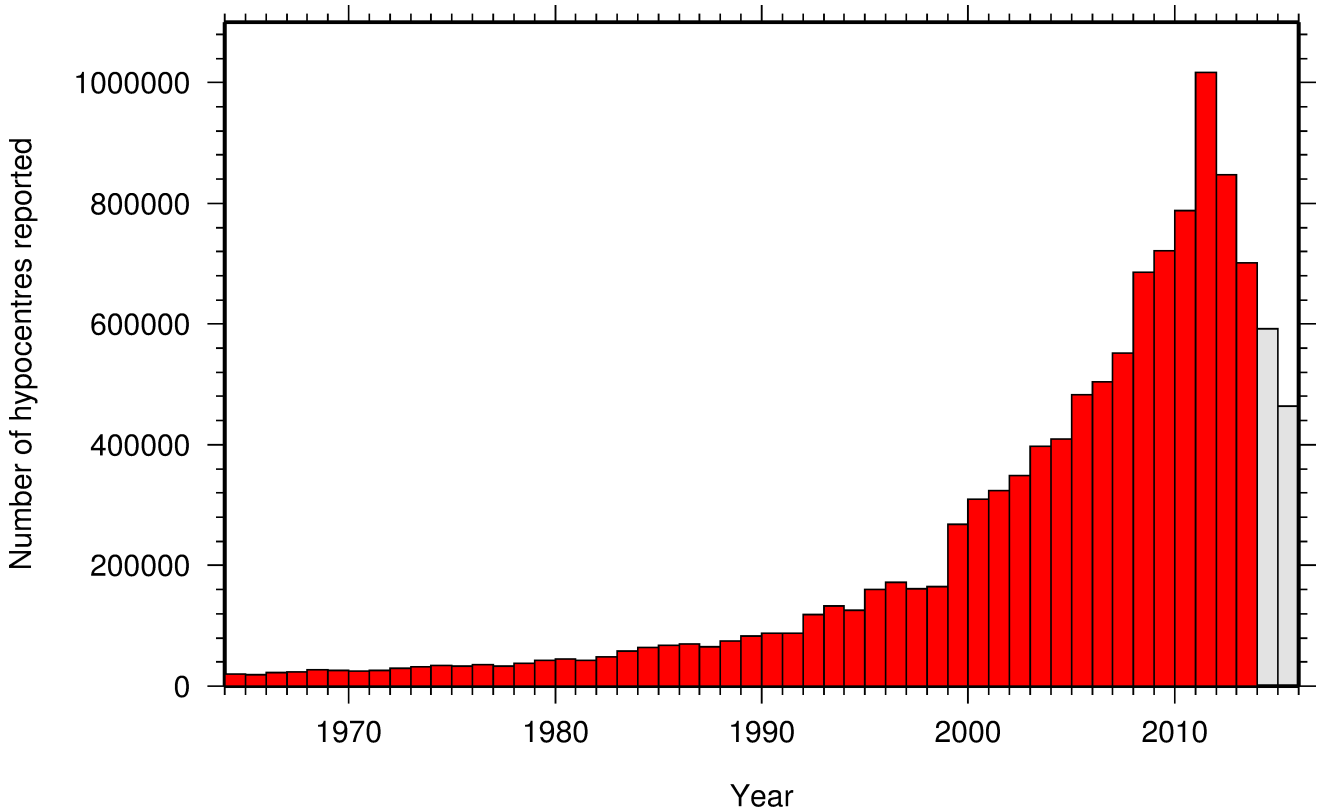


Figure 7.9: Histogram showing the number of hypocentres collected by the ISC for events each year since 1964. For each event, multiple hypocentres may be reported.

All the hypocentres that are reported to the ISC are automatically grouped into events, which form the basis of the ISC Bulletin. For this summary period 339,765 hypocentres (including ISC) were grouped

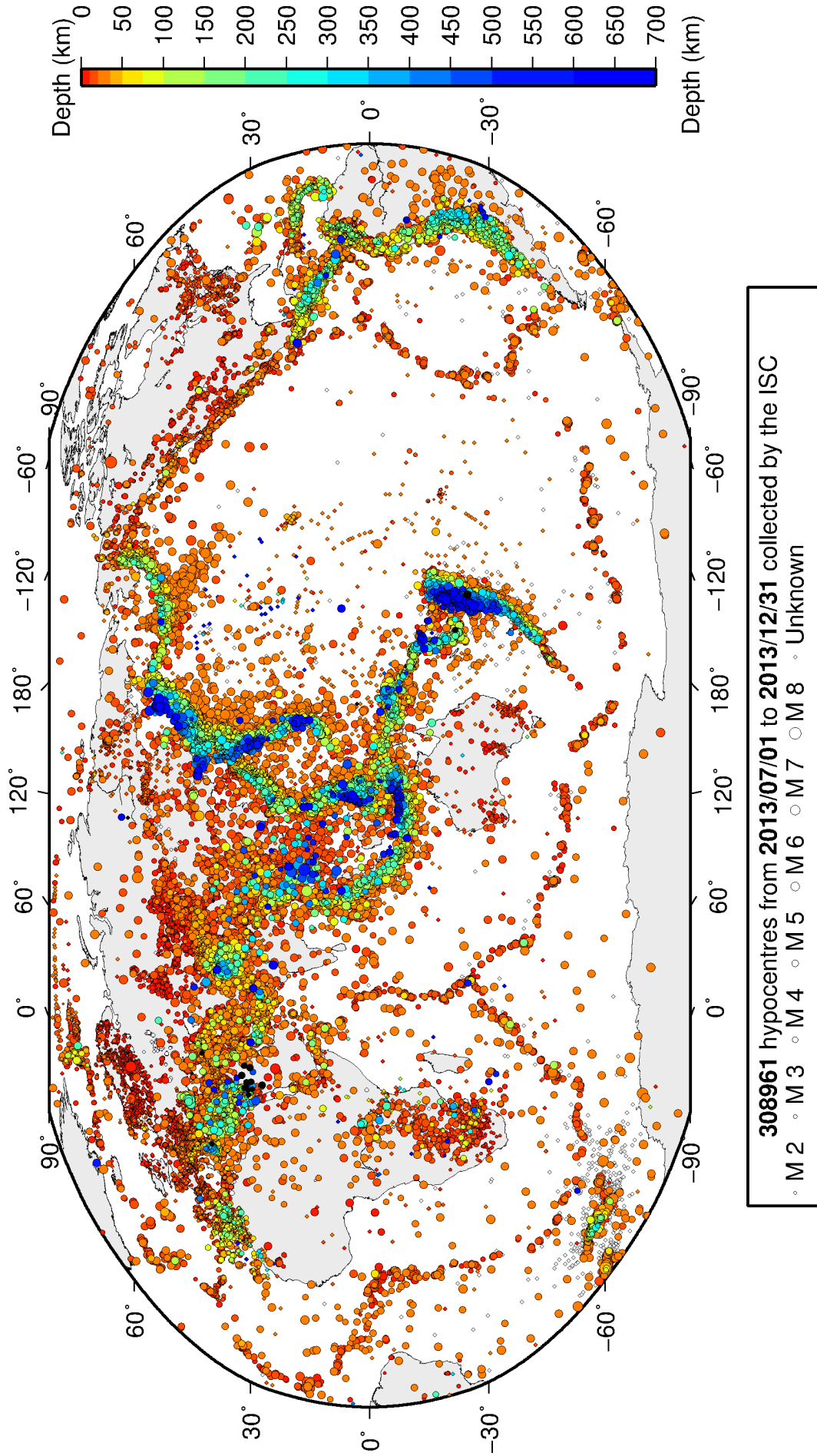


Figure 7.10: Map of all hypocentres collected by the ISC. The scatter shows the large variation of the multiple hypocentres that are reported for each event. The magnitude corresponds with the reported network magnitude. If more than one network magnitude type was reported, preference was given to values of M_W , M_S , m_b and M_L respectively. Compare with Figure 8.2

into 215,951 events, the largest of these having 49 hypocentres in one event. The total number of events shown here is the result of an automatic grouping algorithm, and will differ from the total events in the published ISC Bulletin, where both the number of events and the number of hypocentre estimates will have changed due to further analysis. The process of grouping is detailed in Section 3.3.1 of January to June 2013 Bulletin Summary. Figure 8.2 on page 93 shows a map of all prime hypocentres.

7.5 Collection of Network Magnitude Data

Data contributing agencies normally report earthquake hypocentre solutions along with magnitude estimates. For each seismic event, each agency may report one or more magnitudes of the same or different types. This stems from variability in observational practices at regional, national and global level in computing magnitudes based on a multitude of wave types. Differences in the amplitude measurement algorithm, seismogram component(s) used, frequency range, station distance range as well as the instrument type contribute to the diversity of magnitude types. Table 7.5 provides an overview of the complexity of reported network magnitudes reported for seismic events during the summary period.

	M<3.0	3.0≤M<5.0	M≥5.0
Number of seismic events	166313	31489	392
Average number of magnitude estimates per event	1.3	4.9	26.9
Average number of magnitudes (by the same agency) per event	1.1	2.6	3.9
Average number of magnitude types per event	1.1	4.0	12.8
Number of magnitude types	24	44	41

Table 7.5: Statistics of magnitude reports to the ISC; *M* – average magnitude of estimates reported for each event.

Table 7.6 gives the basic description, main features and scientific paper references for the most commonly reported magnitude types.

Table 7.6: Description of the most common magnitude types reported to the ISC.

Magnitude type	Description	References	Comments
M	Unspecified		Often used in real or near-real time magnitude estimations
mB	Medium-period and Broad-band body-wave magnitude	<i>Gutenberg</i> (1945a); <i>Gutenberg</i> (1945b); <i>IASPEI</i> (2005); <i>IASPEI</i> (2013); <i>Bormann et al.</i> (2009); <i>Bormann and Dewey</i> (2012)	
mb	Short-period body-wave magnitude	<i>IASPEI</i> (2005); <i>IASPEI</i> (2013); <i>Bormann et al.</i> (2009); <i>Bormann and Dewey</i> (2012)	Classical mb based on stations between 21°-100° distance

Table 7.6: *continued*

Magnitude type	Description	References	Comments
mb1	Short-period body-wave magnitude	<i>IDC</i> (1999) and references therein	Reported only by the IDC; also includes stations at distances less than 21°
mb1mx	Maximum likelihood short-period body-wave magnitude	<i>Ringdal</i> (1976); <i>IDC</i> (1999) and references therein	Reported only by the IDC
mbtmp	short-period body-wave magnitude with depth fixed at the surface	<i>IDC</i> (1999) and references therein	Reported only by the IDC
mbLg	Lg-wave magnitude	<i>Nuttli</i> (1973); <i>IASPEI</i> (2005); <i>IASPEI</i> (2013); <i>Bormann and Dewey</i> (2012)	Also reported as MN
Mc	Coda magnitude		
MD (Md)	Duration magnitude	<i>Bisztricsany</i> (1958); <i>Lee et al.</i> (1972)	
ME (Me)	Energy magnitude	<i>Choy and Boatwright</i> (1995)	Reported only by NEIC
MJMA	JMA magnitude	<i>Tsuboi</i> (1954)	Reported only by JMA
ML (MI)	Local (Richter) magnitude	<i>Richter</i> (1935); <i>Hutton and Boore</i> (1987); <i>IASPEI</i> (2005); <i>IASPEI</i> (2013)	
MLSn	Local magnitude calculated for Sn phases	<i>Balfour et al.</i> (2008)	Reported by PGC only for earthquakes west of the Cascadia subduction zone
MLv	Local (Richter) magnitude computed from the vertical component		Reported only by DJA and BKK
MN (Mn)	Lg-wave magnitude	<i>Nuttli</i> (1973); <i>IASPEI</i> (2005)	Also reported as mbLg
MS (Ms)	Surface-wave magnitude	<i>Gutenberg</i> (1945c); <i>Vaněk et al.</i> (1962); <i>IASPEI</i> (2005)	Classical surface-wave magnitude computed from station between 20°-160° distance
Ms1	Surface-wave magnitude	<i>IDC</i> (1999) and references therein	Reported only by the IDC; also includes stations at distances less than 20°
ms1mx	Maximum likelihood surface-wave magnitude	<i>Ringdal</i> (1976); <i>IDC</i> (1999) and references therein	Reported only by the IDC

Table 7.6: *continued*

Magnitude type	Description	References	Comments
Ms7	Surface-wave magnitude	<i>Bormann et al.</i> (2007)	Reported only by BJI and computed from records of a Chinese-made long-period seismograph in the distance range 3°-177°
MW (Mw)	Moment magnitude	<i>Kanamori</i> (1977); <i>Dziewonski et al.</i> (1981)	Computed according to the <i>IASPEI</i> (2005) and <i>IASPEI</i> (2013) standard formula
Mw(mB)	Proxy Mw based on mB	<i>Bormann and Saul</i> (2008)	Reported only by DJA and BKK
Mwp	Moment magnitude from P-waves	<i>Tsuboi et al.</i> (1995)	Reported only by DJA and BKK and used in rapid response
mbh	Unknown		
mbv	Unknown		
MG	Unspecified type		Contact contributor
Mm	Unknown		
msh	Unknown		
MSV	Unknown		

Table 7.7 lists all magnitude types reported, the corresponding number of events in the ISC Bulletin and the agency codes along with the number of earthquakes.

Table 7.7: *Summary of magnitude types in the ISC Bulletin for this summary period. The number of events with values for each magnitude type is listed. The agencies reporting these magnitude types are listed, together with the total number of values reported.*

Magnitude type	Events	Agencies reporting magnitude type (number of values)
M	4184	WEL (1522), SKO (1070), JSO (508), IDG (284), KRAR (268), MOS (167), KOLA (100), VLA (66), ASRS (58), NERS (57), PRU (24), RSPR (19), MIRAS (16), FDF (11), SKHL (10), CMWS (5), CERI (4), SCEDC (3), REN (2), BYKL (1)
mB	2208	BJI (1845), DJA (611), WEL (118), STR (3), IGQ (2)
MB	20	NEIC (20)
mb	24640	IDC (14133), NEIC (6689), NNC (4990), KRNET (4272), BJI (1847), MOS (1801), VIE (1600), MAN (1515), DJA (971), MDD (192), VAO (182), SIGU (50), GII (45), STR (39), NDI (26), DSN (23), OMAN (13), PGC (9), BGS (5), CRAAG (5), NIC (5), IGQ (4), ROM (2), GUC (1), PRE (1), UCR (1), NSSC (1), IGIL (1)
mb1	14581	IDC (14581)
mb1mx	14581	IDC (14581)

Table 7.7: *Continued.*

Magnitude type	Events	Agencies reporting magnitude type (number of values)
mb_Lg	91	NEIC (60), TEH (27), OTT (2), MDD (2), WES (1), OGSO (1)
MB_LG	1	NEIC (1)
mbLg	2897	MDD (2894), WES (1), OGSO (1), NEIC (1)
mbR	45	VAO (45)
mbtmp	14581	IDC (14581)
MC	1	BUT (1)
Mc	1	BER (1)
MD	12006	MEX (3098), LDG (1717), ROM (1381), RSPR (1111), GCG (1023), TRN (732), ECX (597), SVSA (374), GRAL (365), TIR (318), UCR (290), BUC (277), GII (252), SJA (176), HLW (133), PNSN (126), SNET (125), PDG (121), NCEDC (119), DDA (116), LSZ (101), OSPL (96), SSNC (86), EAF (74), JSN (58), SOF (57), INMG (57), UPA (53), BUL (38), NSSC (37), TUN (32), NIC (20), BUT (20), CERI (16), SLM (14), NEIC (7), HVO (7), NDI (3), NAM (3), ISK (3), WES (2), SEA (2), RSNC (1), PGC (1), AAE (1), IGQ (1)
ME	14	NEIC (14)
MH	1	SCEDC (1)
Mjma	568	JSO (494), IGQ (75)
MJMA	63406	JMA (63406)
ML	109433	TAP (20124), ATH (13254), ROM (12847), DDA (9427), ISK (7944), IDC (7642), RSNC (6527), HEL (5412), THE (5097), SJA (3834), GUC (3036), VIE (2806), ANF (2805), UPP (2206), LDG (2185), GEN (1897), AEIC (1687), MAN (1528), BEO (1475), WEL (1474), BER (1380), LJU (1285), SNET (1188), SKO (1109), BUC (1073), PRE (922), CNRM (885), INMG (871), RHSSO (731), THR (645), TEH (606), ECX (579), NAO (574), PGC (565), KRSC (531), BJI (469), JSO (468), SVSA (462), IPEC (441), ISN (426), MRB (424), SFS (410), IGIL (410), NIC (361), NSSC (354), CRAAG (304), OMAN (303), LVSN (284), PDG (278), OSPL (259), UCR (249), NDI (224), DSN (200), KNET (190), WBNET (185), AZER (178), PAS (166), NEIC (159), BGR (149), HLW (148), TUL (128), FIA0 (126), PPT (124), BGS (88), SSNC (87), SCEDC (82), IGQ (76), HVO (75), OTT (71), MIRAS (66), DRS (64), ARE (56), NCEDC (53), REN (45), SCB (43), UPA (31), ARO (27), BNS (26), SEA (26), HYB (26), SGS (24), USSS (24), DMN (19), DNK (18), RISSC (15), BUT (11), LSZ (11), PLV (8), BUG (8), SLC (5), CLL (4), ZUR (3), MOS (2), SSS (2), LIM (2), ZAG (2), SOF (2), TIR (1), INET (1), CSEM (1), HDC (1), PAL (1), LDO (1)
MLh	536	ZUR (413), ASRS (123)
MLSn	345	PGC (345)
MLv	5363	DJA (2226), WEL (1562), STR (928), JSO (508), IGQ (142), ASRS (14)

Table 7.7: *Continued.*

Magnitude type	Events	Agencies reporting magnitude type (number of values)
MN	238	OTT (219), TEH (12), NEIC (10), WES (1), OGSO (1)
mpv	5244	NNC (5244)
MPVA	341	NORS (260), MOS (245), DRS (1)
MS	9562	IDC (7251), MAN (2457), BJI (1520), MOS (426), NSSP (88), OMAN (40), SOME (35), NEIC (33), AZER (10), VIE (8), NDI (4), BGS (2), DSN (2), PGC (1), BER (1)
Ms1	7251	IDC (7251)
ms1mx	7251	IDC (7251)
Ms7	1482	BJI (1482)
Ms_20	145	NEIC (145)
Ms_VX	1	NEIC (1)
MW	7789	SJA (3815), GCMT (1058), RSNC (845), NIED (792), UCR (553), PGC (405), UPA (296), NEIC (116), SSNC (84), MED_RCMT (77), DDA (50), ASIES (48), ROM (22), BRK (14), BER (11), GUC (10), SNET (9), OTT (6), DJA (3), GFZ (3), SLM (3), CRAAG (2), IEC (2), IAG (2), IGIL (1), CSEM (1), SVSA (1), NCEDC (1), NDI (1), PAS (1)
Mw(mB)	125	WEL (118), STR (5), IGQ (2)
Mwb	202	NEIC (202)
Mwc	192	GCMT (190), NEIC (45)
Mwd	2	NEIC (2)
Mwp	53	DJA (47), OMAN (6), HON (1), PMR (1)
MWR	7	NEIC (6), SCEDC (1), REN (1)
Mwr	137	NEIC (91), OTT (16), NCEDC (10), SLM (7), BRK (5), UCR (4), PAS (3), CAR (2), TEH (2), REN (1), GUC (1), RSNC (1), CSEM (1)
Mww	116	NEIC (116)

The most commonly reported magnitude types are short-period body-wave, surface-wave, local (or Richter), moment, duration and JMA magnitude type. For a given earthquake, the number and type of reported magnitudes greatly vary depending on its size and location. The large earthquake of October 25, 2010 gives an example of the multitude of reported magnitude types for large earthquakes (Listing 7.1). Different magnitude estimates come from global monitoring agencies such as the IDC, NEIC and GCMT, a local agency (GUC) and other agencies, such as MOS and BJI, providing estimates based on the analysis of their networks. The same agency may report different magnitude types as well as several estimates of the same magnitude type, such as NEIC estimates of Mw obtained from W-phase, centroid and body-wave inversions.

Listing 7.1: *Example of reported magnitudes for a large event*

```

Event 15264887 Southern Sumatera
Date      Time      Err  RMS  Latitude Longitude  Smaj  Smin  Az  Depth  Err  Ndef  Nsta  Gap  mdist  Mdist  Qual  Author  OrigID
2010/10/25 14:42:22.18  0.27  1.813  -3.5248  100.1042  4.045  3.327  54  20.0  1.37  2102  2149  23  0.76  176.43  m i de ISC  01346132
(#PRIME)

Magnitude  Err  Nsta  Author  OrigID
mb  6.1  61  BJI  15548963
mB  6.9  68  BJI  15548963
Ms  7.7  85  BJI  15548963

```

```

Ns7 7.5 86 BJI 15548963
mb 5.3 0.1 48 IDC 16686694
mb1 5.3 0.1 51 IDC 16686694
mb1mx 5.3 0.0 52 IDC 16686694
mbtmp 5.3 0.1 51 IDC 16686694
ML 5.1 0.2 2 IDC 16686694
MS 7.1 0.0 31 IDC 16686694
Ns1 7.1 0.0 31 IDC 16686694
ms1mx 6.9 0.1 44 IDC 16686694
mb 6.1 243 ISCJB 01677901
MS 7.3 228 ISCJB 01677901
M 7.1 117 DJA 01268475
mb 6.1 0.2 115 DJA 01268475
MB 7.1 0.1 117 DJA 01268475
MLv 7.0 0.2 26 DJA 01268475
7.1 0.4 117 DJA 01268475
Mwp 6.9 0.2 102 DJA 01268475
mb 6.4 49 MDS 16742129
MS 7.2 70 MDS 16742129
mb 6.5 110 NEIC 01288303
ME 7.3 NEIC 01288303
MS 7.3 143 NEIC 01288303
MW 7.7 NEIC 01288303
MW 7.8 130 GCMT 00125427
mb 5.9 KLM 00255772
ML 6.7 KLM 00255772
MS 7.6 KLM 00255772
mb 6.4 20 BGR 16815854
Ms 7.2 2 BGR 16815854
mb 6.3 0.3 250 ISC 01346132
MS 7.3 0.1 237 ISC 01346132

```

An example of a relatively small earthquake that occurred in northern Italy for which we received magnitude reports of mostly local and duration type from six agencies in Italy, France and Austria is given in Listing 7.2.

Listing 7.2: Example of reported magnitudes for a small event

```

Event 15089710 Northern Italy
Date Time Err RMS Latitude Longitude Smaj Smin Az Depth Err Ndef Nsta Gap mdist Mdist Qual Author OrigID
2010/08/08 15:20:46.22 0.94 0.778 45.4846 8.3212 2.900 2.539 110 28.6 9.22 172 110 82 0.41 5.35 m i ke ISC 01249414
(#PRIME)
Magnitude Err Nsta Author OrigID
ML 2.4 10 ZUR 15925566
Md 2.6 0.2 19 ROM 16861451
Ml 2.2 0.2 9 ROM 16861451
ML 2.5 GEN 00554757
ML 2.6 0.3 28 CSEM 00554756
Md 2.3 0.0 3 LDG 14797570
Ml 2.6 0.3 32 LDG 14797570

```

Figure 7.11 shows a distribution of the number of agencies reporting magnitude estimates to the ISC according to the magnitude value. The peak of the distribution corresponds to small earthquakes where many local agencies report local and/or duration magnitudes. The number of contributing agencies rapidly decreases for earthquakes of approximately magnitude 5.5 and above, where magnitudes are mostly given by global monitoring agencies.

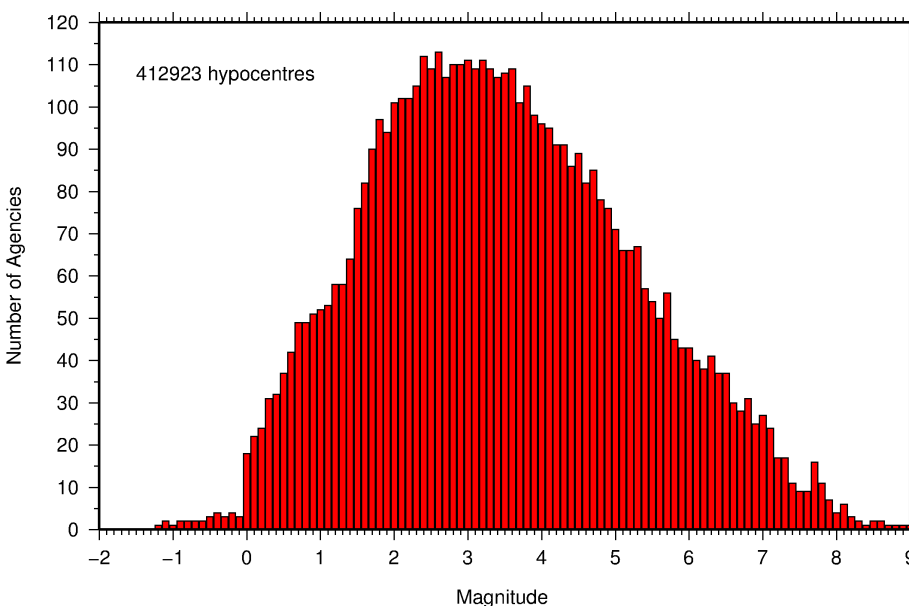


Figure 7.11: Histogram showing the number of agencies that reported network magnitude values. All magnitude types are included.

7.6 Moment Tensor Solutions

The ISC Bulletin publishes moment tensor solutions, which are reported to the ISC by other agencies. The collection of moment tensor solutions is summarised in Table 7.8. A histogram showing all moment tensor solutions collected throughout the ISC history is shown in Figure 7.12. Several moment tensor solutions from different authors and different moment tensor solutions calculated by different methods from the same agency may be present for the same event.

Reports with Moment Tensors	41
Total moment tensors received	4271
Agencies reporting moment tensors	20

Table 7.8: Summary of reports containing moment tensor solutions.

The number of moment tensors for this summary period, reported by each agency, is shown in Table 7.9. The moment tensor solutions are plotted in Figure 7.13.

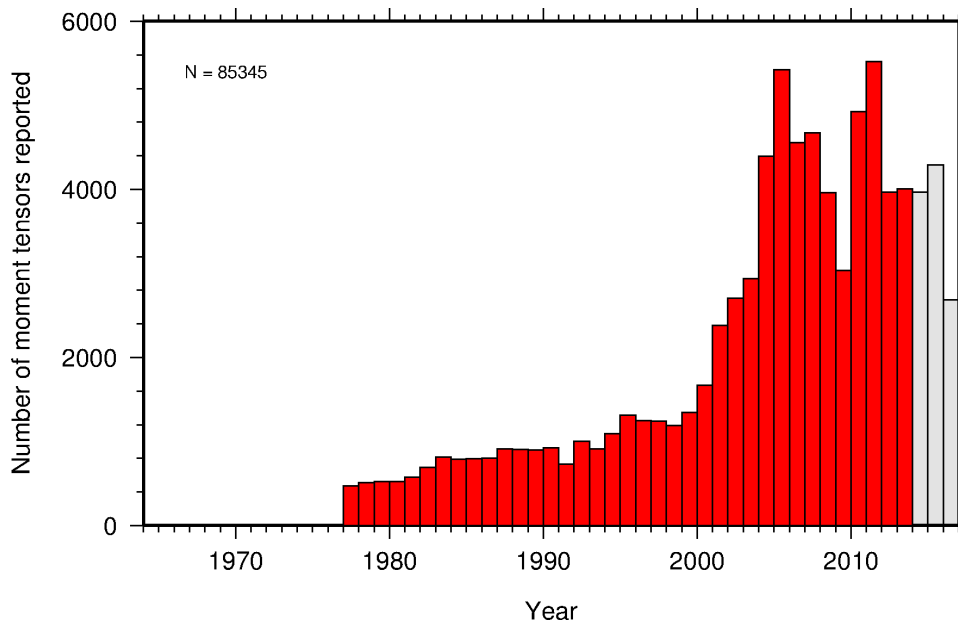
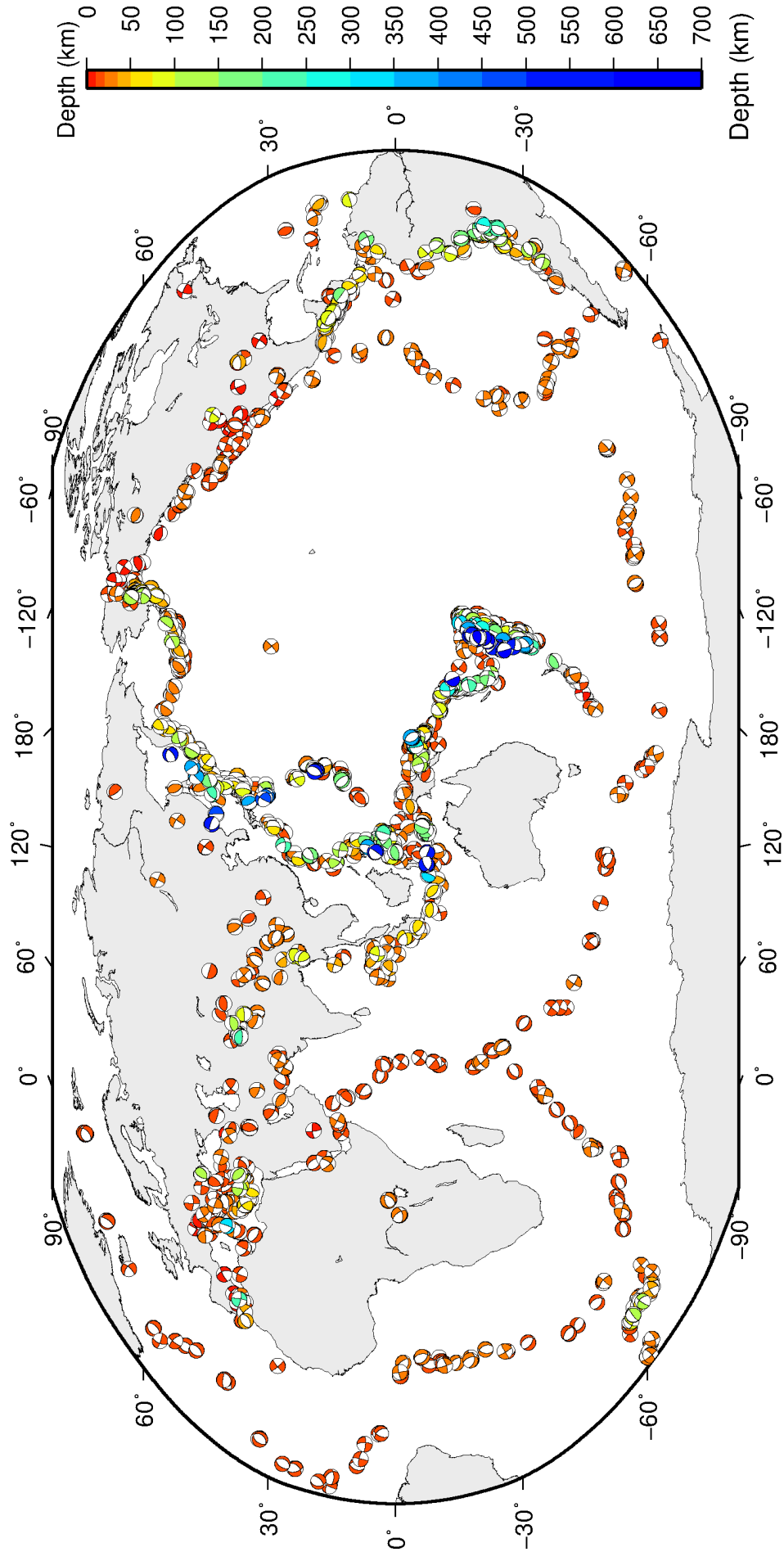


Figure 7.12: Histogram showing the number of moment tensors reported to the ISC since 1964. The regions in grey represent data that are still being actively collected.



ISC Bulletin: 1879 focal mechanism solutions for 1259 events from 2013/07/01 to 2013/12/31

Figure 7.13: Map of all moment tensor solutions in the ISC Bulletin for this summary period.

Agency	Number of moment tensor solutions
NIED	1584
GCMT	1058
NEIC	665
JMA	638
PNSN	126
MED_RCMT	78
ROM	21
AEIC	15
RSNC	15
MOS	14
SJA	11
NCEDC	11
BRK	9
IAG	8
ECX	6
OSPL	5
UCR	5
OTT	4
PAS	3
IGIL	2
HYB	2
REN	2
SLM	2
UPA	2
SEA	1
UAF	1
BGS	1
BUD	1

Table 7.9: Summary of moment tensor solutions in the ISC Bulletin reported by each agency.

7.7 Timing of Data Collection

Here we present the timing of reports to the ISC. Please note, this does not include provisional alerts, which are replaced at a later stage. Instead, it reflects the final data sent to the ISC. The absolute timing of all hypocentre reports, regardless of magnitude, is shown in Figure 7.14. In Figure 7.15 the reports are grouped into one of six categories - from within three days of an event origin time, to over one year. The histogram shows the distribution with magnitude (for hypocentres where a network magnitude was reported) for each category, whilst the map shows the geographic distribution of the reported hypocentres.

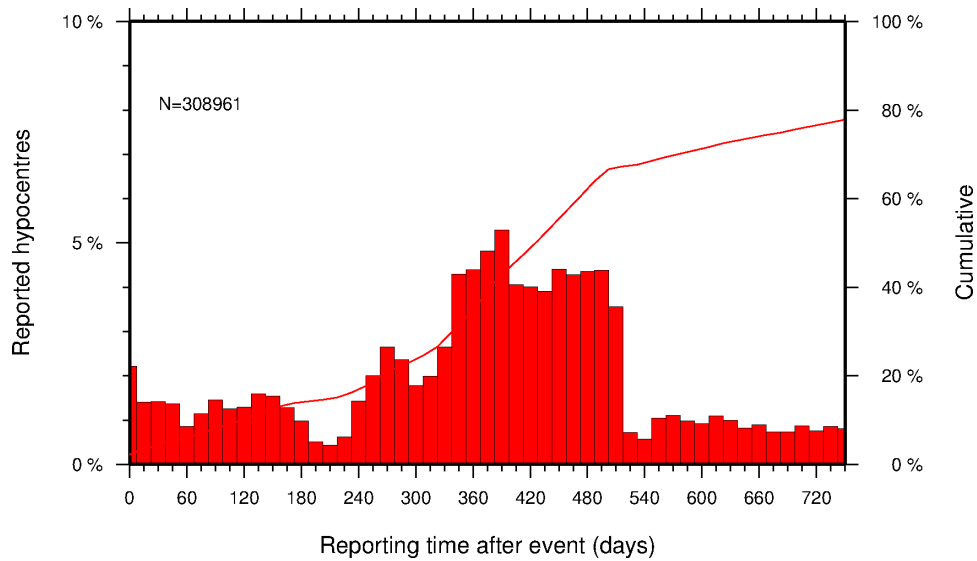


Figure 7.14: Histogram showing the timing of final reports of the hypocentres (total of N) to the ISC. The cumulative frequency is shown by the solid line.

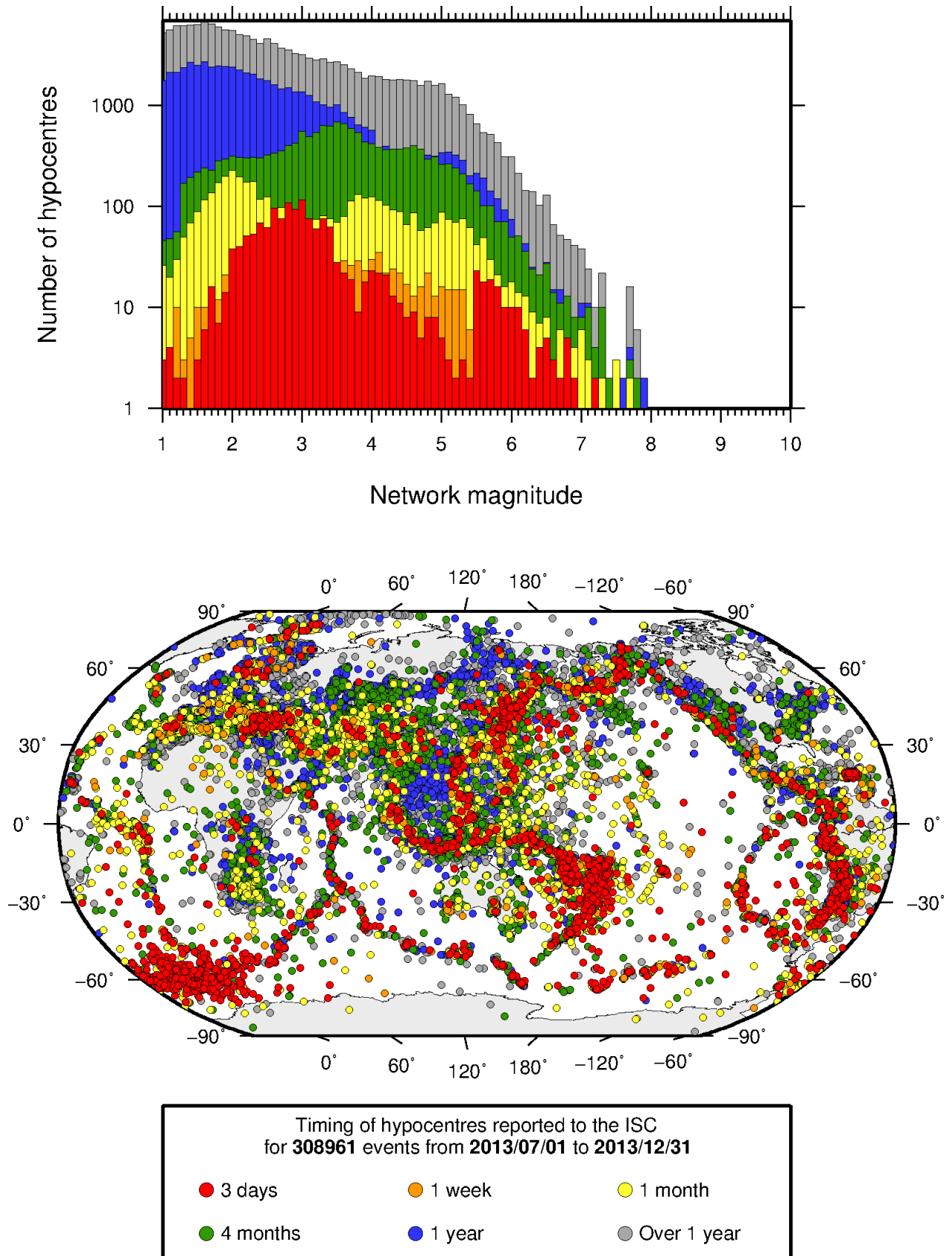


Figure 7.15: Timing of hypocentres reported to the ISC. The colours show the time after the origin time that the corresponding hypocentre was reported. The histogram shows the distribution with magnitude. If more than one network magnitude was reported, preference was given to a value of M_W followed by M_S , m_b and M_L respectively; all reported hypocentres are included on the map. Note: early reported hypocentres are plotted over later reported hypocentres, on both the map and histogram.

8

Overview of the ISC Bulletin

This chapter provides an overview of the seismic event data in the ISC Bulletin. We indicate the differences between all ISC events and those ISC events that are reviewed or located. We describe the wealth of phase arrivals and phase amplitudes and periods observed at seismic stations worldwide, reported in the ISC Bulletin and often used in the ISC location and magnitude determination. Finally, we make some comparisons of the ISC magnitudes with those reported by other agencies, and discuss magnitude completeness of the ISC Bulletin.

8.1 Events

The ISC Bulletin had 207,362 reported events in the summary period between July and December 2013. Some 93% (193,356) of the events were identified as earthquakes, the rest (14,006) were of anthropogenic origin (including mining and other chemical explosions, rockbursts and induced events) or of unknown origin. As discussed in Section 3.3.3 of January to June 2013 Bulletin Summary, typically about 20% of the events are selected for ISC review, and about half of the events selected for review are located by the ISC. In this summary period 13% of the events were reviewed and 8% of the events were located by the ISC. For events that are not located by the ISC, the prime hypocentre is identified according to the rules described in Section 3.3.1 of January to June 2013 Bulletin Summary.

Of the 7,621,203 reported phase observations, 38% are associated to ISC-reviewed events, and 36% are associated to events selected for ISC location. Note that all large events are reviewed and located by the ISC. Since large events are globally recorded and thus reported by stations worldwide, they will provide the bulk of observations. This explains why only about one-fifth of the events in any given month is reviewed although the number of phases associated to reviewed events has increased nearly exponentially in the past decades.

Figure 8.1 shows the daily number of events throughout the summary period. Figure 8.2 shows the locations of the events in the ISC Bulletin; the locations of ISC-reviewed and ISC-located events are shown in Figures 8.3 and 8.4, respectively.

Figure 8.5 shows the hypocentral depth distributions of events in the ISC Bulletin for the summary period. The vast majority of events occur in the Earth's crust. Note that the peaks at 0, 10, 35 km, and at every 50 km intervals deeper than 100 km are artifacts of analyst practices of fixing the depth to a nominal value when the depth cannot be reliably resolved.

Figure 8.6 shows the depth distribution of free-depth solutions in the ISC Bulletin. The depth of a hypocentre reported to the ISC is assumed to be determined as a free parameter, unless it is explicitly labelled as a fixed-depth solution. On the other hand, as described in Section 3.4.3 of January to June

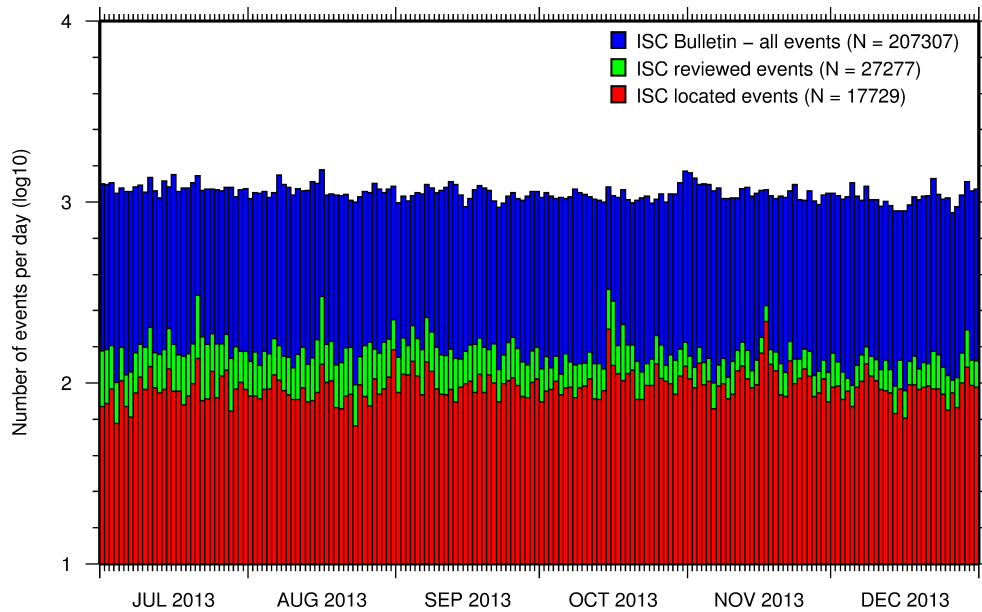


Figure 8.1: Histogram showing the number of events in the ISC Bulletin for the current summary period. The vertical scale is logarithmic.

2013 Bulletin Summary, the ISC locator attempts to get a free-depth solution if, and only if, there is resolution for the depth in the data, i.e. if there is a local network and/or sufficient depth-sensitive phases are reported.

Figure 8.7 shows the depth distribution of fixed-depth solutions in the ISC Bulletin. Except for a fraction of events whose depth is fixed to a shallow depth, this set comprises mostly ISC-located events. If there is no resolution for depth in the data, the ISC locator fixes the depth to a value obtained from the ISC default depth grid file, or if no default depth exists for that location, to a nominal default depth assigned to each Flinn-Engdahl region (see details in Section 3.4.3 of January to June 2013 Bulletin Summary). During the ISC review editors are inclined to accept the depth obtained from the default depth grid, but they typically change the depth of those solutions that have a nominal (10 or 35 km) depth. When doing so, they usually fix the depth to a round number, preferably divisible by 50.

For events selected for ISC location, the number of stations typically increases as arrival data reported by several agencies are grouped together and associated to the prime hypocentre. Consequently, the network geometry, characterised by the secondary azimuthal gap (the largest azimuthal gap a single station closes), is typically improved. Figure 8.8 illustrates that the secondary azimuthal gap is indeed generally smaller for ISC-located events than that for all events in the ISC Bulletin. Figure 8.9 shows the distribution of the number of associated stations. For large events the number of associated stations is usually larger for ISC-located events than for any of the reported event bulletins. On the other hand, events with just a few reporting stations are rarely selected for ISC location. The same is true for the number of defining stations (stations with at least one defining phase that were used in the location). Figure 8.10 indicates that because the reported observations from multiple agencies are associated to the prime, large ISC-located events typically have a larger number of defining stations than any of the reported event bulletins.

The formal uncertainty estimates are also typically smaller for ISC-located events. Figure 8.11 shows the

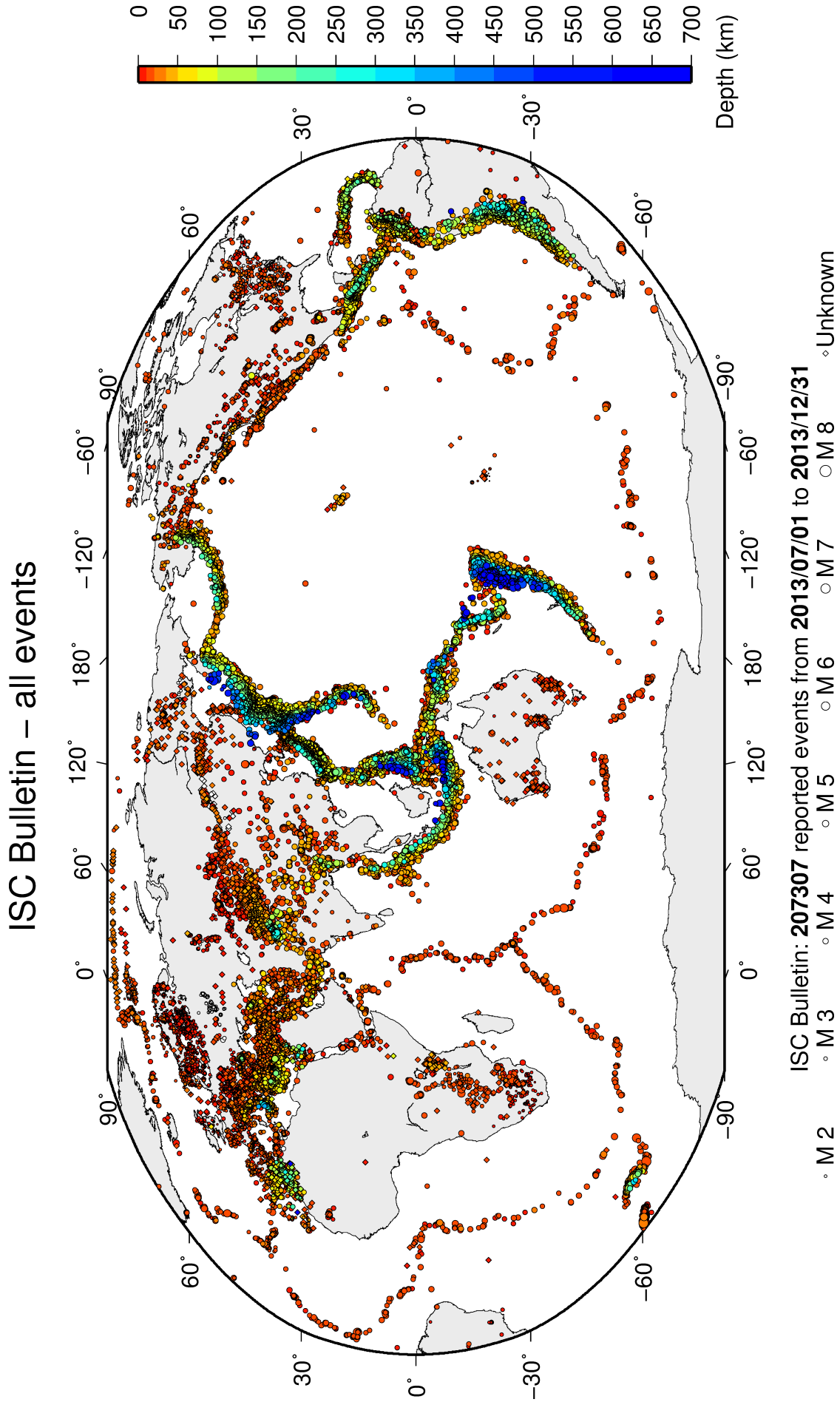
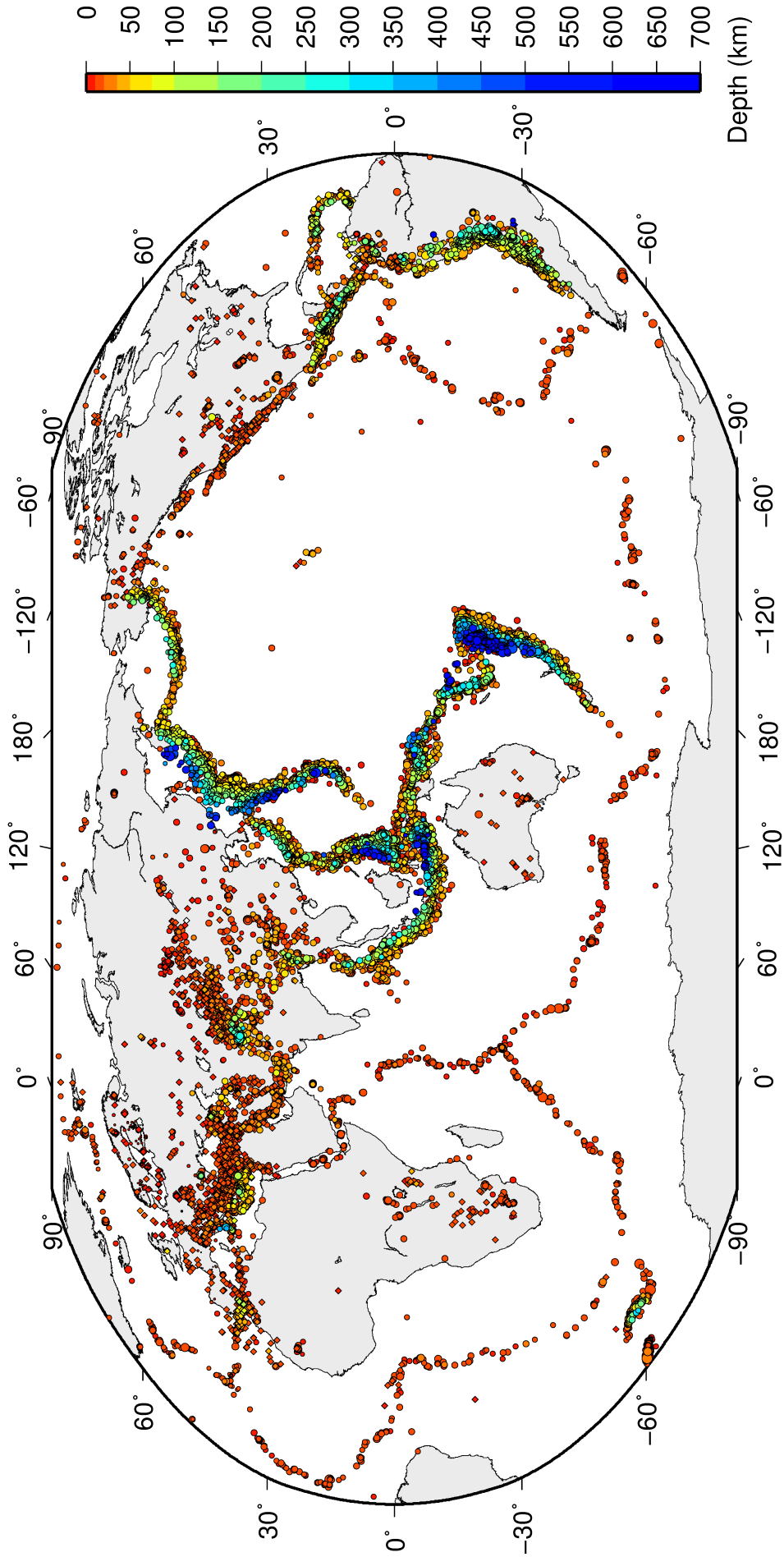


Figure 8.2: Map of all events in the ISC Bulletin. Prime hypocentre locations are shown. Compare with Figure 7.10.

ISC Bulletin – reviewed events



ISC Bulletin: 27277 reviewed events from 2013/07/01 to 2013/12/31

◦ M 2 ◦ M 3 ◦ M 4 ◦ M 5 ◦ M 6 ◦ M 7 ◦ M 8 ◦ Unknown

Figure 8.3: Map of all events reviewed by the ISC for this time period. Prime hypocentre locations are shown.

ISC Bulletin – ISC located events

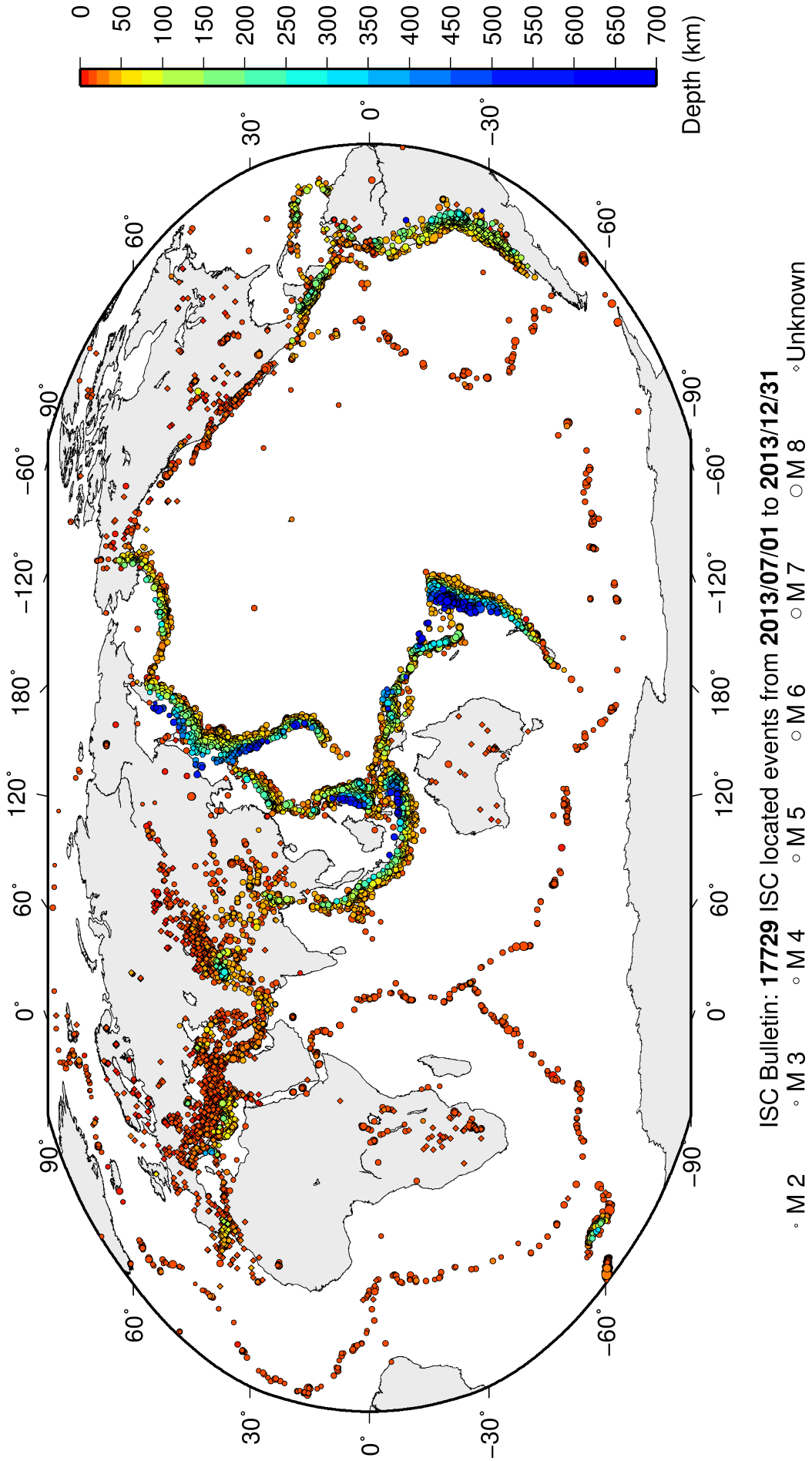


Figure 8.4: Map of all events located by the ISC for this time period. ISC determined hypocentre locations are shown.

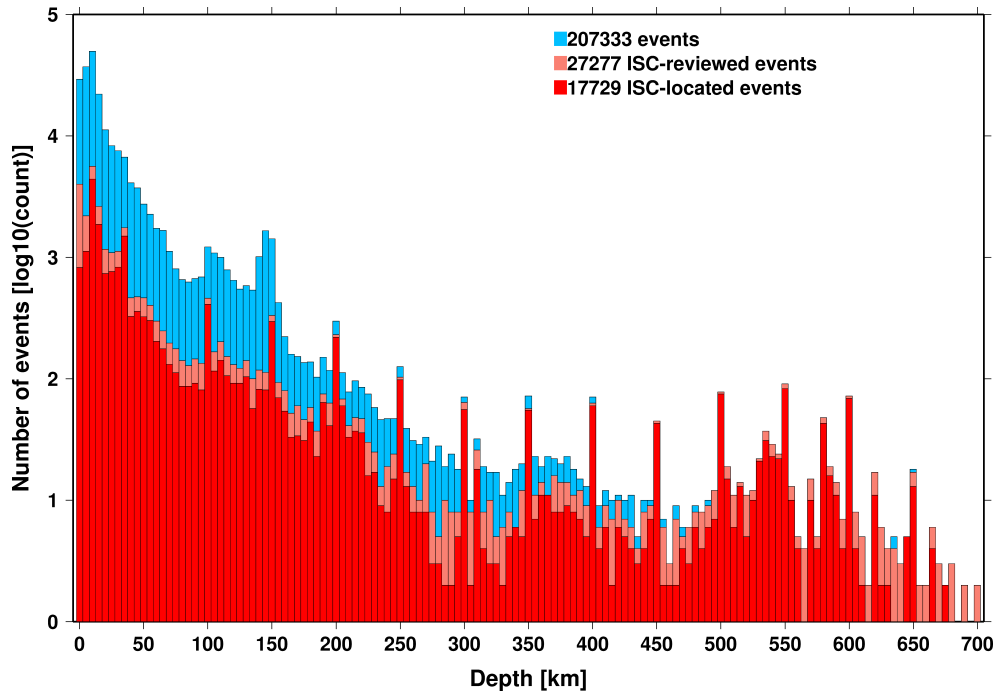


Figure 8.5: Distribution of event depths in the ISC Bulletin (blue) and for the ISC-reviewed (pink) and the ISC-located (red) events during the summary period. All ISC-located events are reviewed, but not all reviewed events are located by the ISC. The vertical scale is logarithmic.

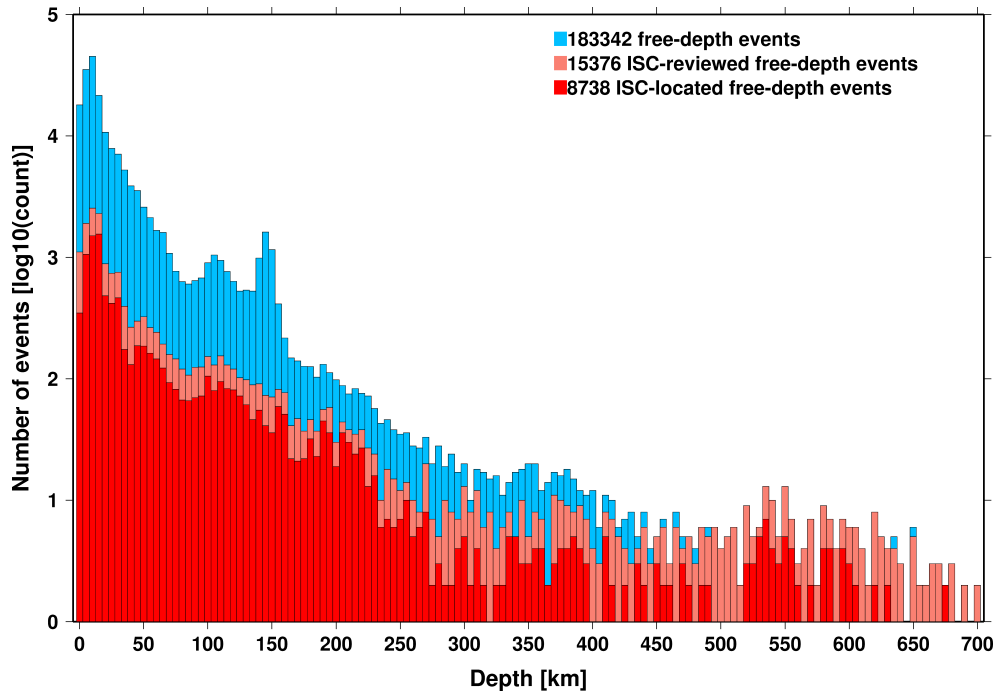


Figure 8.6: Hypocentral depth distribution of events where the prime hypocentres are reported/located with a free-depth solution in the ISC Bulletin. The vertical scale is logarithmic.

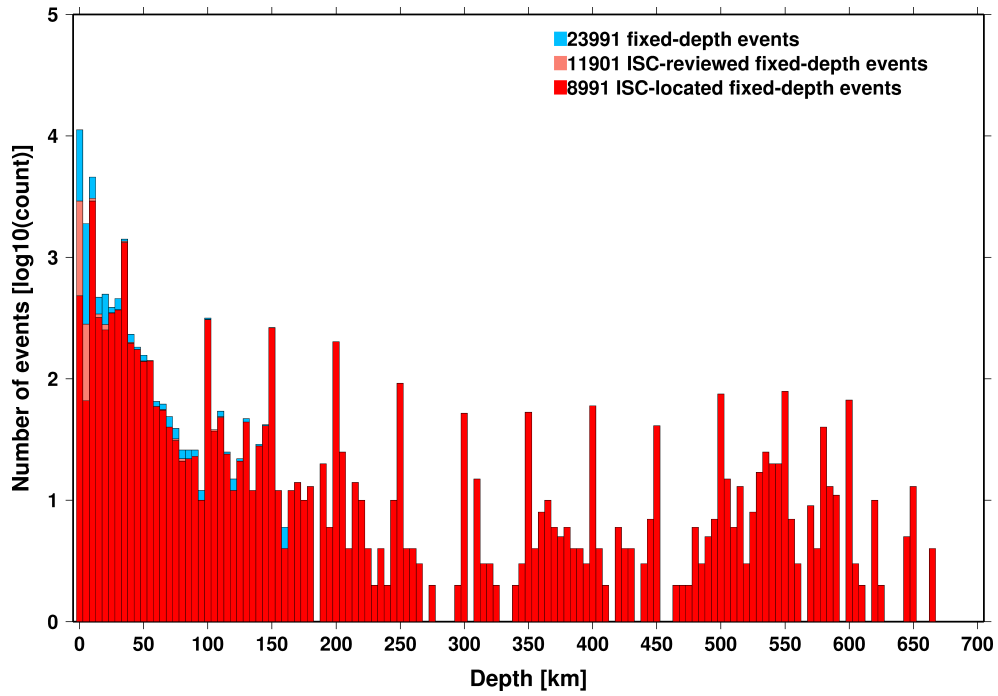


Figure 8.7: Hypocentral depth distribution of events where the prime hypocentres are reported/located with a fixed-depth solution in the ISC Bulletin. The vertical scale is logarithmic.

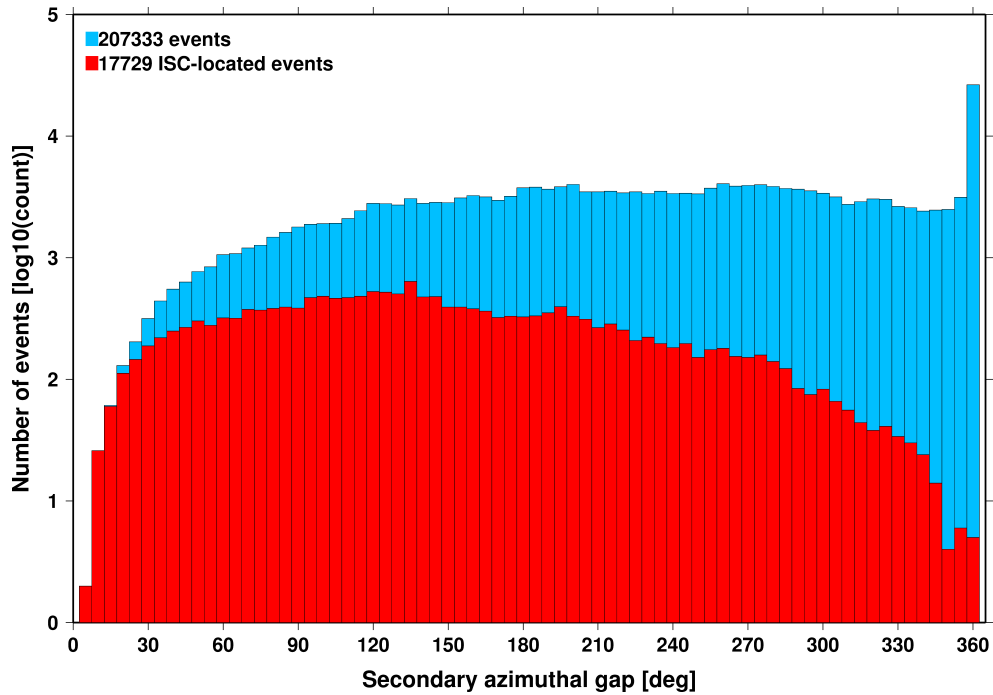


Figure 8.8: Distribution of secondary azimuthal gap for events in the ISC Bulletin (blue) and those selected for ISC location (red). The vertical scale is logarithmic.

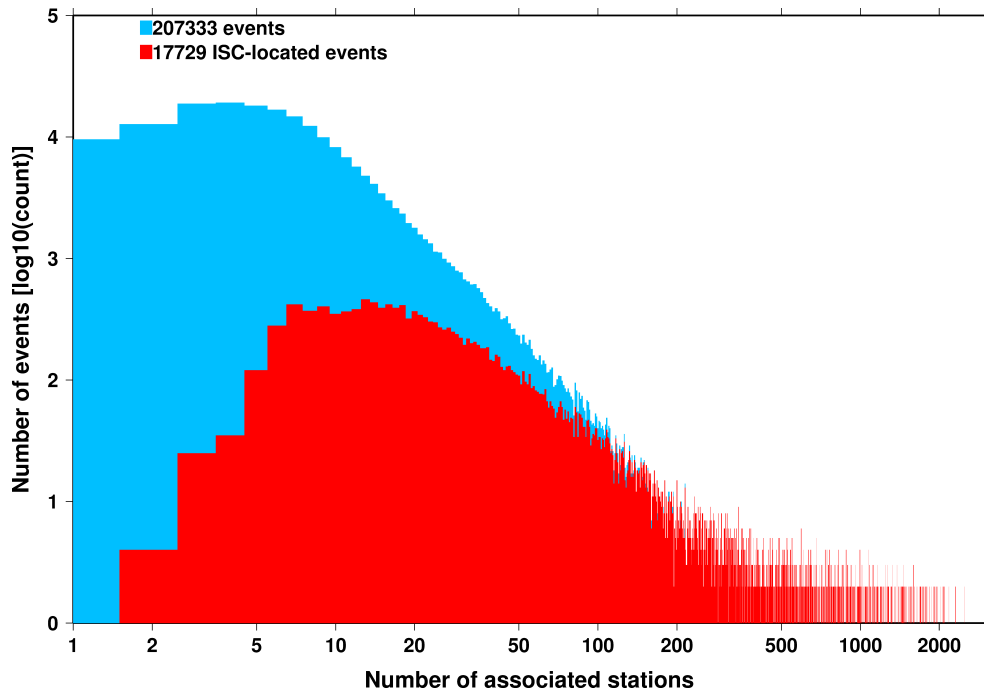


Figure 8.9: Distribution of the number of associated stations for events in the ISC Bulletin (blue) and those selected for ISC location (red). The vertical scale is logarithmic.

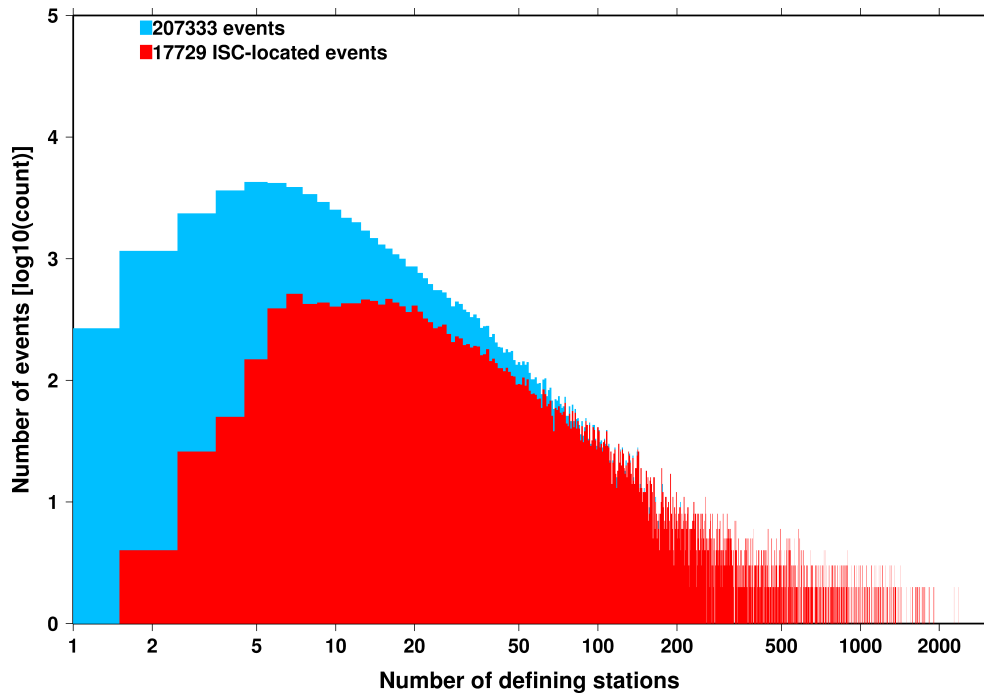


Figure 8.10: Distribution of the number of defining stations for events in the ISC Bulletin (blue) and those selected for ISC location (red). The vertical scale is logarithmic.

distribution of the area of the 90% confidence error ellipse for ISC-located events during the summary period. The distribution suffers from a long tail indicating a few poorly constrained event locations. Nevertheless, half of the events are characterised by an error ellipse with an area less than 184 km², 90% of the events have an error ellipse area less than 1027 km², and 95% of the events have an error ellipse area less than 1655 km².

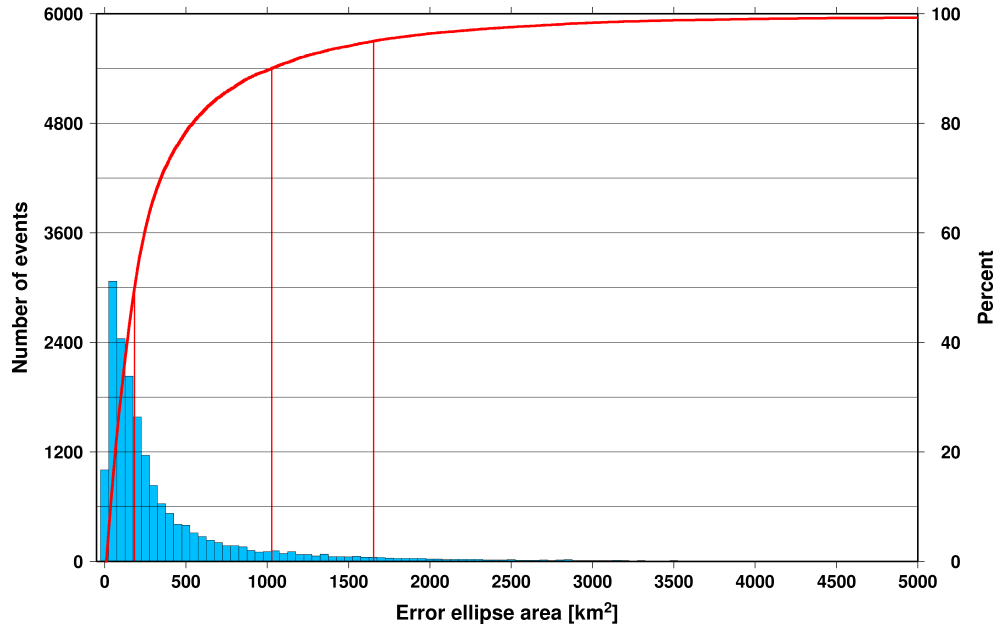


Figure 8.11: Distribution of the area of the 90% confidence error ellipse of the ISC-located events. Vertical red lines indicate the 50th, 90th and 95th percentile values.

Figure 8.12 shows one of the major characteristic features of the ISC location algorithm (Bondár and Storchak, 2011). Because the ISC locator accounts for correlated travel-time prediction errors due to unmodelled velocity heterogeneities along similar ray paths, the area of the 90% confidence error ellipse does not decrease indefinitely with increasing number of stations, but levels off once the information carried by the network geometry is exhausted, thus providing more realistic uncertainty estimates.

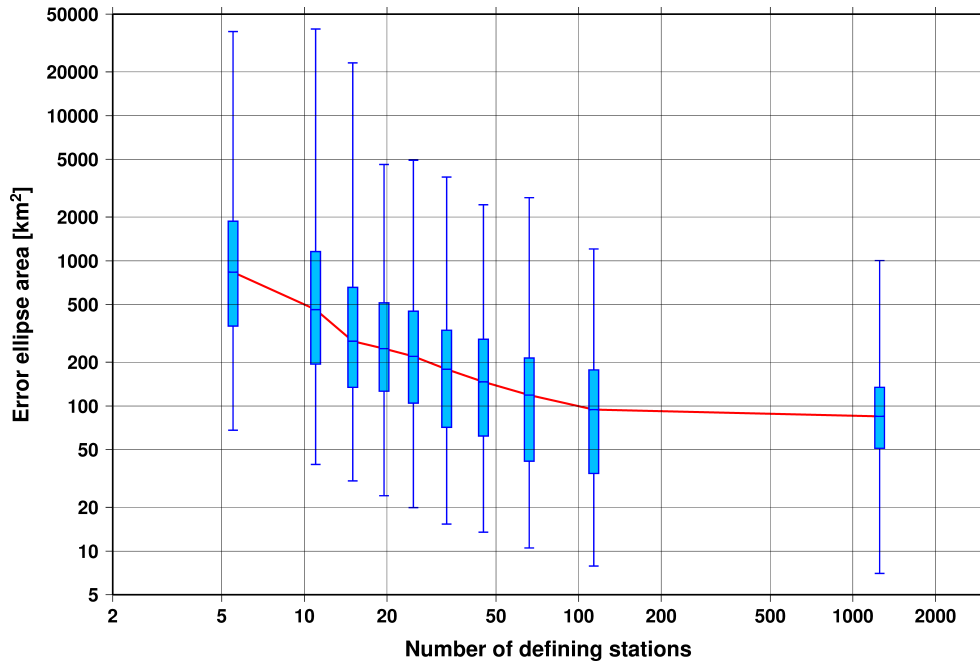


Figure 8.12: Box-and-whisker plot of the area of the 90% confidence error ellipse of the ISC-located events as a function of the number of defining stations. Each box represents one-tenth-worth of the total number of data. The red line indicates the median 90% confidence error ellipse area.

8.2 Seismic Phases and Travel-Time Residuals

The number of phases that are associated to events over the summary period in the ISC Bulletin is shown in Figure 8.13. Phase types and their total number in the ISC Bulletin is shown in the Appendix, Table 10.2. A summary of phase types is indicated in Figure 8.14.

In computing ISC locations, the current (for events since 2009) ISC location algorithm (*Bondár and Storchak, 2011*) uses all *ak135* phases where possible. Within the Bulletin, the phases that contribute to an ISC location are labelled as *time defining*. In this section, we summarise these time defining phases.

In Figure 8.15, the number of defining phases is shown in a histogram over the summary period. Each defining phase is listed in Table 8.1, which also provides a summary of the number of defining phases per event. A pie chart showing the proportion of defining phases is shown in Figure 8.16. Figure 8.17 shows travel times of seismic waves. The distribution of residuals for these defining phases is shown for the top five phases in Figures 8.18 through 8.22.

Table 8.1: Numbers of ‘time defining’ phases (*N*) within the ISC Bulletin for 17729 ISC located events.

Phase	Number of ‘defining’ phases	Number of events	Max per event	Median per event
P	888864	11838	2860	15
Pn	449086	16307	909	15
Sn	153080	14149	221	6
Pb	83811	7735	110	6
PKPdf	65329	3953	1045	3
Pg	64521	6148	117	6
Sg	51409	5936	111	5
Sb	48760	7357	80	4
PKiKP	41910	3231	568	2
S	32786	3495	516	3
PKPbc	29089	3424	316	2

Table 8.1: (continued)

Phase	Number of 'defining' phases	Number of events	Max per event	Median per event
PKPab	18671	2652	377	2
PcP	15214	3377	322	2
pP	10112	1159	551	3
Pdif	8737	972	544	2
PP	8280	1555	158	1
ScP	4594	1066	106	2
SS	3431	963	82	1
sP	2184	735	131	2
PKKPbc	2015	374	82	2
SKSac	1810	321	58	2
SKPbc	1205	277	280	2
pwP	1167	400	63	2
PnPn	998	641	10	1
ScS	995	404	44	1
SnSn	772	450	11	1
pPKPdf	741	316	21	2
PKKPab	568	214	49	1
PKKPdf	516	200	16	2
sS	487	258	26	1
SKiKP	463	265	26	1
pPKPab	379	170	31	1
P'P'df	377	144	27	1
pPKPbc	333	184	17	1
PKSdf	295	271	5	1
PcS	271	223	5	1
SKSdf	259	162	11	1
SKKSac	245	119	12	1
PS	233	79	19	1
SKPab	216	117	8	1
sPKPdf	199	136	7	1
SKPdf	140	59	11	1
PnS	139	94	5	1
sPKPab	131	78	18	1
SP	118	45	16	1
Sdif	115	59	8	1
sPKPbc	108	68	7	1
SKKPbc	56	22	7	2
pPKiKP	51	23	11	1
pS	51	45	3	1
pPdif	30	16	5	1
P'P'bc	20	13	5	1
SKKSdf	16	10	7	1
SPn	13	7	3	2
SKKPab	13	8	3	1
PbPb	12	8	3	1
sPKiKP	11	6	6	1
sPn	8	3	6	1
PgPg	8	2	6	4
PKSab	7	3	5	1
pPn	7	3	4	2
PKSbc	6	6	1	1
SbSb	5	4	2	1
sPdif	4	4	1	1
SKKPdf	4	3	2	1
P'P'ab	4	4	1	1
PKKSbc	2	2	1	1
sSKSac	2	1	2	2
SgSg	2	2	1	1
PgS	1	1	1	1
sSdif	1	1	1	1
S'S'ac	1	1	1	1
PKKSdf	1	1	1	1

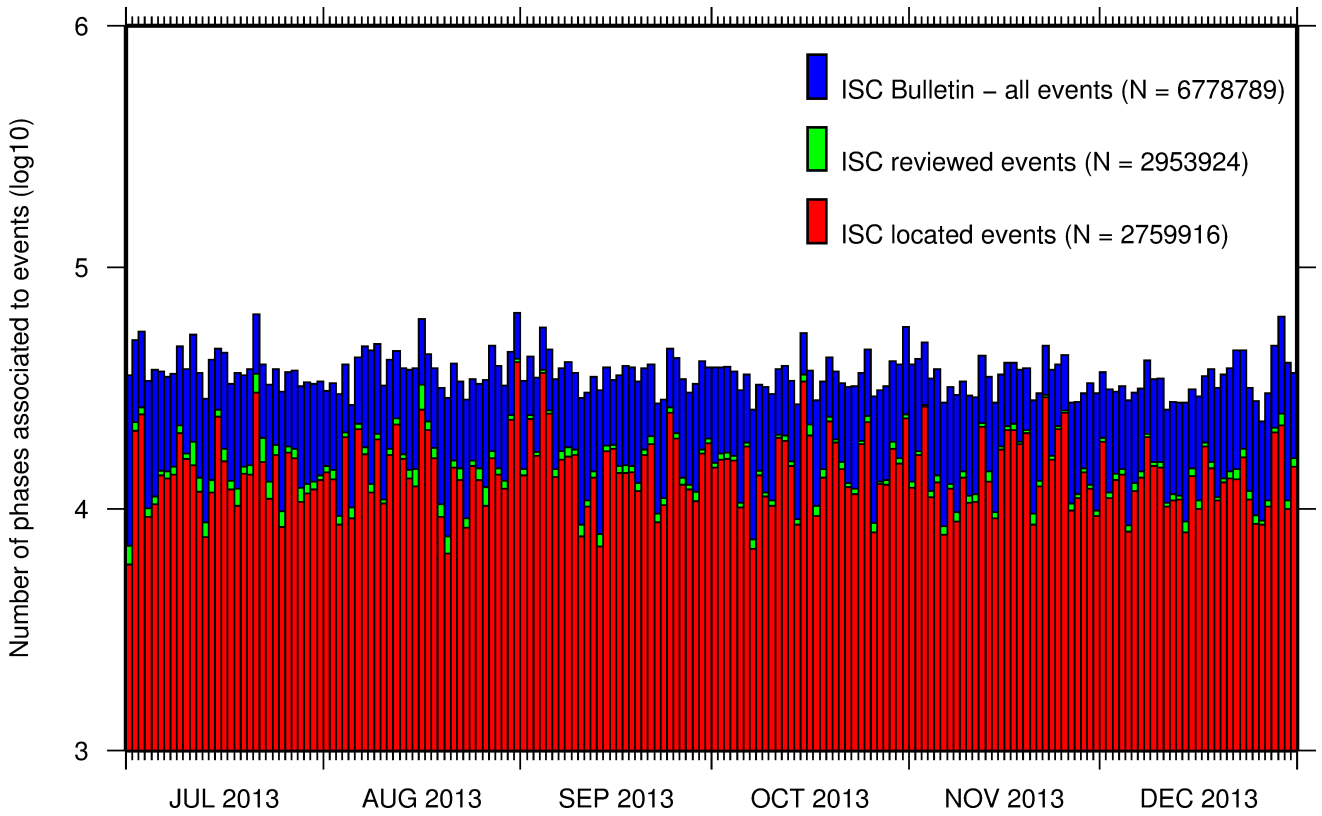


Figure 8.13: Histogram showing the number of phases (N) that the ISC has associated to events within the ISC Bulletin for the current summary period.

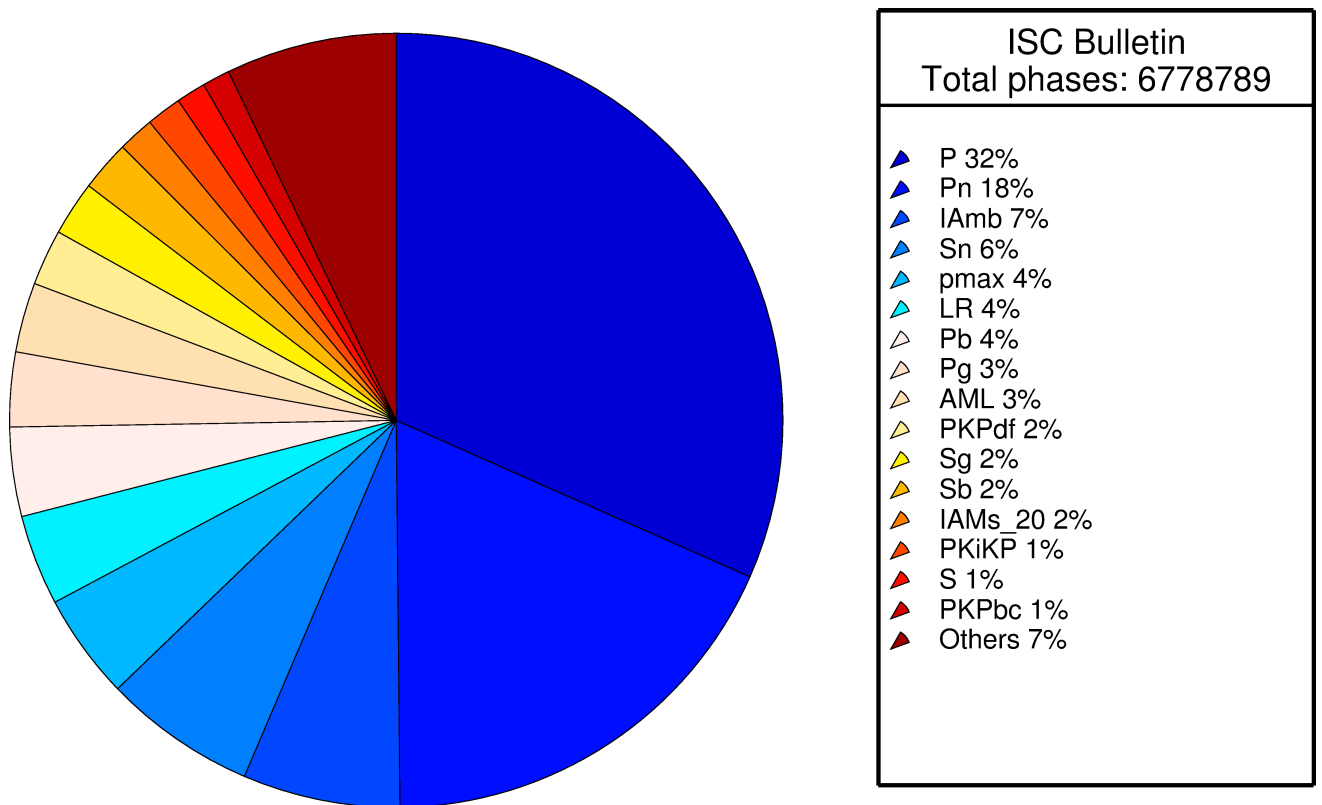


Figure 8.14: Pie chart showing the fraction of various phase types in the ISC Bulletin for this summary period.

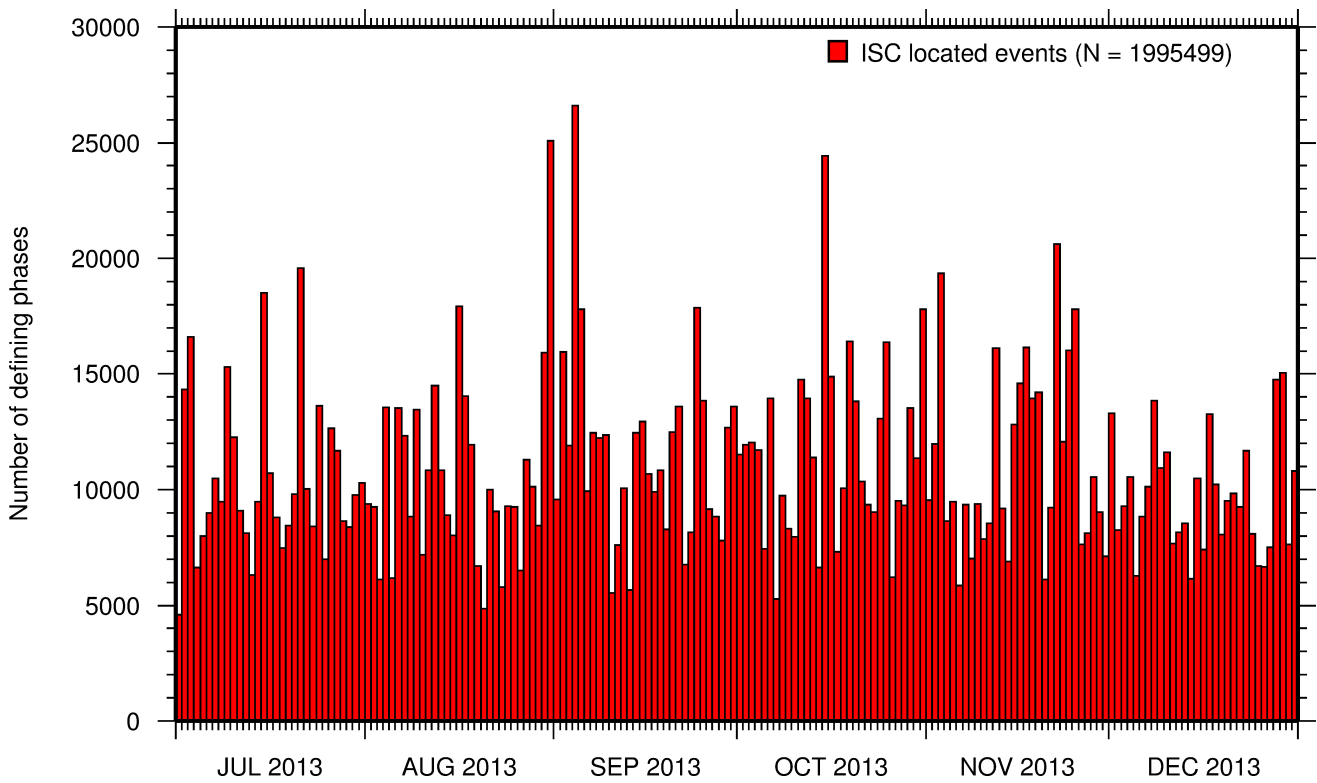


Figure 8.15: Histogram showing the number of defining phases in the ISC Bulletin, for events located by the ISC.

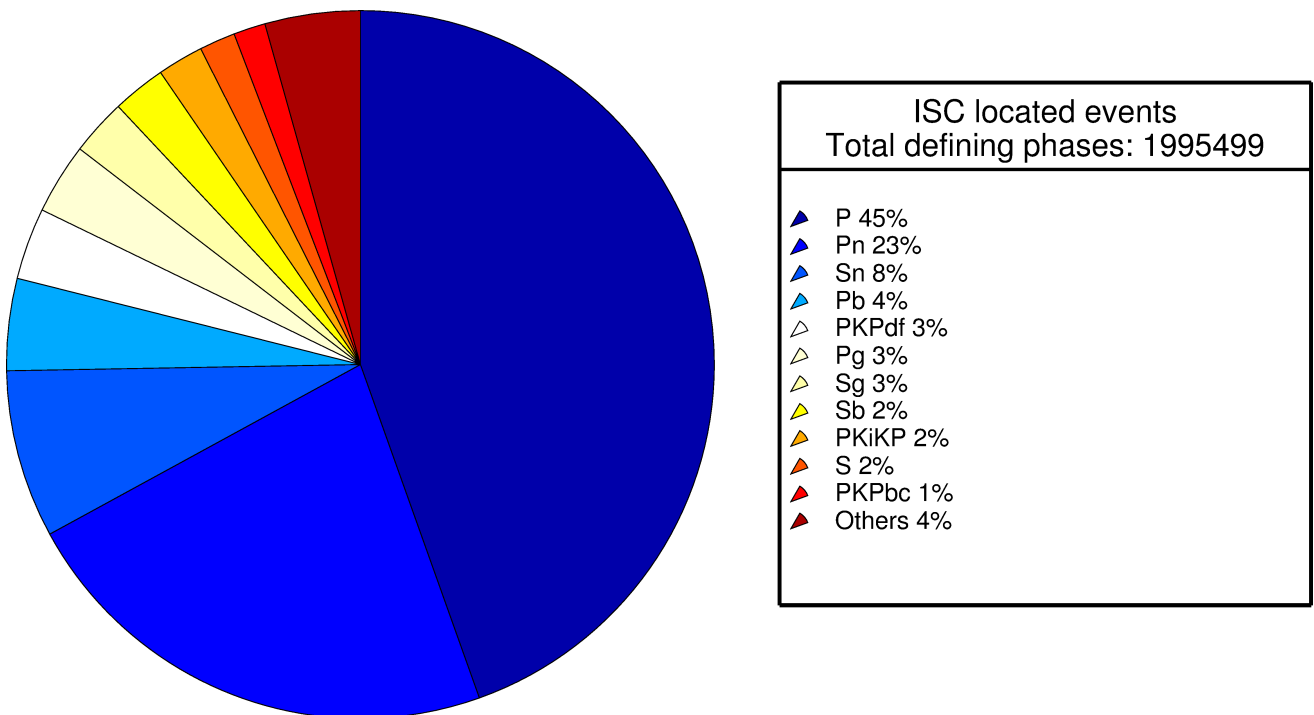


Figure 8.16: Pie chart showing the defining phases in the ISC Bulletin, for events located by the ISC. A complete list of defining phases is shown in Table 8.1.

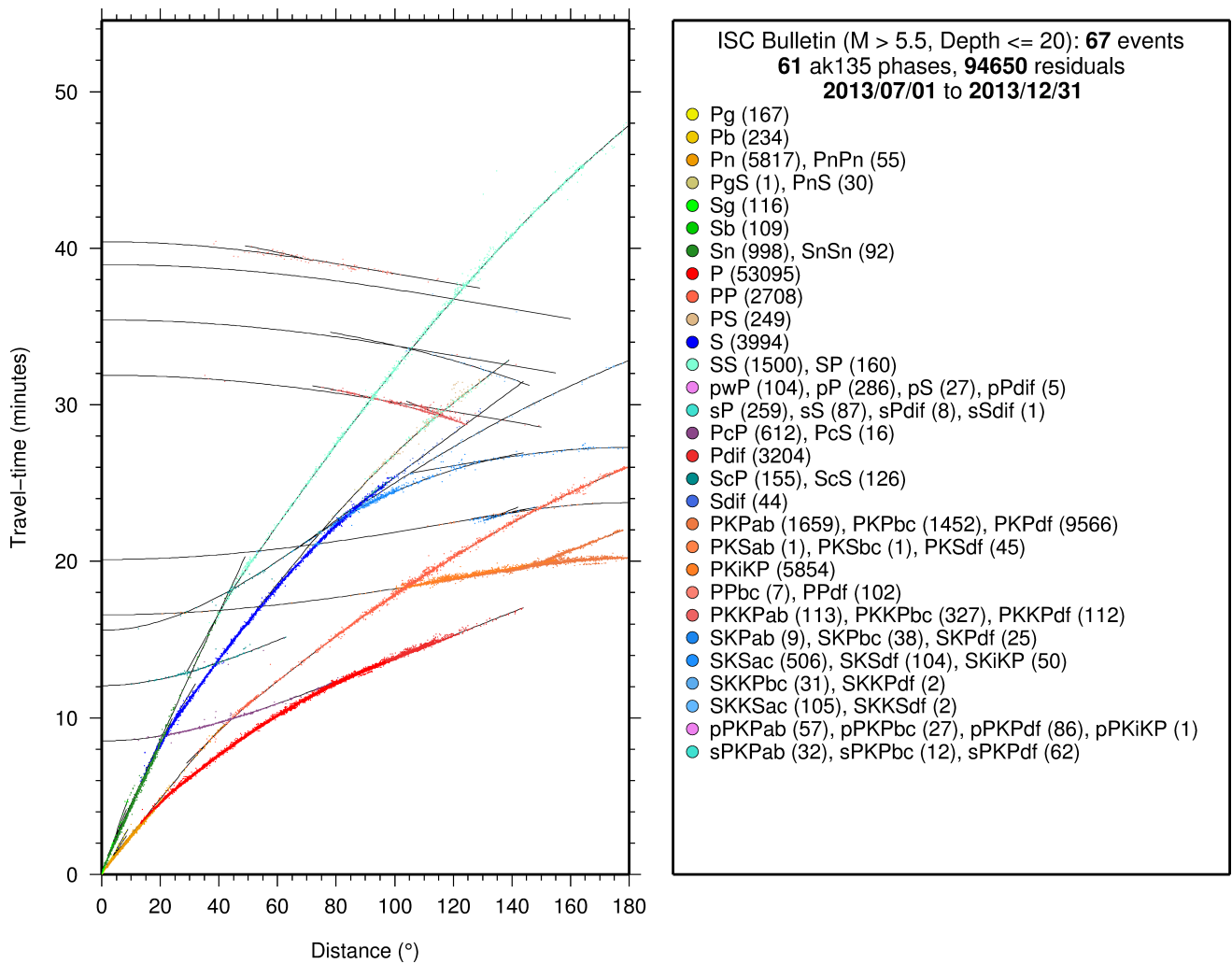


Figure 8.17: Distribution of travel-time observations in the ISC Bulletin for events with $M > 5.5$ and depth less than 20 km. The travel-time observations are shown relative to a 0 km source and compared with the theoretical ak135 travel-time curves (solid lines). The legend lists the number of each phase plotted.

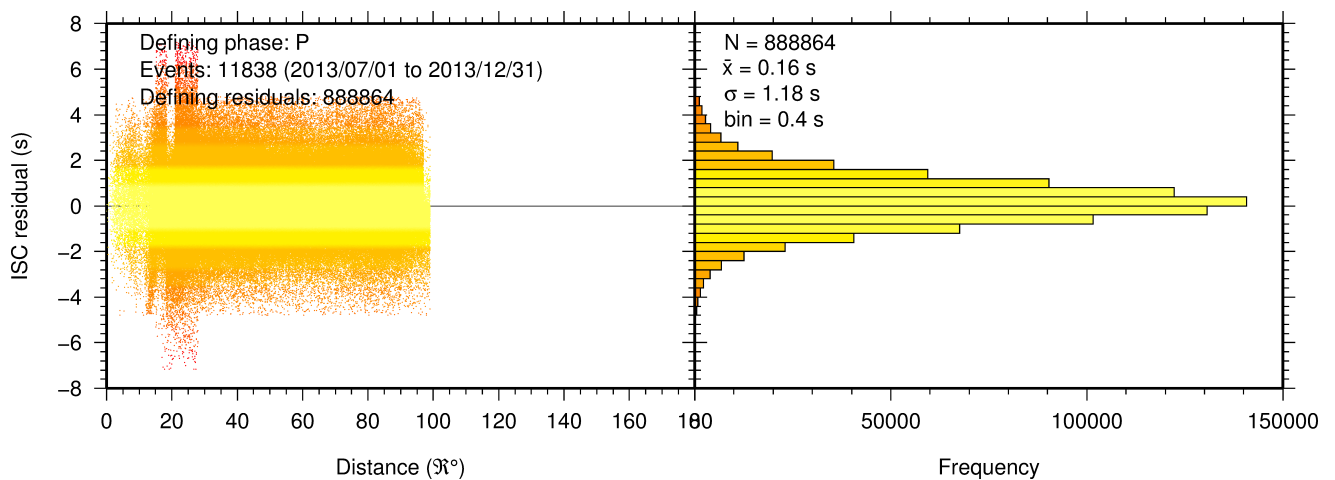


Figure 8.18: Distribution of travel-time residuals for the defining P phases used in the computation of ISC located events in the Bulletin.

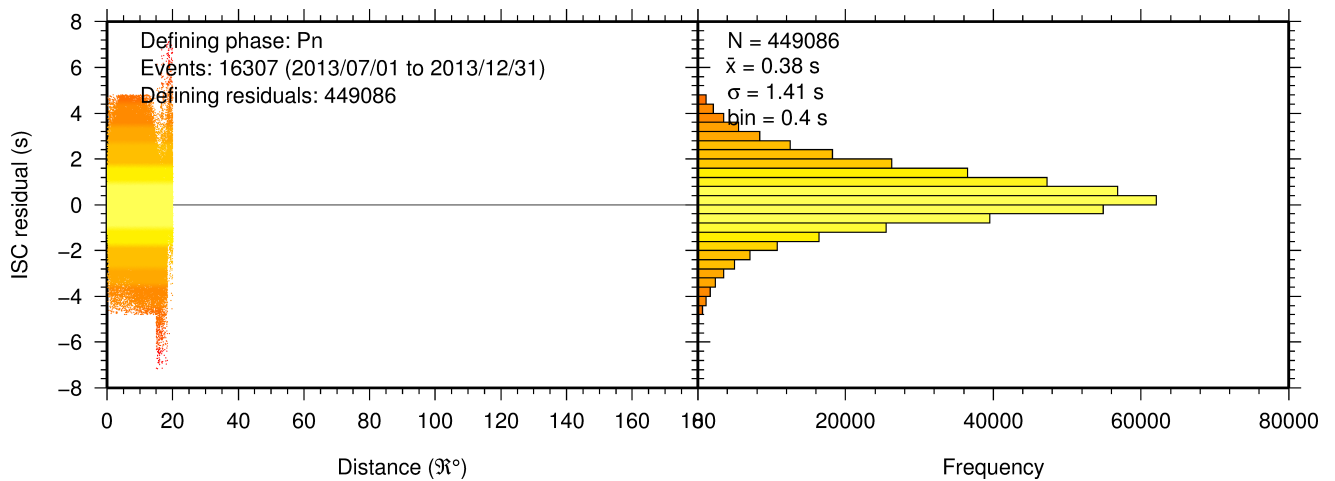


Figure 8.19: Distribution of travel-time residuals for the defining Pn phases used in the computation of ISC located events in the Bulletin.

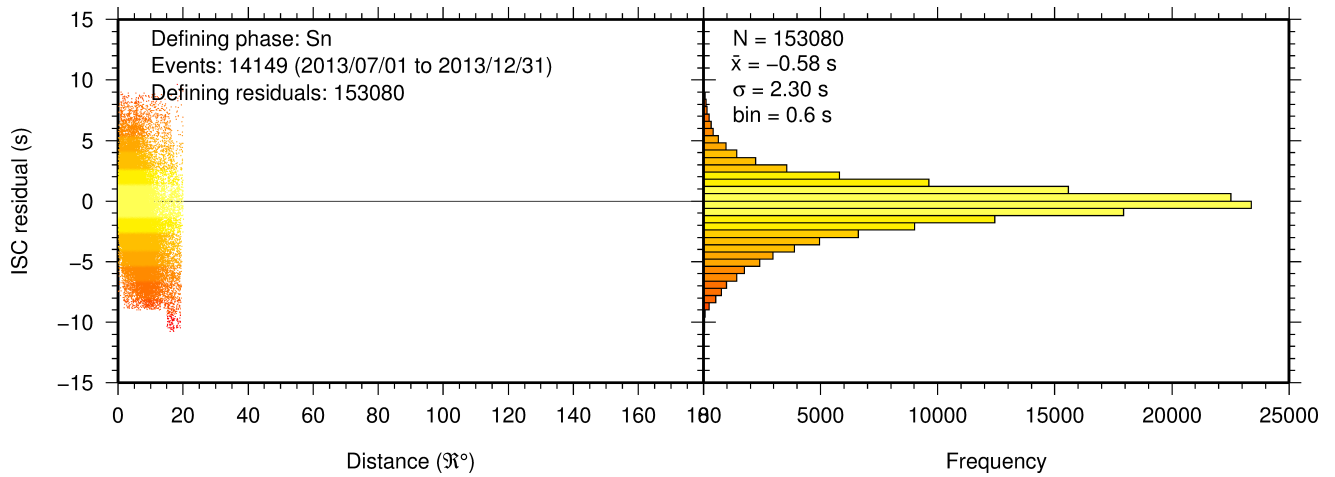


Figure 8.20: Distribution of travel-time residuals for the defining Sn phases used in the computation of ISC located events in the Bulletin.

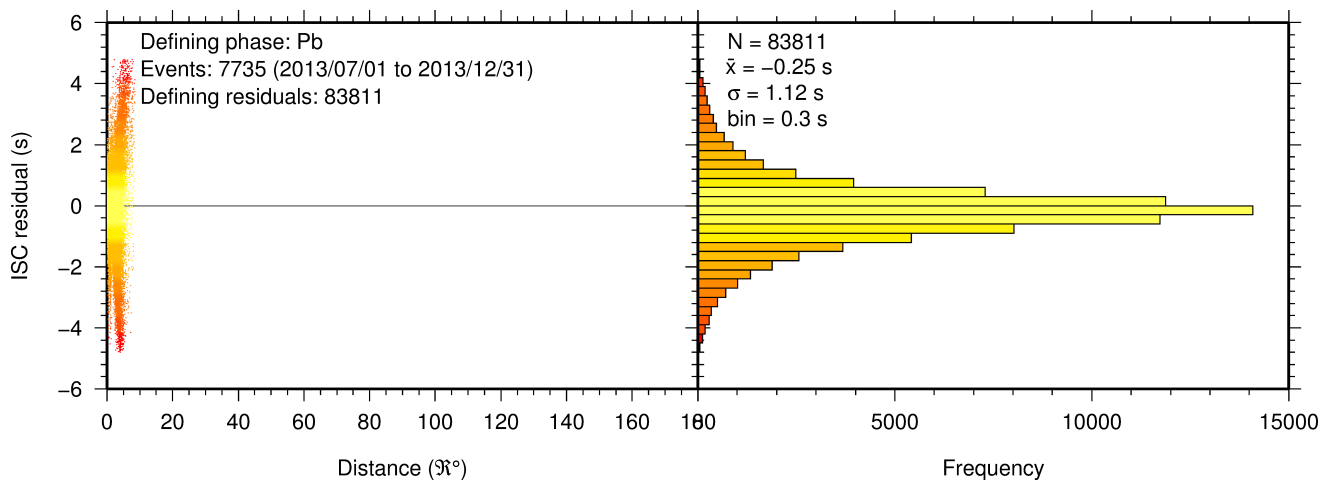


Figure 8.21: Distribution of travel-time residuals for the defining Pb phases used in the computation of ISC located events in the Bulletin.

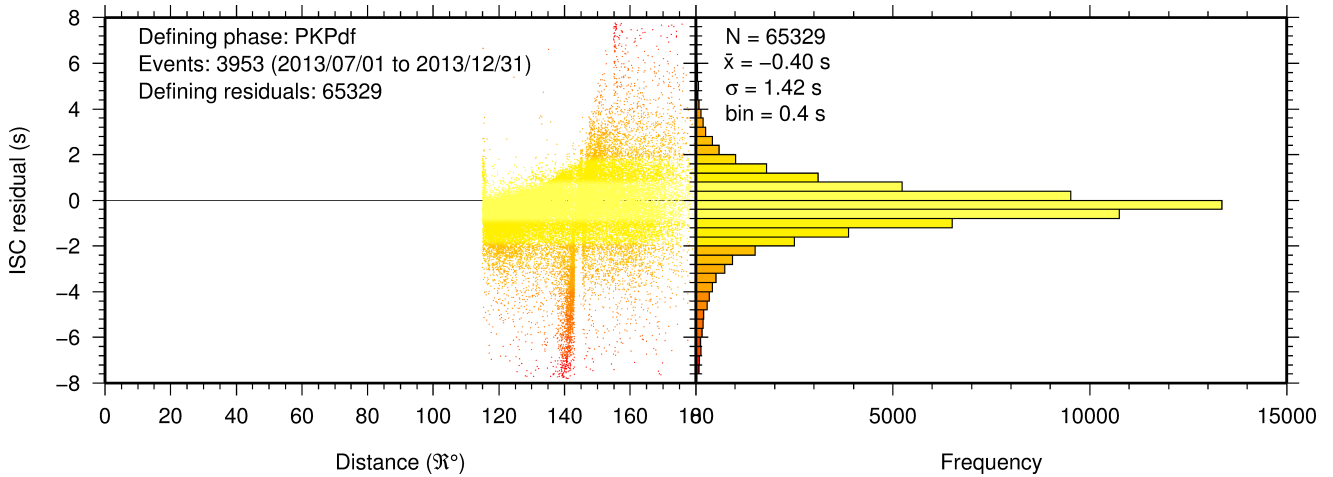


Figure 8.22: Distribution of travel-time residuals for the defining *Pg* phases used in the computation of ISC located events in the Bulletin.

8.3 Seismic Wave Amplitudes and Periods

The ISC Bulletin contains a variety of seismic wave amplitudes and periods measured by reporting agencies. For this Bulletin Summary, the total of collected amplitudes and periods is 762,1203 (see Section 7.3). For the determination of the ISC magnitudes *MS* and *mb*, only a fraction of such data can be used. Indeed, the ISC network magnitudes are computed only for ISC located events. Here we recall the main features of the ISC procedure for *MS* and *mb* computation (see detailed description in Section 3.4 of January to June 2013 Bulletin Summary). For each amplitude-period pair in a reading the ISC algorithm computes the magnitude (a reading can include several amplitude-period measurements) and the reading magnitude is assigned to the maximum A/T in the reading. If more than one reading magnitude is available for a station, the station magnitude is the median of the reading magnitudes. The network magnitude is computed then as the 20% alpha-trimmed median of the station magnitudes (at least three required). *MS* is computed for shallow earthquakes (depth ≤ 60 km) only and using amplitudes and periods on all three components (when available) if the period is within 10-60 s and the epicentral distance is between 20° and 160°. *mb* is computed also for deep earthquakes (depth down to 700 km) but only with amplitudes on the vertical component measured at periods ≤ 3 s in the distance range 21°-100°.

Table 8.2 is a summary of the amplitude and period data that contributed to the computation of station and ISC *MS* and *mb* network magnitudes for this Bulletin Summary.

	<i>MS</i>	<i>mb</i>
Number of amplitude-period data	126442	401529
Number of readings	113110	397452
Percentage of readings in the ISC located events with qualifying data for magnitude computation	14.0	42.1
Number of station magnitudes	107244	353958
Number of network magnitudes	2902	10159

Table 8.2: Summary of the amplitude-period data used by the ISC Locator to compute *MS* and *mb*.

A small percentage of the readings with qualifying data for *MS* and *mb* calculation have more than one amplitude-period pair. Notably, only 14.0% of the readings for the ISC located (shallow) events included qualifying data for *MS* computation, whereas for *mb* the percentage is much higher at 42.1%. This is due to the seismological practice of reporting agencies. Agencies contributing systematic reports of amplitude and period data are listed in Appendix Table 10.3. Obviously the ISC Bulletin would benefit if more agencies included surface wave amplitude-period data in their reports.

Figure 8.23 shows the distribution of the number of station magnitudes versus distance. For *mb* there is a significant increase in the distance range 70°-90°, whereas for *MS* most of the contributing stations are below 100°. The increase in number of station magnitude between 70°-90° for *mb* is partly due to the very dense distribution of seismic stations in North America and Europe with respect to earthquake occurring in various subduction zones around the Pacific Ocean.

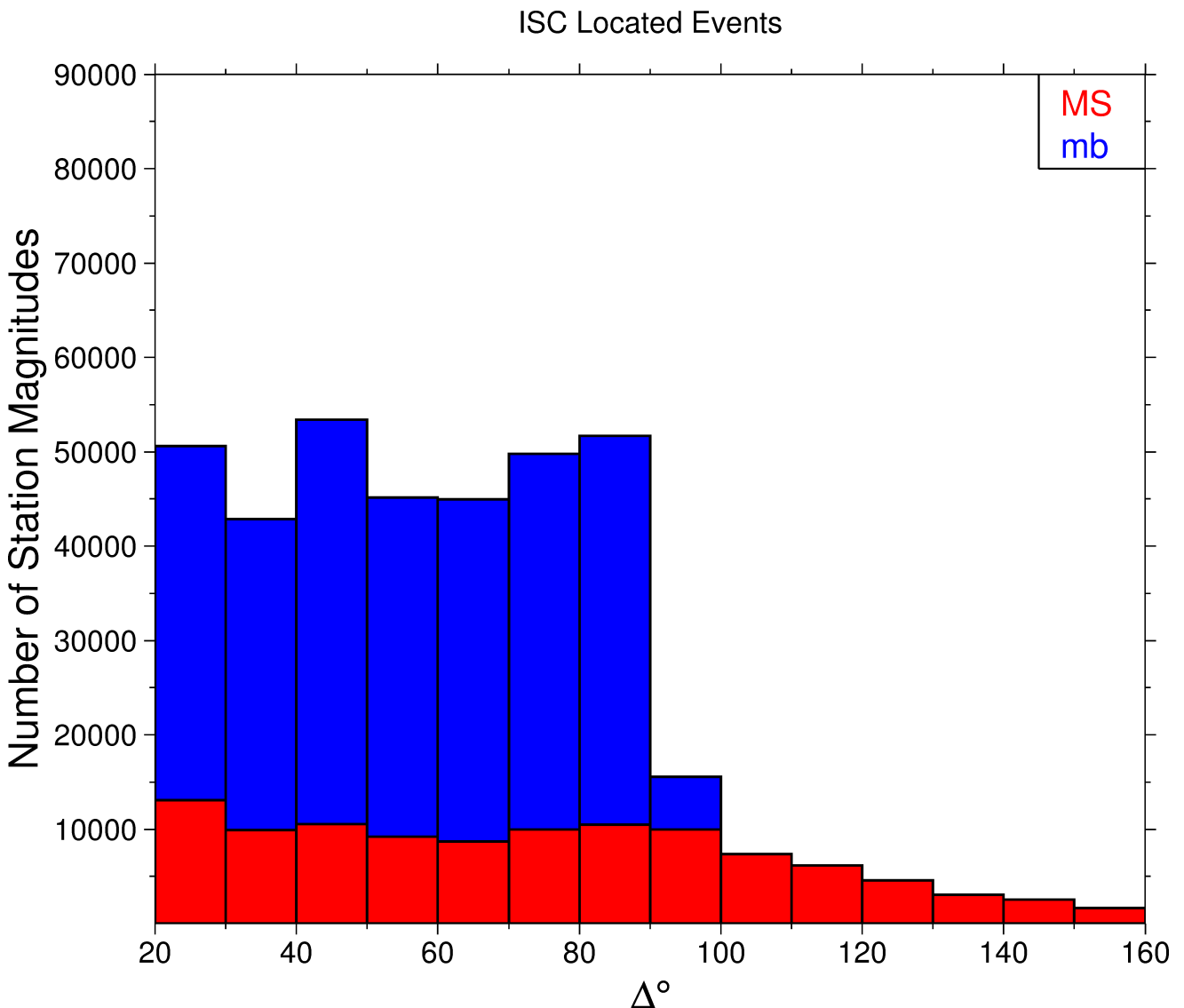


Figure 8.23: Distribution of the number of station magnitudes computed by the ISC Locator for *mb* (blue) and *MS* (red) versus distance.

Finally, Figure 8.24 shows the distribution of network *MS* and *mb* as well as the median number of stations for magnitude bins of 0.2. Clearly with increasing magnitude the number of events is smaller

but with a general tendency of having more stations contributing to the network magnitude.

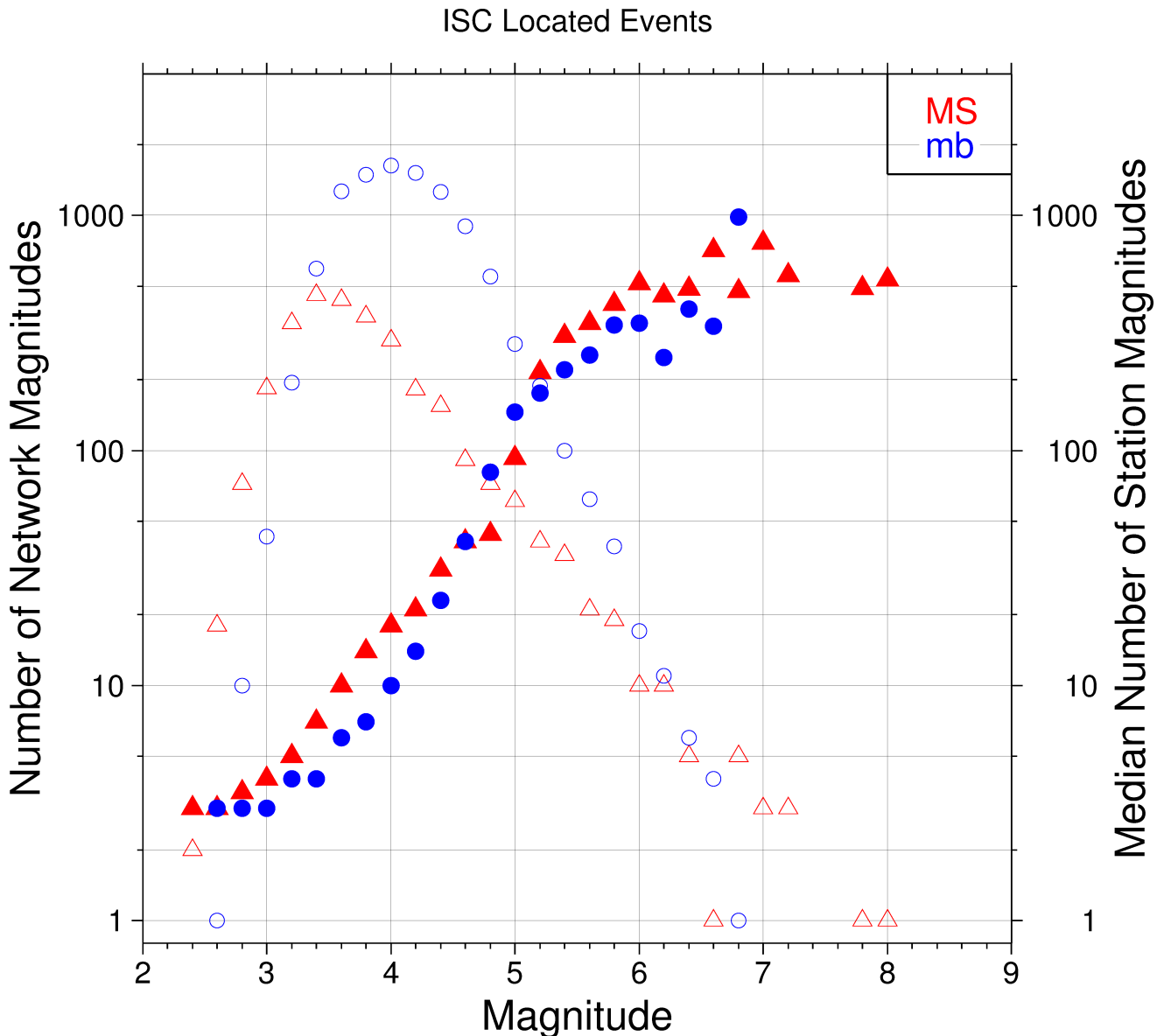


Figure 8.24: Number of network magnitudes (open symbols) and median number of stations magnitudes (filled symbols). Blue circles refer to mb and red triangles to MS. The width of the magnitude interval δM is 0.2, and each symbol includes data with magnitude in $M \pm \delta M/2$.

8.4 Completeness of the ISC Bulletin

The completeness of the ISC Bulletin can be expressed as a magnitude value, above which we expect the Bulletin to contain 100% of events. This magnitude of completeness, M_C can be measured as the point where the seismicity no longer follows the Gutenberg-Richter relationship. We compute an estimate of M_C using the maximum curvature technique of *Woessner and Wiemer (2005)*.

The completeness of the ISC Bulletin for this summary period is shown in Figure 8.25. A history of completeness for the ISC Bulletin is shown in Figure 8.26. The step change in 1996 corresponds with the inclusion of the Prototype IDC (EIDC) Bulletin, followed by the Reviewed Event Bulletin (REB) of

the IDC.

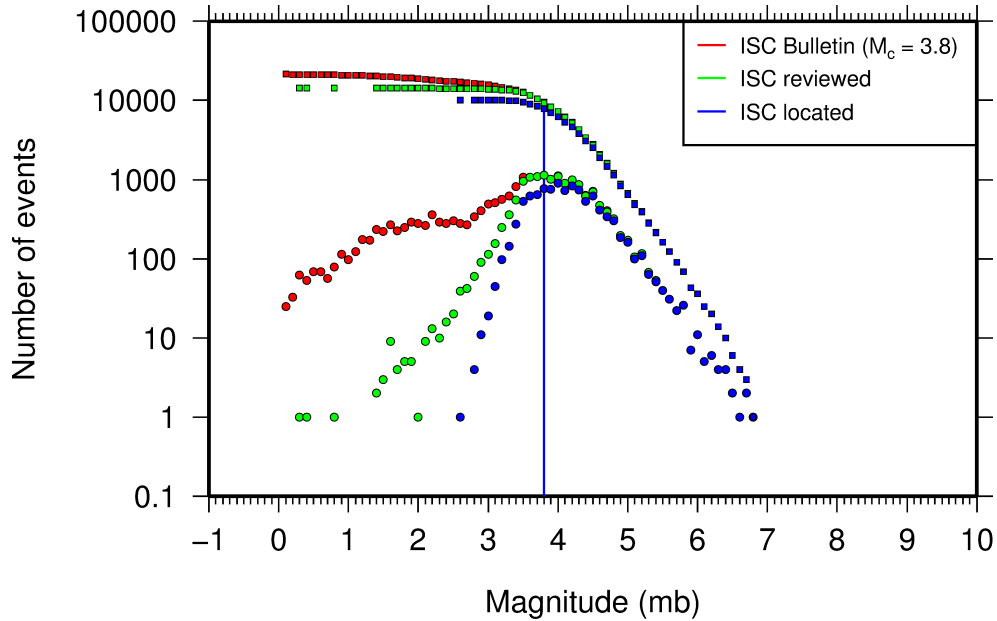


Figure 8.25: Frequency and cumulative frequency magnitude distribution for all events in the ISC Bulletin, ISC reviewed events and events located by the ISC. The magnitude of completeness (M_C) is shown for the ISC Bulletin. Note: only events with values of mb are represented in the figure.

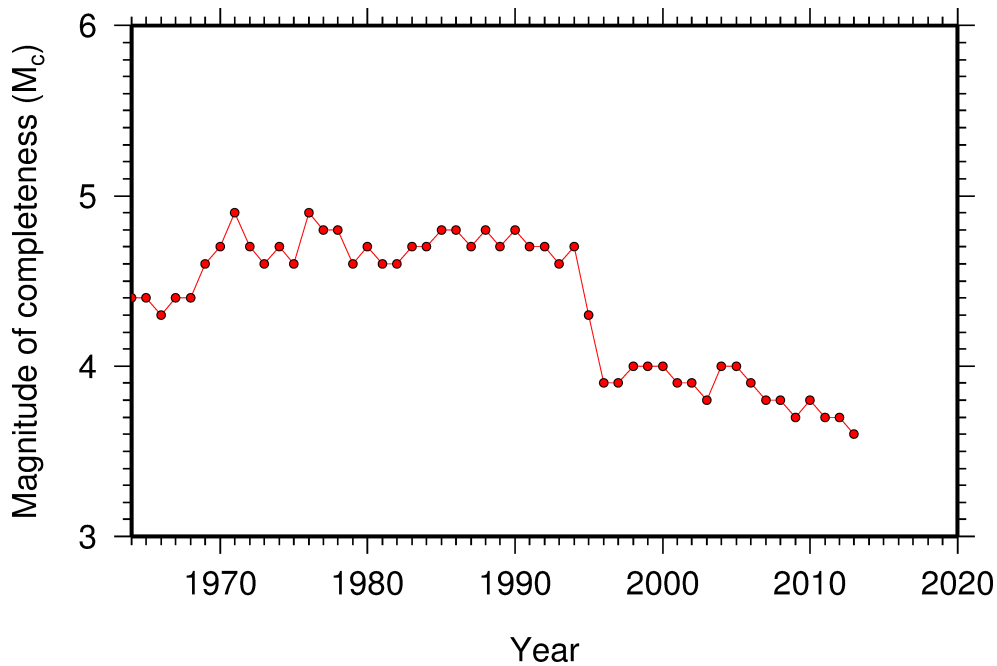


Figure 8.26: Variation of magnitude of completeness (M_C) for each year in the ISC Bulletin. Note: M_C is calculated only using those events with values of mb .

8.5 Magnitude Comparisons

The ISC Bulletin publishes network magnitudes reported by multiple agencies to the ISC. For events that have been located by the ISC, where enough amplitude data has been collected, the MS and mb

magnitudes are calculated by the ISC (MS is computed only for depths ≤ 60 km). In this section, ISC magnitudes and some other reported magnitudes in the ISC Bulletin are compared.

The comparison between MS and mb computed by the ISC locator for events in this summary period is shown in Figure 8.27, where the large number of data pairs allows a colour coding of the data density. The scatter in the data reflects the fundamental differences between these magnitude scales.

Similar plots are shown in Figure 8.28 and 8.29, respectively, for comparisons of ISC mb and ISC MS with M_W from the GCMT catalogue. Since M_W is not often available below magnitude 5, these distributions are mostly for larger, global events. Not surprisingly, the scatter between mb and M_W is larger than the scatter between MS and M_W . Also, the saturation effect of mb is clearly visible for earthquakes with $M_W > 6.5$. In contrast, MS scales well with $M_W > 6$, whereas for smaller magnitudes MS appears to be systematically smaller than M_W .

In Figure 8.30 ISC values of mb are compared with all reported values of mb , values of mb reported by NEIC and values of mb reported by IDC. Similarly in Figure 8.31, ISC values of MS are compared with all reported values of MS , values of MS reported by NEIC and values of MS reported by IDC. There is a large scatter between the ISC magnitudes and the mb and MS reported by all other agencies.

The scatter decreases both for mb and MS when ISC magnitudes are compared just with NEIC and IDC magnitudes. This is not surprising as the latter two agencies provide most of the amplitudes and periods used by the ISC locator to compute MS and mb . However, ISC mb appears to be smaller than NEIC mb for $mb < 4$ and larger than IDC mb for $mb > 4$. Since NEIC does not include IDC amplitudes, it seems these features originate from observations at the high-gain, low-noise sites reported by the IDC. For the MS comparisons between ISC and NEIC a similar but smaller effect is observed for $MS < 4.5$, whereas a good scaling is generally observed for the MS comparisons between ISC and IDC.

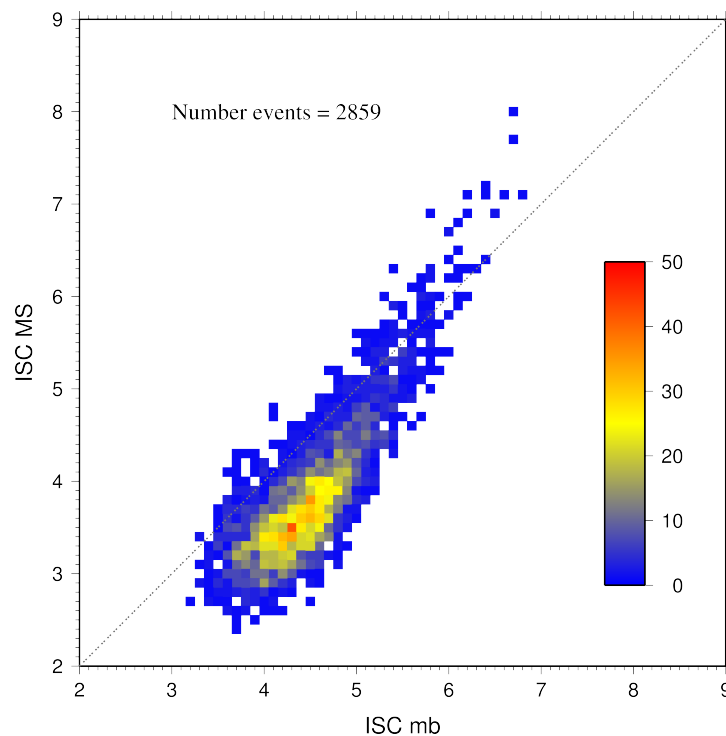


Figure 8.27: Comparison of ISC values of MS with mb for common event pairs.

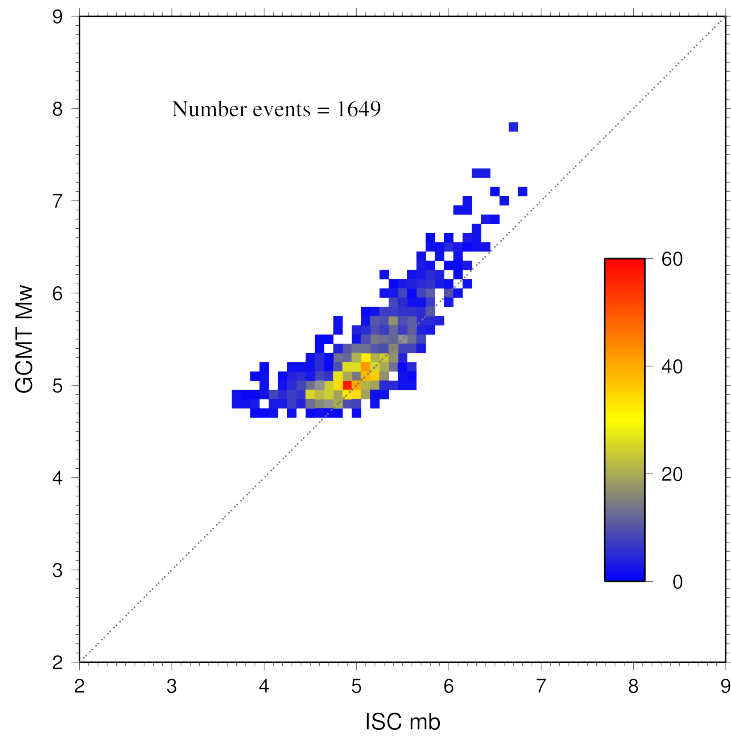


Figure 8.28: Comparison of ISC values of m_b with GCMT M_W for common event pairs.

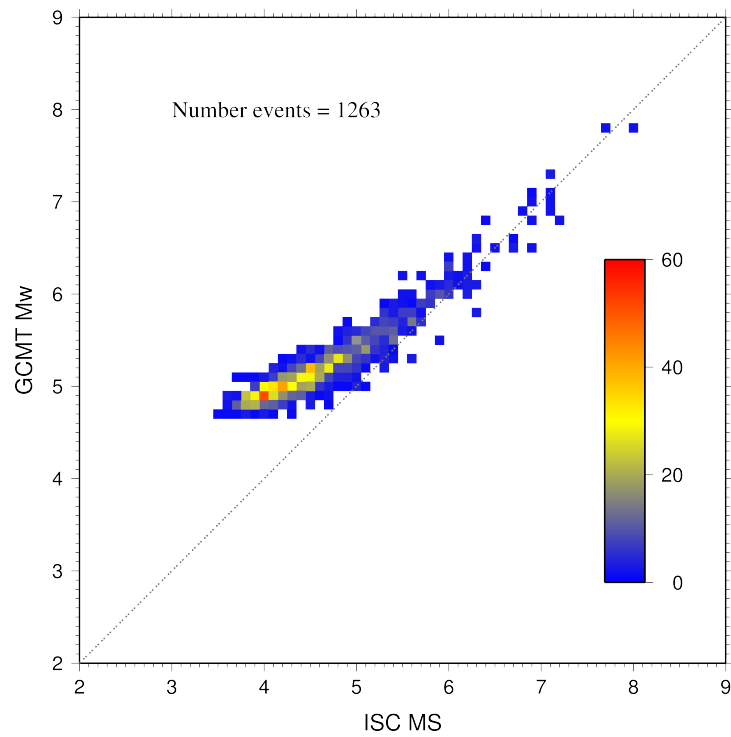


Figure 8.29: Comparison of ISC values of M_S with GCMT M_W for common event pairs.

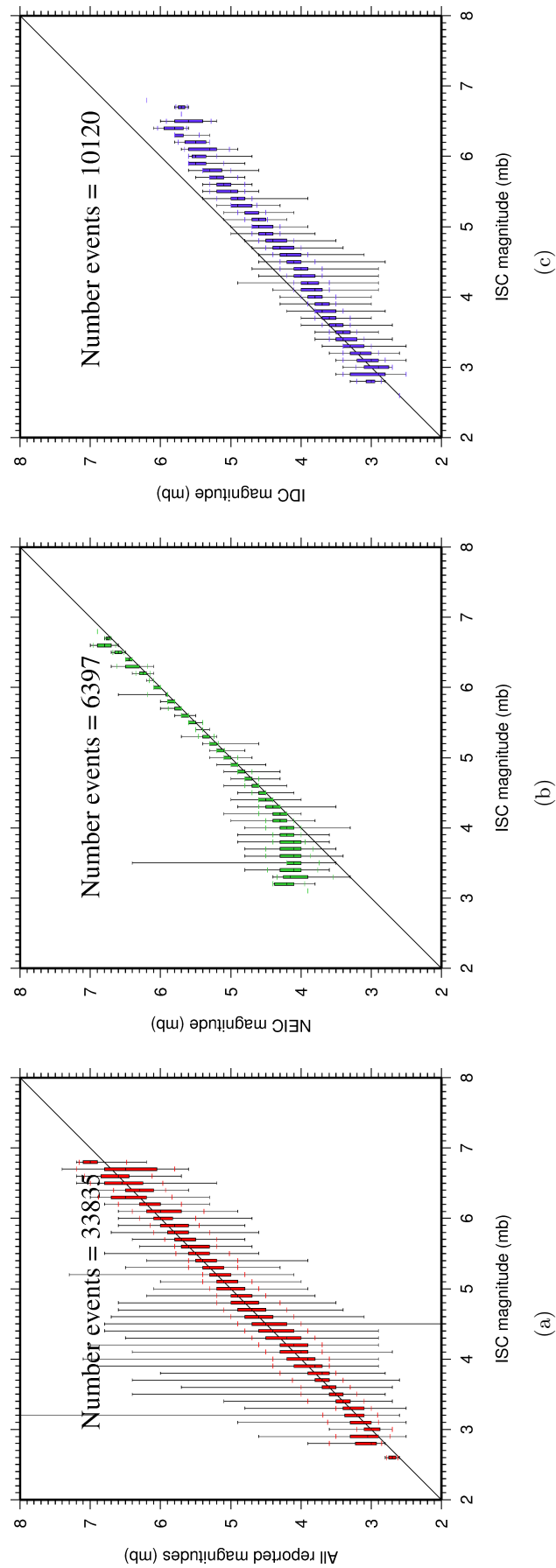


Figure 8.30: Comparison of ISC magnitude data (mb) with additional agency magnitudes (mb). The statistical summary is shown in box-and-whisker plots where the 10th and 90th percentiles are shown in addition to the max and min values. (a): All magnitudes reported; (b): NEIC magnitudes; (c): IDC magnitudes.

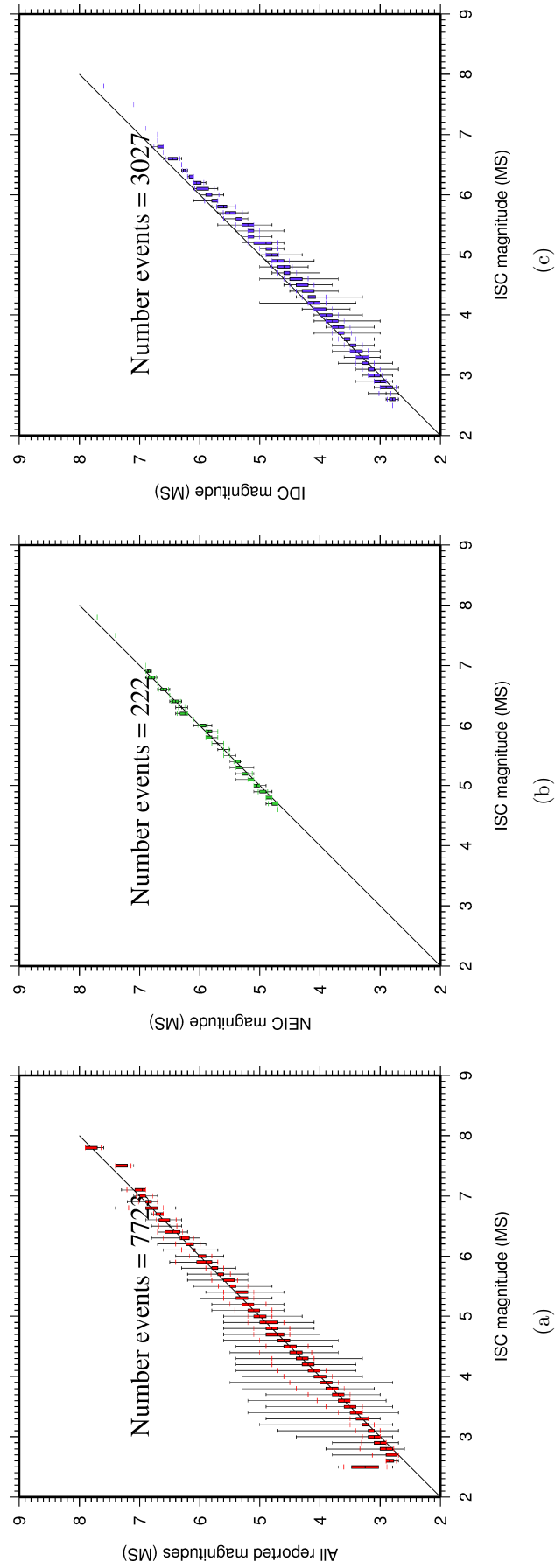


Figure 8.31: Comparison of ISC magnitude data (MS) with additional agency magnitudes (MS). The statistical summary is shown in the box-and-whisker plots where the 10th and 90th percentiles are shown in addition to the max and min values. (a): All magnitudes reported; (b): NEIC magnitudes; (c): IDC magnitudes.

9

The Leading Data Contributors

For the current six-month period, 145 agencies reported related bulletin data. Although we are grateful for every report, we nevertheless would like to acknowledge those agencies that made the most useful or distinct contributions to the contents of the ISC Bulletin. Here we note those agencies that:

- provided a comparatively large volume of parametric data (see Section 9.1),
- reported data that helped quite considerably to improve the quality of the ISC locations or magnitude determinations (see Section 9.2),
- helped the ISC by consistently reporting data in one of the standard recognised formats and in-line with the ISC data collection schedule (see Section 9.3).

We do not aim to discourage those numerous small networks who provide comparatively smaller yet still most essential volumes of regional data regularly, consistently and accurately. Without these reports the ISC Bulletin would not be as comprehensive and complete as it is today.

9.1 The Largest Data Contributors

We acknowledge the contribution of IDC, NEIC, MOS, BJI, BRA, CLL, GCMT and a few others (Figure 9.1) that reported the majority of moderate to large events recorded at teleseismic distances. The contributions of NEIC, IDC, JMA and several others are also acknowledged with respect to smaller seismic events. The contributions of JMA, NEIC, IDC, TAP, ROM, and a number of others are also acknowledged with respect to small seismic events. Note that the NEIC bulletin accumulates a contribution of all regional networks in the USA. Several agencies monitoring highly seismic regions routinely report large volumes of small to moderate magnitude events, such as those in Japan, Chinese Taipei, Turkey, Chile, Italy, Greece, New Zealand, Mexico and Columbia. Contributions of small magnitude events by agencies in regions of low seismicity, such as Finland are also gratefully received.

We also would like to acknowledge contributions of those agencies that report a large portion of arrival time and amplitude data (Figure 9.2). For small magnitude events, these are local agencies in charge of monitoring local and regional seismicity. For moderate to large events, contributions of IDC, USArray, NEIC, MOS are especially acknowledged. Notably, three agencies (IDC, NEIC and MOS) together reported over 80% of all amplitude measurements made for teleseismically recorded events. We hope that other agencies would also be able to update their monitoring routines in the future to include the amplitude reports for teleseismic events compliant with the IASPEI standards.

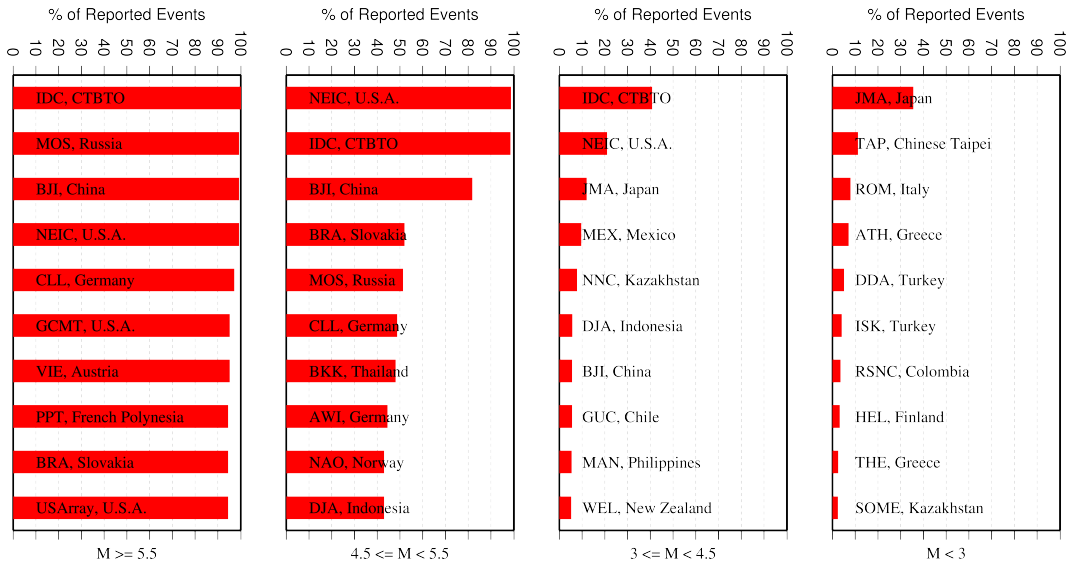


Figure 9.1: Frequency of events in the ISC Bulletin for which an agency reported at least one item of data: a moment tensor, a hypocentre, a station arrival time or an amplitude. The top ten agencies are shown for four magnitude intervals.

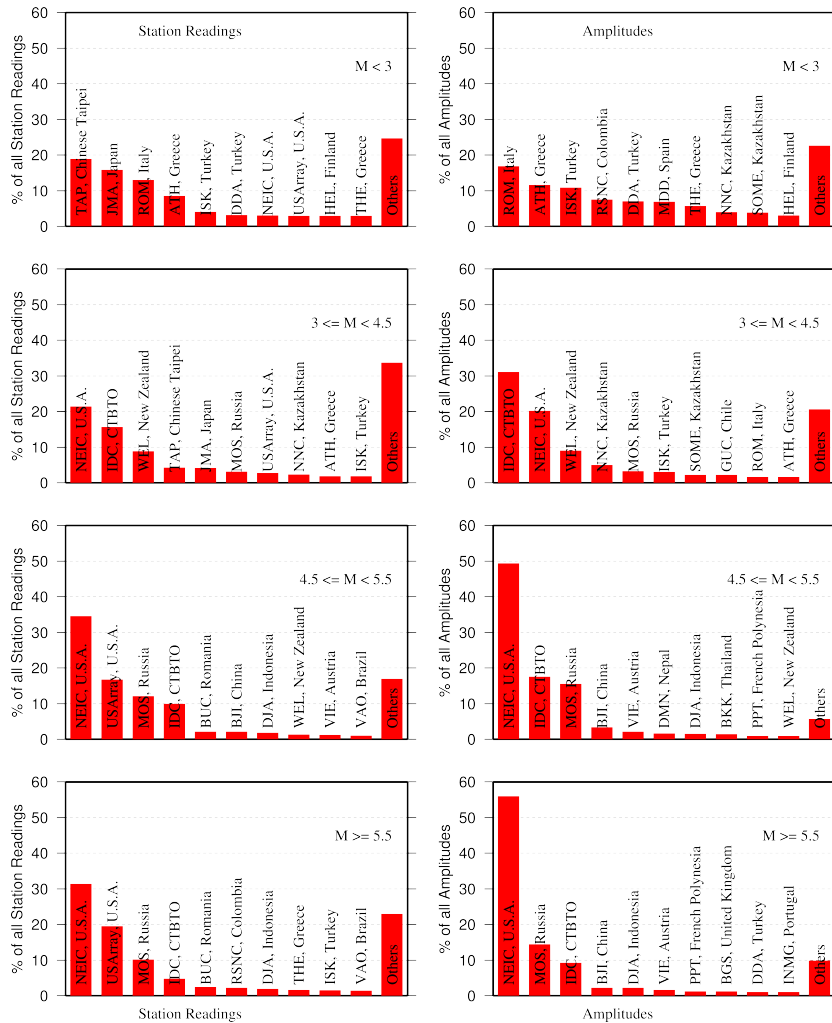


Figure 9.2: Contributions of station arrival time readings (left) and amplitudes (right) of agencies to the ISC Bulletin. Top ten agencies are shown for four magnitude intervals.

9.2 Contributors Reporting the Most Valuable Parameters

One of the main ISC duties is to re-calculate hypocentre estimates for those seismic events where a collective wealth of all station reports received from all agencies is likely to improve either the event location or depth compared to the hypocentre solution from each single agency. For areas with a sparse local seismic network or an unfavourable station configuration, readings made by other networks at teleseismic distances are very important. All events near mid-oceanic ridges as well as those in the majority of subduction zones around the world fall into this category. Hence we greatly appreciate the effort made by many agencies that report data for remote earthquakes (Figure 9.3). For some agencies, such as the IDC and the NEIC, it is part of their mission. For instance, the IDC reports almost every seismic event that is large enough to be recorded at teleseismic distance (20 degrees and beyond). This is largely because the International Monitoring System of primary arrays and broadband instruments is distributed at quiet sites around the world in order to be able to detect possible violations of the Comprehensive Nuclear-Test-Ban Treaty. The NEIC reported over 48% of those events as their mission requires them to report events above magnitude 4.5 outside the United States of America. For other agencies reporting distant events it is an extra effort that they undertake to notify their governments and relief agencies as well as to help the ISC and academic research in general. Hence these agencies usually report on the larger magnitude events. BJI, NAO, MOS, CLL, BRA, AWI, DMN and PRU each reported individual station arrivals for several percent of all relevant events. We encourage other agencies to report distant events to us.

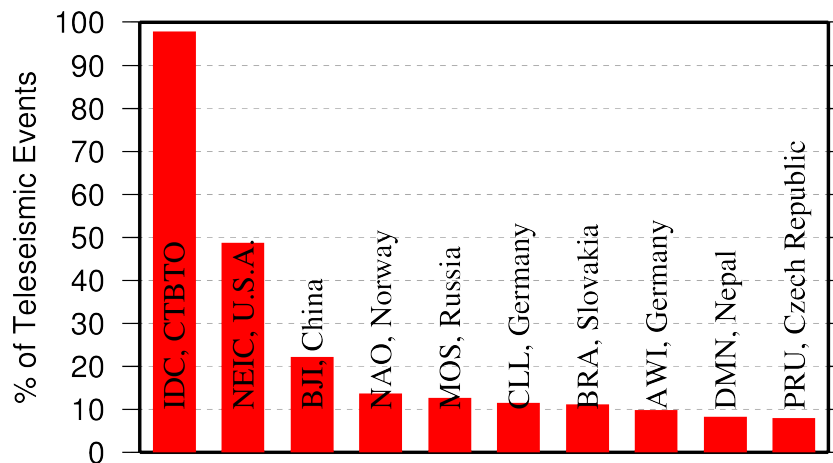


Figure 9.3: Top ten agencies that reported teleseismic phase arrivals for a large portion of ISC events.

In addition to the first arriving phase we encourage reporters to contribute observations of secondary seismic phases that help constrain the event location and depth: S, Sn, Sg and pP, sP, PcP (Figure 9.4). We expect though that these observations are actually made from waveforms, rather than just predicted by standard velocity models and modern software programs. It is especially important that these arrivals are manually reviewed by an operator (as we know takes place at the IDC and NEIC), as opposed to some lesser attempts to provide automatic phase readings that are later rejected by the ISC due to a generally poor quality of unreviewed picking.

Another important long-term task that the ISC performs is to compute the most definitive values of MS and mb network magnitudes that are considered reliable due to removal of outliers and consequent

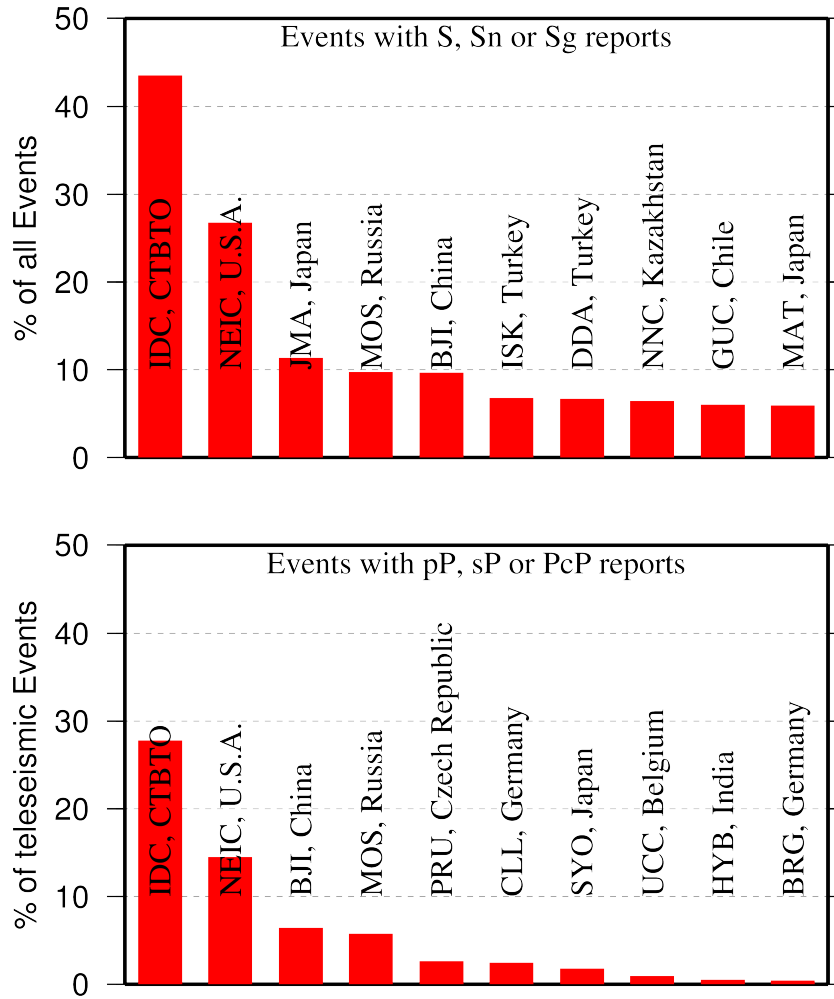


Figure 9.4: Top ten agencies that reported secondary phases important for an accurate epicentre location (top) and focal depth determination (bottom).

averaging (using alpha-trimmed median) across the largest network of stations, generally not feasible for a single agency. Despite concern over the bias at the lower end of m_b introduced by the body wave amplitude data from the IDC, other agencies are also known to bias the results. This topic is further discussed in Section 8.5.

Notably, the IDC reports almost 100% of all events for which M_S and m_b are estimated. This is due to the standard routine that requires determination of body and surface wave magnitudes useful for discrimination purposes. NEIC, MOS, BJI, PPT, PRU, NAO and a few other agencies (Figure 9.5) are also responsible for the majority of the amplitude and period reports that contribute towards the ISC magnitudes.

Since the ISC does not routinely process waveforms, we rely on other agencies to report moment magnitudes as well as moment tensor determinations (Figure 9.6).

Among other event parameters the ISC Bulletin also contains information on event type. We cannot independently verify the type of each event in the Bulletin and thus rely on other agencies to report the event type to us. Practices of reporting non-tectonic events vary greatly from country to country. Many agencies do not include anthropogenic events in their reports. Suppression of such events from reports to the ISC may lead to a situation where a neighbouring agency reports the anthropogenic event

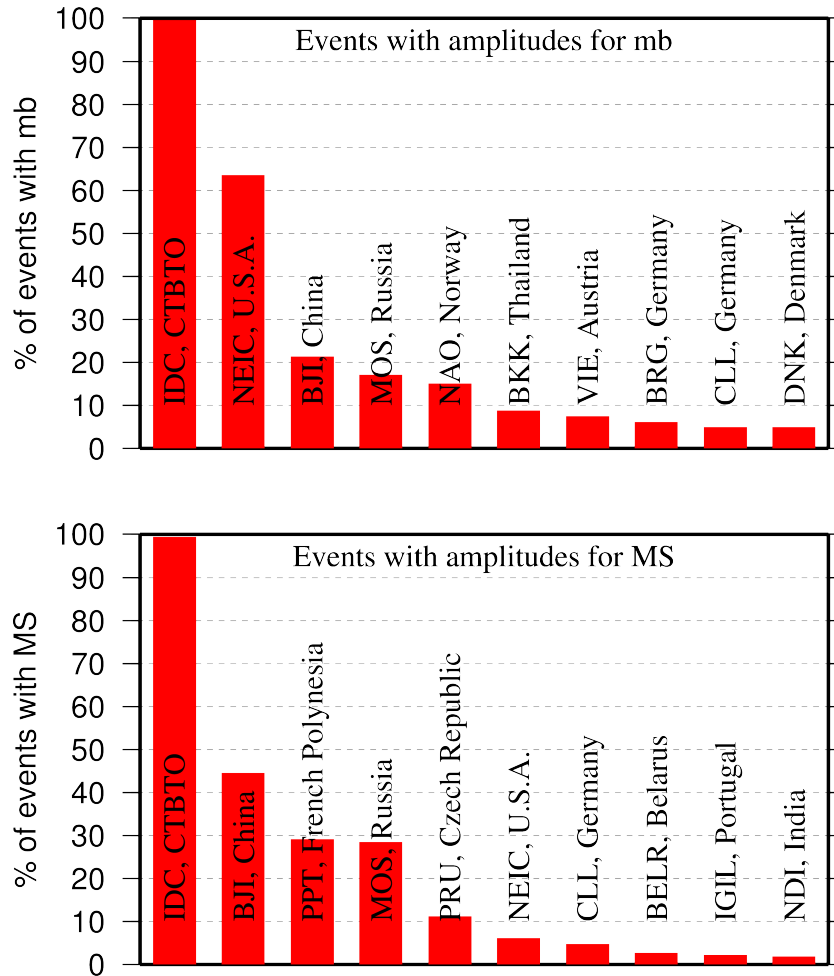


Figure 9.5: Agencies that report defining body (top) and surface (bottom) wave amplitudes and periods for the largest fraction of those ISC Bulletin events with MS/mb determinations.

as an earthquake for which expected data are missing. This in turn is detrimental to ISC Bulletin users studying natural seismic hazard. Hence we encourage all agencies to join the agencies listed on Figure 9.7 and several others in reporting both natural and anthropogenic events to the ISC.

The ISC Bulletin also contains felt and damaging information when local agencies have reported it to us. Agencies listed on Figure 9.8 provide such information for the majority of all felt or damaging events in the ISC Bulletin.

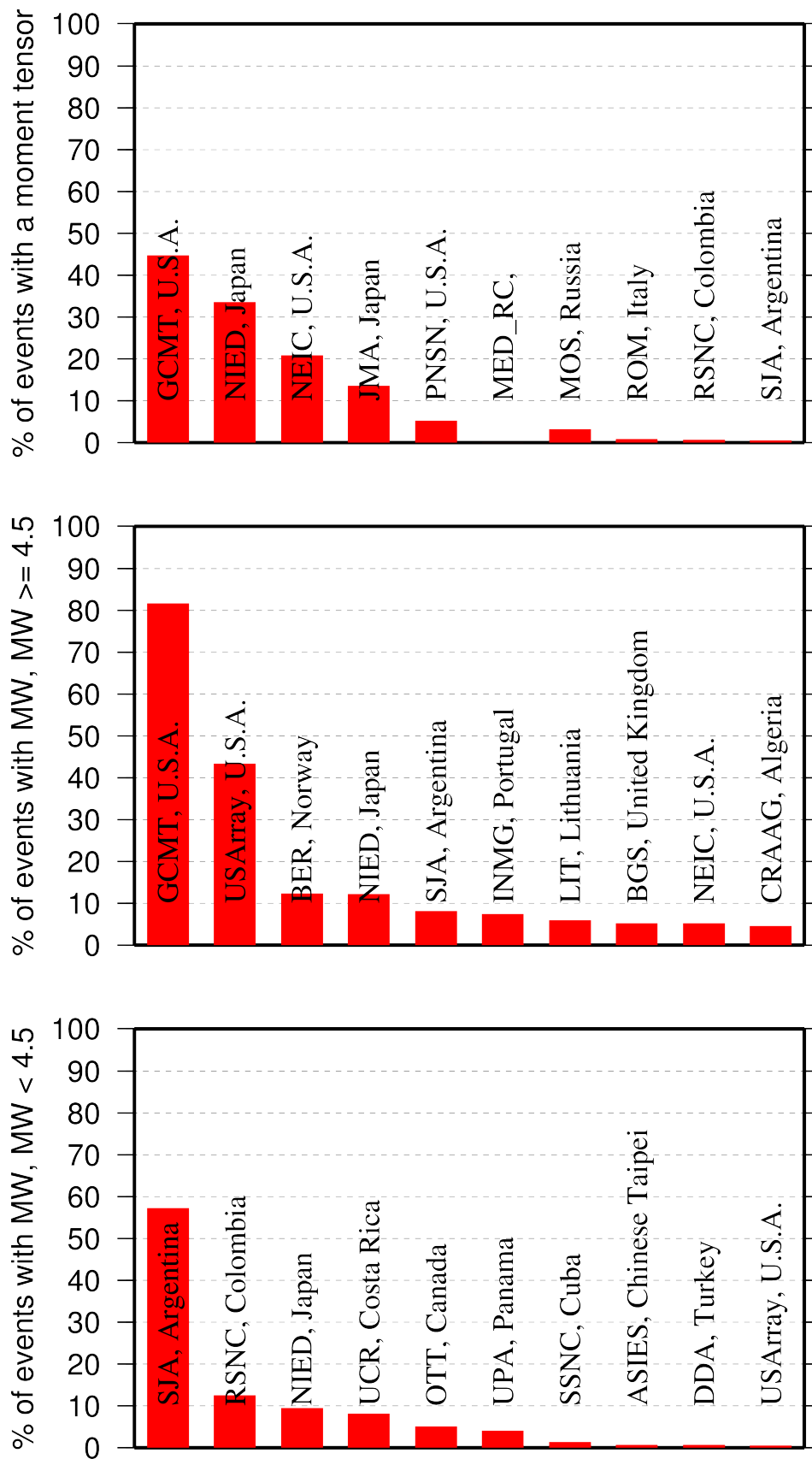


Figure 9.6: Top ten agencies that most frequently report determinations of seismic moment tensor (top) and moment magnitude (middle/bottom for M greater/smaller than 4.5).

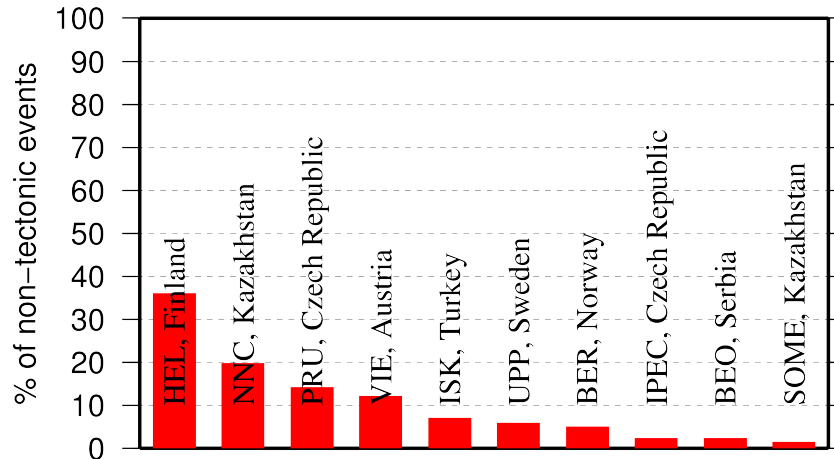


Figure 9.7: Top ten agencies that most frequently report non-tectonic seismic events to the ISC.

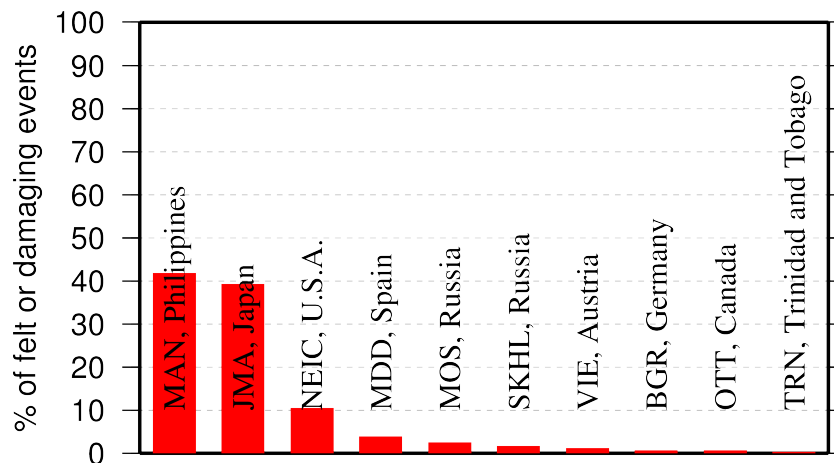


Figure 9.8: Top ten agencies that most frequently report macroseismic information to the ISC.

9.3 The Most Consistent and Punctual Contributors

During this six-month period, 35 agencies reported their bulletin data in one of the standard seismic formats (ISF, IMS, GSE, Nordic or QuakeML) and within the current 12-month deadline. Here we must reiterate that the ISC accepts reviewed bulletin data after a final analysis as soon as they are ready. These data, even if they arrive before the deadline, are immediately parsed into the ISC database, grouped with other data and become available to the ISC users on-line as part of the preliminary ISC Bulletin. There is no reason to wait until the deadline to send the data to the ISC. Table 9.1 lists all agencies that have been helpful to the ISC in this respect during the six-month period.

Agency Code	Country	Average Delay from real time (days)
LDG	France	24
PPT	French Polynesia	25
NAO	Norway	26
LIC	Ivory Coast	33
IGIL	Portugal	36
ISK	Turkey	51
IDC	Austria	59
UCC	Belgium	61
BUL	Zimbabwe	62
ISN	Iraq	66
SVSA	Portugal	67
KRSC	Russia	77
AUST	Australia	84
BEO	Serbia	86
INMG	Portugal	100
BJI	China	106
ATH	Greece	109
THE	Greece	117
DMN	Nepal	135
BGS	United Kingdom	138
BGR	Germany	149
IRIS	U.S.A.	167
QCP	Philippines	196
NERS	Russia	240
BYKL	Russia	241
LSZ	Zambia	254
LIT	Lithuania	275
TEH	Iran	302
NSSC	Syria	302
UPP	Sweden	340
VIE	Austria	346
STR	France	347
PRE	South Africa	353
RSNC	Colombia	356
MOS	Russia	361

Table 9.1: Agencies that contributed reviewed bulletin data to the ISC in one of the standard international formats before the submission deadline.

10

Appendix

Table 10.1: Listing of all 333 agencies that have directly reported to the ISC. The 145 agencies highlighted in bold have reported data to the ISC Bulletin for the period of this Bulletin Summary.

Agency Code	Agency Name
AAA	Alma-ata, Kazakhstan
AAE	University of Addis Ababa, Ethiopia
AAM	University of Michigan, USA
ADE	Primary Industries and Resources SA, Australia
ADH	Observatorio Afonso Chaves, Portugal
AEIC	Alaska Earthquake Information Center, USA
AFAR	The Afar Depression: Interpretation of the 1960-2000 Earthquakes, Israel
ALG	Algiers University, Algeria
ANF	USArray Array Network Facility, USA
ANT	Antofagasta, Chile
ARE	Instituto Geofisico del Peru, Peru
ARO	Observatoire Géophysique d'Arta, Djibouti
ASIES	Institute of Earth Sciences, Academia Sinica, Chinese Taipei
ASL	Albuquerque Seismological Laboratory, USA
ASM	University of Asmara, Eritrea
ASRS	Altai-Sayan Seismological Centre, GS SB RAS, Russia
ATA	The Earthquake Research Center Ataturk University, Turkey
ATH	National Observatory of Athens, Greece
AUST	Geoscience Australia, Australia
AWI	Alfred Wegener Institute for Polar and Marine Research, Germany
AZER	Republic Center of Seismic Survey, Azerbaijan
BCIS	Bureau Central International de Sismologie, France
BDF	Observatório Sismológico da Universidade de Brasília, Brazil
BELR	Centre of Geophysical Monitoring, Belarus
BEO	Seismological Survey of Serbia, Serbia
BER	University of Bergen, Norway
BERK	Berkheimer H, Germany
BGR	Bundesanstalt für Geowissenschaften und Rohstoffe, Germany
BGS	British Geological Survey, United Kingdom
BHUIJ2	Study of Aftershocks of the Bhuj Earthquake by Japanese Research Team, Japan
BIAK	Biak earthquake aftershocks (17-Feb-1996), USA
BJI	China Earthquake Networks Center, China
BKK	Thai Meteorological Department, Thailand
BNS	Erdbebenstation, Geologisches Institut der Universität, Köl, Germany
BOG	Universidad Javeriana, Colombia

Table 10.1: Continued.

Agency Code	Agency Name
BRA	Geophysical Institute, Slovak Academy of Sciences, Slovakia
BRG	Seismological Observatory Berggießhübel, TU Bergakademie Freiberg, Germany
BRK	Berkeley Seismological Laboratory, USA
BRS	Brisbane Seismograph Station, Australia
BUC	National Institute for Earth Physics, Romania
BUD	Geodetic and Geophysical Research Institute, Hungary
BUG	Institute of Geology, Mineralogy & Geophysics, Germany
BUL	Goetz Observatory, Zimbabwe
BUT	Montana Bureau of Mines and Geology, USA
BYKL	Baykal Regional Seismological Centre, GS SB RAS, Russia
CADCG	Central America Data Centre, Costa Rica
CAN	Australian National University, Australia
CANSK	Canadian and Scandinavian Networks, Sweden
CAR	Instituto Sismologico de Caracas, Venezuela
CASC	Central American Seismic Center, Costa Rica
CENT	Centennial Earthquake Catalog, USA
CERI	Center for Earthquake Research and Information, USA
CFUSG	Inst. of Seismology and Geodynamics, V.I. Vernadsky Crimean Federal University, Republic of Crimea
CLL	Geophysikalisches Observatorium Collm, Germany
CMWS	Laboratory of Seismic Monitoring of Caucasus Mineral Water Region, GSRAS, Russia
CNG	Seismographic Station Changalane, Mozambique
CNRM	Centre National de Recherche, Morocco
COSMOS	Consortium of Organizations for Strong Motion Observations, USA
CRAAG	Centre de Recherche en Astronomie, Astrophysique et Géophysique, Algeria
CSC	University of South Carolina, USA
CSEM	Centre Sismologique Euro-Méditerranéen (CSEM/EMSC), France
DASA	Defense Atomic Support Agency, USA
DBN	Koninklijk Nederlands Meteorologisch Instituut, Netherlands
DDA	Disaster and Emergency Management Presidency, Turkey
DHMR	Yemen National Seismological Center, Yemen
DIAS	Dublin Institute for Advanced Studies, Ireland
DJA	Badan Meteorologi, Klimatologi dan Geofisika, Indonesia
DMN	National Seismological Centre, Nepal, Nepal
DNK	Geological Survey of Denmark and Greenland, Denmark
DRS	Dagestan Branch, Geophysical Survey, Russian Academy of Sciences, Russia
DSN	Dubai Seismic Network, United Arab Emirates
DUSS	Damascus University, Syria, Syria
EAF	East African Network, Unknown
EAGLE	Ethiopia-Afar Geoscientific Lithospheric Experiment, Unknown
EBR	Observatori de l'Ebre, Spain
EBSE	Ethiopian Broadband Seismic Experiment, Unknown

Table 10.1: Continued.

Agency Code	Agency Name
ECX	Red Sismica del Noroeste de Mexico (RESOM), Mexico
EFATE	OBS Experiment near Efate, Vanuatu, USA
EHB	Engdahl, van der Hilst and Buland, USA
EIDC	Experimental (GSETT3) International Data Center, USA
EKA	Eskdalemuir Array Station, United Kingdom
ENT	Geological Survey and Mines Department, Uganda
EPSI	Reference events computed by the ISC for EPSI project, United Kingdom
ERDA	Energy Research and Development Administration, USA
EST	Geological Survey of Estonia, Estonia
FBR	Fabra Observatory, Spain
FDF	Fort de France, Martinique
FIA0	Finessa Array, Finland
FOR	Unknown Historical Agency, Unknown - historical agency
FUNV	Fundación Venezolana de Investigaciones Sismológicas, Venezuela
FUR	Geophysikalisches Observatorium der Universität München, Germany
GBZT	Marmara Research Center, Turkey
GCG	INSIVUMEH, Guatemala
GCMT	The Global CMT Project, USA
GDNRW	Geologischer Dienst Nordrhein-Westfalen, Germany
GEM	, Unknown
GEN	Dipartimento per lo Studio del Territorio e delle sue Risorse (RSNI), Italy
GFZ	Helmholtz Centre Potsdam GFZ German Research Centre For Geosciences, Germany
GII	The Geophysical Institute of Israel, Israel
GOM	Observatoire Volcanologique de Goma, Democratic Republic of the Congo
GRAL	National Council for Scientific Research, Lebanon
GSDM	Geological Survey Department Malawi, Malawi
GTFE	German Task Force for Earthquakes, Germany
GUC	Centro Sismológico Nacional, Universidad de Chile, Chile
HAN	Hannover, Germany
HDC	Observatorio Vulcanológico y Sismológico de Costa Rica, Costa Rica
HEL	Institute of Seismology, University of Helsinki, Finland
HFS	Hagfors Observatory, Sweden
HFS1	Hagfors Observatory, Sweden
HFS2	Hagfors Observatory, Sweden
HKC	Hong Kong Observatory, Hong Kong
HLUG	Hessisches Landesamt für Umwelt und Geologie, Germany
HLW	National Research Institute of Astronomy and Geophysics, Egypt
HNR	Ministry of Mines, Energy and Rural Electrification, Solomon Islands
HON	Pacific Tsunami Warning Center - NOAA, USA
HRVD	Harvard University, USA
HRVD_LR	Department of Geological Sciences, Harvard University, USA

Table 10.1: Continued.

Agency Code	Agency Name
HVO	Hawaiian Volcano Observatory, USA
HYB	National Geophysical Research Institute, India
HYD	National Geophysical Research Institute, India
IAG	Instituto Andaluz de Geofisica, Spain
IASPEI	IASPEI Working Group on Reference Events, USA
ICE	Instituto Costarricense de Electricidad, Costa Rica
IDC	International Data Centre, CTBTO, Austria
IDG	Institute of Dynamics of Geosphere, Russian Academy of Sciences, Russia
IEPN	Institute of Environmental Problems of the North, Russian Academy of Sciences, Russia
IGIL	Instituto Geofisico do Infante Dom Luiz, Portugal
IGQ	Servicio Nacional de Sismología y Vulcanología, Ecuador
IGS	Institute of Geological Sciences, United Kingdom
INDEPTH3	International Deep Profiling of Tibet and the Himalayas, USA
INET	Instituto Nicaragüense de Estudios Territoriales, Nicaragua
INMG	Instituto Português do Mar e da Atmosfera, I.P., Portugal
IPEC	The Institute of Physics of the Earth (IPEC), Czech Republic
IPER	Institute of Physics of the Earth, Academy of Sciences, Moscow, Russia
IPGP	Institut de Physique du Globe de Paris, France
IPRG	Institute for Petroleum Research and Geophysics, Israel
IRIS	IRIS Data Management Center, USA
IRSM	Institute of Rock Structure and Mechanics, Czech Republic
ISK	Kandilli Observatory and Research Institute, Turkey
ISN	Iraqi Meteorological and Seismology Organisation, Iraq
ISS	International Seismological Summary, United Kingdom
IST	Institute of Physics of the Earth, Technical University of Istanbul, Turkey
ISU	Institute of Seismology, Academy of Sciences, Republic of Uzbekistan, Uzbekistan
JEN	Geodynamisches Observatorium Moxa, Germany
JMA	Japan Meteorological Agency, Japan
JOH	Bernard Price Institute of Geophysics, South Africa
JSN	Jamaica Seismic Network, Jamaica
JSO	Jordan Seismological Observatory, Jordan
KBC	Institut de Recherches Géologiques et Minières, Cameroon
KEW	Kew Observatory, United Kingdom
KHC	Geofysikalni Ustav, Ceske Akademie Ved, Czech Republic
KISR	Kuwait Institute for Scientific Research, Kuwait
KLM	Malaysian Meteorological Service, Malaysia
KMA	Korea Meteorological Administration, Republic of Korea
KNET	Kyrgyz Seismic Network, Kyrgyzstan
KOLA	Kola Regional Seismic Centre, GS RAS, Russia
KRAR	Krasnoyarsk Scientific Research Inst. of Geology and Mineral Resources, Russia, Russia
KRL	Geodätisches Institut der Universität Karlsruhe, Germany
KRNET	Institute of Seismology, Academy of Sciences of Kyrgyz Republic, Kyrgyzstan

Table 10.1: Continued.

Agency Code	Agency Name
KRSC	Kamchatkan Experimental and Methodical Seismological Department, GS RAS, Russia
KSA	Observatoire de Ksara, Lebanon
KUK	Geological Survey Department of Ghana, Ghana
LAO	Large Aperture Seismic Array, USA
LDG	Laboratoire de Détection et de Géophysique/CEA, France
LDN	University of Western Ontario, Canada
LDO	Lamont-Doherty Earth Observatory, USA
LED	Landeserdbebendienst Baden-Württemberg, Germany
LEDBW	Landeserdbebendienst Baden-Württemberg, Germany
LER	Besucherbergwerk Binweide Station, Germany
LIB	Tripoli, Libya
LIC	Station Géophysique de Lamto, Ivory Coast
LIM	Lima, Peru
LIS	Instituto de Meteorologia, Portugal
LIT	Geological Survey of Lithuania, Lithuania
LJU	Environmental Agency of the Republic of Slovenia, Slovenia
LPA	Universidad Nacional de La Plata, Argentina
LSZ	Geological Survey Department of Zambia, Zambia
LVSN	Latvian Seismic Network, Latvia
MAN	Philippine Institute of Volcanology and Seismology, Philippines
MAT	The Matsushiro Seismological Observatory, Japan
MCO	Macao Meteorological and Geophysical Bureau, Macao, China
MDD	Instituto Geográfico Nacional, Spain
MED_RCMT	MedNet Regional Centroid - Moment Tensors, Italy
MES	Messina Seismological Observatory, Italy
MEX	Instituto de Geofísica de la UNAM, Mexico
MIRAS	Mining Institute of the Ural Branch of the Russian Academy of Sciences, Russia
MOLD	Institute of Geophysics and Geology, Moldova
MOS	Geophysical Survey of Russian Academy of Sciences, Russia
MOZ	Direccao Nacional de Geologia, Mozambique
MRB	Institut Cartogràfic de Catalunya, Spain
MSI	Messina Seismological Observatory, Italy
MSSP	Micro Seismic Studies Programme, PINSTECH, Pakistan
MUN	Mundaring Observatory, Australia
NAI	University of Nairobi, Kenya
NAM	The Geological Survey of Namibia, Namibia
NAO	Stiftelsen NORSAR, Norway
NCEDC	Northern California Earthquake Data Center, USA
NDI	National Centre for Seismology of the Ministry of Earth Sciences of India, India
NEIC	National Earthquake Information Center, USA
NEIS	National Earthquake Information Service, USA
NERS	North Eastern Regional Seismological Centre, GS RAS, Russia
NIC	Cyprus Geological Survey Department, Cyprus

Table 10.1: Continued.

Agency Code	Agency Name
NIED	National Research Institute for Earth Science and Disaster Prevention, Japan
NNC	National Nuclear Center, Kazakhstan
NORS	North Ossetia (Alania) Branch, Geophysical Survey, Russian Academy of Sciences, Russia
NOU	IRD Centre de Nouméa, New Caledonia
NSSC	National Syrian Seismological Center, Syria
NSSP	National Survey of Seismic Protection, Armenia
OBM	Research Centre of Astronomy and Geophysics, Mongolia
OGSO	Ohio Geological Survey, USA
OMAN	Sultan Qaboos University, Oman
ORF	Orfeus Data Center, Netherlands
OSPL	Observatorio Sismologico Politecnico Loyola, Dominican Republic
OSUB	Osservatorio Sismologico Universita di Bari, Italy
OTT	Canadian Hazards Information Service, Natural Resources Canada, Canada
PAL	Palisades, USA
PAS	California Institute of Technology, USA
PDA	Universidade dos Açores, Portugal
PDG	Seismological Institute of Montenegro, Montenegro
PEK	Peking, China
PGC	Pacific Geoscience Centre, Canada
PLV	National Center for Scientific Research, Vietnam
PMEL	Pacific seismicity from hydrophones, USA
PMR	Alaska Tsunami Warning Center, USA
PNNL	Pacific Northwest National Laboratory, USA
PNSN	Pacific Northwest Seismic Network, USA
PPT	Laboratoire de Géophysique/CEA, French Polynesia
PRE	Council for Geoscience, South Africa
PRU	Geophysical Institute, Academy of Sciences of the Czech Republic, Czech Republic
PTO	Instituto Geofísico da Universidade do Porto, Portugal
PTWC	Pacific Tsunami Warning Center, USA
QCP	Manila Observatory, Philippines
QUE	Pakistan Meteorological Department, Pakistan
QUI	Escuela Politécnica Nacional, Ecuador
RAB	Rabaul Volcanological Observatory, Papua New Guinea
RBA	Université Mohammed V, Morocco
REN	MacKay School of Mines, USA
REY	Icelandic Meteorological Office, Iceland
RHSSO	Republic Hydrometeorological Service, Seismological Observatory, Banja Luka, Bosnia-Herzegovina
RISSC	Laboratory of Research on Experimental and Computational Seimology, Italy
RMIT	Royal Melbourne Institute of Technology, Australia
ROC	Odenbach Seismic Observatory, USA

Table 10.1: Continued.

Agency Code	Agency Name
ROM	Istituto Nazionale di Geofisica e Vulcanologia, Italy
RRLJ	Regional Research Laboratory Jorhat, India
RSMAC	Red Sísmica Mexicana de Apertura Continental, Mexico
RSNC	Red Sismológica Nacional de Colombia, Colombia
RSPR	Red Sísmica de Puerto Rico, USA
RYD	King Saud University, Saudi Arabia
SAPSE	Southern Alps Passive Seismic Experiment, New Zealand
SAR	Sarajevo Seismological Station, Bosnia and Herzegovina
SCB	Observatorio San Calixto, Bolivia
SCEDC	Southern California Earthquake Data Center, USA
SDD	Universidad Autonoma de Santo Domingo, Dominican Republic
SEA	Geophysics Program AK-50, USA
SET	Setif Observatory, Algeria
SFS	Real Instituto y Observatorio de la Armada, Spain
SGS	Saudi Geological Survey, Saudi Arabia
SHL	Central Seismological Observatory, India
SIGU	Subbotin Institute of Geophysics, National Academy of Sciences, Ukraine
SIK	Seismic Institute of Kosovo, Unknown
SIO	Scripps Institution of Oceanography, USA
SJA	Instituto Nacional de Prevención Sísmica, Argentina
SJS	Instituto Costarricense de Electricidad, Costa Rica
SKHL	Sakhalin Experimental and Methodological Seismological Expedition, GS RAS, Russia
SKL	Sakhalin Complex Scientific Research Institute, Russia
SKO	Seismological Observatory Skopje, FYR Macedonia
SLC	Salt Lake City, USA
SLM	Saint Louis University, USA
SNET	Servicio Nacional de Estudios Territoriales, El Salvador
SNM	New Mexico Institute of Mining and Technology, USA
SNSN	Saudi National Seismic Network, Saudi Arabia
SOF	Geophysical Institute, Bulgarian Academy of Sciences, Bulgaria
SOME	Seismological Experimental Methodological Expedition, Kazakhstan
SPA	USGS - South Pole, Antarctica
SPGM	Service de Physique du Globe, Morocco
SRI	Stanford Research Institute, USA
SSN	Sudan Seismic Network, Sudan
SSNC	Servicio Sismológico Nacional Cubano, Cuba
SSS	Centro de Estudios y Investigaciones Geotecnicas del San Salvador, El Salvador
STK	Stockholm Seismological Station, Sweden
STR	Institut de Physique du Globe, France
STU	Stuttgart Seismological Station, Germany
SVSA	Sistema de Vigilância Sismológica dos Açores, Portugal
SYO	National Institute of Polar Research, Japan

Table 10.1: Continued.

Agency Code	Agency Name
SZGRF	Seismologisches Zentralobservatorium Gräfenberg, Germany
TAC	Estación Central de Tacubaya, Mexico
TAN	Antananarivo, Madagascar
TANZANIA	Tanzania Broadband Seismic Experiment, USA
TAP	CWB, Chinese Taipei
TAU	University of Tasmania, Australia
TEH	Tehran University, Iran
TEIC	Center for Earthquake Research and Information, USA
THE	Department of Geophysics, Aristotle University of Thessaloniki, Greece
THR	International Institute of Earthquake Engineering and Seismology (IIEES), Iran
TIF	Seismic Monitoring Centre of Georgia, Georgia
TIR	The Institute of Seismology, Academy of Sciences of Albania, Albania
TRI	Istituto Nazionale di Oceanografia e di Geofisica Sperimentale (OGS), Italy
TRN	The University of the West Indies, Trinidad and Tobago
TTG	Titograd Seismological Station, Montenegro
TUL	Oklahoma Geological Survey, USA
TUN	Institut National de la Météorologie, Tunisia
TVA	Tennessee Valley Authority, USA
TZN	University of Dar Es Salaam, Tanzania
UAF	Department of Geosciences, USA
UAV	Red Sismológica de Los Andes Venezolanos, Venezuela
UCC	Royal Observatory of Belgium, Belgium
UCR	Sección de Sismología, Vulcanología y Exploración Geofísica, Costa Rica
UGN	Institute of Geonics AS CR, Czech Republic
ULE	University of Leeds, United Kingdom
UNAH	Universidad Nacional Autónoma de Honduras, Honduras
UPA	Universidad de Panama, Panama
UPIES	Institute of Earth- and Environmental Science, Germany
UPP	University of Uppsala, Sweden
UPSL	University of Patras, Department of Geology, Greece
USAEC	United States Atomic Energy Commission, USA
USCGS	United States Coast and Geodetic Survey, USA
USGS	United States Geological Survey, USA
UUSS	The University of Utah Seismograph Stations, USA
UVC	Universidad del Valle, Colombia
VAO	Instituto Astronómico e Geofísico, Brazil
VIE	Zentralanstalt für Meteorologie und Geodynamik (ZAMG), Austria
VKMS	Lab. of Seismic Monitoring, Voronezh region, GSRAS & Voronezh State University, Russia
VLA	Vladivostok Seismological Station, Russia
VSI	University of Athens, Greece

Table 10.1: Continued.

Agency Code	Agency Name
WAR	Institute of Geophysics, Polish Academy of Sciences, Poland
WBNET	West Bohemia Seismic Network, Czech Republic
WEL	Institute of Geological and Nuclear Sciences, New Zealand
WES	Weston Observatory, USA
WUSTL	Washington University Earth and Planetary Sciences, USA
YARS	Yakutiya Regional Seismological Center, GS SB RAS, Russia
ZAG	Seismological Survey of the Republic of Croatia, Croatia
ZUR	Swiss Seismological Service (SED), Switzerland
ZUR_RMT	Zurich Moment Tensors, Switzerland

Table 10.2: Phases reported to the ISC. These include phases that could not be matched to an appropriate ak135 phases. Those agencies that reported at least 10% of a particular phase are also shown.

Reported Phase	Total	Agencies reporting
P	3183770	ROM (13%), TAP (11%)
S	1518432	TAP (21%), JMA (18%), ROM (15%)
AML	695165	ROM (77%), ATH (19%)
IAmb	304120	NEIC (98%)
NULL	261701	NEIC (37%), RSNC (18%), AEIC (12%)
Pn	188673	NEIC (32%)
Pg	160546	NNC (15%), MDD (12%)
pmax	132276	MOS (78%), BJI (22%)
Sg	121317	LDG (11%)
LR	111596	IDC (49%), BJI (31%), NEIC (15%)
Sn	87249	NEIC (21%), LDG (12%), IDC (11%)
PG	83024	ISK (54%), HEL (17%)
Lg	70221	MDD (43%), NNC (42%)
PN	68060	ISK (67%), MOS (14%)
IAMs_20	67179	NEIC (98%)
IAML	66939	GUC (25%), SJA (24%), DDA (12%)
SG	66906	ISK (32%), HEL (26%), PRU (18%), IPEC (13%)
IAML_P	44121	DDA (100%)
PKP	24852	IDC (55%), BJI (11%)
T	22111	IDC (91%)
pP	18556	BJI (40%), IDC (19%), NEIC (12%)
MLR	17770	MOS (100%)
PKPbc	17271	IDC (62%), NEIC (20%)
A	16847	INMG (51%), SKHL (27%), SVSA (22%)
PKIKP	16539	MOS (97%)
MSG	15848	HEL (100%)
PcP	15722	IDC (61%), NEIC (15%), VIE (11%)
END	14342	ROM (100%)
SN	14175	HEL (50%), ISK (16%), BRA (14%)
PFAKE	12019	NEIC (100%)
PKPdf	11601	NEIC (52%)
PP	11009	BJI (34%), IDC (23%)
Sb	10798	IRIS (99%)
smax	8350	MOS (72%), BJI (28%)
x	8238	NDI (75%), PRU (21%)
PKPab	7703	IDC (43%), NEIC (20%), VIE (13%)
Pb	7518	IRIS (97%)
sP	7321	BJI (85%)
PKiKP	7233	IRIS (40%), VIE (23%), IDC (20%)
SS	6793	MOS (35%), BJI (32%)
PB	6727	HEL (100%)
SB	6246	HEL (100%)
IAMB	6053	TEH (100%)
ScP	4459	IDC (81%)
AMS	4293	PRU (87%)
AMB	4135	SKHL (80%), BJI (18%)
PKP2	3804	MOS (94%)
*PP	2991	MOS (100%)
LG	2949	BRA (80%), OTT (17%)
Pdiff	2491	IRIS (63%), IDC (16%)
mb	2289	BUC (100%)
Trac	2233	OTT (100%)
PKKPbc	2081	IDC (93%)
sS	1962	BJI (94%)
IAmb_Lg	1869	NEIC (100%)
Smax	1651	BYKL (100%)

Table 10.2: (continued)

Reported Phase	Total	Agencies reporting
X	1589	JMA (81%), SYO (18%)
PPP	1493	MOS (77%)
PKhKP	1452	IDC (100%)
IVMs_BB	1440	BER (44%), NEIC (40%), DDA (15%)
LQ	1327	PPT (56%), BELR (16%), INMG (16%)
pPKP	1232	BJI (43%), IDC (31%), PRU (15%)
Pmax	1205	BYKL (97%)
PKHKP	1182	MOS (100%)
SKS	1158	BJI (50%), PRU (15%)
SKPbc	1140	IDC (93%)
AMP	1061	IEPN (57%), HLW (30%)
E	975	ZAG (98%)
SSS	973	MOS (57%), CLL (24%), BELR (11%)
PS	951	MOS (38%), CLL (14%)
ScS	904	BJI (67%), IDC (17%)
L	893	WAR (60%), MOLD (16%)
Pdif	783	BER (21%), NEIC (21%), SFS (12%)
IVmB_BB	766	BER (59%), NEIC (40%)
PA	746	DDA (98%)
LRM	746	MOLD (58%), BELR (42%)
SKP	730	IDC (41%), IRIS (38%)
max	701	BYKL (100%)
sPKP	656	BJI (95%)
PKPAB	655	PRU (100%)
PKPPKP	652	IDC (94%)
PKKP	592	IDC (71%)
SP	535	MOS (25%), BER (19%), PRU (13%), BUD (12%)
*SP	505	MOS (100%)
SKSac	485	BER (45%), VIE (12%), LJU (11%), CLL (11%)
pPKPdf	479	VIE (42%), BER (20%), NEIC (19%)
PKPpre	477	NEIC (66%), IDC (29%)
pPKPbc	451	IDC (62%), VIE (22%)
PKKPab	447	IDC (79%), VIE (16%)
PKP1	426	LIC (89%)
PKS	420	BJI (90%)
ePg	417	ZAG (100%)
PDIFF	391	BRA (53%), PRU (24%), IPEC (15%)
PKPDF	384	PRU (100%)
SKKS	375	BJI (66%)
*SS	366	MOS (100%)
PcS	317	BJI (90%)
pPKPab	292	VIE (53%), IDC (22%), CLL (13%)
Lm	275	CLL (100%)
Sm	247	SIGU (100%)
PPS	245	CLL (52%), MOS (24%), MOLD (16%)
LmV	244	CLL (100%)
PM	242	BELR (99%)
Pm	241	SIGU (100%)
Sgmax	235	NERS (100%)
ePn	229	ZAG (100%)
PKP2bc	227	IDC (100%)
pPKiKP	199	VIE (78%)
PmP	180	BGR (79%), ZUR (21%)
iPg	176	ZAG (100%)
SKPdf	176	BER (56%), VIE (22%), CLL (15%)
SKKPbc	175	IDC (81%), VIE (15%)
Rg	170	DBN (28%), BER (25%), NAO (25%), IDC (14%)

Table 10.2: (continued)

Reported Phase	Total	Agencies reporting
(P)	167	BRG (73%), CLL (26%)
IVmBBB	157	BER (99%)
LmH	150	CLL (100%)
AMd	150	NIC (100%)
P3KPbc	143	IDC (100%)
PCP	141	PRU (63%), LPA (18%), BRG (14%)
Sgm	135	SIGU (100%)
SSSS	135	CLL (100%)
Pgmax	128	NERS (98%)
RG	126	IPEC (52%), HEL (48%)
SmS	124	BGR (96%)
SKPab	114	IDC (83%), VIE (15%)
AMb	108	IGIL (86%), NDI (14%)
P4KPbc	106	IDC (100%)
LMZ	92	WAR (100%)
Lmax	88	CLL (100%)
pPcP	79	IDC (92%)
PKP2ab	70	IDC (100%)
iPn	70	ZAG (100%)
AMs_VX	65	NEIC (100%)
del	64	AUST (91%)
pPdiff	63	VIE (73%), SYO (19%)
SKKSac	62	CLL (61%), IDC (16%), WAR (13%)
m	59	SIGU (100%)
PKKPdf	57	VIE (46%), NEIC (37%), CLL (18%)
PDIF	54	BRA (93%)
Sdif	54	CLL (61%), PPT (20%), WAR (11%)
MSN	53	HEL (77%), BER (23%)
Pgm	51	SIGU (100%)
rx	50	SKHL (100%)
P'P'df	50	VIE (90%)
SH	46	SYO (100%)
pPP	45	CLL (51%), LPA (44%)
SKKP	43	IDC (63%), PRU (14%)
PnPn	41	UCC (63%), SYO (37%)
sPKiKP	41	VIE (51%), UCC (24%), CLL (15%)
SKSdf	41	BER (51%), VIE (39%)
(sP)	40	CLL (100%)
p	40	MAN (100%)
PgPg	39	BYKL (85%), UCC (15%)
Snm	38	SIGU (100%)
LQM	37	BELR (62%), MOLD (38%)
SKSP	35	BELR (43%), MOLD (29%), CLL (29%)
AMPG	33	OSPL (48%), BER (15%), SJA (12%), BGS (12%)
PSKS	31	CLL (100%)
AMSN	30	SJA (87%)
SCP	29	PRU (59%), BRG (31%)
PKSdf	29	BER (69%), CLL (31%)
PKiKPd	29	BUD (100%)
pwP	29	NEIC (100%)
P3KP	29	IDC (100%)
PPPP	28	CLL (100%)
SKiKP	27	AWI (63%), IDC (37%)
(pP)	27	CLL (100%)
sPP	26	CLL (88%), LJU (12%)
SM	23	BELR (96%)
AMSG	23	BER (26%), SJA (22%), BGS (17%), OSPL (17%), LSZ (13%)

Table 10.2: (continued)

Reported Phase	Total	Agencies reporting
SCS	21	LPA (48%), PRU (33%), IPEC (14%)
P*	21	BGR (81%), MOS (14%)
sPKPab	20	UCC (50%), CLL (40%)
AMPN	20	SJA (85%), BER (15%)
SgSg	19	BYKL (100%)
(Sn)	19	OSUB (68%), CLL (32%)
Li	19	MOLD (100%)
IVMsBB	19	BER (84%), BGS (11%)
Plp	19	CLL (100%)
n	19	LIT (100%)
SKIKS	18	LPA (100%)
SDIFF	18	BRG (78%), LPA (22%)
PsP	18	MOLD (61%), BELR (39%)
P*P'bc	17	IDC (76%), NEIC (18%)
pPn	17	UCC (53%), SKHL (35%), SYO (12%)
(PP)	17	CLL (100%)
PKPdiff	17	CLL (100%)
sSS	16	CLL (100%)
sPn	15	UCC (93%)
PKPPKPdf	14	CLL (100%)
(SSS)	14	CLL (100%)
sPKPdf	14	CLL (50%), SYO (50%)
Pnm	13	SIGU (100%)
(SS)	13	CLL (100%)
pScP	13	IDC (100%)
PPlp	13	CLL (100%)
(S)	13	CLL (92%)
s	13	SFS (46%), MAN (46%)
SKKKS	13	BELR (100%)
SDIF	13	PRU (92%)
PKKS	12	PRU (67%), BRG (33%)
PPPprev	12	CLL (100%)
PKPM	12	BELR (100%)
(PKiKP)	12	CLL (100%)
Sglp	11	CLL (100%)
SKPDF	11	BRA (100%)
(SSSS)	11	CLL (100%)
P4KP	11	IDC (100%)
XS	10	PRU (100%)
MPN	10	HEL (100%)
(PPP)	10	CLL (100%)
PKPc	10	WAR (100%)
PSP	9	LPA (89%), MOLD (11%)
S*	9	BGR (100%)
SKIKP	9	LPA (100%)
pPg	9	SKHL (100%)
PbPb	9	UCC (100%)
PPiKP	9	BUD (100%)
SN5	8	LSZ (50%), ISN (50%)
PKiKPc	8	BUD (100%)
(PcP)	8	CLL (100%)
PPM	8	BELR (100%)
sPKPbc	8	CLL (62%), SYO (25%), IDC (12%)
PKPdif	8	NEIC (88%), CLL (12%)
PSPS	8	CLL (100%)
Sdiff	7	LJU (71%), HYB (29%)
SKKPab	7	IDC (100%)

Table 10.2: (continued)

Reported Phase	Total	Agencies reporting
sPPS	7	CLL (100%)
sPPP	7	CLL (100%)
sKSSbc	7	LJU (100%)
P3KPab	7	IDC (100%)
sPDIFF	7	IPEC (57%), BRG (43%)
DMd	7	NEIC (100%)
(PKPab)	7	CLL (100%)
PGDS	7	NDI (100%)
SPP	6	CLL (50%), BELR (17%), HYB (17%), MOS (17%)
pPN	6	IPEC (67%), BRA (33%)
P(2)	6	CLL (100%)
(PKPdf)	6	CLL (100%)
LV	6	CLL (100%)
(Pg)	6	CLL (100%)
R	6	LDG (100%)
PGDN	5	NDI (100%)
SKKPdf	5	CLL (100%)
PSS	5	CLL (100%)
P7KPbc	5	IDC (100%)
RQ	5	MOLD (100%)
pPdf	5	CLL (80%), HYB (20%)
PKiKPC	4	BUD (100%)
(PPS)	4	CLL (100%)
(Sg)	4	CLL (75%), OSUB (25%)
PPPPrev	4	CLL (100%)
sSSS	4	CLL (100%)
sPKIKP	4	IPEC (100%)
PcPPKPre	4	CLL (100%)
SKSp	4	BRA (100%)
sSdiff	4	CLL (100%)
SKKSacre	4	CLL (100%)
P*P	4	ZUR (100%)
(pPKPbc)	4	CLL (100%)
SGSG	4	IPEC (100%)
pSKS	4	IPEC (100%)
sPdf	4	CLL (75%), HYB (25%)
PKKSdf	3	CLL (100%)
sPS	3	CLL (100%)
sSSS	3	CLL (100%)
AP	3	MOS (100%)
PKKSbc	3	CLL (100%)
SKPPKPdf	3	CLL (100%)
Lm(360)	3	CLL (100%)
(sPP)	3	CLL (100%)
Snd	3	BUD (100%)
PN5	3	ISN (67%), LSZ (33%)
PCN	3	NDI (100%)
(PS)	3	CLL (100%)
PKPbc(2)	3	CLL (100%)
(SKSac)	3	CLL (100%)
PKSbc	3	CLL (100%)
PKPdf(2)	3	CLL (100%)
PPmax	3	CLL (100%)
sPcP	3	CLL (100%)
SKPa	3	NAO (67%), BER (33%)
PKPlp	3	CLL (100%)
(sPKiKP)	2	CLL (100%)

Table 10.2: (continued)

Reported Phase	Total	Agencies reporting
SSP	2	CLL (100%)
APKP	2	MOS (100%)
pPS	2	CLL (100%)
sPKKPab	2	CLL (100%)
PNDS	2	NDI (100%)
PKKPpB	2	BRA (100%)
SKKSdf	2	CLL (100%)
XM	2	MOLD (100%)
(PPPP)	2	CLL (100%)
PKIKS	2	LPA (100%)
Lgm	2	SIGU (100%)
PKPab(2)	2	CLL (100%)
SKSSKSac	2	CLL (100%)
Pnc	2	BUD (100%)
LH	2	CLL (100%)
MPKP	2	MOLD (100%)
(PG)	2	BRG (100%)
PGN	2	HEL (100%)
PDS	2	NDI (100%)
(sPKPdf)	2	CLL (100%)
(PKPbc)	2	CLL (100%)
pPPP	2	CLL (100%)
Ec	2	BUD (100%)
PKKSDF	2	BRA (100%)
I	2	ISN (100%)
(Pn)	2	OSUB (50%), CLL (50%)
pg	2	ISN (100%)
PKPPKPbc	2	CLL (100%)
pPPS	1	CLL (100%)
(sPcP)	1	CLL (100%)
pn	1	ISN (100%)
PMP	1	BER (100%)
sPKKPbc	1	CLL (100%)
PPPmax	1	CLL (100%)
SN4	1	ISN (100%)
SSSrev	1	CLL (100%)
(ScS)	1	CLL (100%)
(pPSKS)	1	CLL (100%)
(sSS)	1	CLL (100%)
S4	1	SJA (100%)
I_20	1	NDI (100%)
pSKKSacm	1	CLL (100%)
PPPmax	1	CLL (100%)
sPPPrev	1	CLL (100%)
SPSrev	1	CLL (100%)
sSKPdf	1	CLL (100%)
sPPPP	1	CLL (100%)
(sPdif)	1	CLL (100%)
(sPSKS)	1	CLL (100%)
sScP	1	CLL (100%)
pSKKSacr	1	CLL (100%)
PSPSrev	1	CLL (100%)
(sPPS)	1	CLL (100%)
pSKKSac	1	CLL (100%)
V	1	CLL (100%)
(PN)	1	BRG (100%)
(sS)	1	CLL (100%)

Table 10.2: (continued)

Reported Phase	Total	Agencies reporting
sKKSac	1	CLL (100%)
(SG)	1	OSUB (100%)
sSKP	1	MOLD (100%)
aPKPab	1	CLL (100%)
sPKP1	1	BELR (100%)
PKKPbcma	1	CLL (100%)
i	1	MAN (100%)
Pdiffmax	1	CLL (100%)
(pPKPdf)	1	CLL (100%)
pPdiffma	1	CLL (100%)
OKP	1	BRG (100%)
ePKPab	1	CLL (100%)
SKSsacmax	1	CLL (100%)
pSSrev	1	CLL (100%)
(pPcP)	1	CLL (100%)
PD	1	UPA (100%)
SKKSacma	1	CLL (100%)
sSSP	1	CLL (100%)
O	1	BRG (100%)
N	1	IRIS (100%)
(Sdif)	1	CLL (100%)
RPKKPdf	1	CLL (100%)
Pd0	1	ATH (100%)
SKPPKPbc	1	CLL (100%)
sPg	1	SKHL (100%)
sSSmax	1	CLL (100%)
sPDIF	1	BRA (100%)
sSKKSac	1	CLL (100%)
PDNE	1	NDI (100%)
(SKKPdf)	1	CLL (100%)
SPS	1	CLL (100%)
Pbd	1	BUD (100%)
PKPdiff2	1	CLL (100%)
P7KP	1	IDC (100%)
SKK	1	SFS (100%)
sPN	1	BRA (100%)
pPKPPKPb	1	CLL (100%)
pPKKPbc	1	CLL (100%)
pPmax	1	CLL (100%)
pPKPdiff	1	CLL (100%)
pPKPdif	1	NEIC (100%)
PLR	1	SVSA (100%)
Pdfi	1	SFS (100%)
SSN	1	NDI (100%)
(PKP)	1	CLL (100%)
SSmax	1	CLL (100%)
PL	1	AAE (100%)
sPdiff	1	SYO (100%)
PCS	1	NDI (100%)
CeP	1	BUD (100%)
PC	1	UPA (100%)
Coda	1	SFS (100%)
pPKPPKpd	1	CLL (100%)
(sKKSac)	1	CLL (100%)
Sgd	1	BUD (100%)
-	1	INMG (100%)
(sn)	1	CLL (100%)

Table 10.2: (continued)

Reported Phase	Total	Agencies reporting
SKKSacr	1	CLL (100%)
LRM1	1	BELR (100%)
SKIK	1	LPA (100%)
PKPdfmax	1	CLL (100%)
KIKP	1	BUD (100%)
PKKPDF	1	BRA (100%)
pSP	1	CLL (100%)
3PKPdf	1	CLL (100%)
P'P'ab	1	IDC (100%)
pPKKKPab	1	CLL (100%)
PGCS	1	NDI (100%)
(SKKSac)	1	CLL (100%)
(Sb)	1	CLL (100%)
Pnd	1	BUD (100%)
sPKSdf	1	CLL (100%)
(PSKS)	1	CLL (100%)
Pd1	1	ATH (100%)
Pnmax	1	CLL (100%)
(pPSPS)	1	CLL (100%)
SSPrev	1	CLL (100%)
pPKP1	1	BELR (100%)
PSSrev	1	CLL (100%)
(pPP)	1	CLL (100%)
Pd2	1	ATH (100%)
pZP	1	SYO (100%)
PcPPKPrm	1	CLL (100%)
Pcp	1	SYO (100%)
Se	1	BER (100%)
SMZ	1	BJI (100%)
SPPmax	1	CLL (100%)
PPPPmax	1	CLL (100%)
sP(2)	1	CLL (100%)
H	1	CLL (100%)
Cod	1	SFS (100%)
pPDIF	1	BRA (100%)
pPDIFF	1	BRG (100%)
pSPP	1	CLL (100%)
(SN)	1	OSUB (100%)
PKPaf	1	BER (100%)
sPSKS	1	CLL (100%)
(SSrev)	1	CLL (100%)
PKPPKPab	1	CLL (100%)

Table 10.3: Reporters of amplitude data

Agency	Number of reported amplitudes	Number of amplitudes in ISC located events	Number used for ISC <i>mb</i>	Number used for ISC <i>MS</i>
ROM	549892	33211	0	0
NEIC	430134	281168	163572	51498
IDC	299800	283629	116649	33973
ATH	134152	12778	0	0
MOS	128793	124387	66866	12381
NNC	96016	32102	78	0
WEL	74334	20190	0	0
ISK	70061	16576	0	0
MDD	66414	11914	0	0
BJI	66199	60552	13826	17752
SOME	61925	18996	528	0
DDA	52604	11088	0	0
RSNC	48091	3590	0	0
VIE	41111	21510	8274	0
DJA	38866	22951	4887	0
THE	35202	5496	0	0
LDG	20634	5153	8	0
MAN	17902	4045	0	0
GUC	16974	6084	0	0
SJA	16371	4472	63	0
HEL	16130	262	0	0
DMN	13846	13211	0	0
BKK	12370	11110	5924	0
INMG	11555	5505	2196	0
PPT	10757	8566	1143	2421
PRU	10273	4962	0	2920
BUC	9238	2089	0	0
SKHL	8148	5595	0	0
BER	7960	1956	8	3
YARS	7843	289	0	0
JSO	7416	2451	381	0
LJU	6362	375	0	0
TEH	6052	4185	0	0
NDI	5659	4809	1044	240
PRE	4574	448	3	0
SKO	4281	465	0	0
PDG	4252	2910	0	0
MRB	4134	301	0	0
SVSA	4113	430	252	0
BGS	3994	3110	1608	820
BRG	3955	2427	663	0
NIC	3897	1521	0	0
BYKL	3532	1028	0	0
SNET	3473	1450	0	0

Table 10.3: Continued.

Agency	Number of reported amplitudes	Number of amplitudes in ISC located events	Number used for ISC <i>mb</i>	Number used for ISC <i>MS</i>
WBNET	3448	0	0	0
CLL	2637	2398	515	205
ZUR	2427	544	0	0
KNET	2393	771	0	0
OTT	2232	356	0	0
NSSC	2185	1032	3	0
NAO	2046	2007	1525	0
LIT	2026	1985	1483	0
ASRS	1933	721	0	0
DNK	1853	1588	1113	0
LIC	1768	1565	880	0
LVSN	1717	27	0	0
ECX	1424	275	0	0
THR	1421	630	0	0
IPEC	1311	171	0	0
IEPN	884	675	9	0
ISN	873	333	0	0
OSPL	872	330	0	0
IGIL	871	447	88	150
UCC	865	681	534	0
MOLD	761	463	82	0
UCR	749	633	0	0
SIGU	716	509	0	0
WAR	700	670	12	506
BELR	612	584	0	240
SSNC	600	84	0	0
NERS	365	56	0	0
DBN	283	204	102	0
MIRAS	265	37	0	0
HYB	258	177	56	0
BGR	181	51	0	0
SCB	111	92	0	0
UPA	61	16	0	0
PLV	47	26	0	0
LSZ	35	14	0	0
JSN	1	0	0	0
MEX	1	1	0	0
BEO	1	1	0	0

11

Glossary of ISC Terminology

- Agency/ISC data contributor

An academic or government institute, seismological organisation or company, geological/meteorological survey, station operator or author that reports or contributed data in the past to the ISC or one of its predecessors. Agencies may contribute data to the ISC directly, or indirectly through other ISC data contributors.

- Agency code

A unique, maximum eight-character code for a data reporting agency (e.g. NEIC, GFZ, BUD) or author (e.g. ISC, EHB, IASPEI). Often the agency code is the commonly used acronym of the reporting institute.

- Arrival

A phase pick at a station is characterised by a phase name and an arrival time.

- Associated phase

Associated phase arrival or amplitude measurements represent a collection of observations belonging to (i.e. generated by) an event. The complete set of observations are associated to the prime hypocentre.

- Azimuthal gap/Secondary azimuthal gap

The azimuthal gap for an event is defined as the largest angle between two stations with defining phases when the stations are ordered by their event-to-station azimuths. The secondary azimuthal gap is the largest azimuthal gap a single station closes.

- BAAS

Seismological bulletins published by the British Association for the Advancement of Science (1913-1917) under the leadership of H.H. Turner. These bulletins are the predecessors of the ISS Bulletins and include reports from stations distributed worldwide.

- Bulletin

An ordered list of event hypocentres, uncertainties, focal mechanisms, network magnitudes, as well as phase arrival and amplitude observations associated to each event. An event bulletin may list all the reported hypocentres for an event. The convention in the ISC Bulletin is that the preferred (prime) hypocentre appears last in the list of reported hypocentres for an event.

- Catalogue

An ordered list of event hypocentres, uncertainties and magnitudes. An event catalogue typically lists only the preferred (prime) hypocentres and network magnitudes.

- CoSOI/IASPEI

Commission on Seismological Observation and Interpretation, a commission of IASPEI that prepares and discusses international standards and procedures in seismological observation and interpretation.

- Defining/Non-defining phase

A defining phase is used in the location of the event (time-defining) or in the calculation of the network magnitude (magnitude-defining). Non-defining phases are not used in the calculations because they suffer from large residuals or could not be identified.

- Direct/Indirect report

A data report sent (e-mailed) directly to the ISC, or indirectly through another ISC data contributor.

- Duplicates

Nearly identical phase arrival time data reported by one or more agencies for the same station. Duplicates may be created by agencies reporting observations from other agencies, or several agencies independently analysing the waveforms from the same station.

- Event

A natural (e.g. earthquake, landslide, asteroid impact) or anthropogenic (e.g. explosion) phenomenon that generates seismic waves and its source can be identified by an event location algorithm.

- Grouping

The ISC algorithm that organises reported hypocentres into groups of events. Phases associated to any of the reported hypocentres will also be associated to the preferred (prime) hypocentre. The grouping algorithm also attempts to associate phases that were reported without an accompanying hypocentre to events.

- Ground Truth

An event with a hypocentre known to certain accuracy at a high confidence level. For instance, GT0 stands for events with exactly known location, depth and origin time (typically explosions); GT5 stands for events with their epicentre known to 5 km accuracy at the 95% confidence level, while their depth and origin time may be known with less accuracy.

- Ground Truth database

On behalf of IASPEI, the ISC hosts and maintains the IASPEI Reference Event List, a bulletin of ground truth events.

- IASPEI

International Association of Seismology and Physics of the Earth Interior, www.iaspei.org.

- International Registry of Seismograph Stations (IR)

Registry of seismographic stations, jointly run by the ISC and the World Data Center for Seismology, Denver (NEIC). The registry provides and maintains unique five-letter codes for stations participating in the international parametric and waveform data exchange.

- ISC Bulletin

The comprehensive bulletin of the seismicity of the Earth stored in the ISC database and accessible through the ISC website. The bulletin contains both natural and anthropogenic events. Currently the ISC Bulletin spans more than 50 years (1960-to date) and it is constantly extended by adding both recent and past data. Eventually the ISC Bulletin will contain all instrumentally recorded events since 1900.

- ISC Governing Council

According to the ISC Working Statutes the Governing Council is the governing body of the ISC, comprising one representative for each ISC Member.

- ISC-located events

A subset of the events selected for ISC review are located by the ISC. The rules for selecting an event for location are described in Section 3.3.4 of January to June 2013 Bulletin Summary; ISC-located events are denoted by the author ISC.

- ISC Member

An academic or government institute, seismological organisation or company, geological/meteorological survey, station operator, national/international scientific organisation that contribute to the ISC budget by paying membership fees. ISC members have voting rights in the ISC Governing Council.

- ISC-reviewed events

A subset of the events reported to the ISC are selected for ISC analyst review. These events may or may not be located by the ISC. The rules for selecting an event for review are described in Section 3.3.3 of January to June 2013 Bulletin Summary. Non-reviewed events are explicitly marked in the ISC Bulletin by the comment following the prime hypocentre "Event not reviewed by the ISC".

- ISF

International Seismic Format (www.isc.ac.uk/standards/isf). A standard bulletin format approved by IASPEI. The ISC Bulletin is presented in this format at the ISC website.

- ISS

International Seismological Summary (1918-1963). These bulletins are the predecessors of the ISC Bulletin and represent the major source of instrumental seismological data before the digital era. The ISS contains regionally and teleseismically recorded events from several hundreds of globally distributed stations.

- Network magnitude

The event magnitude reported by an agency or computed by the ISC locator. An agency can report several network magnitudes for the same event and also several values for the same magnitude type. The network magnitude obtained with the ISC locator is defined as the median of station magnitudes of the same magnitude type.

- Phase

A maximum eight-character code for a seismic, infrasonic, or hydroacoustic phase. During the ISC processing, reported phases are mapped to standard IASPEI phase names. Amplitude measurements are identified by specific phase names to facilitate the computation of body-wave and surface-wave magnitudes.

- Prime hypocentre

The preferred hypocentre solution for an event from a list of hypocentres reported by various agencies or calculated by the ISC.

- Reading

Parametric data that are associated to a single event and reported by a single agency from a single station. A reading typically includes one or more phase names, arrival time and/or amplitude/period measurements.

- Report/Data report

All data that are reported to the ISC are parsed and stored in the ISC database. These may include event bulletins, focal mechanisms, moment tensor solutions, macroseismic descriptions and other event comments, as well as phase arrival data that are not associated to events. Every single report sent to the ISC can be traced back in the ISC database via its unique report identifier.

- Shide Circulars

Collections of station reports for large earthquakes occurring in the period 1899-1912. These reports were compiled through the efforts of J. Milne. The reports are mainly for stations of the British Empire equipped with Milne seismographs. After Milne's death, the Shide Circulars were replaced by the Seismological Bulletins of the BAAS.

- Station code

A unique, maximum six-character code for a station. The ISC Bulletin contains data exclusively from stations registered in the International Registry of Seismograph Stations.

12

Acknowledgements

We thank Danila Chebrov and his colleagues at Kamchatka Branch of the Geophysical Survey of Russian Academy of Sciences for kindly accepting our invitation and submitting the article on notable earthquakes for this issue of the Summary.

We are also grateful to the developers of the Generic Mapping Tools (GMT) suite of software (Wessel and Smith, 1998) that was used extensively for producing the graphical figures.

Finally, we thank the ISC Member Institutions, Data Contributors, Funding Agencies (including NSF Award EAR-1417970 and USGS Award G15AC00202) and Sponsors for supporting the long-term operation of the ISC.

References

- Balfour, N., R. Baldwin, and A. Bird (2008), Magnitude calculations in Antelope 4.10, *Analysis Group Note of Geological Survey of Canada*, pp. 1–13.
- Bisztricsany, E. A. (1958), A new method for the determination of the magnitude of earthquakes, *Geofiz. Kozl.*, pp. 69–76.
- Bondár, I., and D. Storchak (2011), Improved location procedures at the International Seismological Centre, *Geophysical Journal International*, 186, 1220–1244.
- Bormann, P., and J. W. Dewey (2012), The new iaspei standards for determining magnitudes from digital data and their relation to classical magnitudes, is 3.3, *New Manual of Seismological Observatory Practice 2 (NMSOP-2)*, P. Bormann (Ed.), pp. 1–44, doi:10.2312/GFZ.NMSOP-2_IS_3.3,10.2312/GFZ.NMSOP-2, <http://nmsop.gfz-postsdam.de>.
- Bormann, P., and J. Saul (2008), The new IASPEI standard broadband magnitude mB, *Seism. Res. Lett.*, 79(5), 698–705.
- Bormann, P., R. Liu, X. Ren, R. Gutdeutsch, D. Kaiser, and S. Castellaro (2007), Chinese national network magnitudes, their relation to NEIC magnitudes and recommendations for new IASPEI magnitude standards, *Bulletin of the Seismological Society of America*, 97(1B), 114–127, doi:10.1785/012006007835.
- Bormann, P., R. Liu, Z. Xu, R. Ren, and S. Wendt (2009), First application of the new IASPEI teleseismic magnitude standards to data of the China National Seismographic Network, *Bulletin of the Seismological Society of America*, 99, 1868–1891, doi:10.1785/0120080010.
- Choy, G. L., and J. L. Boatwright (1995), Global patterns of radiated seismic energy and apparent stress, *J. Geophys. Res.*, 100(B9), 18,205–18,228.
- Dziewonski, A. M., T.-A. Chou, and J. H. Woodhouse (1981), Determination of earthquake source parameters from waveform data for studies of global and regional seismicity, *J. Geophys. Res.*, 86, 2825–2852.
- Engdahl, E. R., and A. Villaseñor (2002), Global seismicity: 1900–1999, *International Handbook of Earthquake Engineering and Seismology, International Geophysics series*, 81A, 665–690.
- Engdahl, E. R., R. van der Hilst, and R. Buland (1998), Global teleseismic earthquake relocation with improved travel times and procedures for depth determination, *Bulletin of the Seismological Society of America*, 88, 722–743.
- Gutenberg, B. (1945a), Amplitudes of P, PP and S and magnitude of shallow earthquakes, *Bulletin of the Seismological Society of America*, 35, 57–69.
- Gutenberg, B. (1945b), Magnitude determination of deep-focus earthquakes, *Bulletin of the Seismological Society of America*, 35, 117–130.
- Gutenberg, B. (1945c), Amplitudes of surface waves and magnitudes of shallow earthquakes, *Bulletin of the Seismological Society of America*, 35, 3–12.
- Hutton, L. K., and D. M. Boore (1987), The ML scale in southern California, *Bulletin of the Seismological Society of America*, 77, 2074–2094.
- IASPEI (2005), Summary of magnitude working group recommendations on standard procedures for determining earthquake magnitudes from digital data, <http://www.iaspei.org/commissions/CSOI.html#wgmm>, http://www.iaspei.org/commissions/CSOI/summary_of_WG_recommendations_2005.pdf.

- IASPEI (2013), Summary of magnitude working group recommendations on standard procedures for determining earthquake magnitudes from digital data, http://www.iaspei.org/commissions/CSOI/Summary_of_WG_recommendations_20130327.pdf.
- IDC (1999), IDC processing of seismic, hydroacoustic and infrasonic data, *IDC Documentation*.
- Kanamori, H. (1977), The energy release in great earthquakes, *J. Geophys. Res.*, *82*, 2981–2987.
- Lee, W. H. K., R. Bennet, and K. Meagher (1972), A method of estimating magnitude of local earthquakes from signal duration, *U.S. Geol. Surv.*, Open-File Rep.
- Nuttli, O. W. (1973), Seismic wave attenuation and magnitude relations for eastern North America, *J. Geophys. Res.*, *78*, 876–885.
- Richter, C. F. (1935), An instrumental earthquake magnitude scale, *Bulletin of the Seismological Society of America*, *25*, 1–32.
- Ringdal, F. (1976), Maximum-likelihood estimation of seismic magnitude, *Bulletin of the Seismological Society of America*, *66*(3), 789–802.
- Tsuboi, C. (1954), Determination of the Gutenberg-Richter's magnitude of earthquakes occurring in and near Japan, *Zisin (J. Seism. Soc. Japan)*, *Ser. II*(7), 185–193.
- Tsuboi, S., K. Abe, K. Takano, and Y. Yamanaka (1995), Rapid determination of M_w from broadband P waveforms, *Bulletin of the Seismological Society of America*, *85*(2), 606–613.
- Vaněk, J., A. Zapotek, V. Karnik, N. V. Kondorskaya, Y. V. Riznichenko, E. F. Savarensky, S. L. Solov'yov, and N. V. Shebalin (1962), Standardization of magnitude scales, *Izvestiya Akad. SSSR., Ser. Geofiz.*(2), 153–158, pages 108–111 in the English translation.
- Woessner, J., and S. Wiemer (2005), Assessing the quality of earthquake catalogues: estimating the magnitude of completeness and its uncertainty, *Bulletin of the Seismological Society of America*, *95*(2), doi:10/1785/012040,007.

GDI Protocol



ULTRA LOW LATENCY TRANSMISSION

A rapid data transmission protocol that dramatically reduces latency, ideal for earthquake early warning systems.

GDI uses a flexible packetisation scheme for true, real-time transmission that can deliver waveforms, sample by sample, as they are acquired by the datalogger.

By adapting its transmission to the available communications bandwidth GDI achieves the fastest possible speed for data flow.

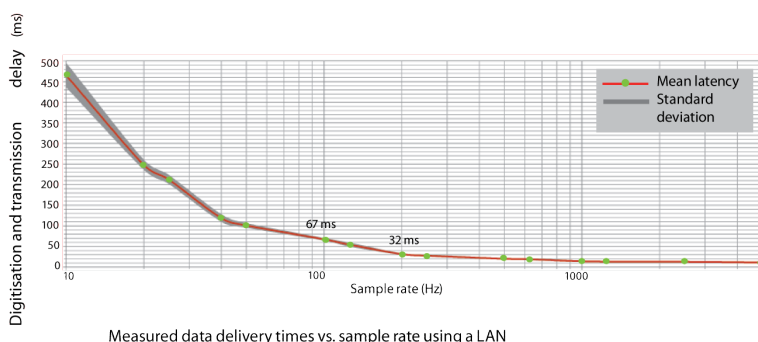
Traditional delays associated with protocols with fixed length packets such as SEEDlink (miniSEED packets) are overcome. In addition, as the packet header is significantly smaller than with SEEDlink (4 bytes as opposed to 64 bytes in SEEDlink), bandwidth requirements are reduced.

Unlike SEEDlink protocol, GDI also delivers per-channel metadata in SEED format and machine readable State of Health (SoH) information.

GDI available as free-licence source code

GDI source code is available as a free download for further development or integration into existing EEW networks, visit www.guralp.com for further details.

In addition, through partnership with Gempa, GDI protocol is also supported via a plug-in to the CAPS module of SeisCompPro for simple integration into existing seismic monitoring infrastructure.



Download the free-licence GDI source code here:

<http://git.guralp.com>

For more information see the GDI project wiki here:

http://git.guralp.com/open-source/gdi_simple_client/wikis/home

Key features

Free-licence source code for incorporation into your EEW network

Supported via a plug-in for the CAPS module of SeisCompPro

Rapid data transmission for earthquake early warning systems on all scales

Bandwidth-adaptive packetisation scheme drives efficient data flow

Responsive sample-by-sample streaming dispatches data instantly

Delivers per-channel metadata in SEED format and machine readable State of Health (SoH)

Significantly reduced packet headers for higher transmission efficiency

Already available, in combination with low latency causal filtering, in Güralp Minimus digitiser - for data latency of ~40 ms

GDI and the Güralp Minimus

The greatest benefit of GDI is achieved when it is combined with low latency filtering, such as the causal filtering in the Güralp Minimus digitiser. In this example, digitisation and transmission can be achieved in ~40 ms, significantly less than the data latencies of 1 s, typically achieved with SEEDlink.



GURALP MINIMUS

Güralp Systems Limited
Midas House, Calleva Park
Aldermaston, Reading
RG7 8EA, UK

T +44 118 981 9056
F +44 118 981 9943
E sales@guralp.com



Kestrel™ SeismoGeodetic 160-09 System

The ideal instrument for real-time earthquake characterization and hazard mitigation from Trimble

- ▶ Combines seismic recording with GNSS Geodetic Measurements
- ▶ 220 Channel GNSS Receiver
- ▶ GNSS Precise Point Positioning (PPP); positions and displacements on board
- ▶ ANSS Class A Triaxial Accelerometer

For further information email MonSol_Sales@trimble.com
www.trimble.com/monitoring



© 2016 Trimble Inc. All rights reserved. PN 022506-201 (1/2016)

REFATEK
A TRIMBLE BRAND

TECHNOLOGY THAT
transforms

TRANSFORMING THE WAY THE WORLD WORKS





Earthquake Early Warning Rapid Response

Where to be utilized?

- ✓ High seismic risk areas
- ✓ Regions with known active faults or fault zones
- ✓ Densely populated and urban areas
- ✓ Industrial facilities and lifelines

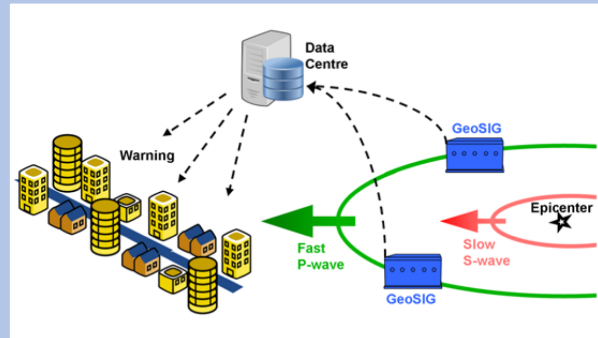
What are the Features and Benefits?

- ✓ Detecting primary non-destructive waves as soon as an earthquake occurs
- ✓ Estimating the magnitude and location of earthquake
- ✓ Indicating approaching destructive waves
- ✓ Real-time operation within scientific reliability
- ✓ Rapid calculation of estimated damages after shake
- ✓ Thematic mapping for damage assessment and action plan (disaster management)
- ✓ Notification of user groups or involved parties
- ✓ Mitigation of risk due to earthquake exposure
- ✓ Automated decision making and emergency actions such as shutdown of facilities
- ✓ Continued monitoring for aftershock events
- ✓ Disaster awareness, prevention and management

Professional Advice and Support from concept to deployment

Our professional and experienced consultants are ready to provide you with the best impartial advice and support from the outset.

Our knowledge of earthquake early warning, seismic monitoring and rapid response systems coupled with an in-depth understanding of our instruments will provide you with an unparalleled advantage to achieve the best results for your requirements on time and on budget.



Overview

Earthquakes are perilous and inevitable natural events, causing severe damage and loss of life.

There is no proven method to forecast the precise occurrence time of an earthquake nor its location or size.

Yet, utilising state of the art scientific methodologies as done in GeoSIG Earthquake Early Warning (EEW) solution, it is now possible to quite accurately assess the location and size as soon as an earthquake emerges using its non-destructive primary waves.

Thus, warnings about a potential strong shaking can be generated almost instantaneously, until destructive secondary seismic waves arrive.

Based on fast and reliable communication channels, this provides the crucial seconds to take measures which may help reduce catastrophic impacts of seismic events.

After an earthquake, GeoSIG Rapid Response (RR) solution provides analytic and thematic information on the aftermath of the earthquake in terms of shake maps consisting of observed ground motion parameters as well as estimated damage distribution.

Our Services

Advice

Consulting

Technical Proposal

Financial Offer

Planning

Installation

Training

Maintenance

How does it work?

GeoSIG instruments provide an EEW option, which is based on and tested against the latest worldwide scientific developments. Currently available methodologies are:

- ✓ Japan Meteorological Agency (JMA)
- ✓ Elarms
- ✓ Presto
- ✓ TaucPd

Depending on specific project requirements, GeoSIG instruments are deployed within and around a seismic hazard region and continuously monitor ground motions.

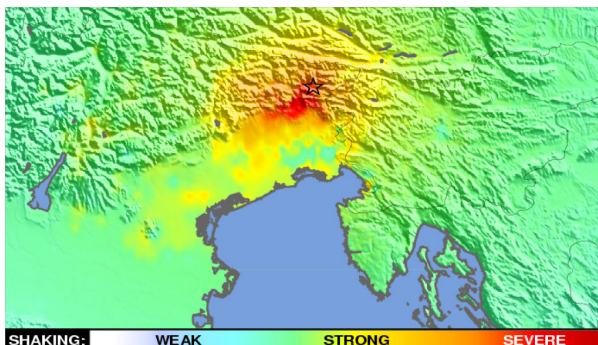
As soon as an earthquake emerges, the fast moving primary seismic wave is detected and analysed on the fly to generate and transmit a notification either directly or via a data centre (improved reliability using several stations) to a target vulnerable area before the arrival of the slower moving destructive seismic waves to that area.

Most beneficial warning is achieved for areas within 20 to 100 km distance from the source of the earthquake.

The notification can be used for various actions such as

- ✓ issuing an audio/visual emergency signal
- ✓ pushing alerts to mobile devices
- ✓ feeding data in decision making systems
- ✓ activating automated emergency reaction systems
- ✓ notifying emergency organisations and personnel and many more.

Once the earthquake event is completed, the continuously collected data is optionally analysed in an automated fashion by GeoSIG RR solution in a data centre within minutes. The results of the analyses are output in the form of shake maps as well as tabular reports that can be transmitted to disaster management organisations, decision makers and general public.



We provide useful advice and a unique integrated approach that can help you achieve your endeavour for

Earthquake Early Warning Rapid Response

In many countries where high seismic risks are present, EEWR systems have been in operation for many years.

It is all about mitigating risk and knowing that your investment in installing an EEWR system can be a sound protection against earthquakes in particular in areas where such risks are high.



Case Studies

Refer to our website www.geosig.com and learn more about our EEWR projects.

- ✓ Ignalina Nuclear Power Plant, Lithuania
- ✓ TGV Méditerranée Railway, France
- ✓ Sakhalin II Oil and Gas Project, Russia
- ✓ Istanbul Metropolitan Area, Turkey

Contact us

for a comprehensive consultation and discussion on your requirements:

Phone +41 44 810 21 50
Email sales@geosig.com
Web www.geosig.com

GeoSIG Ltd
Wiesenstrasse 39
8952 Schlieren
Switzerland

Australian Earthquake Observatory Celebrates 40 Years of Earthquake Monitoring

The Seismology Research Centre was established in Melbourne, Australia in 1976 as part of a tertiary education institute which was later incorporated into RMIT University. Founded by Gary Gibson and first employee Russell Cuthbertson (who still both work at the SRC part time), the SRC is now directed by Adam Pascale (celebrating 25 years with the Centre) and the observatory is managed by Wayne Peck (27 years with SRC), who all contribute to the SRC's wealth of local earthquake knowledge.

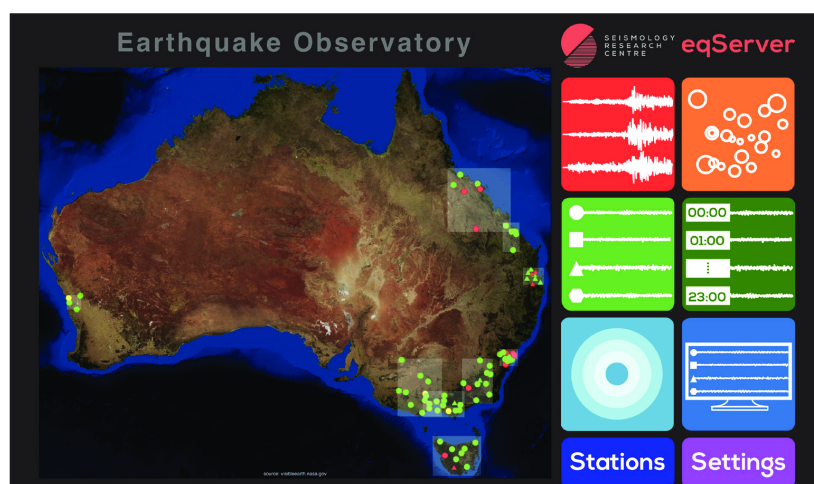
One of the first research projects was to monitor for reservoir induced seismicity at the planned Thomson Dam site, about 100km east of Melbourne. Recording local seismicity for several



SEISMOLOGY
RESEARCH
CENTRE

years prior to construction produced a solid baseline of natural seismicity, clearly showing the activation of reservoir induced seismicity once the dam was completed and water impoundment began. Regular earthquake activity continued for decades, with the largest being a magnitude 5.0 earthquake 11km from the dam, with little impact to the well engineered structure. Still monitored today, Thomson Dam is Melbourne's main water supply.

Providing monitoring services to industry generated funding for the continued earthquake research within the academic setting and allowed the SRC to begin developing their own digital seismic recording equipment and earthquake data processing software. Effectively operating as a self-funded business, RMIT University sold the SRC to private industry in 1998, now owned by ESS Earth Sciences, a Melbourne-based environmental monitoring technology company. With the support of ESS engineering and production departments, and the expansion of the dedicated seismology team, the SRC in 2016 continues to excel at the core function of operating as a high-resolution earthquake observatory, providing rapid emergency response services to industry, as well as continuing the development of some of the best seismic hardware and software available in the market today.



The Seismology Research Centre will soon be releasing their latest waveform analysis software application for Windows, Mac & Linux. To get your free copy of the amazingly user-friendly MiniSEED data viewer, **Waves**, register for an email notification at: src.com.au/news/

GECKO The 7th Generation Kelunji Seismograph Designed by Seismologists; Engineered for Simplicity

Low noise 32-bit ADCs with constant GPS-lock timing
Built-in keypad and display - no laptop required for setup
Rugged IP67 waterproof bodies - only 135mm diameter
Removable SD card stores >1 year of MiniSEED data at 100sps
Lowest cost professional grade recorder; 3 year warranty
Ethernet and 3G cell modem telemetry options
Integrated sensor and internal battery options

- **3-channel recorder accepts any make/model sensor**
- **Low cost $\pm 2g$ to $\pm 400g$ MEMS accelerograph**
- **Low noise $\pm 2g$ or $\pm 4g$ feedback accelerograph**
- **Short Period seismometer - flat 1Hz to 100Hz**
- **Broadband seismometer - 200sec to 1500Hz**



Gecko Compact



Gecko Rugged & SMA



**Gecko SMA-HR
Helix & Prism**



For more information: email sales@esearth.com

www.esearth.com

www.src.com.au

gecko.kelunji.net

Developed by the Seismology Research Centre, a division of ESS Earth Sciences
Designed and manufactured in Melbourne, Australia

